miRNA dynamics in T cell activation

Ana Rodríguez Galán

PhD Thesis

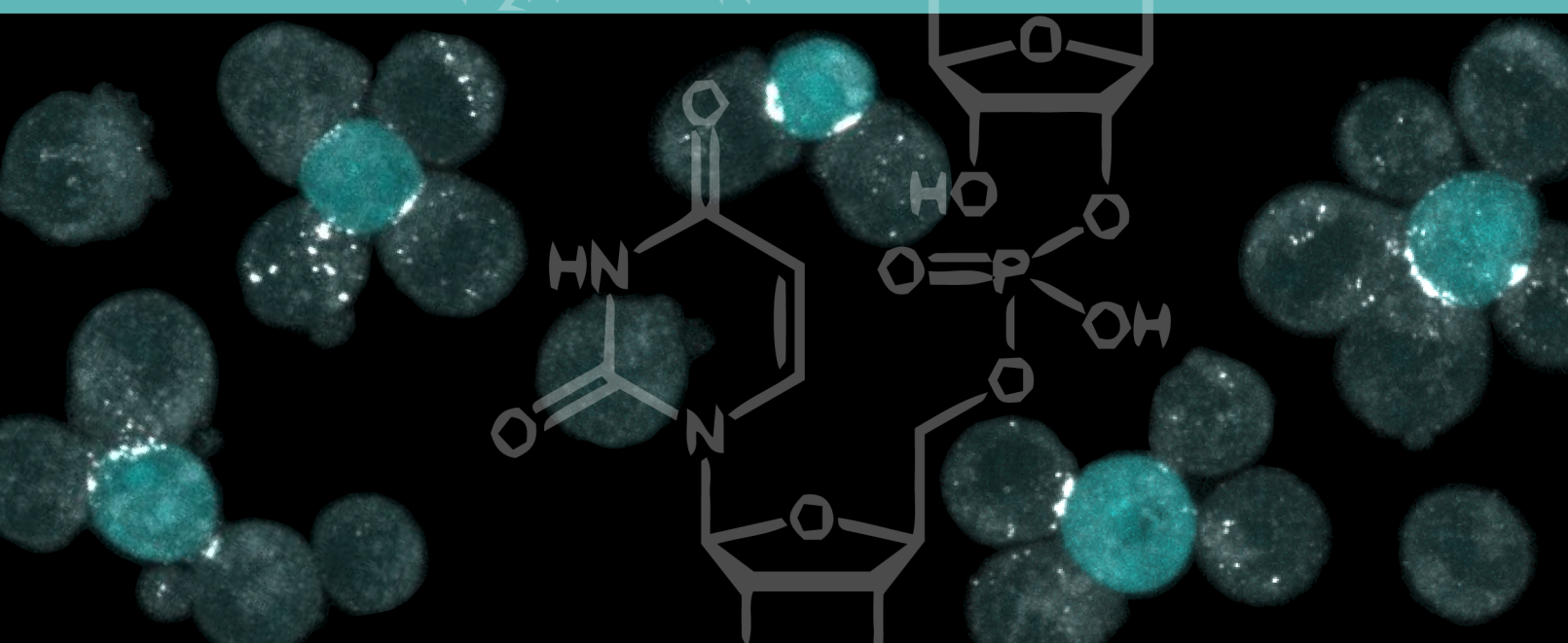

Universidad Autónoma de Madrid

Departamento de Bioquímica

Facultad de Medicina

MiRNA dynamics in T cell activation

Memoria presentada por la Licenciada en Bioquímica:

Ana Rodríguez Galán

Para optar al título de Doctor por la Universidad Autónoma de Madrid.

Director de tesis: **Dr. Francisco Sánchez Madrid**, Doctor en Ciencias Biológicas y Catedrático de Inmunología de la Universidad Autónoma de Madrid.

Este trabajo ha sido realizado en el
Centro Nacional de Investigaciones Cardiovasculares (CNIC) y
Servicio de Inmunología del Hospital Universitario de la Princesa.

Madrid, 2021

A mis padres,

a Clara,

a Javi

Ante él se encontraba el Árbol, su Árbol, ya terminado, si tal cosa puede afirmarse de un árbol que está vivo, cuyas hojas nacen y cuyas ramas crecen y se mecen en aquel aire que Niggle tantas veces había imaginado y que tantas veces había intentado en vano captar.

Miró el Árbol, y lentamente levantó y extendió los brazos.

"Es un don", dijo.

[…] Todas las hojas sobre las que él había trabajado estaban allí, más como él las había intuido que como había logrado plasmarlas. Y había otras que sólo fueron brotes en su imaginación y muchas más que hubieran brotado de haber tenido tiempo. No había nada escrito en ellas; eran sólo hojas exquisitas; pero todas llevaban una fecha, nítidas como las de un calendario. Se veía que algunas de las más hermosas y características, las que mejor reflejaban el estilo de Niggle, habían sido realizadas en colaboración con el señor Parish: no hay otra forma de decirlo.

Hoja de Niggle, J.R.R. Tolkien

Agradecimientos

Agradecimientos

Me encanta leer los agradecimientos de una tesis, incluso cuando no conozco a la persona que los ha escrito. Será que, aunque nos apasionen los datos, siempre buscamos a las personas, y en estas páginas es donde mejor se ve que la ciencia la hacen personas que sufren y se alegran. Sobre todo, se ve que los pequeños y grandes logros se alcanzan con el esfuerzo de muchos, y de muchos otros que los sostienen.

'A Ana la traemos de Inglaterra como sea', le dijo Paco a mi madre cuando se acercó para solucionar unos papeles de la beca, unas palabras que mi familia años después sigue recordando con mucho cariño. Esta misma determinación y seriedad de Paco con cada pequeña cosa, es una pieza esencial de todos los proyectos de este laboratorio. Gracias Paco, por acogerme en tu grupo, por darme tanta libertad, pero también un apoyo seguro en los momentos decisivos. Gracias por tu rotundo optimismo, tan necesario en esta aventura en la que las probabilidades de éxito son tan pequeñas.

Gracias Lola, porque has sido una gran compañía durante esta tesis, desde los primeros días en la Princesa; gracias por tus buenos consejos científicos y personales; gracias, porque sin darte cuenta, con tu presencia, me empujaste a seguir aquí cuando llegué a pensar que éste no era mi sitio. Gracias Hortensia, Ali Vara, Aitana y Eva, porque me recibisteis con los brazos abiertos. Gracias Hort, porque si cualquiera tuviéramos que hacer todas tus tareas perderíamos la cabeza y en medio de todas ellas todavía sacas tiempo para atender cualquier necesidad. Gracias a Mari Ángeles, por estar pendiente de todo y sacarnos de los peores problemas. Gracias a Almudena y a Laura Grau que también nos ayudan con la gestión de tantos trámites.

Gracias a Noa y a Danay, porque me han ayudado con muchas dudas y siempre me han dado buenas sugerencias. Gracias a Eugenio que ha sido maestro y manual de referencia en muchos experimentos de esta tesis. Gracias Eugenio, Rocío, Noelia, Rafa, Javi, Norman y Álvaro, por haber abierto vuestra amistad a las nuevas incorporaciones que fuimos llegando más tarde, porque siempre es una alegría compartir cualquier rato con vosotros. Gracias Dani, porque tenerte cerca ha sido cada vez más importante, por el apoyo en los retos y por todo lo que he disfrutado nuestras conversaciones. Gracias a Irene que ha aportado muchas ideas y saber hacer a esta tesis, gracias por tu esfuerzo generoso en que las cosas sean siempre más fáciles y mejores para todos. Irene y Marta me han sacado de las peores crisis científicas y su ayuda ha sido imprescindible en los experimentos más difíciles. Gracias Marta también por tu sinceridad, y por tus

ánimos. Gracias a Cristina, por todo lo que me enseñó cuando llegué y porque con su trabajo abrió las puertas a los proyectos de esta tesis. Gracias a Olga y a María Laura, que han sido hermanas mayores de laboratorio, una presencia amable y divertida, cuánto os he echado de menos desde que os fuisteis. Gracias a Raquel por su sensibilidad y su disponibilidad, por preocuparse por todos. Gracias a Nieves por ser un ejemplo de iniciativa y asertividad, y una estupenda vecina de sitio. Gracias a Raúl por su cercanía y su dulzura. Sara, me acuerdo del primer día que viniste a conocer el laboratorio, después de hablar contigo pensé que serías una persona con la que me encantaría trabajar. Ahora sé que es verdad, me has regalado un final de tesis en la mejor compañía, y además, de la mejor ciencia: la que se hace y se piensa en equipo. Gracias también por ser tan detallista con todos. Gracias a todas las incorporaciones más recientes: Amelia, María, Diego, Marta, Silvia, que nos traen la emoción de los comienzos y ánimos renovados.

Gracias a Bea, a Raquel y a Chemari por estar siempre disponibles y aportarnos tanto. Gracias a Almudena y a Virginia de las que he podido aprender mucho estos años. Gracias Ester, por atreverte con todo con una valentía contagiosa, porque siempre es un gusto trabajar contigo. Gracias Sonia, por tu sonrisa y por ayudarnos en tantas emergencias. Gracias a todo el grupo de Almudena, de Jacob y de Pilar que hacen de la 2N un lugar mejor.

Gracias a las unidades del Cnic, que facilitan tanto nuestro trabajo diario. Gracias a Manuel por los análisis bioinformáticos, que son una parte fundamental de este proyecto, y gracias a Fátima por sus buenas orientaciones. Gracias a Emilio y al equipo de proteómica, que han sido una pieza clave de este trabajo. Gracias a Eli por estar siempre pendiente de nosotros y ser tan eficiente. Gracias a Elena, Mariano, Ligos y Raquel, que consiguen que citometría funcione tan bien.

Gracias a todo el grupo de Stepanka, que me hicieron sentir en casa durante la estancia. Gracias a Dasa, por su amistad y por ayudarme a ser mas libre. Gracias a Zuzka, por tanta entrega generosa con los proyectos de todos, por dedicarme tanto tiempo.

Y ahora, volviendo a los comienzos de esta historia… Gracias a mis profesores del colegio Casvi, una etapa que recuerdo como un tesoro. En especial gracias a José Vicente y a Inma. En sus clases me encontré con una belleza enorme, que me cambió los planes universitarios. Valoramos poco las cosas que pasan en las clases de secundaria, pero ahí descubrí el asombro de que un proceso como la fotosíntesis fuera algo que se pudiera comprender átomo a átomo. Y darme cuenta de que vivimos en un

mundo que podemos entender en sus pedacitos más pequeños, ha sido el salto de aprendizaje más grande de todos estos años de estudio e investigación.

Gracias también a los profesores de la Complutense. Gracias a Inmaculada Fernández que me abrió las primeras puertas de un laboratorio y a todos los grupos que después me dieron la oportunidad de trabajar con ellos: Pedro Reche, Eleanor Riley y Adrian V Hill. Gracias a Martin por ser una de las personas con las que más he disfrutado trabajando. Gracias a Ahmed por ser un regalo enorme en un año difícil. Gracias a Alex por su disponibilidad y su perseverancia.

Gracias a mis amigos, que han sido una parte esencial del camino hasta aquí y un apoyo fundamental. Gracias a Elena, por ser mi amiga más antigua, por lo que significan tantos años de estar cerca. Gracias a María Aguirre, por las conversaciones infinitas, nos faltan horas para todo lo que nos queda por contarnos. Gracias a Guio y a Miguel Ángel por ser tan acogedores. Gracias a Roy, por valorar tanto la amistad, por darnos tanto cariño. Gracias a Semites V, Vanesa, Nacho, N Castillo, Esther, Joaquín, Reyes y Rosi por ser luces preciosas.

Gracias María por haberme acompañado desde el primer día de universidad, y por cada día que lo sigues haciendo. Gracias Nuria por tu familiaridad y tu ternura (que ya crearon hace años a Petunia), por ser mi memoria. Gracias Ana Raso y Alicia, sigo recordando nítidamente pensar que ojalá llegáramos a ser amigas las primeras veces que os vi, y no puedo estar más agradecida de que de verdad haya pasado. Gracias a las personas maravillosas que se fueron sumando: mi feténica Eugenia, Irene, Ana, Teresa, Boris, Toni, Dani y ahora nuestra pequeña Carla. Gracias a los amigos que aún viviendo tan lejos están muy cerca: Salvo, Keith, Naya, Dion, Natasha, Gonzalo, Deanna, Olivia, John, Nikki, Imogen, Dusham y Alicja. Gracias a Christine por estar tan pendiente y cuidarme tanto.

Gracias a Elena por aparecer como un oasis en un desierto y convertirse en un alma gemela de intereses tan distintos como suelos hidráulicos y limones preservados. Gracias a Carla V y a Clara Serra que también han sido un regalo de este tiempo de tesis. Gracias a Seve, Antonio, L Quintás, Almacellas, Teo y Prades, sin los que habría perdido la paz estos años y que tanto me han descubierto del sentido de las cosas. Gracias a los amigos de Universitas, en los que he visto la mirada y la pasión que yo quiero tener.

Gracias a mis padres y a Clara. Me acuerdo de donde estaba exactamente cuando me di cuenta de que los que yo creía que habían sido éxitos de mi esfuerzo, nunca hubieran ocurrido si no me hubierais dado el mejor lugar para crecer. Gracias papá, por

ser el trampolín que me ha lanzado al mundo, aunque siempre hayas creído que tus intentos eran infructuosos. Gracias por poner en marcha ese motorcillo, que no se quiere perder ningún tren. Gracias mamá por cada vez que me has repetido que si éste y todos los otros proyectos fallaban no me ibas a seguir queriendo lo mismo, sino más. Gracias porque tres palabras tuyas levantan el peor de mis desánimos: arriba los corazones. Gracias Clara, por ser mi primera compañera en todo, por darle tanto valor a estar en casa, a jugar, a estar juntos, por ser maestra de todos. Gracias a mis abuelos, tíos y primos, que han sido siempre un abrazo para mí. Gracias a mi familia adoptiva por darme también tanto cariño.

Gracias Javi. Gracias por haberme alimentado este último año, por despertarte en mitad de la noche para que al salir del laboratorio de Brno hiciera el camino a casa hablando contigo, gracias por tu paciencia con los horarios terribles y por cada hora que me has esperado en el parking del hospital. Gracias por vivir cada uno de mis proyectos como si fueran tuyos, y porque contigo se construyen los mejores. Gracias porque, después de media vida cerca de ti, cada día me siento aún más afortunada por ser parte de este equipo.

Gracias por todos y por todo a quien sostiene mi vida a cada instante y me hace siempre hija. Gracias por el privilegio de hundir las manos, la cabeza y el corazón en tanta belleza, que tanto se me escapa. Gracias por la oportunidad de pintar un poco de este árbol, AMDG.

Resumen

Resumen

La expresión de microARNs en células T cambia ampliamente en respuesta a la activación. A las pocas horas, ocurre una bajada global en los niveles de microARNs, sobre la que destacan microARNs individuales que aumentan o disminuyen su expresión. En este trabajo, hemos seguido por secuenciación la cinética temprana de expresión de microARNs y sus modificaciones post-transcripcionales en células primarias humanas T CD4+ activadas por estimulación de receptor de células T o con IFN I. Se han identificado por su expresión diferencial un grupo de microARNs que no se habían vinculado antes con activación de células T. Los microARNs que disminuyen sus niveles presentan más uridilación en su extremo 3', confirmando observaciones previas del laboratorio realizadas en células T de ratón. Los microARNs que aumentan su expresión presentan un enriquecimiento en adenilación en su extremo 3'. En medio de un contexto adverso en el que parece probable que opere un mecanismo activo de degradación de microARNs, es posible que la adición de adenina en 3' suponga una protección que podría utilizarse para mejorar la estabilidad de microARNs en terapia.

La estimulación del receptor de células T aumenta la expresión de las exoribonucleasas Dis3L2 y Eri1 (descritas por su capacidad de degradar preferentemente sustratos uridilados) y de las enzimas transferasas de uridina TUT4 y TUT7, que podrían estar uridilando sus sustratos. Buscando otras enzimas que pudieran jugar un papel en la degradación de microARNs en células T, se identificó ISG20L2 como una exoribonucleasa (3' a 5') capaz de interaccionar preferencialmente con microARNs uridilados. ISG20L2 degrada microARNs con una eficiencia que se ve afectada por los nucleótidos que encuentra en el extremo 3'. También identificamos que los aminoácidos D267, D183 and E185 están implicados en la actividad catalítica de ISG20L2.

Estudiando los posibles sustratos de ISG20L2 en células T, por el momento, los microARNs no parecen ser la población más afectada por el silenciamiento de esta enzima, al menos en células J77 no activadas. Sin embargo, el ARN mensajero de moléculas inmunoreguladoras como AHR, NKG2D, CTLA4, CD137, TIM3, PD-L1 y CD69, se acumuló en ausencia de ISG20L2. Pese a que se ha descrito que ISG20L2 está implicada en biogénesis de ribosomas, la proliferación y supervivencia de clones J77 deficientes en esta enzima no se vieron comprometidas. Sin embargo, sí se observaron cambios en la regulación de moléculas importantes para la activación T como CD69, CD3ε, CD25, CTLA-4, PD-1 e IL2.

Summary

Summary

MiRNA repertoire of T cells undergoes extensive changes in response to activation. Beyond a global decrease in miRNA levels few hours after activation, some individual miRNAs are specifically up-regulated or down-regulated. We have assessed miRNA expression and post-transcriptional modification kinetics in human primary CD4+ T cells upon stimulation by T cell receptor (TCR) or with IFN I, using Next Generation Sequencing. Multiple miRNAs not related before with T cell activation profile have been identified as differentially expressed. Downregulated miRNAs presented higher 3' uridylation, consistently with previous studies from our laboratory in mouse cells. Adenylation was overrepresented in upregulated miRNAs. In the midst of an adverse environment, with the likely presence of active miRNA degradation mechanisms, miRNAs multiplying their levels may use 3' adenine as a protective signal. This potential strategy could open a new avenue to improve miRNA stability for therapy in T cells.

Upon TCR stimulation, exoribonucleases Dis3L2 and Eri1 (previously described for its preferential degradation of uridylated substrates) upregulated their levels; together with terminal uridylyl transferases TUT4 and TUT7, that could be labelling their substrates. In the search of other relevant exoribonucleases in T cell context, we identified through mass spectrometry ISG20L2, a previously described 3' to 5' exoribonuclease, as an enzyme with a preferential interaction for uridylated miRNAs. We show ISG20L2 degrades miRNAs, with an efficiency influenced by nucleotides present at 3' edge. In addition, we identify residues D267, D183 and E185 are involved in catalytic activity.

In our search to find ISG20L2 substrates in T cells, so far miRNAs have not been found as the most affected population, at least in J77 non-activated cells. However, mRNA levels of various immunoregulatory molecules were largely affected, with upregulation of AHR, NKG2D, CTLA4, CD137, TIM3, PD-L1 and CD69.

KO J77 clones were generated to study ISG20L2 function in T cells. IS20L2 had been described to be involved in ribosome biogenesis, but proliferation and cell survival of KO clones were not impaired. Remarkably, specific key molecules for T cell activation CD69, CD3ε, CD25, CTLA-4, PD-1 and IL2 were dysregulated.

Index

Index

List of Abbreviations

List of Abbreviations

A	alanine
ADAR	Adenosine Deaminase Acting on RNA
ADGRD1	ADhesion G protein-coupled Receptor D1
AHR	Aryl Hydrocarbon Receptor
AP-1	Activator Protein-1
APC	Antigen Presenting Cell
APOBEC	APOlipoprotein B mRNA editing Enzyme, Catalytic polypeptide-like
AQP3	AQuaPorin 3
BCG	mycobacterium bovis Bacillus Calmette–Guerin
BCL2	B-Cell Lymphoma 2
BCL2L2	BCL2-Like protein 2
BIM	BCL-2 Interacting Mediator of cell death
BLIMP-1	B Lymphocyte-Induced Maturation Protein
BSA	Bovine Serum Albumin
CD	Cluster of Differentiation
CMAC	7-amino-4 chloromethylcoumarin
COBALT	COnstraint-Based multiple ALignment Tool
CPM	Count Per Million
CRISPR	Clustered Regularly Interspace Short Palindromic Repeats
cSMAC	central SupraMolecular Activation Cluster
CTLA4	Cytotoxic T Lymphocyte-associated Antigen 4
D	aspartic
DAG	DiAcylGlycerol
DGCR8	DiGeorge síndrome Critical Region 8
Dis3L2	Dis3 Like 3'-5' exoribonuclease 2
E	glutamic
EDTA	EthyleneDiamine Tetraacetic Acid
EGR-1	Early Growth Response protein 1
EIF2	Eukaryotic Initiation Factor-2
ELISA	Enzyme-Linked ImmunoSorbent Assay
Eri1	Exoribonuclease 1
EVL	Ena-VASP-Like
FOXP3	FOrkhead boX P3
GFP	Green Fluorescence Protein
GITR	Glucocorticoid-Induced TNFR-Related
GLD-2	cytoplasmic poly(A) polymerase (cytoPAPs)
gMFI	geometric Mean Fluorescence Intensity
gp33-41	glycoprotein 33-41
GVHD	Graft Versus Host Disease
H2AX	H2A histone family member X
HCV	Hepatitis C Virus
HDAC4	Histone DeACetylase 4
hnRNPM	heterogeneous nuclear RiboNucleoProtein M
ICOS	Inducible T-cell COStimulator
IFN	InterFeroN
IKK	IκB Kinase

IL	InterLeukin
IP3	Inositol-1,4,5-triPhosphate
IPA	Ingenuity Pathway Analysis
IPTG	IsoPropyl β-d-1-ThioGalactopyranoside
IRE1α	Inositol-Requiring Enzyme 1 α
IS	Immune Synapse
ISG20L2	Interferon-Stimulated 20 kDa exonuclease-Like 2
ITAM	Immunoreceptor Tyrosine-based Activation Motifs
ITK	Interleukin-2-inducible T-cell Kinase
KO	Knock Out
LARP7	LA-Related Protein 7
LAT	Linker of Activated T cells
LFA1	Lymphocyte Function-associated Antigen 1
lncRNA	long non-coding RNA
LPS	LipoPolySaccharide
MAPK	Mitogen-Activated Protein Kinases
MCMV	Murine CytoMegaloVirus
MCP-1	Monocyte Chemoattractant Protein-1
MCPIP-1	MCP-1-Induced Protein-1
MHC	Major Histocompatibility Complex
min	minutes
miR(NA)	microRNA
MTOC	MicroTubule-Organizing Centre
mTOR	mammalian Target Of Rapamycin
ncPAP	non-canonical Poly(A) Polymerases
NF-κB	Nuclear Factor-κB
NFAT	Nuclear Factor of Activated T cells
NGS	Next Generation Sequencing
NK	Natural Killer
NTA	Non-Template Additions
OVA	OVAlbumin
PAPD	poly(A) RNA polymerase GLD2
PARN	Poly(A)-specific RiboNuclease
PBMC	Peripheral Blood Mononuclear Cells
PBS	Phosphate Buffered Saline
PD-1	Programmed Death 1
PD-L1	Programmed Death Ligand 1
PI(3,4,5)P3	PhosphatidylInositol (3,4,5)-trisPhosphate
PI(4,5)P2	PhosphatidylInositol 4,5-bisPhosphate
PI3K	PhosphatidylInositol 3-Kinase
PIP2	PhosphatidylInositol-4,5-biPhosphate
PKC	Protein Kinase C
PKD2	Polycystic Kidney Disease 2
PLCγ1	PhosphoLipase C, gamma 1
PMA	Phorbol Myristate Acetate
PP2AA	Serine/threonine-protein phosphatase 2

pre-miRNA	precursor miRNA
pri-miRNA	primary miRNA
PTEN	Phosphatase and TENsin homolog
PtM	Post-transcriptional Modifications
RISC	RNA-Induced Silencing Complex
RNAP III	RNA Polymerase III
RNAseq	RNA Next generation sequencing
RP	Ribosomal Protein
rRNA	ribosomal RNA
RSV	Respiratory Syncytial Virus
RT	Room Temperature
RT-qPCR	Reverse Transcription-quantitative Polymerase Chain Reaction
SDN	Small RNA Degrading Nuclease
SEE	*Staphylococcus aureus* Enterotoxin E
SEM	Standard Error of the Mean
SHP2	(SH2)-containing protein tyrosine Phosphatase 2
snoRNA	small nucleolar RNA
TBS	Tris Buffer Saline
TCR	T Cell Receptor
TDMD	Target RNA-Directed MiRNA Degradation
TENT	TErminal Nucleotidyl Transferase
Tfh	T follicular helper cells
TGF-β	Transforming Growth Factor-β
Th1/2	T helper
TIGIT	T-cell immunoreceptor with IG and ITIM domains
TIM3	T cell immunoglobulin and mucin domain-containing protein 3
TNF	Tumor Necrosis Factor
TNF-α	Tumor Necrosis Factor-α
TNFR	Tumor Necrosis Factor Receptor
TRAFs	TNFR-Associated-Factors
Treg	regulatory T cell
tTreg	thymic-derived regulatory T cells
TUT	Terminal Uridylyl Transferase
UTR	UnTranslated Region
VASP	VAsodilator-Stimulated Phosphoprotein
VISTA	V-domain Ig Suppressor of T cell Activation
VLA4	Very Late Antigen-4
WB	Western Blot
WT	Wild Type
ZAP70	ζ chain-Associated Protein kinase 70
α	anti

Introduction

Introduction

1. Immune system overview, a focus on T cells

The immune system is formed by a diverse network of cells and soluble factors, which have been organized in two sections: innate and adaptive. Both immune arms work in continuous collaboration in order to protect an organism against external threats. Innate and adaptive immunity are able to specifically distinguish pathogen sequences from self-structures. The innate immune system is ready to act immediately against conserved common general patterns, while the adaptive immune system is able to mount an immune response generated precisely against the particular antigen sequences of the current infection.

The first line of defence offered by the innate immune system is achieved through monocyte derived cells (dendritic cells and macrophages), granulocytes (basophils, eosinophils and neutrophils), mast cells and complement proteins. The adaptive immune system takes a longer time to mount an antigen driven response, due to the requirements of clonal selection and expansion, but in turns tailors a highly effective immunity towards a much larger diversity of antigens and is able to maintain a pool of memory cells able to act more rapidly on a re-infection. Adaptive responses rely mainly on specific antibodies generated by B lymphocytes (humoral immunity against pathogens and their toxins) and T cell responses, both helper (CD4+ T cells) and cytotoxic (CD8+ T cells). CD8+ T cells are able to recognize and eliminate infected cells and CD4+ T cells orchestrate function and recruitment of other immune cells through cytokine secretion.

T cell activation and signalling

T cell effector function is conditioned by the detection of foreign antigens on cellular surfaces, while precisely trained to tolerate self-peptides. The mechanism enabling this antigen surveillance consists on the interaction between the T cell receptor (TCR) and a cognate antigenic peptide presented on the Major Histocompatibility Complex (MHC) molecule. B lymphocytes, dendritic cells and macrophages, are professional antigen presenting cells (APCs) able to display peptides derived from internalized antigens on their MHC II molecules, which are recognized by CD4+ T cells. In contrast, CD8+ T cells recognize MHC I molecules bearing intracellular peptides, which are expressed on every nucleated cell, including APCs. This TCR-MHC interaction occurs in the context of the immune synapse, a highly specialized structure formed in the contact area between T cells and APCs (1–3).

T cell activation requires this specific TCR peptide recognition and the presence of co-stimulation. Costimulatory signals are provided by surface receptors expressed on the T lymphocytes that interact with specific ligands on APCs, and can be either activatory (such as CD28 and ICOS) or inhibitory (like CTLA-4 and PD-1). Among multiple pathways downstream of the TCR: PI3K, AKT and mTOR are crucial mediators of T cell activation. These signals are counter-balanced by negative regulators such as PTEN and BIM. These activating and inhibiting events are integrated into a net response that triggers the activation and/or repression of transcription factors (NFAT, AP-1, NF-κB, and others) essential for expression of immune effector molecules, e. g. cytokines.

The T cell receptor is a protein complex composed of several chains with a transmembrane region and intracellular and extracellular domains of various lengths, specifically it includes: a heterodimer of α/β or γ/δ chains, and CD3γ, CD3δ, CD3ζ and two CD3ε. When a specific peptide is recognized by the variable extracellular domain of the α/β or γ/δ chains, a conformational change exposes to phosphorylation intracellular domains, such as ITAMs, in ε, γ, δ and ζ chains (4,5). This interaction has been mimicked in this work using αCD3 antibodies, which were combined with αCD28 to provide co-stimulatory signals (6,7); or in J77 and Raji co-cultures, through incubation with SEE, which brings together TCR and MHC II molecules (8,9). ZAP70 binds to phosphorylated ITAMs and activates LAT, which recruits PLCγ1 (10–12). PIP_2 (phosphatidilinositol-4,5-biphophate), located at the plasma membrane, is hydrolysed by PLCγ1 into the second messengers IP_3 (inositol-1,4,5-triphosphate) and DAG (diacylglycerol). IP_3 induces calcium release from the endoplasmic reticulum; which leads to NFAT nuclear translocation, and together with DAG and other stimuli, activates NF-κB (13). DAG activates various PKCs (serine/threonine kinases), both leading to PKD2 activation (required for cytokine production) (14,15). In addition, DAG localized accumulation is one of the mechanisms promoting cytoskeleton rearrangement and centrosome polarization (16), which enables a directional secretion of vesicles and cytokines (17–19). Ca^{2+} influx can be artificially induced with a ionophore, such as ionomycin, which is used here in combination with PMA, a potent PKC activator (20).

T cell differentiation

Activation of naïve CD4+ T cells, usually occurs in lymph nodes or lymphoid associated organs, and leads to differentiation into a particular effector subset: Th1, Th2, Th9, Th17, Th22, Tfh or Treg (21). TCR and co-receptor signalling together with environmental cytokines determine the most appropriate T helper cell phenotype that the newly activated cell must acquire to better coordinate adaptive immune responses. Th1 and Th2 which were first described (22), are characterized to target intracellular and

extracellular pathogens, respectively. Later Th9, Th17 and Th22 have been also related to clearance of parasites and extracellular bacteria; Tfh to promote humoral responses and Treg to play an essential anti-inflammatory roles. Each subset is characterized by the expression of a specific transcription factor (Tbet, GATA3, PU.1, RORγt, AHR, Bcl-6 and Foxp3) and a set of characteristics cytokines.

2. T cell regulation by miRNAs

MiRNAs are small (~19-24 nucleotides) single-stranded non-coding RNA species that act as post-transcriptional modulators; they control gene expression, either by promoting mRNAs degradation or repressing their translation (23). More than 2500 human mature miRNA sequences have been already listed in MirBase (24) although the total amount of miRNAs is likely up to ten times higher (25). Friedman et al. estimated that miRNAs could modulate around 60% of protein-coding genes, indicating the relevance of these regulatory pathways in gene expression (26).

Dicer is an RNase III endonuclease that controls miRNA biogenesis. It processes precursor miRNA (pre-miRNA) into mature miRNA forms (27–29). Constitutive Dicer KO mice display embryonic lethality (30), indicating the relevance of this enzyme in development. Lineage-specific, Dicer-deficient models were therefore required to study the consequences of reduced miRNA function in a tissue-specific manner.

Dicer-deficient CD4+ T cells were hyper-responsive to TCR stimulation and produced IL-2 in the absence of co-stimulation (31). After activation, CD4+ Dicer-deficient mice showed reduced proliferation, higher levels of apoptosis and a bias towards Th1 differentiation and IFN-γ release (32). In Th1 differentiation, IFN-γ production and a decline in IL-2 secretion occurred earlier in Dicer-deficient than in wild-type CD4+ T cells (32). Th2 cells presented reduced levels of GATA3 mRNA and failed to suppress IFN-γ expression (32). Consistently, similar phenotypes were observed in T cells lacking Drosha or its RNA-binding cofactor DGCR8, which forms a complex responsible for primary miRNA transcript processing. Drosha-deficient naïve CD4+ T cells differentiated into Th1 and Th2, but expressed higher levels of IFN-γ than control cells (33). Similarly, DGCR8-deficient T lymphocytes showed reduced proliferation and an increase in IFN-γ secretion (34). A number of very comprehensive reports have addressed the role of miRNAs in T cell differentiation (35–39).

CD4-specific Dicer deficiency also affects the regulatory T cell compartment, impairing Tregs development in the thymus and reducing their numbers in peripheral

lymphoid organs (40). In addition, deficient naïve CD4+ T cells activated in the presence of TGF-β expressed significantly less FOXP3 than control cells (40). Besides, several studies have demonstrated that miRNA disruption in Treg cells leads to autoimmune diseases (33,41,42).

Dicer-deficient CD8+ T lymphocytes responded more rapidly to activation *in vitro*, as indicated by faster CD69 up-regulation and an earlier proliferative response, although their survival was reduced after two days (43). CD8+ Dicer KO cells also showed a delay in CD69 down-regulation after removal of the TCR-activating stimulus, suggesting a sustained activation of cytotoxic lymphocytes in the absence of miRNAs (43). Furthermore, CD8+ Dicer-deficient cells failed to produce an efficient *in vivo* effector response, including lower proliferation and impaired cytokine production (IFN-γ and TNF-α) (43).

In summary, these models with impaired miRNA synthesis machinery highlight the importance of miRNA as positive (booster) and/or negative (brake) regulators of T cell development and function. MiR-146a mainly acts as a “brake” miRNA, as miR-146a-deficient mice develop chronic inflammation and autoimmunity (44). CD4+ and CD8+ T cells from miR-146a deficient mice display less apoptosis and increased proliferation and expression of activation markers (CD25 and CD69) and effector cytokines (IL2, IFN-γ and IL-17A) (45). Likewise, miR-125b is another negative regulator of T cell function, contributing to the maintenance of the naïve state in human CD4+ T cells, in which it appears at high levels (46). This effect is at least partly achieved via targeting key molecules for T cell activation, e.g. BLIMP-1, IL-2Rβ, IL-10Rα and IFN-γ (46). Conversely, other miRNAs boost the immune response. For instance, miR-142-deficient mouse T cells showed reduced proliferation, deregulated cytokine expression and decreased secretion of pro-inflammatory cytokines such as IFN-γ, IL-17 and IL2 in response to activation (47,48). Other examples of enhancer miRNAs are miR-155 and miR-17~92; miR-155-depleted mice are immunodeficient (49), whereas miR-17~92-deficient T cells exhibited reduced antitumoral responses (50).

As it has been previously described, T cell responses result from the integration of a complex network of activatory and inhibitory signals. In this context, miRNA targeting of key immunoregulatory molecules boosts or dampens immune functions, to preserve homeostasis while supporting the full development of effector functions. Figure I1 aims to highlight the network behaviour involved in miRNA function: individual miRNAs interact with a set of targets and each target in turn can be regulated by several miRNAs. In addition, mRNA regulation can occur at different levels, either through miRNA directly targeting the molecule or indirectly regulating its expression via targeting its receptor and/or transcription factors. In fact, our current knowledge is limited by the difficulty of

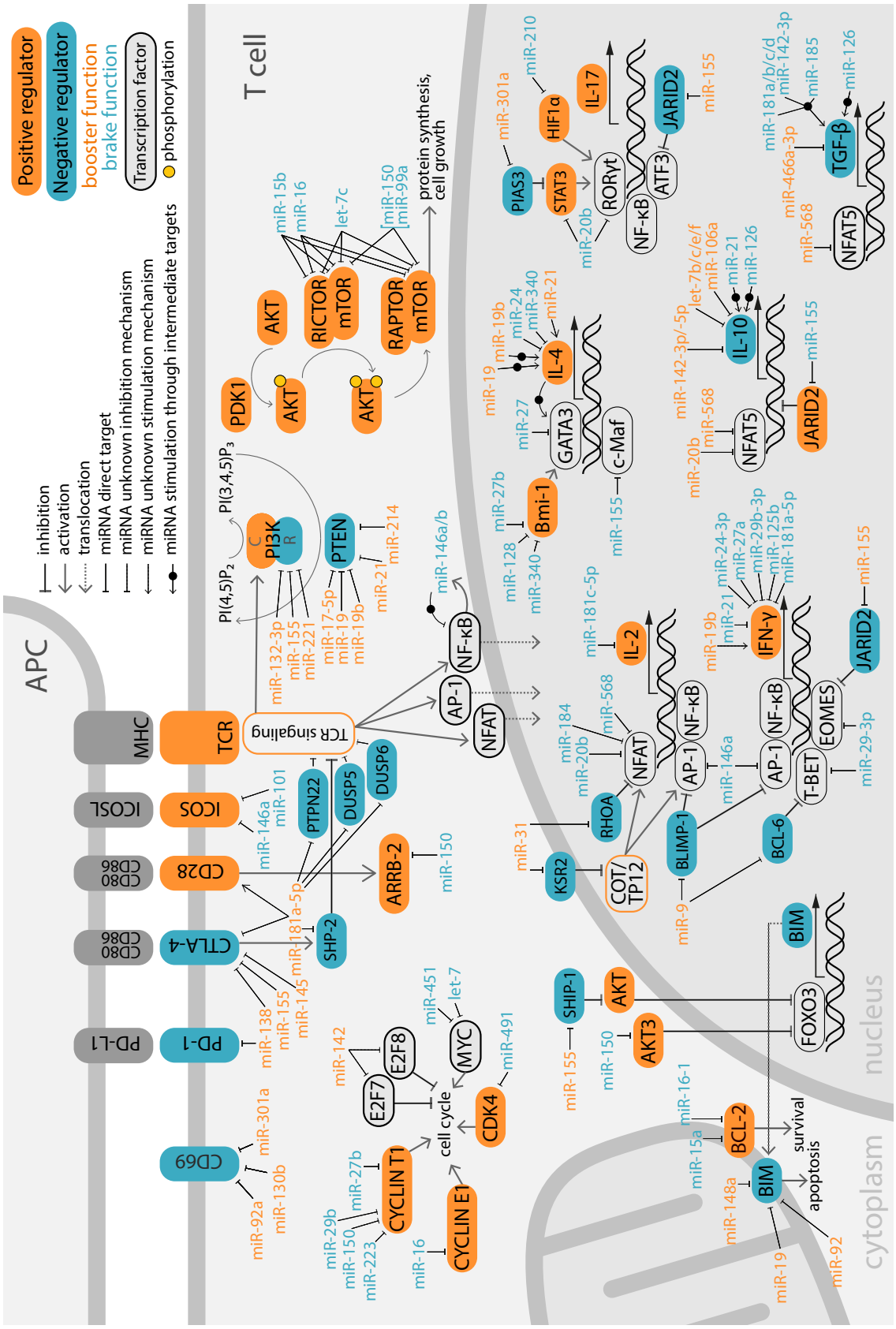
Positive regulator
Negative regulator
booster function
brake function
Transcription factor
phosphorylation
inhibition
activation
translocation
miRNA direct target
miRNA unknown inhibition mechanism
miRNA unknown stimulation mechanism
miRNA stimulation through intermediate targets
APC
T cell
cytoplasm
nucleus
MHC
TCR
ICOSL
ICOS
CD28
CD80 CD86
CTLA-4
CD80 CD86
PD-L1
PD-1
CD69
TCR singaling
PI(4,5)P2
PI(3,4,5)P3
PI3K
PTEN
PDK1
AKT
RICTOR
mTOR
RAPTOR
mTOR
protein synthesis, cell growth
PTPN22
DUSP5
DUSP6
SHP-2
ARRB-2
SHIP-1
AKT
AKT3
FOXO3
BIM
BCL-2
BIM
survival
apoptosis
CDK4
CYCLIN E1
CYCLIN T1
cell cycle
E2F7
E2F8
MYC
AP-1
NF-κB
NFAT
RHOA
COT/ TP12
KSR2
IL-2
BLIMP-1
AP-1
NF-κB
BCL-6
AP-1
NF-κB
T-BET
EOMES
IFN-γ
JARID2
Bmi-1
GATA3
c-Maf
IL-4
NFAT5
IL-10
JARID2
PIAS3
STAT3
HIF1α
RORγt
NF-κB
ATF3
JARID2
IL-17
NFAT5
TGF-β
miR-132-3p
miR-155
miR-221
miR-17-5p
miR-19
miR-19b
miR-21
miR-214
miR-146a/b
miR-15b
miR-16
let-7c
miR-150
miR-99a
miR-146a
miR-101
miR-155
miR-145
miR-181a-5p
miR-138
miR-142
miR-451
let-7
miR-491
miR-150
miR-92a
miR-130b
miR-301a
miR-29b
miR-150
miR-223
miR-27b
miR-16
miR-15a
miR-16-1
miR-148a
miR-19
miR-92
miR-155
miR-150
miR-31
miR-184
miR-20b
miR-568
miR-181c-5p
miR-128
miR-340
miR-27b
miR-9
miR-146a
miR-19b
miR-21
miR-24-3p
miR-27a
miR-29b-3p
miR-125b
miR-181a-5p
miR-155
miR-29-3p
miR-155
miR-19
miR-27
miR-19b
miR-24
miR-340
miR-21
miR-155
miR-20b
miR-568
miR-142-3p/-5p
let-7b/c/e/f
miR-106a
miR-21
miR-126
miR-301a
miR-210
miR-20b
miR-155
miR-181a/b/c/d
miR-142-3p
miR-185
miR-466a-3p
miR-568
miR-126

Figure I1. Overview of miRNA modulation on positive and negative immune-regulator molecules (previous page).
Signalling coming from TCR and costimulatory molecules is integrated by the T lymphocyte promoting cell survival, proliferation and production of effector molecules, such as cytokines. This complex network is fine-tuned by miRNAs that target key immunoregulatory molecules, supporting either T cell activation (booster) or inhibition (brake). MiRNAs exert their function by targeting the mRNA 3'UTR in the cytoplasm, although for simplicity sake some have been depicted in the nucleus, close to their targeted immunoregulators. In PI3K, C and R designated the catalytic and regulatory subunits, respectively.

considering more than one miRNA in experimental designs, which increases its technical complication, but also enable models that simulate the complexity of the physiological scenarios.

3. MiRNAs dynamics in T cell activation

Given miRNA potential to fine-tune immune responses (39,51–53), it is not surprising miRNA repertoire undergoes extensive changes upon T cell activation (54–60). This intense remodelling highlights miRNA function is constrained by a specific spatiotemporal frame related to the signals that induce T cell-based effector functions. Figure I2 summarizes miRNA species described to be either upregulated or downregulated upon T cell stimulation. Different studies have yielded data that may appear contradictory, likely due to T cell subset differences, the origin of the sample (murine or human) and the strategy and length of stimulation. Additional differences stem from the strategy used to evaluate miRNA expression, being arrays the most commonly employed technique, together with RT-qPCR and Northern Blot.

Despite variability, some trends are very consistent, including downregulation of miR-26a, miR-26b, miR-150, miR-181a, miR-223 and miR-342-3p; and upregulation of miR-155 and the miR-17~92 cluster (particularly miR-17-5p, miR-18a-5p and miR-19b). MiR-146a was downregulated in mouse T cells, but upregulated in human upon activation, while miR-31 behaved in the opposite way, suggesting the existence of species-specific regulatory mechanisms.

In addition to variations in miRNA expression, it would be essential to consider the total abundance of each miRNA in the cell. Interestingly, only 7 miRNAs accounted for around 60% of the total sequencing reads in CD8+ T cells (57).

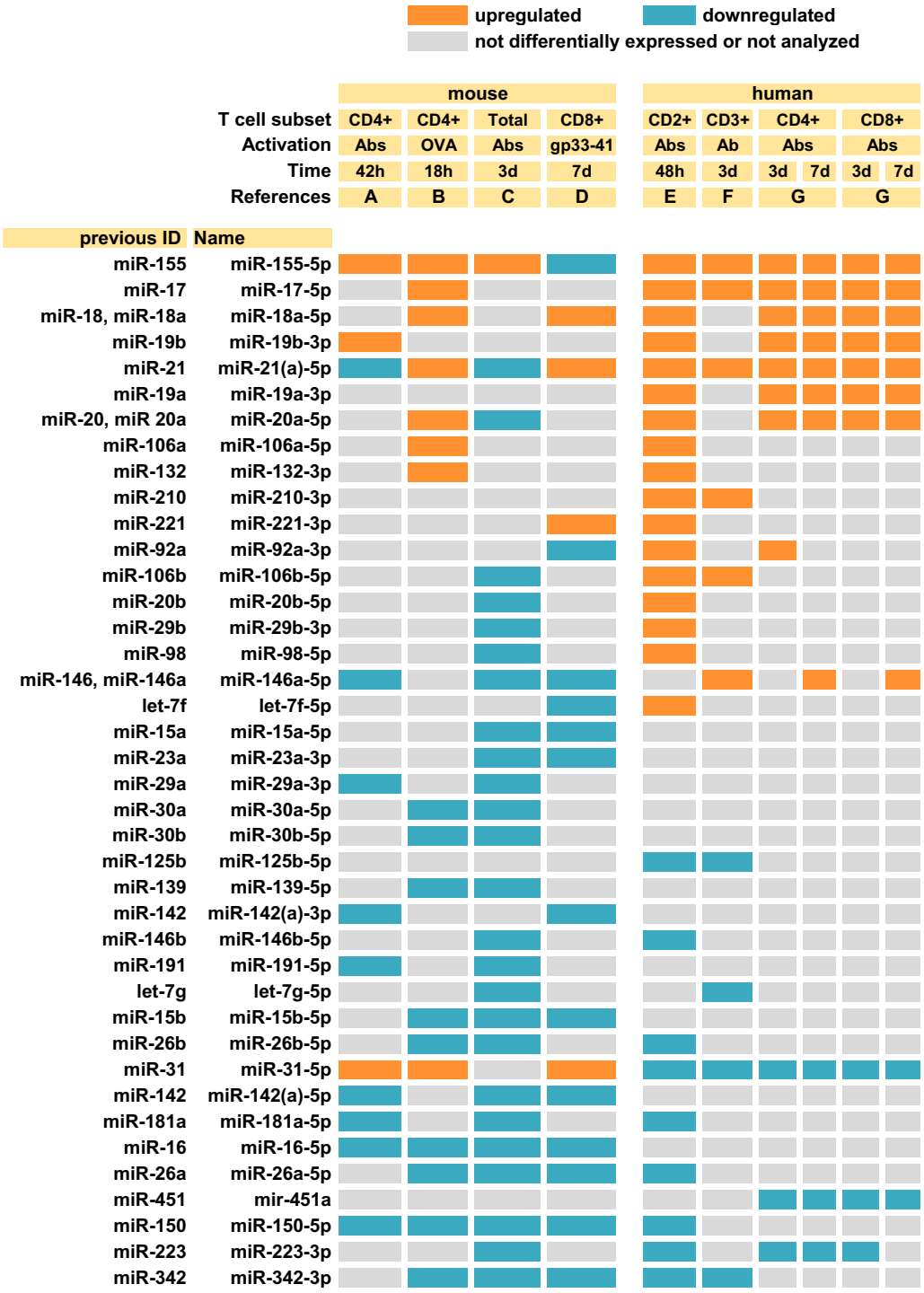

Figure I2. MiRNAs differentially expressed upon T cell stimulation.
MiRNAs described in at least two different studies are summarized. Different subsets of T cells (both mouse and human) were activated with either antibodies against CD3 alone (Ab), or together with antibody against CD28 (Abs), or with specific peptides (OVA or gp33-41). Cells were stimulated during different lengths of time ranging from 18h to 7 days. The studies included in the table are: A ((54)), B ((55)), C((56)), D((57)), E((58)), F((59)), G((60)). Whenever more than one detection method was used, only consistent data obtained with at least two techniques was selected [(57)]. Most studies evaluated miRNA expression with miRNAs arrays, some together with RT-qPCR and Northern Blot.

Beyond individual miRNA changes, it is important to highlight that miRNA levels undergo a global downregulation upon stimulation. In this regard, almost three times higher total miRNA arrays hybridization signal has been detected in mouse CD8+ naive T cells compared to activated cells (57); similarly, an independent study found a significant downregulation of the total amount of miRNA in stimulated mouse and human CD4+ T cells compared to non-stimulated controls as early as 4 h after activation (54).

4. Regulation of miRNA tunover

MiRNA levels are the result of both biogenesis and degradation processes. RNA Pol II transcribes primary miRNA (pri-miRNAs) under de control of RNA Pol II-associated transcription factors, enhancers and epigenetic regulators (61–63). Two RNase III enzymes, Drosha and Dicer, are responsible for miRNA biogenesis with their sequential processing of pri-miRNAs. First, the microprocessor complex (Drosha/DGCR8) generates a hairpin precursor miRNA (pre-miRNA, 70-100nt) in the nucleous which is exported to the cytosol. Second, Dicer cleaves the pre-miRNA into a double-stranded miRNA duplex (18-22nt). These steps are tightly regulated by RNA-binding proteins which bind to miRNA precursos and regulate Drosha and Dicer activity (64). A minority of miRNA follow non-canonical biogenesis pathways independent of Drosha or Dicer processing, such as miRNAs generated from snoRNAs or mirtrons generated via pre-mRNA splicing (64). Upon loading onto Argonaute protein, where only one strand is retained (mature miRNA), miRNAs are stabilized (65), presenting half-lives ranging from hours to days. In fact, downregulation of Argonaute proteins during T cell activation has been suggested to be responsible for the global miRNA downregulation previously mentioned (54). MiRNA bound to Argonaute are the core component of the miRNA-induced silencing complex (miRISC), where miRNA interact with 3'-UTRs of target mRNAs and exert their effector function (66,67).

MiRNA degradation, critical to achieve a dynamic repertoire, is not as well understood as miRNA biogenesis. A series of endonucleases have been described to already degrade pre-miRNAs, preventing Dicer processing and terminating miRNA biogenesis: IRE1α, MCPIP-1 (Regnase-1) and PMR1. During endoplasmic reticulum stress, IRE1α degrades pre-miRNA involved in repression of *Caspase-2* mRNA (68). Regnase-1 downregulates a broad range of pre-miRNAs (69). PMR1 promotes breast cancer cell motility by cleaving miR-200 family (preferentially between UG dinucleotides) (70).

Certain 'global' mature miRNA degradation mechanisms have been suggested, such as TDMD (target RNA-directed miRNA degradation). In TDMD, miRNAs bound to

Argonaute with high complementarity to their target mRNAs, are tailed at 3' and trimmed (71–75). In NK cells and CD4+ T cells, Eri1 exonuclease has been described to reduce miRNA levels (76). Other ribonucleases have been described in a variety of organisms with a selective specificity: SDNs degrade miRNAs containing a 3'-OH group in *Arabidopsis thaliana* (77); Xrn-1 and Xrn-2 degrade 5'-monophosphate miRNAs in *Caenorhabditis elegans* (78,79); RRP41 (a core component of the exosome complex) and XRN1 degrade miR-382 in HEK293T cells (80); PNPT1 （$PNPase^{old-35}$) degrades miRNA-221 in melanoma cells (81); and the endonuclease TSN cleaves miRNA with CA or UA dinucleotides, promoting cell cycle progression (G_1 to S phase transition) in human cells (82). Other ribonucleases have been described to be guided by post-transcriptional modifications such as PARN or Dis3L2, and are discussed in the following section.

5. MiRNAs post-transcriptional modifications

Next Generation Sequencing (NGS) has identified not only nucleotide additions to the expected genomic miRNA sequences, but also trimmings and substitutions (83,84). Post-transcriptional Modifications (PtMs) generate multiple variants of the same miRNA (isomiRs) that differ in their 5', 3' or internal modifications. PtMs modulate biogenesis, stability and function (67,85,86). Several mechanisms elicit PtMs on the canonical miRNA sequence including: alternative processing by Drosha or Dicer, RNA editing and non-template nucleotide addition.

During sequential cleavage in miRNA biogenesis, Drosha (pri-miRNA => pre-miRNA) and Dicer (pre-miRNA => miRNA duplex) excisions are slightly flexible, becoming a source of 5' and 3' isomiRs (87–93).

Other forms of PtMs derive from RNA editing which include conversion of adenosine (A) to inosine (I) by ADARs (adenosine deaminases acting on RNA) (94–97); or deamination of cytidine (C) to uridine (U) by APOBECs (apolipoprotein B mRNA editing enzyme, catalytic polypeptide-like) (98,99). Since I is a guanosine (G) analog, A-to-I editing is equivalent to an A-to-G mutation. For miRNAs, A-to-I editing is well-characterized (100,101), whereas the physiological relevance of C-to-U modification is currently unknown.

Additional enzymes responsible for miRNA PtMs are TErminal Nucleotidyl Transferases (TENTs). TENTs catalyse non-template additions (NTAs) of nucleotides mainly at the 3' end ('tailing') (102). TENTs are often flexible substrate-wise, but those with a preference towards adding adenosine are known as non-canonical poly(A) polymerases (ncPAPs). Other TENTs prefer to add uridine, namely terminal uridyl

transferases (TUTases). Uridylation and adenylation are the most typical 3' end modifications across animal miRNAs (103–107). Multiple studies have explored these modifications and their consequences in detail. Conclusions often appear contradictory, which likely result from the specific biological context, including different species, cell type or cellular compartment. For instance, GLD-2 (PAPD4/TENT2) 3' monoadenylation seems to stabilize specific miRNA populations in human fibroblasts (108) and miR-122 in the liver (109). In mouse early embryos, 3' mono- and oligoadenylation appears to protect certain miRNAs in a context of large degradation (110). However, PAPD5 (TENT4B/GLD4/TUT3) adenylates miR-21-5p on 3', promoting its degradation by PARN (Poly(A)-specific ribonuclease) (111). In human monocytes, knocking down PAPD4 showed no overall effect of 3' adenylation on miRNA stability, but adenylation instead altered miRNA effectiveness through reduction of their incorporation into the RNA-induced silencing complex (RISC, the complex where miRNAs induce mRNA degradation or inhibit their translation) (105). Uridylation also promotes diverse outcomes on miRNA. Pre-let-7 miRNA can be uridylated at its 3' by TUT4 (ZCCHC11) or TUT7 (ZCCHC6) (112,113). Lin28 (an RNA-binding protein) binds to pre-let-7 and favours oligouridylation (10-20 uridines), which inhibits subsequent Dicer processing and serves as a signal for Dis3L2 degradation (112–116). In the absence of Lin28, pre-let-7 undergoes monouridylation to pursue its maturation process (117). Let-7 promotes cell differentiation, and the regulatory mechanism triggered by Lin28 expression maintains pluripotency in stem cells (112,118). Non-templated uridine addition also occurs on mature miRNA, such as miR-26, which has been described to undergo 3'-uridylation by ZCCHC11 (TUT4) (119). MiR-26a and miR-26b uridylation has been shown to reduce their ability to repress IL-6 (119). Beyond pre-let-7, Dis3L2 has been also described to degrade Ago-bound mature miRNAs after TUT oligourydilation (120).

6. An unknown T cell ribonuclease?

Global miRNA decay occurring in T cells only few hours after stimulation (54,57) and a specific downregulation of uridylated miRNAs in activated mouse CD4+ T cells (121), seem to point to the existence of an active degradation mechanism that would act preferentially on miRNAs bearing 3' uridines. Dis3L2 and Eri1 could be responsible for this intense and rapid miRNA degradation. Dis3L2 ability to degrade uridylated miRNAs has just been discussed, and Eri1 is another 3' to 5' exonuclease which degrades oligouridylated histone mRNAs (122) and reduces miRNA levels in CD4+ T cells and NK

cells (76). These enzymes and other undescribed ribonucleases could be behind T cell activation miRNA decay.

Objectives

Objectives

Part I

-Study early changes occurring at the level of miRNA expression and post-transcriptional modifications in human primary CD4+ T cell activation.

-Identify potential enzymes degrading uridylated miRNAs in activated T cells.

Part II

This second stage was proposed after identifying ISG20L2, a previously described 3' to 5' exoribonuclease, as a candidate for uridylated miRNA degradation in T cells:

-Evaluate ISG20L2 activity as a miRNA degrading enzyme.

-Design a CRISPR-Cas9 strategy to silence ISG20L2.

-Identify ISG20L2 substrates.

-Study ISG20L2 expression upon T cell activation.

-Analyse ISG20L2 function in T cells.

Materials and Methods

Materials and Methods

1. Reagents and antibodies

Details of reagents are indicated in the corresponding sections. Antibodies used in this thesis work are gathered in Table M1. Plasmids pEGFP-C1-ISG20L2 and pGEX-ET-1-ISG20L2 (GST) were a kind gift from Jean-Jacques Diaz (Cancer Research Center of Lyon, France).

Antibody	Host species	Manufacturer	Catalog number	Application
αTubulin- FITC	Mouse	Sigma-Aldrich	F2168	if
CD19 PerCP-Cy5.5	Mouse	Tonbo Biosciences	65-0199-T100	cyt
CD25 PECy7	Mouse	Biolegend	302612	cyt
CD3(OKT3)	Mouse	Biolegend	317302	if
CD69 V450	Mouse	BD Biosciences	560740	cyt
Cleaved Caspase-3 AF647	Rabbit	Cell Singaling	9602S	cyt
Dis3L2	Rabbit	Nobus biologicals	NBP1-84740	wb
Eri1/THEX1	Rabbit	Cell Signaling	4049	wb
ERMs 90/3	Rabbit	+	+	wb
GFP	Mouse	Takara Bio	632381	wb
ISG20L2	Rabbit	Proteintech	24639-1-AP	wb
Ki67 PECy7	Rat	Biolegend	652426	cyt
p150 (glued)	Mouse	BD Pharmingen	610474	wb
TUT4/ZCCHC11	Goat	Pro Sci incorporated	46-610	wb
TUT7/ZCCHC6	Rabbit	Proteintech	25196-1-AP	wb
anti-goat HRP	Rabbit	ThermoFisher Scientific	31402	wb
anti-rabbit HRP	Goat	ThermoFisher Scientific	31460	wb

Table M1. Antibodies used in this thesis.
In the application column: wb (western blot), if (immunofluorescence), cyt (flow cytometry). (+) kindly provided by Heinz Furthmayr, Stanford University, CA

2. Cell culture

Human primary CD4+ T cell isolation and activation

Human peripheral blood mononuclear cells (PBMCs) were isolated from buffy coats, obtained from healthy donors, by separation on Biocoll Separating Solution (Biochrom, L6115) according to standard procedures. Non-adherent cells were separated from PBMCs after a 30 min adherence step at 37 °C. CD4+ T cells were purified from non-adherent cells using Human Resting CD4+ T cell Isolation Kit (STEMCELL Technologies, 17962). A specific reagent to isolate resting T cells was selected to avoid the presence of pre-activated CD4+ T cells in sequencing samples. In experiments performed to evaluate protein expression, CD4+ T cells were isolated with EasySep Human CD4+ T Cell Isolation Kit (STEMCELL Technologies, 17952).

For T cell stimulation, we treated CD4+ T cells with either αCD3αCD28 (ImmunoCult™ Human CD3/CD28 T Cell Activator; STEMCELL Technologies, 10971) or IFN I (1:1000, Human IFN Alpha Hybrid (Universal Type I IFN); PBL ASSAY SCIENCE, 11200-1). Cells were cultured in RPMI 1640 (Gibco), supplemented with 10% fetal bovine serum (FBS, Sigma), 20mM Hepes (Hyclone), 0.3mg/mL L-glutamine (Hyclone), 100 U/mL penicillin (Gibco) and 100 μg/mL streptomycin (Gibco).

These studies were performed according to the principles of the Declaration of Helsinki and approved by the local Ethics Committee for Basic Research at the Hospital La Princesa (Madrid), informed consent was obtained from all human volunteers.

Human lymphoid cell lines culture and activation

Jurkat-derived T cell line J77 E6.1 (Vαl.2 Vβ8+ TCR) and lymphoblastoid B cell line Raji, were obtained from ATCC. These human cell lines were cultured in the same media used for primary cells and routinely tested for potential mycoplasm contamination.

J77 cells were activated (in the RPMI supplemented media used for primary cells, but containing only 5% FBS) either with PMA (phorbol 12-myristate 13-acetate, 5ng/mL; Sigma-Aldrich, p-8139) and ionomycin (250ng/mL; Sigma-Aldrich, I0634), or with Raji cells and SEE. In this second approach, Raji cells were incubated with SEE (0.5 μg/mL; Toxin Technologies, PE404), for 30 min at 37ºC. SEE pulsed cells were washed and cultured with T cells. For flow cytometry assays 150 000 cells J77 and 150 000 Raji cells were plated in P96 wells; and for RNA isolation $1.2 \cdot 10^6$ J77 and 120 000 Raji, in P48 wells. Plates were centrifuged at low speed to favour earlier proximity between cells and incubated at 37ºC. Co-cultures without SEE were prepared in parallel to use as controls.

3. RNA isolation, library preparation and NGS

smallRNAseq in human primary CD4+ T cells

Three independent experiments were performed with resting CD4+ T cells isolated from different healthy donors. Samples were collected at 0h and after αCD3αCD28 or IFN I stimulation during 3h, 6h and 24h. The 21 samples were lysed in QIAzol Lysis Reagent (Qiagen, 79306) and RNA was extracted using the miRNeasy Mini Kit (Qiagen, 217004). In order to reduce phenol-based reagent contaminations, purified RNA samples were precipitated using sodium acetate (3M, 0.1x sample volume) and ethanol (100%,3x sample volume). RNA integrity was evaluated using an Agilent 2100 Bioanalyzer (Eukaryote Total RNA Nano assay).

A total of 200 ng of total RNA were used to generate barcoded miRNA-seq libraries using the NEBNext Multiplex SmallRNA Library Prep Set for Illumina (New England Biolabs). Briefly, 3´ and 5´ SR adapters were first ligated to the RNA sample. Next, reverse transcription followed by PCR amplification was used to enrich cDNA fragments with adapters at both ends. The quantity and quality of the miRNA libraries were determined using the Agilent 2100 Bioanalyzer High Sensitivity DNA chip.

Libraries were sequenced on a HiSeq2500 (Illumina) to generate 60 bases single reads. FastQ files for each sample were obtained using bcltofastQ 2.20 Software software (Illumina). NGS experiments were performed in the Genomics Unit of the CNIC.

smallRNAseq in J77 cells (control and ISG20L2 knockdown)

RNA was isolated, as described for primary cells, from GFP+ cells 72h after electroporation with pSpCas9(BB)-2A-GFP (control cells), or pSpCas9(BB)-2A-GFP-sgRNA_target1 and pSpCas9(BB)-2A-GFP-sgRNA_target6 (knockdown cells). Three independent experiments were performed and isolated RNA was used both for smallRNAseq and mRNAseq detailed in the next paragraph. The same smallRNAseq protocol detailed for primary cells was followed with two exceptions. Here, 100 ng of total RNA were used for library generation. In addition, RNA sample was not limited to the miRNA size (cutting a gel band) in order to include also other small RNAs.

mRNAseq in J77 cells (control and ISG20L2 knockdown)

Total RNA (100 ng) was used to generate barcoded RNA-seq libraries using the NEBNext Ultra II Directional RNA Library preparation kit (New England Biolabs) according to manufacturer's instructions. First, poly A+ RNA was purified using poly-T oligo-attached magnetic beads followed by fragmentation and first and second cDNA strand synthesis. Next, cDNA ends were repaired and adenylated. The NEBNext adaptor

was then ligated followed by second strand removal, uracile excision from the adaptor and PCR amplification. The size of the libraries was checked using the Agilent 2100 Bioanalyzer and the concentration was determined using the Qubit® fluorometer (ThermoFisher).

Libraries were sequenced on a HiSeq2500 (Illumina) to generate 60 bases single reads. FastQ files for each sample were obtained using CASAVA v1.8 software (Illumina).

4. RNA-Seq data analysis

smallRNAseq in human primary CD4+ T cells

Sequencing reads were pre-processed by means of a pipeline that used FastQC (http://www.bioinformatics.babraham.ac.uk/projects/fastqc/) to assess read quality; and Cutadapt (123) to trim sequencing reads, eliminating Illumina adaptor remains, and to discard those that were shorter than 15 nt or longer than 35 nt after trimming. Around 80% of the reads from any of the samples were retained. Resulting reads were aligned against a collection of 2657 human, mature miRNA sequences extracted from miRBase (release 22), to obtain expression estimates with RSEM (124). Percentages of reads participating in at least one reported alignment were around 40%. Expected expression counts were then processed with an analysis pipeline that used Bioconductor package Limma (125) for normalization (using TMM method) and differential expression testing, taking into account that samples had been obtained in three batches, and considering only 626 miRNA species for which expression was at least 1 count per million (CPM) in 3 samples. Changes in gene expression were considered significant if associated to Benjamini-Hochberg adjusted p-value < 0.1. Clustering of expression profiles and production of heatmaps were performed with Genesis (126). Epi-transcriptomic modifications were detected with Chimira (127), an online tool that, after alignment of miRNA-Seq reads against miRBAse records, identifies mismatched positions to classify them and to quantify multiple types of 3'-modifications (uridylation, for example), as well as 5'-modifications and internal modifications or variations. Count tables produced by Chimira were further processed with ad-hoc produced R-scripts to normalize modification counts by library size and to calculate summary statistics across groups of replicate samples. Analyses were restricted to the collection of 626 miRNA species with detectable expression.

Two core analysis were performed by Ingenuity Pathway Analysis (Content version: 49932394 (Release Date: 2019-11-14), one with all miRNAs differentially expressed at

least one time point of stimulation with αCD3αCD28 and a second one with the corresponding IFN-I regulated miRNAs. MiRNA-target networks were buildt with miRNet loading the highest upregulated and downregulated miRNAs for each treatment (128). Ven diagrams were elaborated with Venny:
(https://bioinfogp.cnb.csic.es/tools/venny/index.html).

smallRNAseq in J77 T cells (control vs ISG20L2 KD)

Bioinformatic analysis was performed as just described for primary cells, but without imposing a maximum read length of 35nt with the purpose of including other small RNAs apart from miRNAs. Percentages of reads participating in at least one reported alignment were around 47%. sRNAtoolbox (https://arn.ugr.es/srnatoolbox/) was used to quantify the abundance of the different types of small RNA detected.

mRNAseq in J77 T cells (control vs ISG20L2 KD)

Data analysis was performed as described for primary cells, with these variations:
-After trimming, discarded sequences are those shorter than 30nt.
-Reads were mapped against reference transcriptome GRCh38.91. Percentages of reads participating in at least one reported alignment were around 84%.

5. Data and code availability for miRNAs PtMs

GEO submission

All raw and processed sequencing data generated in this study have been submitted to the NCBI Gene Expression Omnibus (GEO; www.ncbi.nlm.nih.gov/geo/) under accession number GSE156287.

UCSC genome browser sessions

Alignments are accessible at the following UCSC Genome Browser session:

* https://genome.ucsc.edu/s/mjgommo/CD4T_IFN_I
* https://genome.ucsc.edu/s/mjgommo/CD4T_aCD3aCD28

Each session has been configured to allow the visualization of 13 custom tracks, which consist in:
- miRBase_mature track: representing the coordinates of all mature miRNAs described in miRBase, release 22.

-12 BAM alignment tracks, corresponding to three replicate samples for the control condition (0h) and each of the time points (3h, 6h, 24h) for IFN I or αCD3αCD28 treatment.

MiRNA detection and quantification has been performed in this study by aligning NGS processed reads against a transcriptomic reference consisting in all mature miRNA sequences described in miRBAse, release 22, for Homo sapiens. To produce genomic alignments that were fully congruent with those generated for quantification, BAM alignments displayed in the UCSC tracks have been generated with RSEM using a genomic reference constructed with the mature miRNA coordinates described in miRBase, release 22, exclusively. For this reason, coverage is expected only on the intervals corresponding to regions that code for mature miRNAs. MIMAT IDs are used to identify such intervals because they are guaranteed to be unique (locus specific). Visualization of the tracks may require reloading the page, because of timeout issues.

In-house scripts

Chimira results describing miRNA modifications consist in a separate table for each sample. A specialized, in-house R script (CHIMProcessor.R) was developed to process the collection of output files, as well as several other auxiliary files, in order to normalize modification frequencies by library size, merge frequency information from replicate samples, filter data using various parameters and generate combined tables and preliminary plots. The script is available from GitHub, at:

* https://github.com/mjgommo/CD4T_miRNA_MOD

6. Immunoblotting

Cells extracts were prepared in lysis buffer (50mM Tris pH 7.5, 150mM NaCl, 1%NP-40, 5mM EDTA, 50mM NaF, 5mM DTT) supplemented with a protease inhibitor cocktail (Complete, Roche). Cell lysates were cleared of debris and nuclei by centrifugation (15000g, 15 min), mixed with Laemli solution and β-mercaptoethanol (2% final volume) and boiled 5 min at 90ºC. Proteins were separated on 8-10% SDS-PAGE gels and transferred to a nitrocellulose membrane. Membranes were incubated with primary specific antibodies and peroxidase conjugated secondary antibodies. Chemoluminescence was measured with LAS-3000 (Fujifilm). Band intensities were quantified with Image Studio Lite (LI-COR Biosciences), normalized to ERMs values and relativized to unstimulated conditions (when no band was detected at 0 h, background was taken as reference signal).

7. Cell electroporation

Prior to transfection cells were washed first with PBS, and afterwards with Opti-MEN (Gibco). Cells were then resuspended in Opti-MEN at $30 \cdot 10^6$ cells/mL and 400μL ($12 \cdot 10^6$ cells/mL) were added to each 4mm Bio-Rad cuvette together with corresponding plasmids (a total of 10μg of DNA). Cells were electroporated with a Gene Pulser Xcell Electroporation System (Bio-Rad) at 240mV and 975μF. After electroporation cells were cultured in media containing 5% FBS (instead of 10% FBS used for cell maintenance). Death cells were discarded using Biocoll Separating Solution (Biochrom, L6115). GFP+ cells were sorted either as a pool or individually to a P96-well plate for clone isolation. For miRNA pull-down experiments cells were lysed without prior sorting.

8. MiRNA pull down

Streptavidin dynabeads (Dynabeads MyOne Streptavidin C1; Invitrogen, 65001) were loaded with biotinylated miRNAs according to manufacturer instructions. Per condition, $12\text{-}20 \cdot 10^6$ J77 cells were lysed in 1mL of buffer*[1]; and after nuclei and debris clearance, incubated overnight with beads (50μL). UV-Crosslink (400x100mJ; Stratalinker UV crosslinker, Stratagene) was performed and beads were extensively washed*[2] (6-7 times). Finally, beads were prepared in 20μL of washing buffer for mass spectrometry or boiled in Laemli for western blot analysis. For ISG20L2-GFP pull-down validation, lysed J77 cells had been previously electroporated with pEGFP-C1-ISG20L2.

*[1] Lysis buffer: PBS, NP40 1%, NaCl 150mM, EDTA 5mM, NaF 50mM, DTT 5mM, Complete (Roche Diagnostics, 11836145001) and PhosSTOP (Roche, 4906837001).

*[2] Washing buffer: PBS, NP40 0.05%, NaCl 150mM, EDTA 5mM, NaF 50mM, DTT 5mM and Complete.

9. Mass spectrometry analysis

Protein digestion

Proteins were subjected to in-gel tryptic digestion as described previously (129).

Mass spectrometry

The resulting peptides were analysed by liquid chromatography coupled to tandem mass spectrometry (LC-MS/MS) on an Easy nLC-1200 nano-HPLC apparatus (Thermo

Scientific, San Jose, CA, USA) coupled to a hybrid quadrupole-orbitrap mass spectrometer (Q Exactive HF, Thermo Scientific). The dried peptides were taken up in 0.1% (v/v) formic acid and then loaded onto a PepMap100 C18 LC pre-column (75µm I.D., 2cm, Thermo Scientific) and eluted on line onto an analytical NanoViper PepMap 100 C18 LC column (75µm I.D., 50cm, Thermo Scientific) with a continuous gradient consisting of 8-30% B in 90 min (B = 80% ACN, 0.1% formic acid) at 200 nL/min. Peptides were ionized using a Picotip emitter nanospray needle (New Objective). Each MS run consisted of enhanced FT-resolution spectra (120 000 resolution) in the 400–1200 m/z range followed by data-dependent MS/MS spectra of the 20 most intense parent ions acquired along the chromatographic run. The AGC target value in the Orbitrap for the survey scan was set to 1 000 000. Fragmentation in the linear ion trap was performed at 30% normalized collision energy with a target value of 10 000 ions. The full target was set to 30 000, with 1 microscan and 50 ms injection time, and the dynamic exclusion was set to 0.5 min.

Peptide identification

For peptide identification the MS/MS spectra were searched with the Sequest algorithm implemented in Proteome Discoverer 1.4 (Thermo Scientific). Database searching against human protein sequences from the UniProt database (March 2017, 158 382 entries) was performed with the following parameters: trypsin digestion with 2 maximum missed cleavage sites; precursor and fragment mass tolerances of 800 ppm and 0.02 Da, respectively; Cys carbamidomethylation as static modifications; and Met oxidation as a dynamic modification. The results were analysed using the probability ratio method (130) and a false discovery rate (FDR) for peptide identification was calculated based on the search results against a decoy database using the refined method (131).

10. MiRNA degradation assays

Catalytic mutants and protein expression

Mutants were obtained using QuickChange II Site-Directed mutagenesis Kit (Agilent) on ISG20L2-GST (pGEX-4T-1) with the following primers (introduced mutations are depicted bold and grey):

NAF: D267 (GAC) => A267 (G**C**C)

Forward:

5’-CTCACAGGGAAGATAGTGGTGGGGCATGCCATCCACAACG**C**CTTCAAAGCC-3’

Reverse:
5'-GGTGAGGGACTTGGGGTGAAAGTACTGAAGGGCTTTGAAGGCGTTGTGGAT-3'
IACAM: D183 (GAC) => A183 (G**C**C), E185 (GAG) => A185 (GCG)
Forward:
5'-GCATCCCAGAAGTTGCCACGGAAGATGGTGGCAATTGCCTGTGCGATGGTG-3'
Reverse:
5'-GGAACTAACATGCCCCTTTGGTCCTGTGCCCACCATCGCACAGGCAATTGC-3'

ISG20L2-GST (pGEX-4T-1) mutants (NAF and IACAM) were expressed in *E.coli* RIPL strain with 0.2mM IPTG induction and overnight incubation at 16ºC. ISG20L2-GST (pGEX-4T-1) WT was expressed in p-Lys strain with 0.2mM IPTG induction and 30 min incubation at 30ºC (to avoid degradation at larger culture times). Bacteria were lysed through sonication in buffer containing Tris HCl 50mM pH 7.5, NP40 0.1% KCl 100mM, β-mercaptoethanol 1mM, Glicerol 5% and protease inhibitor. Proteins were affinity purified with Glutathione Sepharose beads (GE Healthcare) and concentrated (Protein Concentrator 30000 MWCO PES, Thermo Scientific Pierce).

RNA degradation assays

RNA degradation assays were performed incubating the purified proteins with radioactively labelled (5′ end-^{32}P) substrates, at 37ºC. RNAs used were: miRNA-151, miRNA-151-AA, miR-151-UU, miR-151-CC, U30 and A30. Degradation assays were performed in TrisHCl 10mM pH 7.6, KCl 50mM, $MgCl_2$ 5mM, DTT 10mM, 0.8 units/μL RNAsin (Promega; used to prevent unintentional degradation by potential contaminants: RNAse A, B and C) and BSA 0.01%. Reaction was developed in 10μL and stopped with formamide buffer (formamide 80%, bromophenol blue 0.1%, xylene cyanol 0.1% and EDTA 5mM). Samples were resolved on 20% poly-acrylamide denaturing gels containing urea 8M. Radioactively labelled RNA was detected with a phosphorimaging screen in a FLA-9000 phosphorimager (FujiFilm).

11. Generating CRISPR-Cas9 ISG20L2 KO clones

CRISPR-Cas9 plasmids including sgRNA targeting human ISG20L2 were obtained following the protocol described by Ran et al. (132). Plasmid pSpCas9(BB)-2A-GFP (PX458) (available from AddGene) was modified to incorporate specific sgRNA (single guide RNA). Target sequences were selected using CHOPCHOP (133,134) (http://chopchop.cbu.uib.no). For each target sequence, a pair of oligos was designed

including an overlapping region with the plasmid, followed by G (if the target sequence does not present a G on 5') to facilitate transcription (Table M2). Oligos were phosphorylated (T4 Polynucleotide Kinase; Thermo Scientific, EK0031) and annealed, and plasmid digested (FastDigest *Bbs*I; Fermentas/Thermo Scientific, FD1014); prior to the ligation reaction (T4 DNA ligase; Promega, M1801). Finally, plasmids purified from DH5α transformed with the ligation product and cultured under ampicillin selection, were sequenced to confirm the specific sgRNA incorporation.

Target sequence	PAM	Plasmid overlapping nucleotides
Target 1		Fwd: CACCGTTGTGGACTACCGAACCAGG
TTGTGGACTACCGAACCAGGTGG		Rev: AAACCCTGGTTCGGTAGTCCACAAC
Target 6		Fwd: CACCGGGAGCTCTTCTTCTGAGAG
GGGAGCTCTTCTTCTGAGAGCGG		Rev: AAACCTCTCAGAAGAAGAGCTCCC
Target 8		Fwd: CACCGAGAAGCGGAGGCTCTTAGAA
AGAAGCGGAGGCTCTTAGAACGG		Rev: AAACTTCTAAGAGCCTCCGCTTCTC

Table M2. Oligos used to generate CRISPR-Cas9 plasmids with specific sgRNA. G was added in 5', when target sequence did not start with G in 5', to favour RNA Pol III transcription. Fwd: forward, Rev: reverse

J77 cells were transfected with a combination of two plasmids with sgRNA directed towards two different targets (1+6 or 6+8). One GFP+ cell was sorted to each well (96-well plate), containing pre-conditioned media. This media was obtained from a J77 cell culture after centrifuging at high speed, and filtering the supernatant with a 0.22µm strainer. For genotyping forward and reverse primers were designed to amplify by PCR a region (856nt) including all targets (1,6 and 8):

Forward (ISG20L2 genomic): CCTCTTTTCATCCATAAGCCAC

Reverse (ISG20L2 genomic): TAGACCTCTCTCCATCCACCTC

Knock out clones were identified for removal of fragments 1-6 (274nt) or 6-8 (302nt), leading to an amplification of a smaller region (582 and 554, respectively). Genomic DNA was isolated with Gentra Puregene cell kit (Qiagen, 158745-K). PCR was performed with REDExtract-N-Amp PCR Reaction mix (Sigma-Aldrich, R4775), and resolved in 3% agarose (Agarose D1 Low EEO, Covalab) gels stained with ethidium bromide (Sigma-Aldrich, E-1510).

12. qPCR (quantitative real-time PCR)

For RNA extraction, 100μL of chloroform (Sigma-Aldrich, C2432) were added to 500μL of QIAzol (Qiagen, 79306) lysed sample, and the mix was shaken vigorously. After 12000g centrifugation for 15 min at 4ºC, aqueous phase (which contains RNA, while DNA is retained at interphase and proteins at the pink bottom phase) was transferred to a new tube. RNA was precipitated by addition of 250μL of isopropanol and overnight incubation at -20ºC. Samples were centrifuged at 12000g for 10-30 min and supernatants discarded. Pellet were washed with ethanol 75%, centrifuged 7500g (5 min, 4ºC) and resuspended in RNAse free H_2O.

Reverse transcription was performed with the High Capacity cDNA Reverse Transcriptase kit (Applied Biosystems, 4368814). Quantitative real-time PCR (qPCR) was prepared by triplicate using SYBR green GoTaq qPCR Master Mix (Promega, A6001) and run in a 7900 HT Fast Real-Time PCR system (Life technologies). Primers are detailed in Table M3. Data were analysed with SDS2.4 (Applied Biosystems) and QBasePlus (Biogazelle). Expression levels were normalized taking as reference β-actin, B2M (β2-microglobulin), GAPDH (Glyceraldehyde-3-phosphate dehydrogenase) HPRT1(hypoxanthine phosphoribosyltransferase 1) and/or YWHAZ (Tyrosine 3-Monooxygenase/Tryptophan 5-Monooxygenase Activation Protein Zeta).

Table M3. mRNA qPCR primer sequences.

Gene	Forward primer	Reverse primer
AC073111.3-201/2	GCAACGGCACAGTTGCAGAG	GGCAGGTCTTCTTACTGGATGT
AC090198.1-201	GTCCTTGAGAGACAGCAAATGA	TCTCTCGCAAGGGTAGAGGT
AC240565.2	CCCCGCTTTTGACTTTCGGT	AGGCAGGAGCTTTGGACTC
AHR	ATGGATCAATACTTCCACCTC	TTTGGCATCACAACCAATAG
AL078644.1	GGTCTGTTTTGTCTGCGTGC	GGGCCCCAGTAGGTTAGGAT
AMIGO3	CGAGTACGTATGCTTGGCCT	GCTGGTGTTGCAGTAAAGCC
AQP3	ACCAGCTTTTTGTTTCGGGC	GGCTGTGCCTATGAACTGGT
B-Actin	ATCATGTTTGAGACCTTCAA	AGATGGGCACAGTGTGGGT
B2M	GAGGCTATCCAGCGTACTCCA	CGGCAGGCATACTCATCTTTT
BCL2	GATTGTGGCCTTCTTTGAG	GTTCCACAAAGGCATCC
BCL2L11	ATGCAAGGAGGGTATTTTTG	CGTAACAGTCGTAAGATAACC
BCL2L2	CCTTTGGAATGGAAGCTTAG	GAGGGAATGTTTTCTCCTTG

Gene	Forward primer	Reverse primer
CD137	ACAACCATTTATGAGACCAG	ACATCCTCCTTCTTCTTCTTC
CD25	GACGTCCATATTTACAACAGAG	TCTACTCTTCCTCTGTCTCC
CD69	CAGCAAAGACTTTCACTGTAG	CATTTTCTTGTCCACTCTCC
CTLA4	TTGCTAAAGAAAAGAAGCCC	AAAGTTAGAATTGCCTCAGC
DOCK10	CGGAGCCTGTTGAGACCTG	CTAGGCTTTTCTTGCCGCTG
EEF1A1	TATCCACCTTTGGGTCGCTT	GTGGGGTGGCAGGTATTAGG
FP236241.1	ATTCAGGCAACTGAGGGGTG	AACCAGTCCTTCCACCAACC
GAPDH	ACAGTTGCCATGTAGACC	TTGAGCACAGGGTACTTTA
GITR	AATTCAGTTTTGGCTTCCAG	CAGTCTGTCCAAGGTTTG
H2AX	GGCCTCCCAGGAGTACTAAGA	CTCTTTCCATGAGGGCGGTG
HPRT1	CCTGGCGTCGTGATTAGTGAT	AGACGTTCAGTCCTGTCCATAA
IDH1	GGCTGTGGTTGTGAGTCTGA	TAGTTTATCGCCTGCCGGG
IFN γ	GGTAACTGACTTGAATGTCC	TTTTCGCTTCCCTGTTTTAG
IL2	AGGGATCTGAAACAACATTC	GCCTGATATGTTTTAAGTGGG
ISG20L2	GAGATGTGCTTTATGACGAG	TCTTCCCTGTGAGTATCTTC
KI67	GACAGAGGTTCCTAAGAGAG	AACAATCAGATTTGCTTCCG
LAG3	TATAACCTCACTGTTCTGGG	TCTAGTCGAAGGGTAAAGTC
LEF1	AGAGAGAGAAACTACAGGAATC	CCACCATGTTTCAGATGTAG
LINC00324	GCAGCATGCTCTGCAACGAA	GGTTACCGACTTGGTGCCAT
LINC00449	CTGGTTGGGAGCAGGCTAAG	ACTGCCCAATGCAAGAATGC
MTOR	GGAGGAGAAATTTGATCAGG	GGGCAACAAATTAAGGATTG
NKG2D	AGGACAAAATGACCAAAGAC	CTTGGGGATATCTGAATTGC
PD-L1	ATGCCCCATACAACAAAATC	GACATGTCAGTTCATGTTCAG
PD1	CTCCAGGCATGCAGATCC	GGCCTGTCTGGGGAGTCTA
RHOH	GCCTTTGCCACTTCTTGGAG	AGCCTAGTCTTCAACTGGTGTG
RIMBP3C	GGAAGGAGATACAGGCGCTC	CTCCGGCATTTGACTGGTCT
RPL22	GCCATGGCTCCTGTGAAAAAGC	GTTCCCAGCTTTTCCGTTCAC
RPL22L1	TTTTGAGCAATTTCTACGGG	TCAATGTGAACAACATTCCC
SCARNA9	AGCCTAATCATTTCTGGGCAA	GCTCAGGTCAAGTGTAGAAACC
SNORD3A	ACGAGGAAGAGAGGTAGCGT	ATCAATGGCTGACGGCAGTT
TIGIT	GTACTTCTGCATCTATCACAC	GGGCTTTCTTCTTTCTAGTC
TIM3	CTCTGACTTTTCTTCTGCAAG	ACCTTGTAAGTAGTAGCAGC
TNFAIP3	GCCAAGAGAGATCACACCCC	GCGATCCTTTCGCAAAGTCC

Gene	Forward primer	Reverse primer
TTLL1	TGGAAAATACCTCTATCTGGACTTT	CCCGGGACCACTTTTTGATCT
TUBA1A	GAAGCAGCAACCATGCGTGA	TCTCCTCCCCCAATGGTCTT
ULK1	GTTCCAAACACCTCGGTCCT	CCAACTTGAGGAGATGGCGT
VISTA	CCCAGGATAGTGAAAACATC	TTCAATCCCTTGAATGTTGC
YWHAZ	AACTTGACATTGTGGACATC	AAAACTATTTGTGGGACAGC
ZNF322P1	GCATTCATTGGAGAGCCTTACT	GGGCCTGATAAGACAGGAGC

Table M3. mRNA qPCR primer sequences.

13. Flow cytometry

Cells were blocked with γ-globulin (100µg/mL) in PBE (PBS, BSA1%, EDTA 5mM) at 4ºC for 20 min. Afterwards, cells were stained with corresponding conjugated surface antibodies (1:200, in PBE) at 4ºC for 30 min. Cells were washed with PBS and Propidium Iodide (Sigma-Aldrich, P4864), DAPI (Invitrogen, D3571) or TO-PRO-3 (Invitrogen, T3605) were added to distinguish dead cells.

Whenever staining included intracellular antibodies, instead of adding viability dyes at the end, cells were incubated during the blocking step with FYDCS (Fixable Yellow Dead Cell Stain: LIVE/DEAD® Fixable Yellow Dead Cell Stain Kit, for 405 nm excitation; Invitrogen, L34968) in PBS instead of PBE. After surface staining, cells were fixed and permeabilized with FIX&PERM Cell Permeabilization Kit (Invitrogen, GAS-003). Intracellular antibodies were incubated overnight at 1:100 dilution in permeabilization medium.

Proliferation was evaluated staining cells prior to cell culture with CellTrace Violet Cell Proliferation (Invitrogen, C34557).

For Annexin V apoptosis assay, cells were washed twice with PBS and incubated with Annexin V (1:40; BD Pharmingen, 550474) for 15 min in binding buffer (HEPES/NaOH 10mM, pH 7.4; NaCl 140mM; $CaCl_2$ 2,5mM).

Cells were acquired in a FACS Canto 3L or LSRFortessa (BD Biosciences). Software used for acquisition was BD FACSDiva (BD Biosciences) and samples were analysed with FlowJo (BD Biosciences).

14. Immunofluorescence

Raji cells were stained with CMAC cell tracker (10μM; Molecular Probes, C2110) and pulsed with SEE (0.5μg/mL; Toxin Technologies, PE404) for 30 min at 37ºC. 150000 Raji cells and 150000 J77 cells were plated on each Poly-L-Lys-coated (50μg/mL, 1h, 37ºC) slide, and incubated at 37ºC for 30 min. Cells were fixed with 2% paraformaldehyde in PBS, washed with TBS and permeabilized with 0.2% TritonX-100 (Sigma) in TBS (5min, RT). Cells were blocked for 30 min (γ-globulin 100μg/mL, BSA 3%, azide 0.2% in TBS), incubated with primary antibodies (biotinylated CD3 OKT3 and Tubulin-FITC, both 1:100 in blocking buffer), washed, and incubated with stretavidin-647 (Invitrogen, S-21374) and phalloidin conjugated to Alexa Fluor 568 (for actin staining) (both 1:200 in blocking buffer). Slides were mounted on Prolong (Molecular Probes, p36930) and images were captured with a Leica SP5 confocal microscope fitted with a 63x oil objective.

Maximal projections were assembled using Leica software and analysed with Fiji (ImageJ) (https://imagej.net/Fiji) and Imaris (Oxford Instruments). Accumulation of CD3ε at immune synapse was quantified using 'Synapse Measures' plugin for Fiji, developed by Calabia-Linares et al. (135). Imaris was used to model Raji B cell surfaces and measure T cell MTOC distance to synaptic contact area (136).

15. ELISA

J77 cells were stimulated with PMA and ionomycin, and supernatants were collected either at 20 or 45 h. IL2 detection was performed by ELISA (Human IL-2 ELISA Kit, Diaclone, 851500010). Manufacturer's instructions were followed, but samples were incubated overnight.

16. Statistical analysis

Graphs represent median and interquartile range for experiments with more than 4 replicates. In miRNAseq modification study, where data from 3 donors were available, mean and SEM were represented.

GraphPad Prism was used to perform statistical analyses according with the specific experimental designs. For non-parametric group analysis Kruskal-Wallis test and Dunn's multiple comparisons were applied. Mann-Whitney test was used whenever comparing

two groups (to avoid normality assumption).

Fisher's Exact Test p-value, with a 0.05 threshold value, was the statistical test used with Ingenuity Pathway analyses.

Significance is represented in graphs with the following symbols: * p-value<0.05, ** p-value<0.01, *** p-value<0.001; **** p-value<0.0001. For certain experiments, low but non-significant p-values are indicated with text. Non-significant comparisons are indicated as: ns.

Results

Results

Part I

In order to gain a mechanistic insight in the early changes occurring, upon T cell activation, at the level of miRNA expression and miRNA post-transcriptional modifications (PtMs); we have studied the effect of αCD3αCD28 and IFN I stimulation in human primary CD4+ T cells through Next Generation Sequencing (NGS). Since large changes in total miRNA levels occur very early (54), 3, 6 and 24 h were selected for our time course. Additionally, we evaluated the expression of several enzymes which could play an important role in miRNA remodelling.

1.1. MiRNA modulation by αCD3αCD28

A total of 120 miRNAs were found to be differentially expressed (adjusted p value <0.1, 62 upregulated and 58 downregulated) upon stimulation of resting human CD4+ T cells with αCD3αCD28 for 3, 6 and 24 h by NGS analysis [Fig. 1.1AB]. The most upregulated miRNAs (fold change indicated in brackets) at 24 h were miR-4455 (122x), miR-222-5p (24x), miR-7974 (21x), miR-155-3p (18x) and miR-4521 (15x) [Fig. 1.1B]. Remarkably, miR-1281 showed a 14-fold change upregulation at 3 h which was maintained at 6 h, but vanished at 24 h. The most downregulated miRNAs at 24h were miR-4485-3p (-11x), miR-4695-3p (-5x), miR-570-3p (-4x) and miR-1260a (-4x). With the exception of miR-155-3p, none of these miRNAs had been associated previously to T cell activation, probably due to the lack of studies using an unbiased approach such as NGS. Consistent with previous evidence (137), we also found downregulation of miR-150 and miR-223; while miR-155, miR-17-5p and miR-18a-5p were upregulated. Ingenuity pathway analysis (IPA) indicated that differentially expressed miRNAs were mainly involved in processes related to cell development, growth, proliferation and movement [Fig. 1.3A]. Networks of predicted targets for the miRNAs with the highest up- and down-regulation show large overlapping with 59 genes targeted by at least 2 of the 6 most upregulated miRNAs and 149, targeted by at least 2 of the 6 most downregulated [Fig. 1.4A].

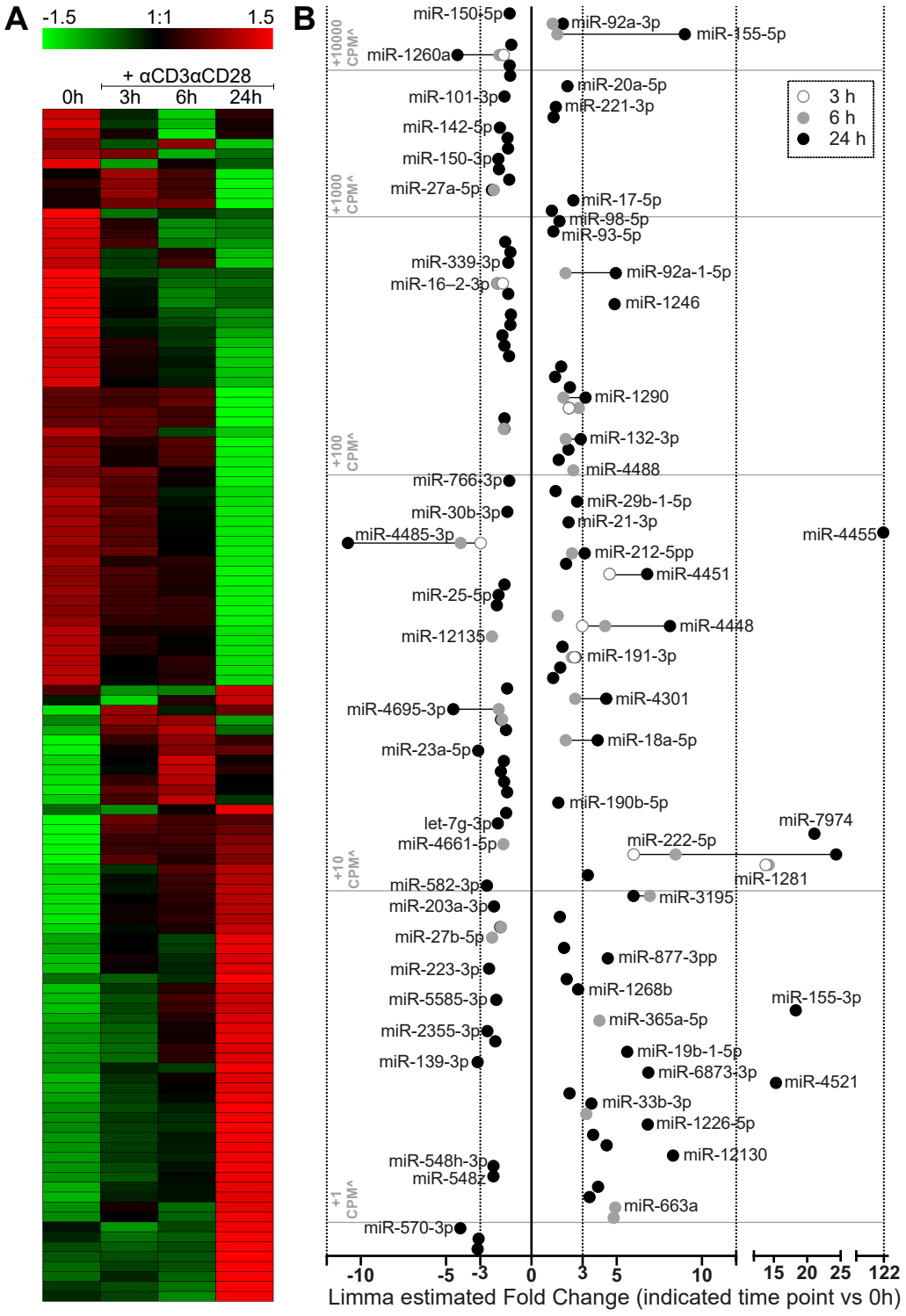

Figure 1.1. Differential miRNA expression 3h, 6h and 24h after αCD3αCD28 stimulation of human primary CD4+ T cells.
A) The heatmap represents relative expression values for a non-redundant collection of differentially expressed miRNAs (adjusted p-value <0.1), detected after stimulation with αCD3αCD28 for 3h, 6h, and 24h. B) Log fold change of differentially expressed miRNAs at 3, 6 and 24h compared to 0h. Representative miRNAs names are included, particularly those with higher fold changes. MiRNAs detected with higher CPMs occupy higher positions in Y axis.

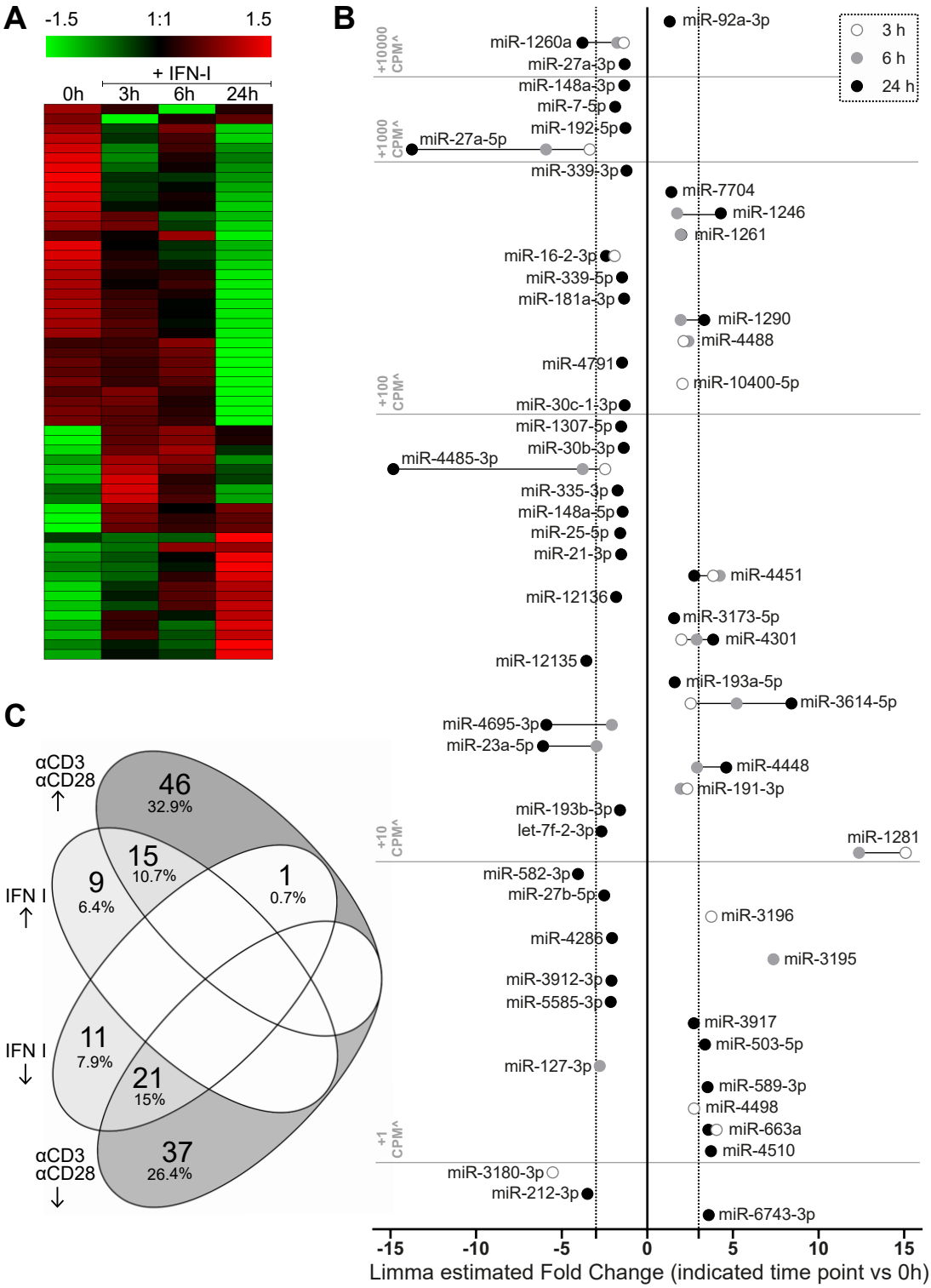

Figure 1.2. Differential miRNA expression 3h, 6h and 24h after IFN I stimulation of human primary CD4+ T cells.
A) The heatmap represents relative expression values for a non-redundant collection of differentially expressed miRNAs (adjusted p-value <0.1), detected after stimulation with IFN I for 3h, 6h, and 24h. B) Log fold change of differentially expressed miRNAs at 3, 6 and 24h compared to 0h. MiRNAs detected with higher CPMs occupy higher positions in Y axis. C) Venn diagram with miRNAs differentially up and down-regulated by IFN I and αCD3αCD28.

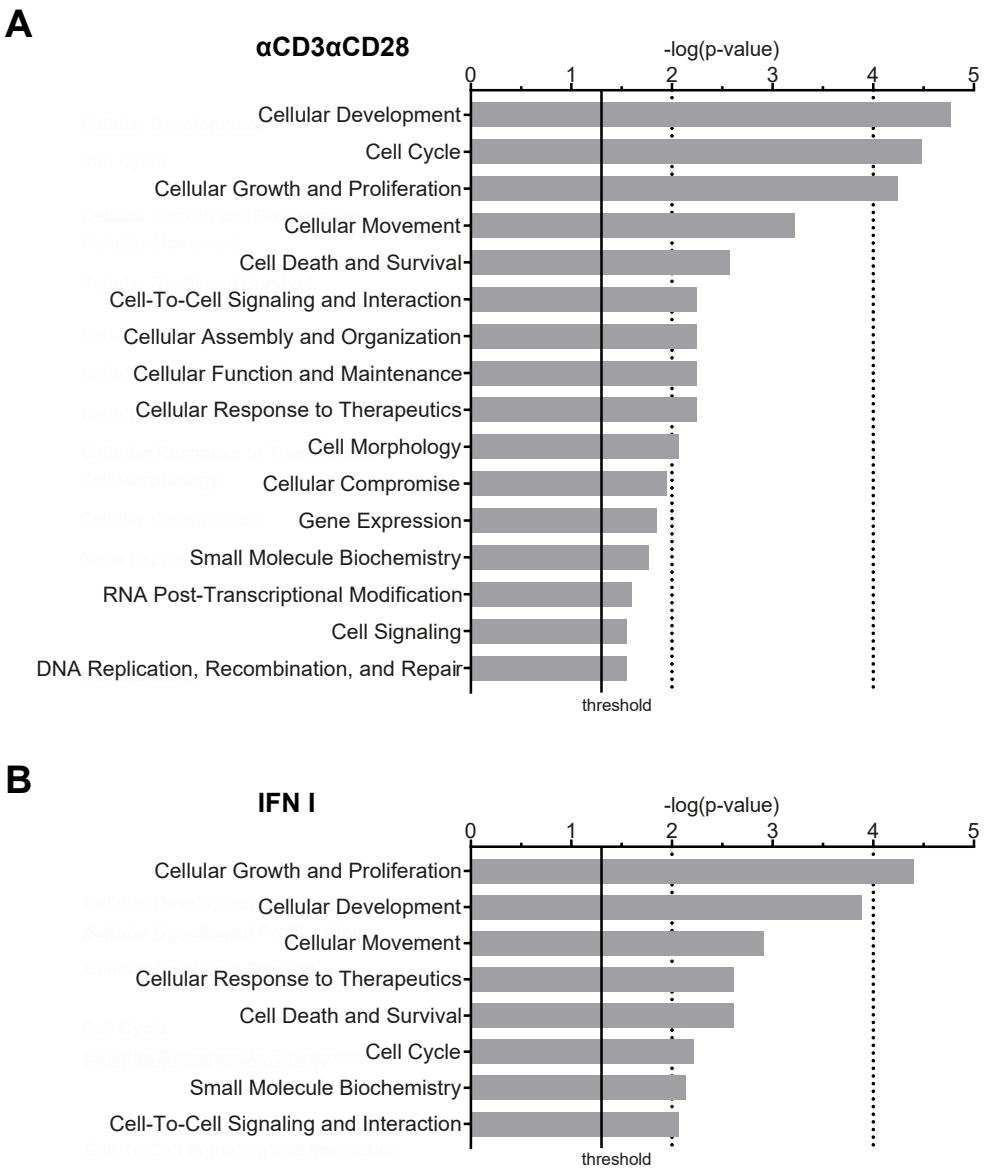

Figure 1.3. Ingenuity Pathway Analysis: molecular and cellular functions.
Core analysis performed with Ingenuity Pathway Analysis on differentially expressed miRNA (adjusted value <0.1) associated to their highest fold change during stimulation. Graphs include molecular and cellular functions found to be significantly represented for αCD3αCD28 miRNAs (A) and IFN I miRNAs (B). Fisher's Exact Test p-value, threshold value 0.05, displaying only entities that have a –log(p-value) greater than 1.3.

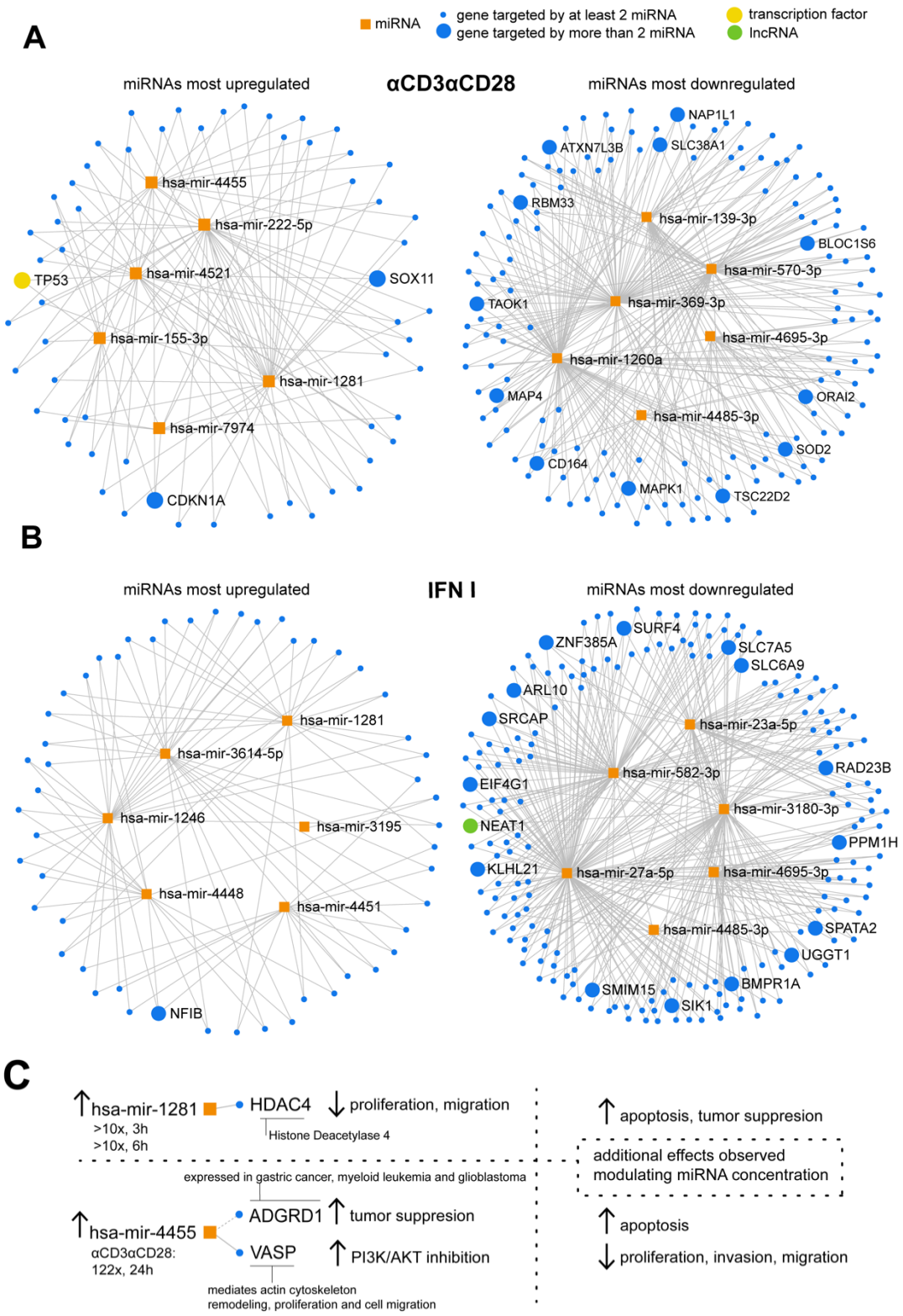

Figure 1.4. MiRNA predicted targets.
Targets predicted for the 6 miRNAs with highest up (left) and down-regulation (right) in αCD3αCD28 (A) and IFN I (B) sets. Networks include gene targets predicted for at least two of the selected miRNAs. Data were generated using miRNet, applying a degree filter of 1 in all but miRNAs nodes. C) Summary of targets and functions described for miRNA with a strong differentiated behaviour: miR-1281 and miR-4455.

1.2. MiRNA modulation by IFN I

In a separate set, resting human CD4+ T cells were stimulated with IFN type I. IFN I significantly altered the expression levels of 57 miRNAs (adjusted p value <0.1): 24 microRNAs were upregulated, and 33 were downregulated [Fig. 1.2A,B]. Compared with the data in Fig. 1.1, we found that 37 miRNAs were common to the IFN I and αCD3αCD28 subsets (15 upregulated and 21 downregulated in both stimulations, and 1 miRNA regulated in opposite directions) [Fig. 1.2C].

The most upregulated miRNAs (fold change indicated in brackets) at 24 h were miR-1281 (15x, 3h), miR-3195 (7x, 6h) and miR-3614-5p (8x, 24h). The most downregulated miRNAs at 24h were miR-27a-5p (-14x) and miR-4485 (-15x) [Fig. 1.2AB]. IPA revealed that most processes controlled by IFN I-regulated miRNAs were very similar to those observed for cells stimulated through αCD3αCD28, mainly: cell development, movement, growth and proliferation [Fig. 1.3B]. Predicted targets show a more intense network overlapping among the 6 most downregulated miRNA with 189 targets common to at least 2 miRNAs; while 52 genes would be targeted by at least 2 of the six most upregulated [Fig. 1.4B].

1.3. Post-transcriptional Modifications kinetics in T cell activation

A global assessment of Post-transcriptional Modifications (PtMs) indicated that miRNAs in our samples underwent extensive 3'-end modification compared to their canonical sequences [Fig. 1.5A]. Unexpectedly, C addition was highly represented in our samples at the most modified position: 0 or '3p end nucleotide'. A and C modifications were similarly represented in this position, much more frequently than U and G [Fig. 1.5A]. Modifications at 5' end and ADAR editing (A to G) were detected on a very limited basis. According to the global profile, positions 0 (3p end) and +1 (3p end +1), were by far the most heavily modified, followed by positions -1 and +2 [Fig. 1.5A]. For this reason, nucleotide modifications at the 3' end were analysed in greater detail in an attempt to discover specific sequences that could guide miRNA dynamics in T cells. PtMs patterns found in the 3' end (positions -4 to 4) were evaluated (data not shown), indicating that the most common modifications across the different samples were: C, A, U and G mono-additions, and A and U oligo-additions. 'AU' was the most frequent multi-nucleotide modification, although sequences combining more than one nucleotide were clearly underrepresented. We also detected UAGU modifications at position -4, as well as AGU

and AGUU at -3. We evaluated the presence of U, A, C, G and of UU+, AA+, CC+, GG+ (homopolymers of two or more equal nucleotides) at highly modified 3'-end positions. The results were conjoined for the different stimulation time points [Fig. 1.5B]. Analysed PtMs remained stable during activation and were clearly associated to a specific 3' end position [Fig. 1.5B].

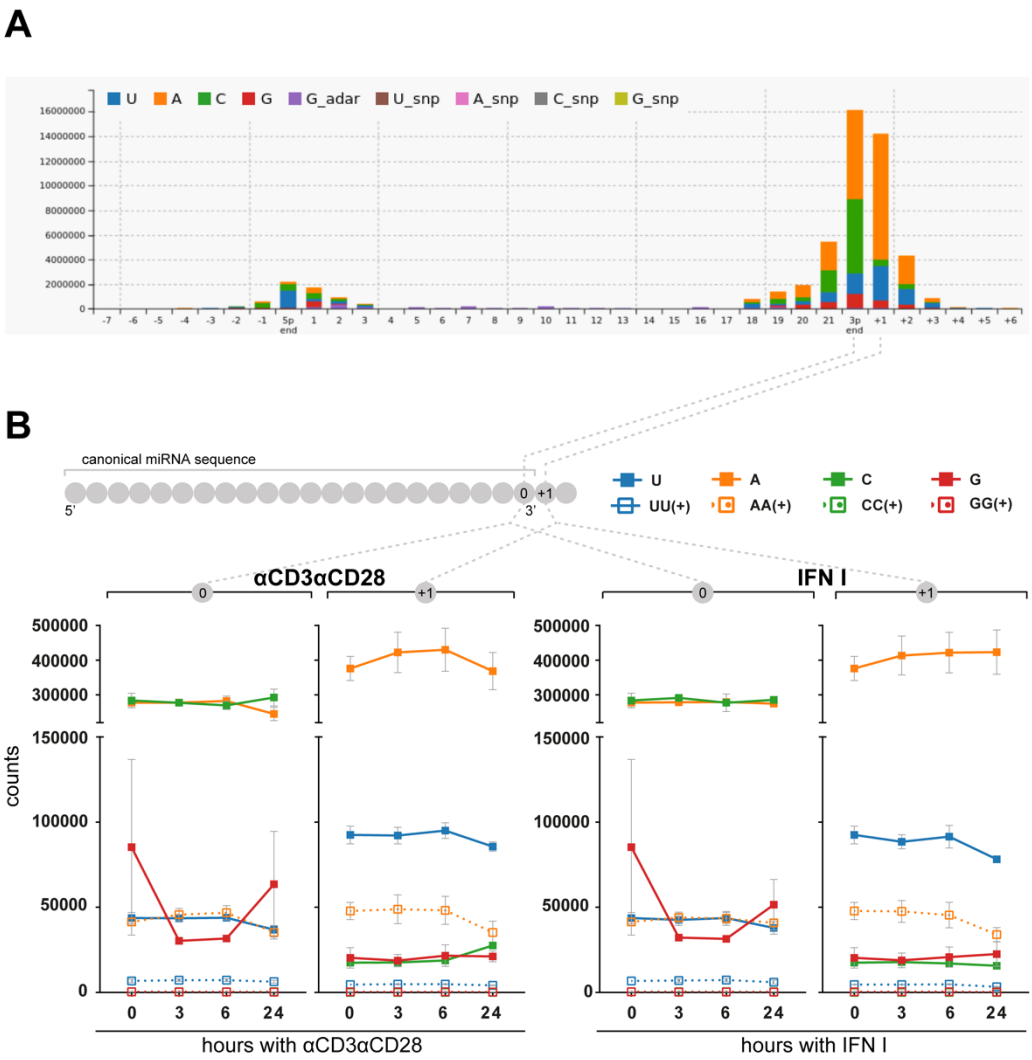

Figure 1.5. Post-transcriptional miRNA modifications: a global view.
A) Global post-transcriptional modifications (PtMs) profile for all 21 sequenced samples generated by Chimira. B) Kinetics of most abundant PtMs (mono-additions: U, A, C, G; and oligo-additions: ≥UU, ≥AA, ≥CC, ≥GG) at positions '3p-end' (0) and '3p-end + 1' (+1), in the population of 626 expressed miRNA species in unstimulated conditions and during activation with αCD3αCD28 (left) or IFN I (right). Mono-additions refer to the specific nucleotide on their own or followed by a different nucleotide, but not followed by the same nucleotide. Oligo-additions include PtMs with two or more equal nucleotides.

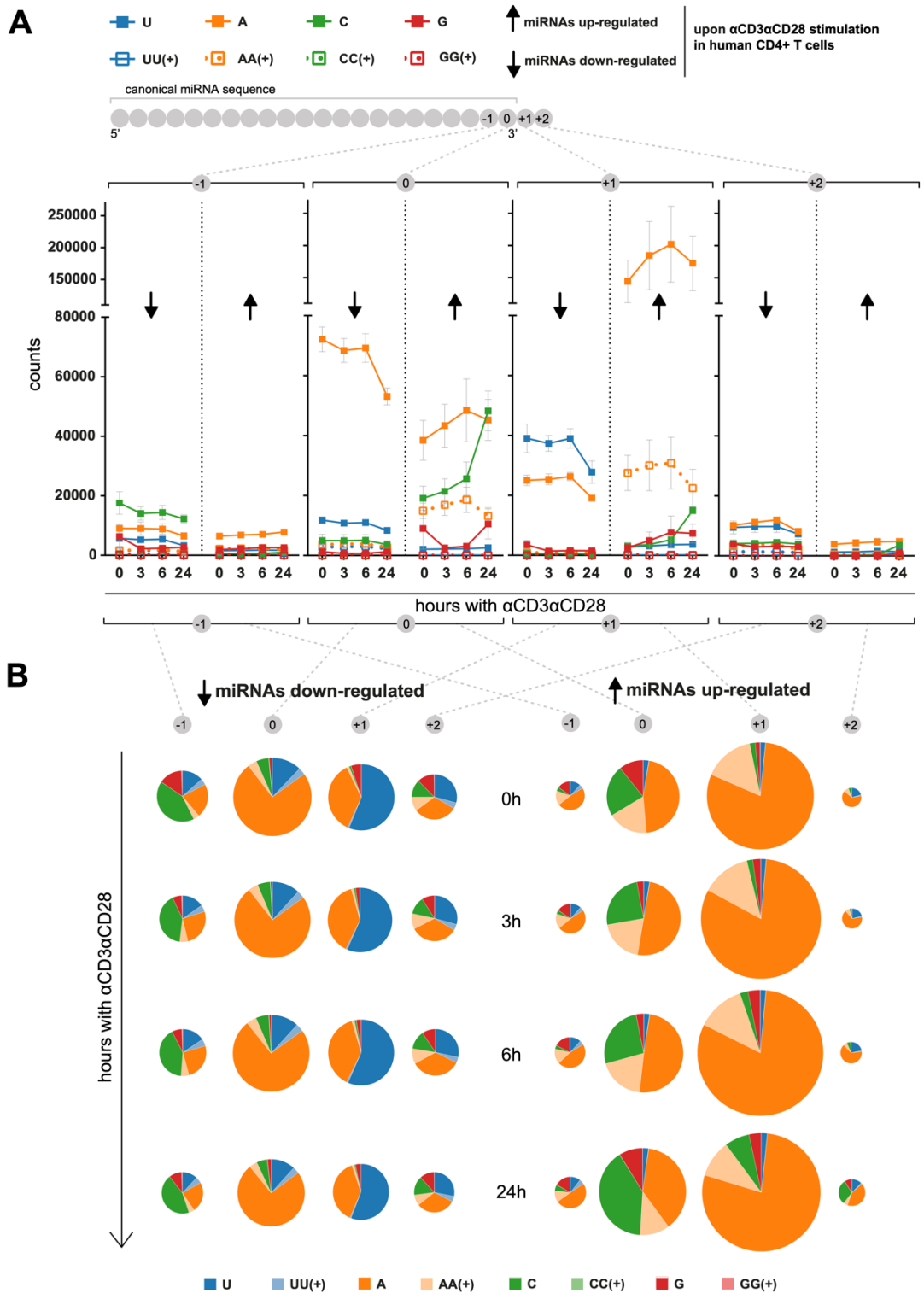

Figure 1.6. Kinetics of miRNA post-transcriptional modifications for αCD3αCD28 differentially expressed miRNAs.
Kinetics of most abundant PtMs (mono-additions: U, A, C, G; and oligo-additions: ≥UU, ≥AA, ≥CC, ≥GG) at positions '3p-end -1' (-1), '3p-end' (0), '3p-end + 1' (+1) and '3p-end + 2' (+2); for up-regulated miRNAs (left) and down-regulated miRNAs (right) with an adjusted p-value <0.1. Mean and SEM (from three independent experiments) were plotted for each modification counts at specific positions across time points (A) and as pie charts whose area is proportional to the total number of counts for the specific position at indicated time points (B).

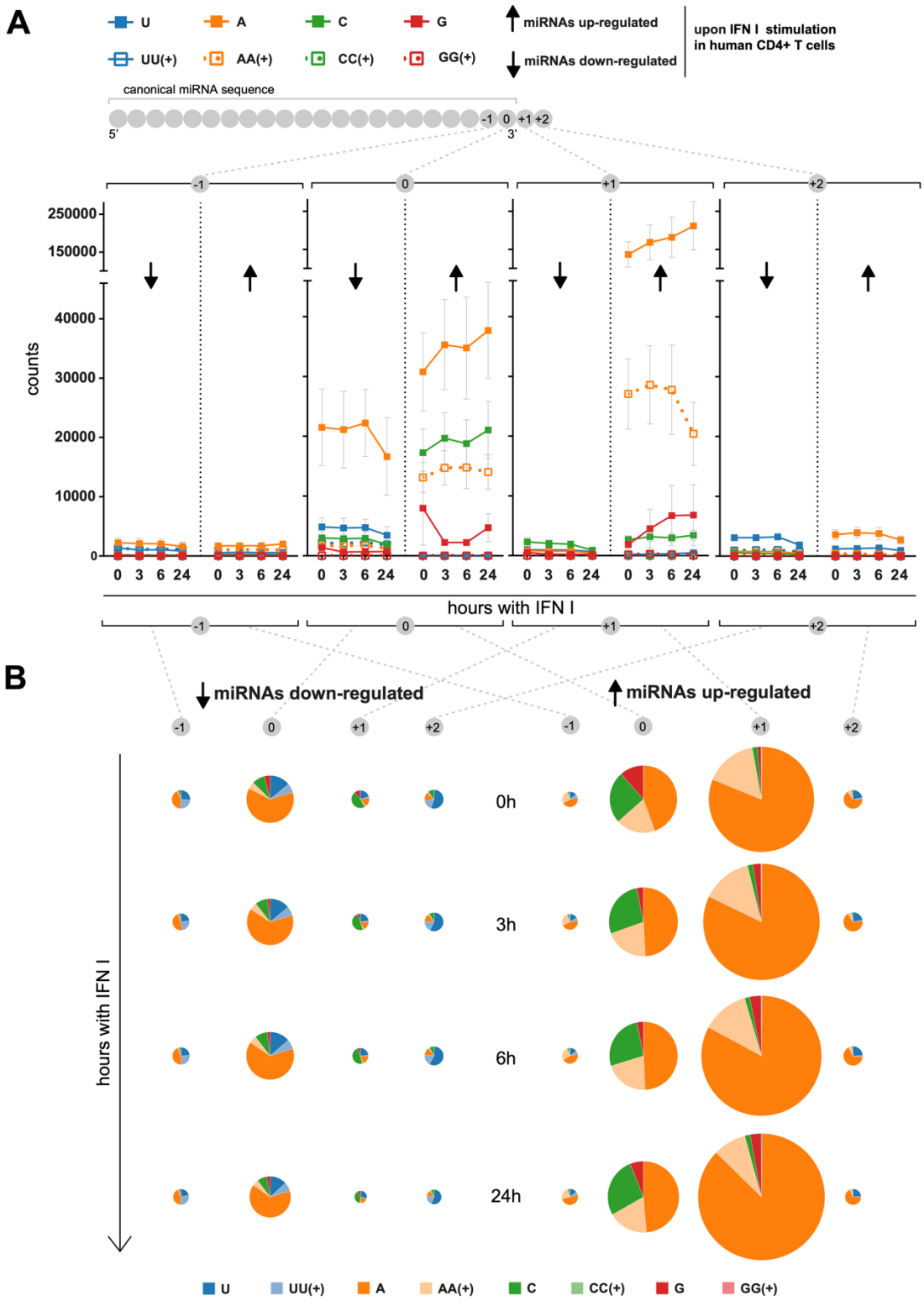

Figure 1.7. Kinetics of miRNA post-transcriptional modifications for IFN I differentially expressed miRNAs.
Kinetics of most abundant PtMs (mono-additions: U, A, C, G; and oligo-additions: ≥UU, ≥AA, ≥CC, ≥GG) at positions '3p-end' (0) and '3p-end + 1' (1) and '3p-end + 2' (2), for up-regulated miRNAs (left) and down-regulated miRNAs (right) with an adjusted p-value <0.1. Mean and SEM (from three independent experiments) were plotted for each modification counts at specific positions across time points (A) and as pie charts whose area is proportional to the total number of counts for the specific position at indicated time points (B).

To assess whether PtMs could be guiding the differential miRNA expression described in Fig. 1 and Fig. 2, modifications at positions -1, 0, +1 and +2, were represented considering only data from miRNA upregulated or downregulated, either upon αCD3αCD28 stimulation [Fig. 1.6AB] or IFN I [Fig. 1.7AB]. Data divided according to differential regulation, revealed the presence of a specific 'PtMs barcode' for each population. Upregulated miRNAs were more extensively modified, with the distinct signature of high levels of A addition at +1 and C addition at 0 [Fig. 1.6AB, Fig. 1.7AB]. αCD3αCD28 downregulated miRNAs show reduced levels of these specific modifications and a marked presence of U additions, mostly at +1 [Fig. 1.6AB]. Adenine additions at position +1 were much higher in upregulated miRNAs with counts of A mono-additions around 140000-210000, while downregulated miRNAs counts did not go beyond 30000 in αCD3αCD28 stimulation [Fig. 1.6A] or 2000 in IFN I [Fig. 1.7A]. Additions of two or more adenines were also a specific signature of upregulated miRNAs at 0 and +1 [Fig. 1.6A, Fig. 1.7A]. Strikingly, miRNAs found to be upregulated showed around 20000 cytosine counts at position 0 before stimulation [Fig. 1.6A, Fig. 1.7A], which remain stable upon IFN I stimulation [Fig. 1.7A] and grew up to around 50000 counts after 24h of αCD3αCD28 stimulation [Fig. 1.6A], whereas downregulated miRNAs maintained their cytosine counts around 5000 and below across all time points [Fig. 1.6A, Fig. 1.7A; position 0].

To gain a better understanding of the most abundant modifications in upregulated miRNAs, we identified the individual miRNAs exhibiting higher adenylation at position 1 and cytosylation at position 0 [Fig. 1.8-1.11]. A higher number of modified miRNAs were found in αCD3αCD28 stimulation [Fig. 1.8, 1.9], than in IFN I [Fig. 1.10, 1.11]. A group of miRNAs were found to be significantly cytosylated [Fig. 1.9, 1.11]. Nevertheless, miR-3195 on its own seems to account for the differential accumulation of cytosylation in upregulated miRNAs. Remarkably, a higher frequency of adenylation was found in upregulated miRNAs [Fig. 1.8, 1.10]. MiR-92a-3p, the upregulated miRNA with higher expression both in αCD3αCD28 [Fig. 1.1] and IFN I [Fig. 1.2] stimulations, counts with 31-42% of reads with an adenine at position 1 in all evaluated time points. In αCD3αCD28 stimulation, we have identified a group of upregulated miRNAs which present a higher frequency of adenylation [Fig. 1.8].

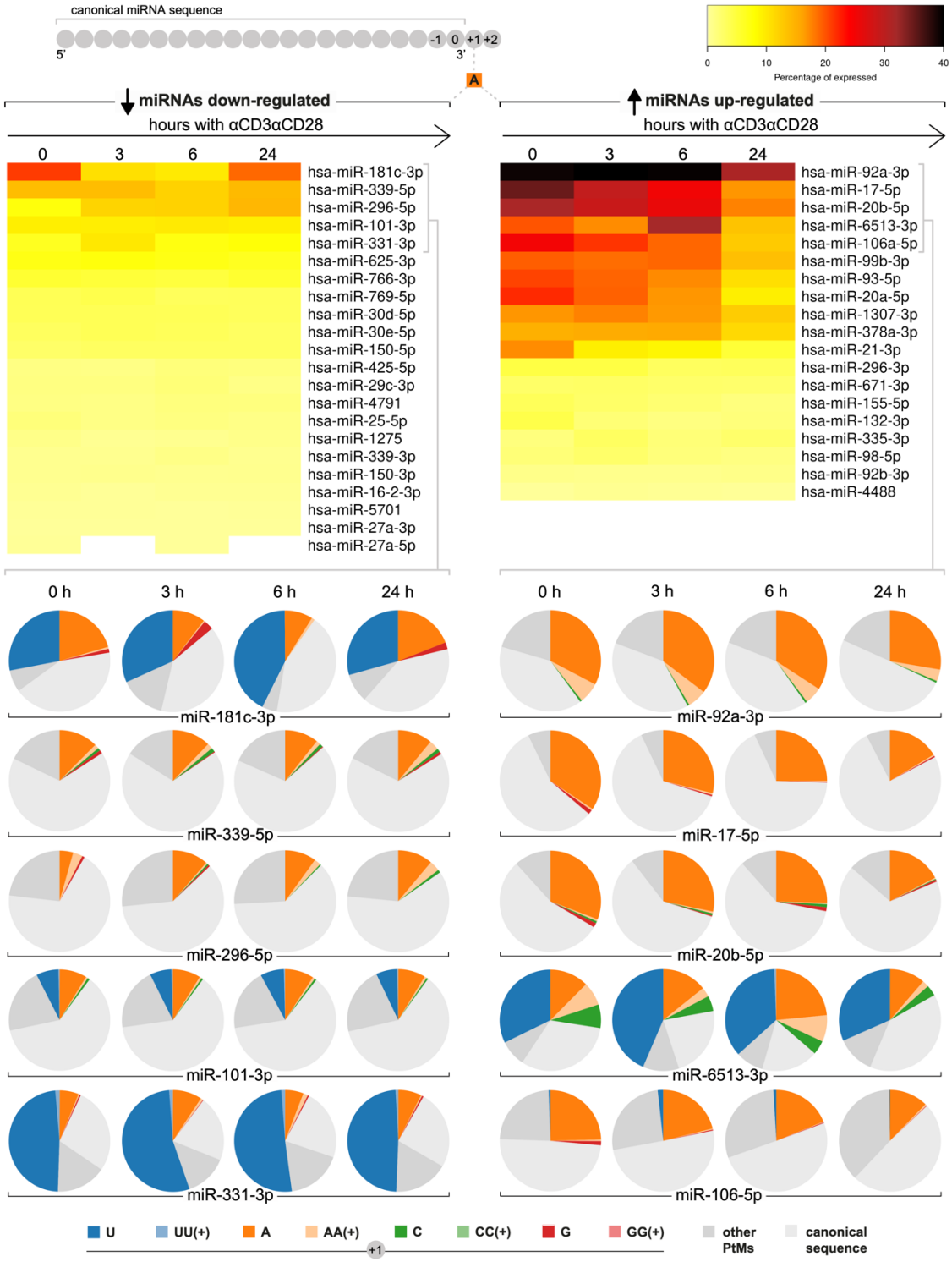

Figure 1.8. MiRNAs with significant adenylation at position 1 (αCD3αCD28). Heatmaps include upregulated (right) and downregulated (left) miRNAs with significant adenylation at position 1, detected in αCD3αCD28 stimulation. Reads with adenine at position 1 are normalized to total reads, in order to visualize the frequency of adenylation for each miRNA. Pie charts are included below for the 5 miRNAs most adenylated within each group. These graphs show in colour the percentage of reads with specific modifications at position 1, while reads with modifications at other positions and unmodified reads are depicted in gray.

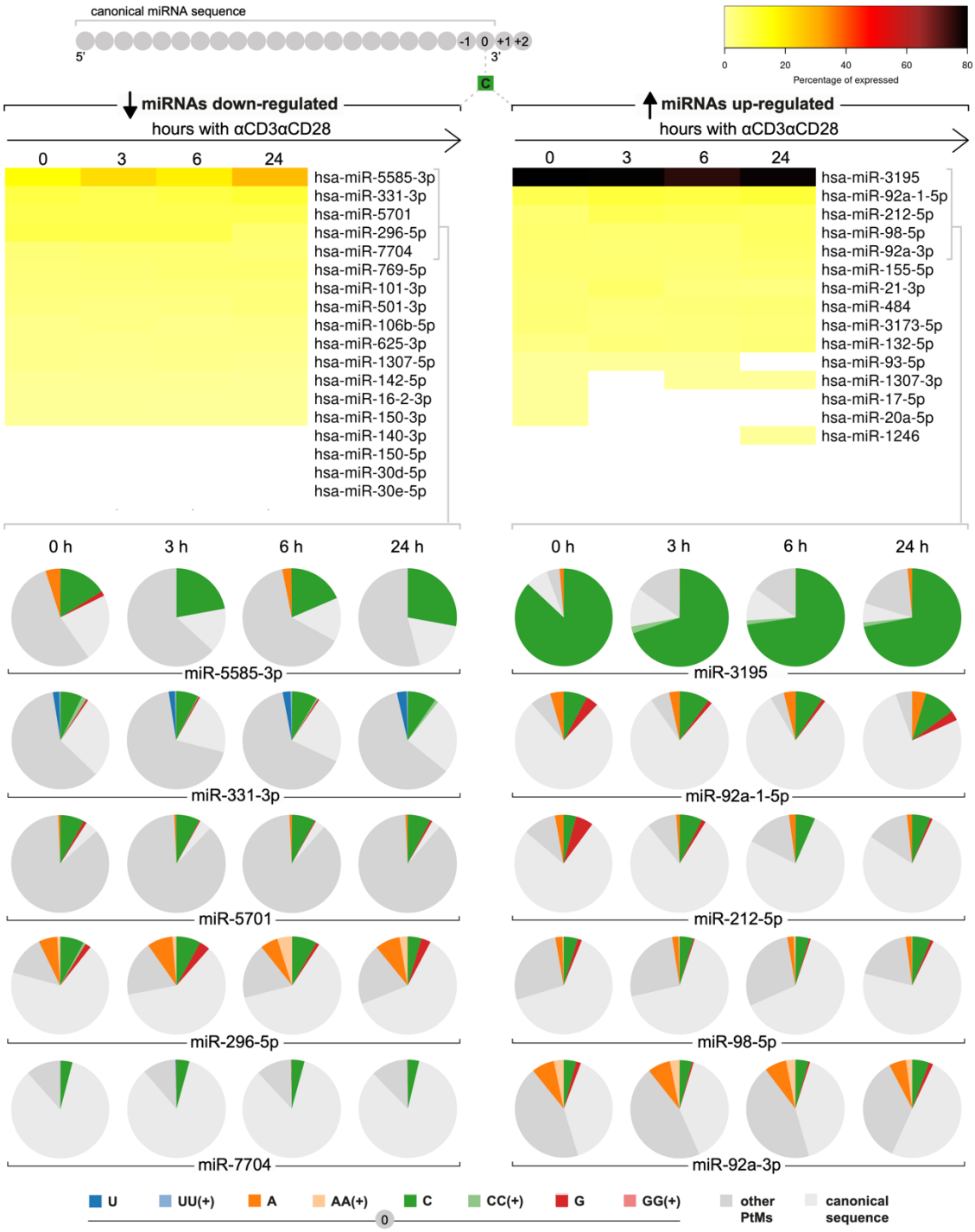

Figure 1.9. MiRNAs with significant cytosylation at position 0 (αCD3αCD28). Heatmaps include upregulated (right) and downregulated (left) miRNAs with significant cytosylation at position 0, detected in αCD3αCD28 stimulation. Reads with cytosine at position 0 are normalized to total reads, in order to visualize the frequency of cytosylation for each miRNA. Pie charts are included below for the 5 miRNAs most adenylated within each group. These graphs show in colour the percentage of reads with specific modifications at position 0, while reads with modifications at other positions and unmodified reads are depicted in gray.

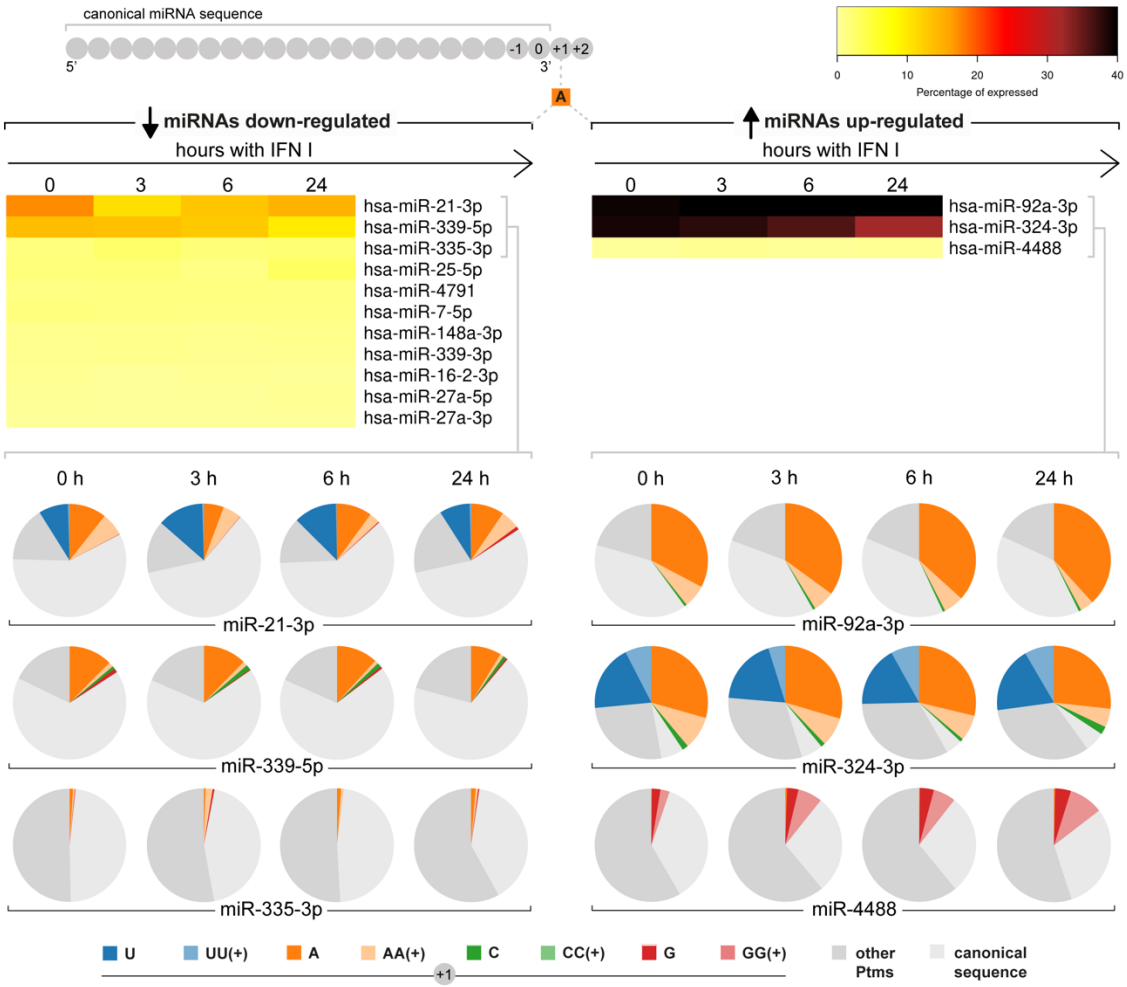

Figure 1.10. MiRNAs with significant adenylation at position 1 (IFN I).
Heatmaps include upregulated (right) and downregulated (left) miRNAs with significant adenylation at position 1, detected in IFN I stimulation. Reads with adenine at position 1 are normalized to total reads, in order to visualize the frequency of adenylation for each miRNA. Pie charts are included below for the 3 miRNAs most adenylated within each group. These graphs show in colour the percentage of reads with specific modifications at position 1, while reads with modifications at other positions and unmodified reads are depicted in gray.

Figure 1.11. MiRNAs with significant cytosylation at position 0 (IFN I) (next page).
Heatmaps include upregulated (right) and downregulated (left) miRNAs with significant cytosylation at position 0, detected in IFN I stimulation. Reads with cytosine at position 0 are normalized to total reads, in order to visualize the frequency of cytosylation for each miRNA. Pie charts are included below for the 3 miRNAs most adenylated within each group. These graphs show in colour the percentage of reads with specific modifications at position 0, while reads with modifications at other positions and unmodified reads are depicted in gray (continued).

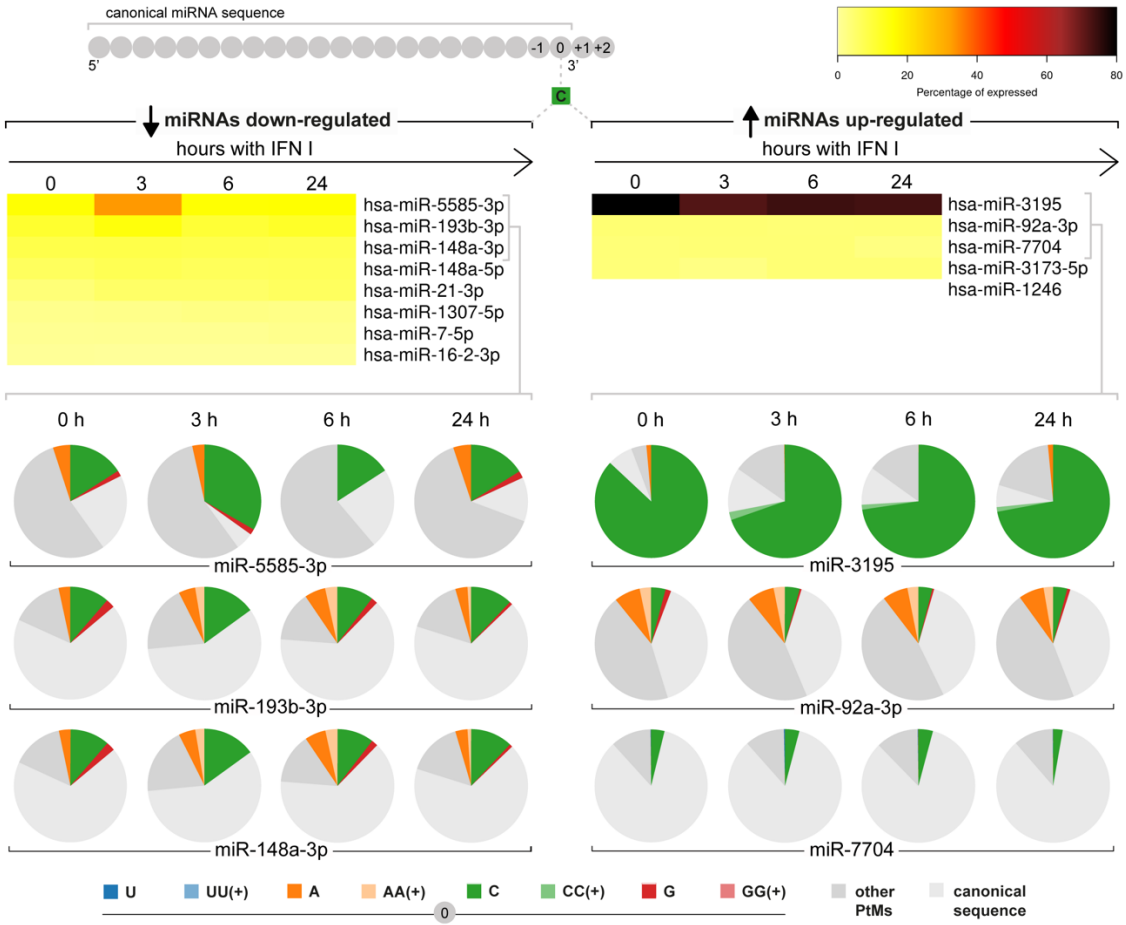

Figure 1.11. MiRNAs with significant cytosylation at position 0 (IFN I). Read full legend in previous page.

1.4. Dis3l2, Eri1, TUT4 and TUT7 regulation upon T-cell activation

In addition, we evaluated the expression kinetics of four proteins related to RNA metabolism: TUT4 and TUT7 (terminal uridylyl transferases), and Dis3L2 and Eri1 (exonucleases that preferentially degrade uridylated RNA (115,116,122)). For these experiments, we stimulated human CD4+ T cells from seven donors with αCD3αCD28 during various times up to 48 h. A significant average upregulation was found after activation for all evaluated enzymes [Fig. 1.12A-D]. Early upregulation of Eri1 and Dis3L2 could be driving global miRNA downregulation upon T-cell activation. The overexpression of TUT4 and TUT7, could be indicating a higher uridylation activity, which could mark miRNA for degradation by Eri1 and Dis3L2.

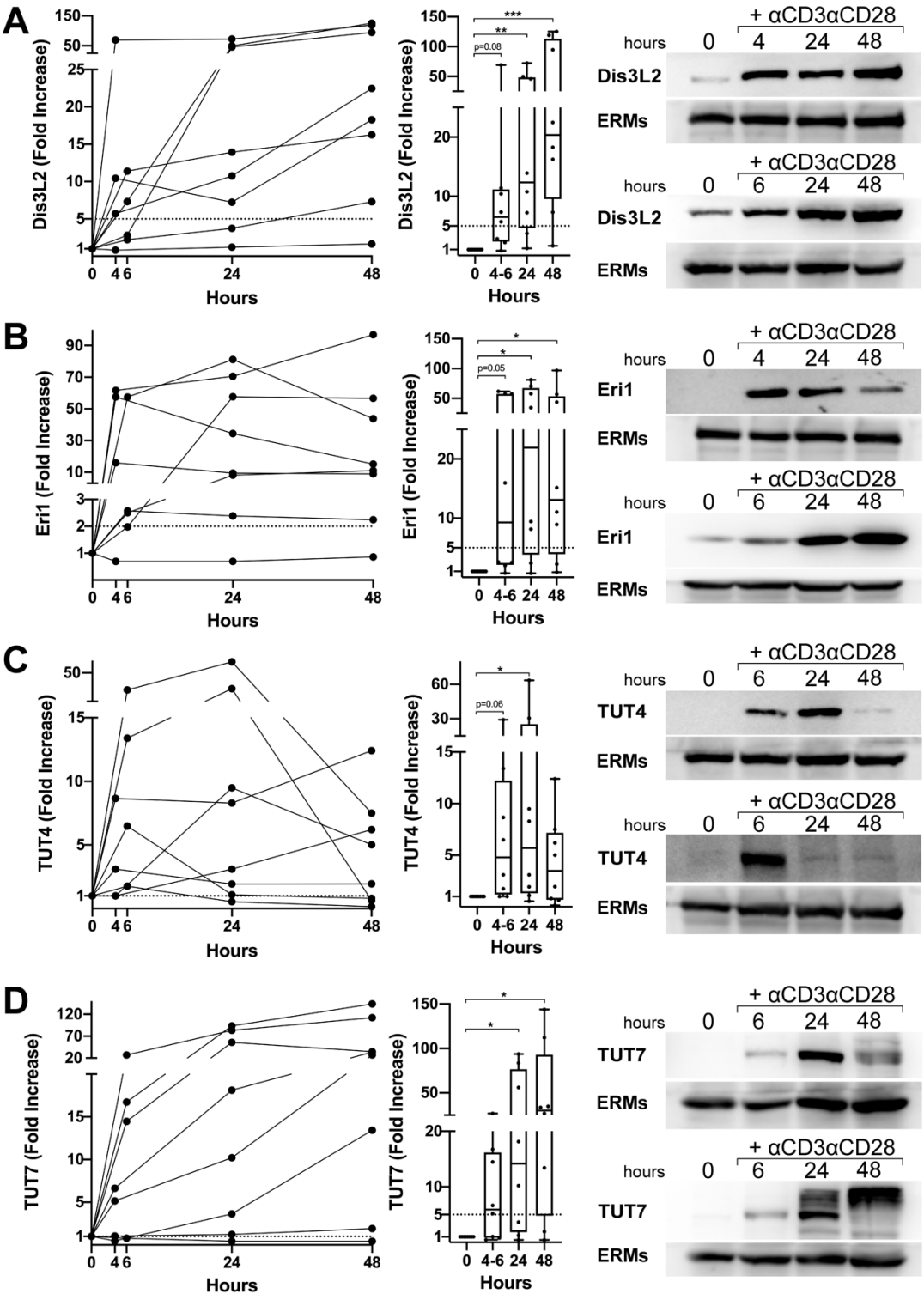

Figure 1.12. Expression of uridylated RNA degrading enzymes (Dis3L2 and Eri1) and terminal uridyl transferases (TUT4 y TUT7) upon CD4+ T cell activation.
Western blot analysis of protein expression in human primary CD4+ T cell stimulated with αCD3αCD28, assessing Dis3L2 (A), Eri1 (B), TUT4 (C) and TUT7 (D). Fold increase compared to non-stimulation was represented for each donor to observe evolution upon activation (left panel) and using group median and interquartile range with whiskers ranging from minimum to maximum values (middle panel). Right panels include two examples for each protein to highlight inter-donor variability in upregulation kinetics. Band intensities were normalized to ERMs values and relativized to unstimulated conditions. Statistical analysis: Kruskal-Wallis test, Dunn's multiple comparisons test [* p-value <0.05, ** p-value<0.01, *** p-value<0.001; 0.05<p-value<0.1: indicated with numbers].

Part II

In this second part we present the data obtained studying ISG20L2, a potential candidate for specific miRNA degradation in T cells. We describe how ISG20L2 was identified, an approach towards potential RNA targets and a first understanding of its role in T cell function.

2.1. Looking for a U' exonuclease

In order to find out an enzyme which could be behind degradation of uridylated miRNAs in T cell activation, a pull-down experiment was performed using miRNAs with different 3' ends. Three isoforms (canonical, with two additional 3' adenines or with two additional 3' uridines) of two different biotinylated miRNA were bound to streptavidin magnetic beads and incubated with a lysate of activated mouse CD4+ T cells [Fig. 2.1A]. By analysing proteins which were retained to the beads through mass spectrometry, we detected peptides from a previously identified 3' to 5' exonuclease, ISG20L2, only when the pull-down was performed with uridylated miRNAs: 4 peptides for miRNA-25-UU and 2 peptides for miR-151-UU [Fig. 2.1B]. These results were validated repeating the experiment in J77 cells and analysing proteins bound to beads through Western Blot [Fig. 2.1C]. Initially, these experiments were conducted overexpressing ISG20L2-GFP in J77 and later interaction with endogenous ISG20L2 was evaluated [Fig. 2.1C]. In both cases, ISG20L2 was found to present higher affinity for uridylated miRNAs than for their canonical or adenylated forms. Interestingly, ISG20L2 interaction with miR-151-AA was stronger than with the canonical miR-151, while interaction with miR-25-AA was not as high. These data point to a strong capacity of nucleotides added on 3' to favour ISG20L2 target recognition, but also to an influence of the miRNA sequence itself determining this interaction. This is particularly relevant for Dis3L2, an exonuclease previously described for its capacity to degrade specifically uridylated miRNAs. Here, we blotted Dis3L2 and detected it interacts preferentially with uridylated miRNA-25, with a pattern of interaction similar to ISG20L2, but barely recognizes miR-151 [Fig. 2.1C].

Table 2.1 includes all 'nuclease proteins' identified by mass spectrometry for the described pull-down experiment performed in mouse activated T cell and a subsequent experiment using human T lymphoblasts. ISG20L2 is the only enzyme with more peptides found both in miR-25 and miR-151 uridylated miRNAs compared to their canonical forms in both experiments [Table 2.1]. With human cells, only an ISG20L2 peptide per sample was detected interacting with 25-UU, 151-UU and 151-AA [Table

2.1]. This very limited peptide count could be due to a low protein input. The pull-down performed with human lymphoblasts included two additional conditions: beads with

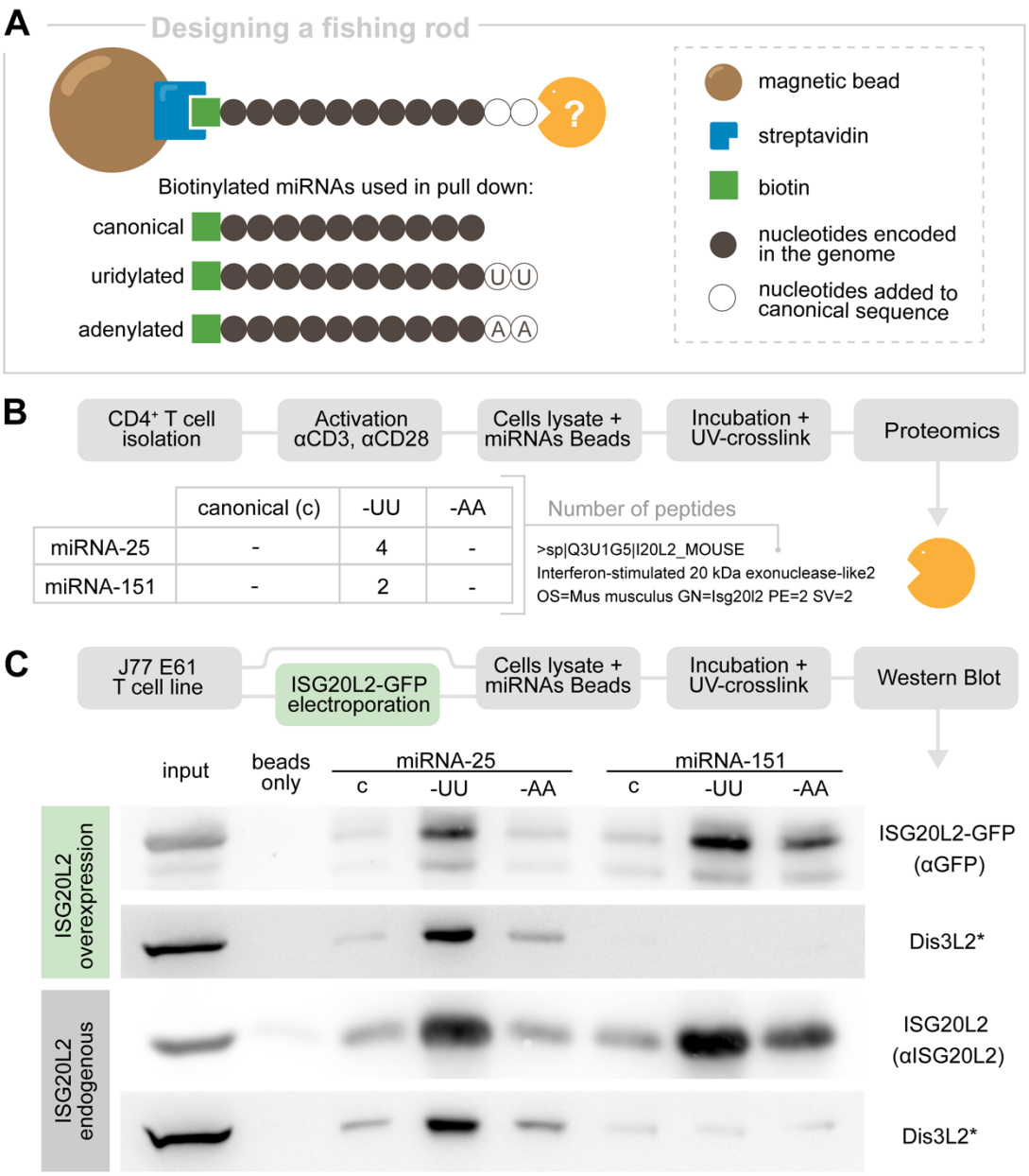

Figure 2.1. ISG20L2 binds uridylated miRNA in T cells.
A) Pull-down experiment design: biotinylated miRNAs either in their canonical sequence or with a 3' addition of two uridines or two adenines were incubated first with T cell lysates, UV-crosslink to maintain RNA-protein interactions and lastly streptavidin beads were added. B) Amount of ISG20L2 peptides identified through mass spectrometry using a lysate of activated CD4+ T cells. C) Validation of ISG20L2 preferential interaction with uridylated miRNAs performing the pull-down experiment in J77 E61 either relying on ISG20L2 GFP overexpression (top) or ISG20L2 endogenous expression (bottom). Overexpression ISG20L2 images (top) show blot with anti-GFP and with anti-Dis3L2. ISG20L2 endogenous images (bottom) show blot with anti-ISG20L2 and with anti-Dis3L2. Endogenous Dis3L2, an exonuclease described to degrade uridylated miRNAs, is shown as a positive control of U-interaction.

Accession	Protein name	Beads	miRNA-25	miRNA-25-UU	miRNA-25-AA	miRNA-151	miRNA-151-UU	miRNA-151-AA	Poly(U)	Poly(A)
	MOUSE:									
P52760	Ribonuclease UK114					1			X	X
Q3U1G5	**ISG20L2**			**4**			**2**		**X**	**X**
	HUMAN:									
Q8IYB7	**Dis3L2**			**3**					**14**	
Q9H9L3	**ISG20L2**			**1**			**1**	**1**		
Q99575	Ribonucleases P/MRP protein subunit POP1			2	2	2	1	2	6	1
Q9H0D6	5'-3' exoribonuclease 2				1				4	
Q9UPY3	Endoribonuclease Dicer									4
O43414	ERI1 exoribonuclease 3									1
P78346	Ribonuclease P protein subunit p30									1
Q9NRR4	Ribonuclease 3								1	
B4DI15	cDNA FLJ60550, weakly similar to Exosome complex exonuclease RRP44 (EC 3.1.13.-)								1	
P78345	Ribonuclease P protein subunit p38		1	1		1			1	
P51530	DNA replication ATP-dependent helicase/nuclease DNA2		1					1		

Table 2.1. Nuclease proteins identified by biotinylated miRNA pull-down. Proteins described as 'nuclease' identified by mass spectrometry in pull-down samples. X is depicted when the condition was not included in the experiment.

poly(U) and poly(A). The idea behind using this homopolymeric RNA stretches was to have an additional option to identify RNA degrading enzymes that would target an RNA with more than one or two added uridines. Dis3L2 peptides were only detected in human samples, interacting with miR-25-UU and poly(U) [Table 2.1]. No peptides belonging to Eri1 (Q8IV48, ERI1 gene; thought to be a likely candidate for degradation of uridylated miRNA), were identified, nor was it visible by western blot in any bead samples, only in lysate input (data not shown). Eri1 exoribonuclease 3 (O43414, ERI3 gene) is an Eri1 paralog, but only one peptide was detected in poly(A) beads [Table 2.1].

Table 2.2 (mouse) and Table A.3 (human, annexes) show proteins found to interact more strongly with uridylated miRNAs. The list has been compiled considering differential peptide detection comparing uridylated miRNA with canonical forms, and subtracting non-specific binding (number of peptides bound to beads without biotinylated RNAs). Table A.5 gathers an additional list of proteins not included in Tabe A.3, which were found to have a differential interaction towards poly(U). Table A.4 shows proteins with preferential interaction with poly(A).

Accession	Protein name	Beads	miR-25	miR25 -UU	miR25 -AA	miR-151	miR151 -UU	miR151-AA
Q8K310	Matrin-3		4	23	13	1		
Q8BVY0	Ribosomal L1 domain-containing protein 1	1		8	2	2	2	5
Q9Z204	Heterogeneous nuclear ribonucleoproteins C1/C2	1	2	5	2		5	1
Q05CL8	La-related protein 7			5			2	
P09405	Nucleolin		11	15	8	5	7	11
P32067	Lupus La protein homolog		2	5	2		3	1
Q3U1G5	Interferon-stimulated 20 kDa exonuclease-like 2			4			2	
Q3TEA8	Heterochromatin protein 1-binding protein 3			4				1
Q9CZM2	60S ribosomal protein L15		2	4	2	1	3	4
Q91VC3	Eukaryotic initiation factor 4A-III						4	
P62717	60S ribosomal protein L18a	1	4	6	3	3	5	8
Q8BHD7	Polypyrimidine tract-binding protein 3		1	4	2			
P62900	60S ribosomal protein L31			3	1	2	2	1
Q99ME9	Nucleolar GTP-binding protein 1			2			1	3
Q922P9	Putative oxidoreductase GLYR1			3				
Q9ESX5	H/ACA ribonucleoprotein complex subunit 4	3	6	9	6	5	7	11
O09167	60S ribosomal protein L21	3	2	5	2	3	5	3
O55142	60S ribosomal protein L35a	1	2	3	1	1	3	2
P53026	60S ribosomal protein L10a	1		2	1		1	2
P62827	GTP-binding nuclear protein Ran	1		1			2	
P62960	Nuclease-sensitive element-binding protein 1			2	1	1	1	1
P62889	60S ribosomal protein L30		1	2			1	2
Q8VEK3	Heterogeneous nuclear ribonucleoprotein U		1	2	1	1	2	2
Q922K7	Probable 28S rRNA (cytosine-C(5))-methyltransferase		1	1			2	1
Q9CQS2	H/ACA ribonucleoprotein complex subunit 3			2	1			1
Q9Z2X1	Heterogeneous nuclear ribonucleoprotein F			1	1		1	1
P43277	Histone H1.3			1	1		1	
Q8VDW0	ATP-dependent RNA helicase DDX39A				1		2	
P62082	40S ribosomal protein S7			1			1	1
Q6P5B0	RRP12-like protein			2				

Table 2.2. Mouse proteins with peptides enriched in uridylated miRNA beads. Proteins with a sum of at least 2 peptide counts more in uridylated miRNA samples than in canonical and beads samples. Keratins (7) have been removed from the list. Ribosomal proteins have a blue background and ribonucleoproteins a green one. ISG20L2 is indicated in yellow.

Ribosomal proteins and ribonucleoproteins are abundantly represented in these lists, which is not surprising due to their RNA interacting function. Proteins previously described to interact with uridylated RNA, such as Lupus La protein and LARP7, were enriched in the correspondent samples. La protein (targeted by autoantibodies in patients suffering Sjögren's syndrome or systemic lupus erythematosus) and its homolog in mouse, interact with the UUU-3'OH of nascent RNAP III (RNA polymerase III) transcripts, protecting them from degradation (138–140). La-related protein 7 (LARP7) recognizes the same motif in a specific RNAP III transcripts subset (141). Therefore, these proteins serve as a positive control of specific interaction with uridylated RNA. In our data: Lupus La protein homolog, La-related protein 7 [Table2.2] and Lupus La protein [Table A.3] are enriched in uridylated substrates. In addition, hnRNPM (heterogeneous

nuclear ribonucleoprotein M), which has been described to bind poly(U) and poly(G) RNA (142), is highly represented here in poly(U) beads and more abundant in uridylated miRNAs compared to their canonical forms in human samples [Table A.3] (in mouse samples peptides detected in uridylated miRNAs did not surpass the background threshold). A large number of Matrin-3 peptides have been detected in miR-25-UU and poly(U) beads [Table 2.1, Table A.3]. This RNA-binding protein has been described to have a role in mRNA stabilization (143) and to interact with hnRNPM (144) .

In summary, these results support ISG20L2 preferentially interacts with uridylated miRNAs and is the strongest nuclease candidate found here to play a potential role in a uridylated-guided miRNA remodelling in T cells.

2.2. ISG20L2 degrades miRNA

ISG20L2 belongs to a family of 3' to 5' exoribonucleases: DEDDh (145), which is characterized for the presence of four conserved core of acidic residues (one glutamate (E) and three aspartates (D)) distributed in three separated sequence segments and a common catalytic mechanism involving metal ions (146–148). A fifth also conserved histidine completes the DEDD residues leading to the DEDDh family name. These residues provide a binding site for the two divalent metal ions and play a critical role in the active site.

ISG20L2 was aligned with other two closely related DEDDh enzymes, ISG20L1 (AEN) and ISG20, using COBALT (Constraint-based Multiple Alignment Tool) [Fig 2.2AB]. These proteins share a high homology, particularly in the catalytic region (identified by COBALT as DNAQ_like_exo (or DEDD) in ISG20 and ISG20L1; while ISG20L2 catalytic region is recognized as ISG20) [Fig. 2.2A]. In order to generate ISG20L2 catalytic mutants, critical positions in the active site were hypothesized by association with ISG20 and ISG20L1. The conserved D residues are marked in yellow, green and blue following the positions described in UniProt to be involved in metal binding by ISG20 (bold and underlined residues) [Fig. 2.2B].

Two strategies were designed in order to generate two different mutants: NAF and IACAM. NAF was generated mutating D267 to alanine (A), by producing a punctual mutation to change adenine to cytosine in the central position of the corresponding codon [Fig. 2.2C]. IACAM includes two A substitutions: replacing D183 and E185 [Fig. 2.2C].

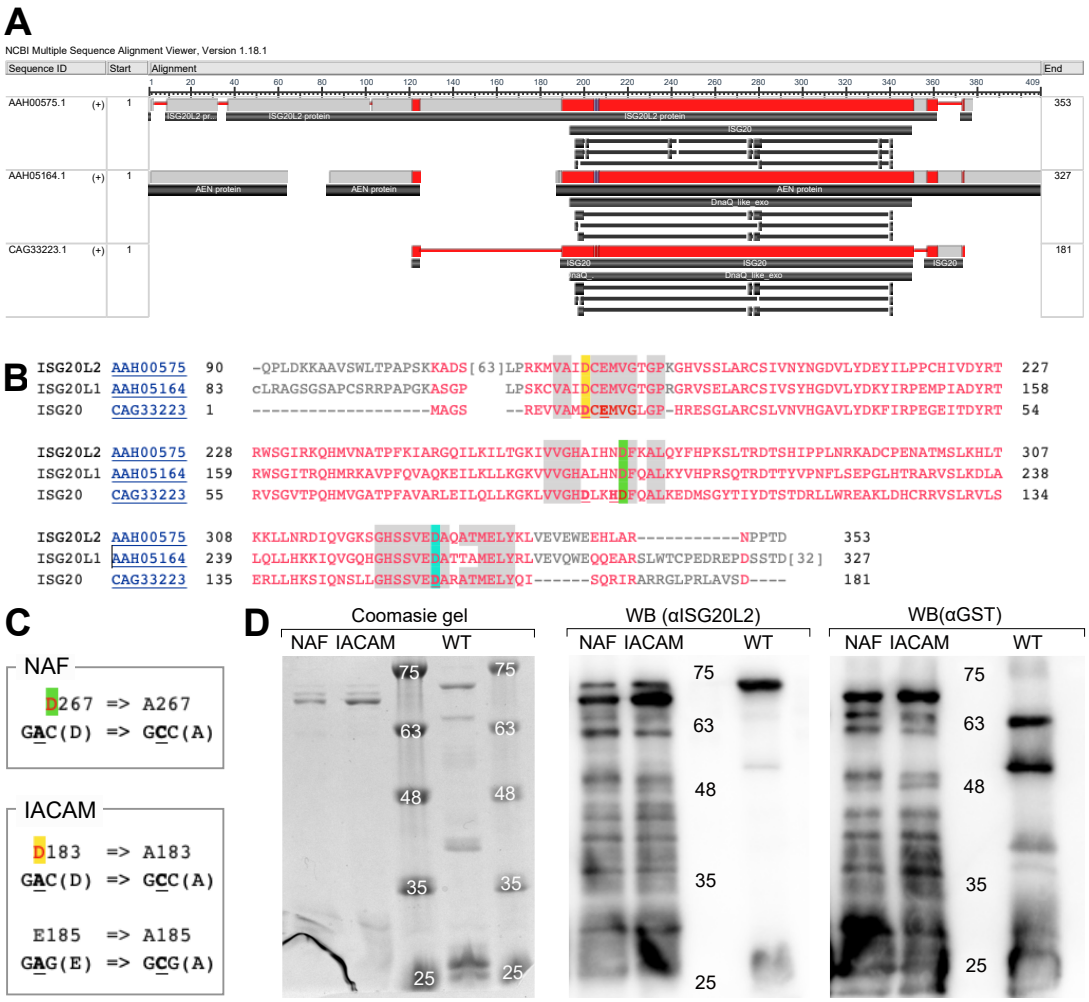

Figure 2.2. ISG20L2 catalytic mutants.
A) Alignment of conserved regions in the catalytic centre of ISG20L2, ISG20L1 (AEN) and ISG20 generated by COBALT (Constraint-based Multiple Alignment Tool). Red indicates highly conserved alignment columns (with no gaps) (column-method based on residue's relative entropy threshold). DnaQ_like_exo region refers to DnaQ-like (or DEDD) 3'-5' exonuclease domain superfamily. Regions identified without text included due to space limitations refer to active sites and substrate binding sites. B) Sequence alignment of ISG20L2, ISG20L1 and ISG20. Bold and underlined residues have been described to be key sites for ISG20 catalytic activity. Aspartic (D) conserved residues are coloured in yellow, green and blue. C) Mutations introduced to generate catalytic mutants NAF and IACAM. D in 267 is mutated to alanine (A) through a one base nucleotide exchange (A to C) to generate NAF mutant. IACAM mutant is achieved by D183 and glutamic (E) 185 mutation to A. D) WT and catalytic mutants fused to GST obtained after affinity purification and concentration (left: coomasie gel, middle: wb with anti-ISG20L2, right: wb with anti-GST).

WT and catalytic mutants were fused to GST in a pGEX-4T-1 plasmid [Fig. 2.2D]. WT ISG20L2-GST was extremely difficult to express in bacteria, while NAF and IACAM were easily overexpressed at various conditions (RIPL strain, induced with IPTG 0.2mM, overnight at 16ºC was a particularly good scheme). Expression of ISG20L2-SMT3 in

pET28 plasmid was also attempted but bacteria grew extremely slowly. Finally, WT ISG20L2-GST was produced using a p-Lys strain induced with 0.2mM IPTG for only half an hour, to avoid degradation found at larger induction times.

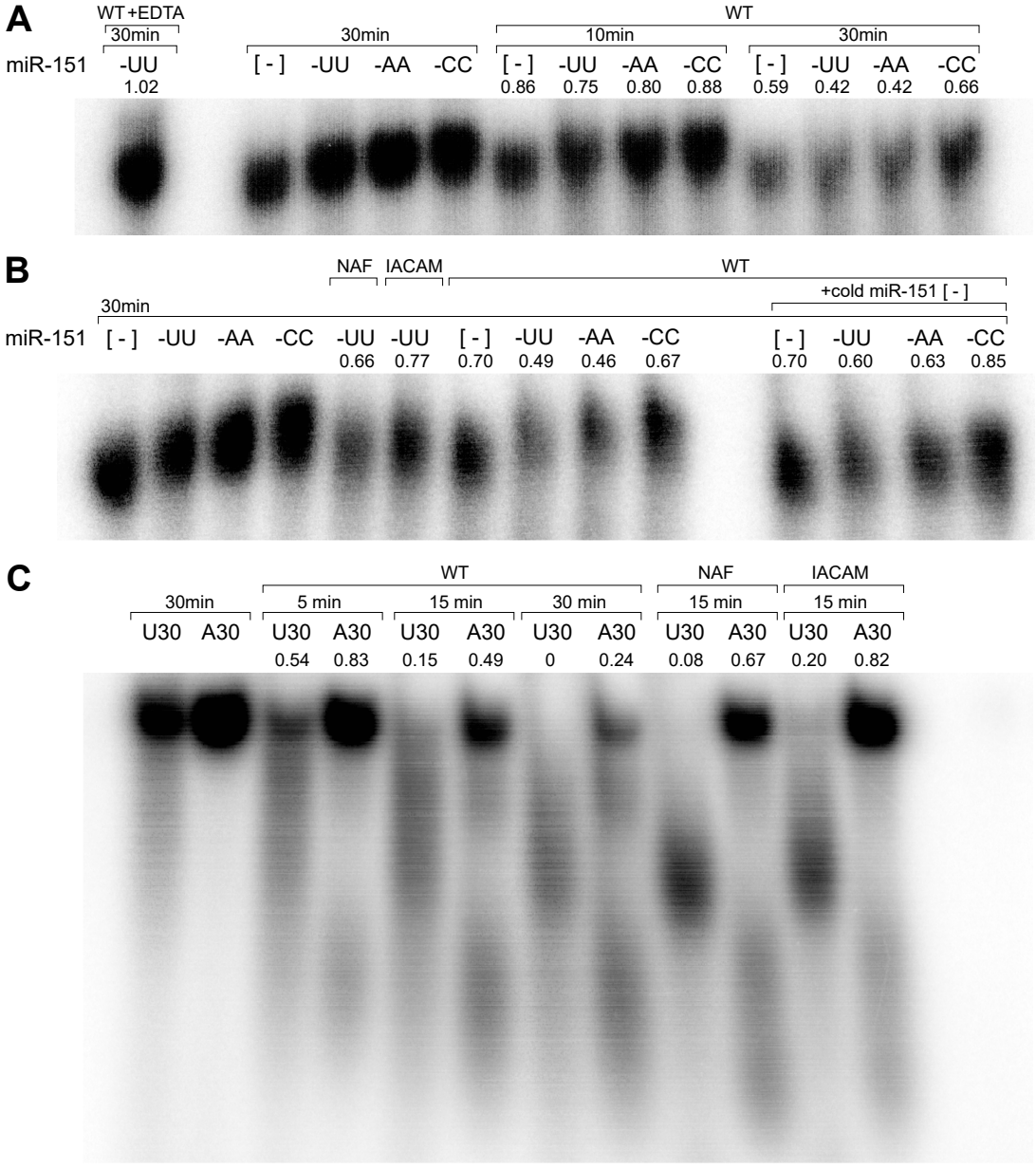

Figure 2.3. ISG20L2 degrades miRNAs with an efficiency influenced by terminal 3' end nucleotides.
Degradation assays performed in the presence of WT, NAF or IACAM proteins incubated with various miR-151 isoforms (canonical [-], uridylated (miR-151-UU), adenylated (miR-151-AA), cytosylated (miR-151-CC)) (A, B) or homopolymeric stretches of 30 adenines (A30) or 30 uridines (U30) (C). RNA incubated in absence of protein for the time corresponding with the longest assay are included in every gel, and used as a reference for normalization of non-degraded quantifications. EDTA was added to test dependence on divalent cations (A). +cold miR-151[-] indicates the degradation assay was conducted in the presence of unlabeled canonical miRNA (C).

Figure 2.3AB shows degradation experiments performed with miR-151 isoforms. As expected, ISG20L2 catalytic activity is inhibited in the absence of free divalent cations (chelated by EDTA) [Fig 2.3A]. ISG20L2 degraded miR-151-UU and miR-151-AA at similar rates, with greater efficiency than miR-151 and miR-151-CC [Fig. 2.3AB]. Degradation experiments in the presence of non-radioactively labelled miR-151 (cold miR-151), reveal a protective effect of the cytosine additions [Fig. 2.3B]. NAF and IACAM mutants degraded miRNAs with a reduced efficiency compared to WT, particularly the double mutant IACAM [Fig. 2.3B]. Therefore, ISG20L2 residues D267, D183 and E185 are involved in the exoribonucleolytic enzymatic activity.

Poly(U) and poly(A) stretches of 30 nucleotides were used with the aim of revealing a potential substrate preference not visible in our experimental setting when comparing miRNAs which only differ in two terminal nucleotide additions. U30 3' ends were degraded more efficiently by ISG20L2 than A30 3' ends [Fig. 2.3C]. NAF and IACAM mutants degraded U30 at a similar rate than the WT, while showing a reduced A30 degradation, as if poly(U) degradation was so favoured than even overcomes the active site mutations [Fig. 2.3C]. While degradation bands in Fig. 2.3AB were very diffuse and did not show specific bands, degradation smear in Fig. 2.3C presented a differential degradation pattern between U30 and A30.

These results show ISG20L2 is able to degrade miRNAs and its catalytic activity can be modulated by miRNA 3' end nucleotides.

2.3. ISG20L2 is upregulated in T cell stimulation

ISG20L2 expression was evaluated in resting human CD4+ T cells samples isolated from human donors and stimulated with αCD3αCD28, or with type I IFN. Cells were incubated for 6 to 72 h and analysed by Western Blot. A representative western blot image is shown in Fig 2.4A, together with ISG20L2 kinetics for both activations with seven donors [Fig. 2.4B]. ISG20L2 was upregulated after activation in every donor, except for D5, which counted with higher ISG20L2 basal levels maintained through stimulation.

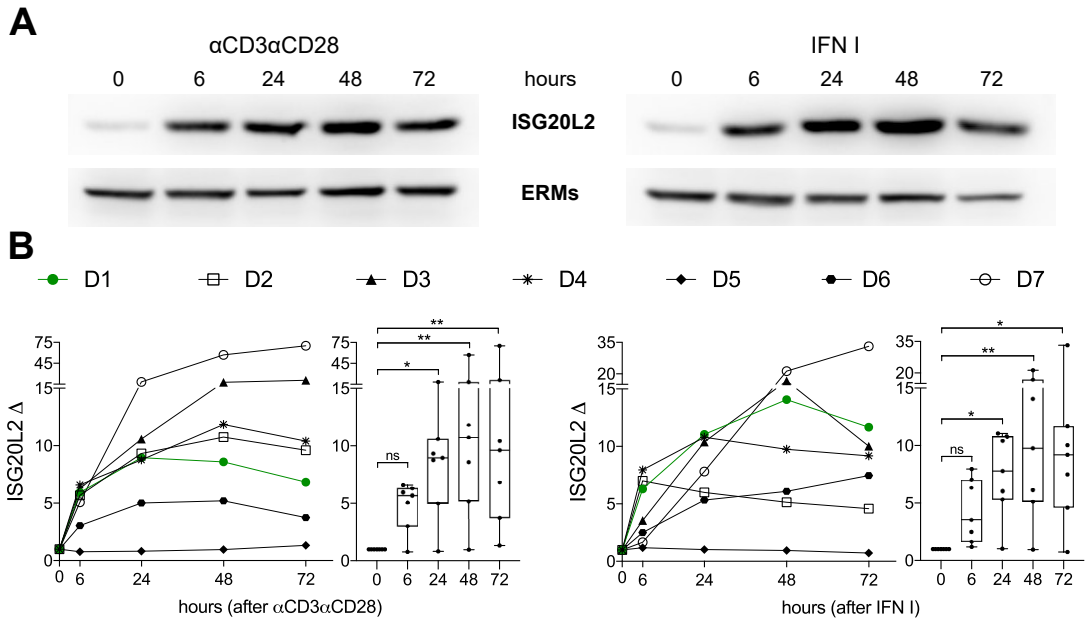

Figure 2.4. ISG20L2 is upregulated in human T cells upon stimulation.
CD4+ resting T cells were isolated from healthy human donors and stimulated either with antibodies αCD3αCD28 (left panels) or with type IFN I (right panels). Cells were incubated for 6 to 72 h and analysed by Western Blot. A) Blot images obtained for a representative donor (D1). B) ISG20L2 fold change increment taking 0 h as a reference, measured for seven donors. Statistical analysis: Kruskal-Wallis test, Dunn's multiple comparisons test [* p-value <0.05, ** p-value<0.01, ns: non-significant].

2.4. ISG20L2 silencing using CRISPR-Cas9

Three sequences were selected for CRISPR-Cas9 targeting in ISG20L2 exon 2 using the web-based tool CHOPCHOP (133,149) [Fig. 2.5A]. Targets 8 and 6, closer to the translation initiation site were chosen attempting to disrupt protein translation as soon as possible. Target 1 is located in the predicted catalytic region (which is extended also along exons 3 and 4). sgRNAs were designed for the selected targets and included individually in the plasmid pSpCas9(BB)-2A-GFP (PX458) (132). These plasmids were electroporated in pairs with the aim of removing the region between each couple. GFP expression allowed cell sorting of the positively transfected cells [Fig. 2.5B]. Gene editing is expected to occur in a fraction of GFP+ cells, generating a pool of ISG20L2 WT, HT and KO cells [Fig. 2.5B]. Probably due to a relatively short life span, testing ISG20L2 expression in this GFP+ pool revealed silencing was achieved after 48 h [Fig. 2.5C].

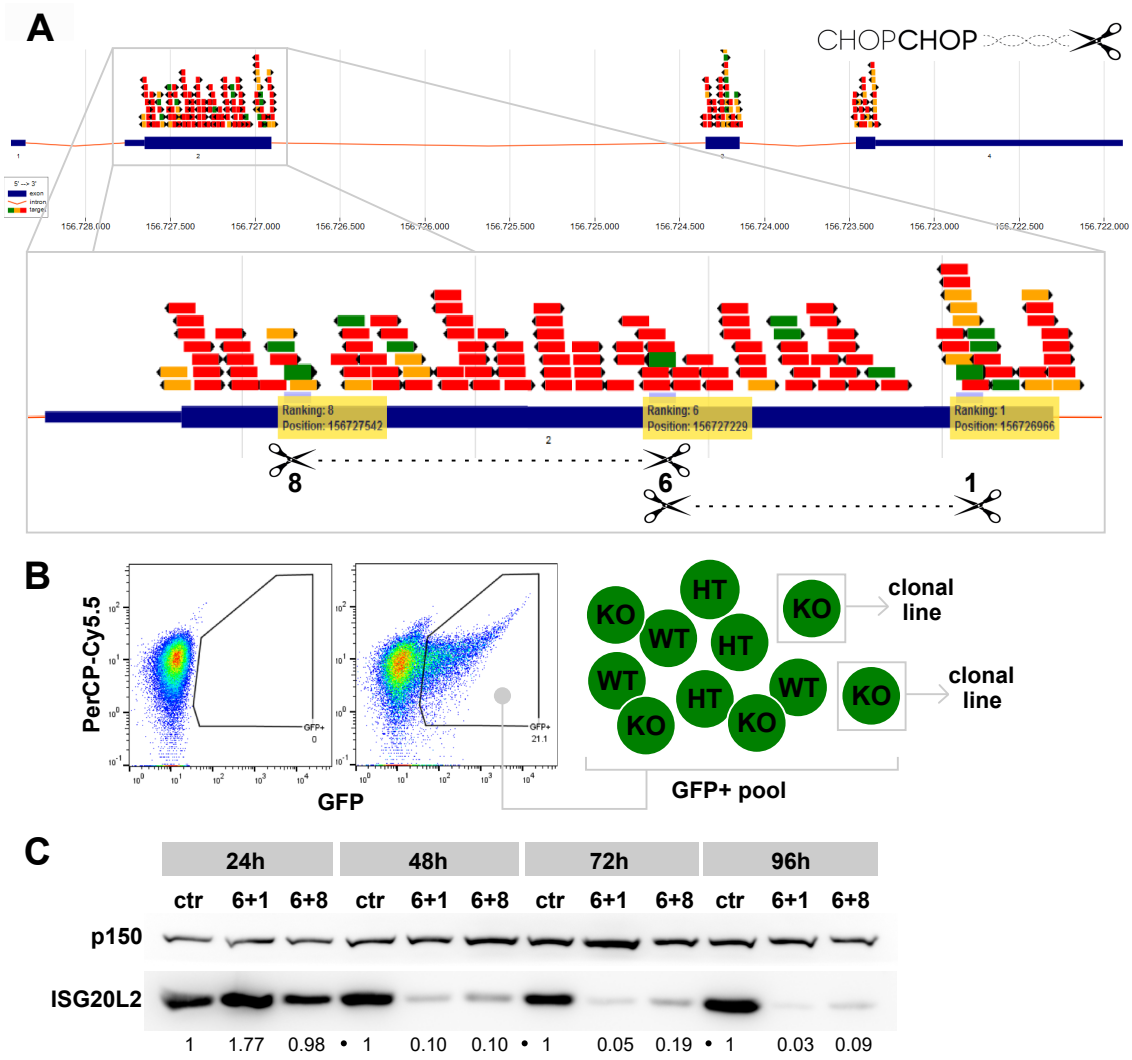

Figure 2.5. ISG20L2 is silenced 48h after CRISPR-Cas9 electroporation.
A) Location of the 3 target positions selected in exon 2 with CHOPCHOP. B) Positively electroporated cells were sorted for GFP+ expression and either used as a pool or further cultured to obtain clonal lines from single cells. C) ISG20L2 silencing in GFP+ pool (obtained with two different strategies: targeting 6+1 or 6+8 positions) at various time points. ISG20L2 expression has been quantified taking p150 as loading control, and normalizing each time point to the expression of the control sample (electroporated with CRISPR-Cas9 without sgRNA).

In order to generate clonal KO cell lines, GFP+ sorting was also performed collecting single cells into 96-well plates. Interestingly, these cells only survived when cultured in pre-conditioned media. A total of 31 clones were isolated following 6+1 strategy; and 9, with 6+8 [Fig 2.6]. Although punctual mutations may have occurred, deletion of the region delimited by the target pair (582 nt, 6+1; 554 nt, 6+8), was analysed finding 4 hetero clonal lines [Fig. 2.6A].

Isolated lines presented variable ISG20L2 expression [Fig. 2.6B]. The largest ISG20L2 reduction was observed for the clone HT(6+8/6) [Fig. 2.6B]. However, since

ISG20L2 expression was not completely abrograted and with the aim of obtaining a set of clones to test as biological replicates in functional experiments, a second round of electroporation was performed. HT23(6+1) was electroporated again with plasmids targeting 6 and 1, and HT6(6+8) with 6 and 8. Again if a whole KO (with both 8-6 or 6-1 regions removed, not only punctual mutations) was generated, it did not survive, since we only found HT clones through genotyping [Fig. 2.7AC]. Only 2 clonal lines were isolated for 6+1 with a moderate reduction in ISG20L2 expression [Fig. 2.7B]. 6+8 strategy yielded 83 clones, including two WT lines, most likely due to contamination of the J77 culture used to generate the pre-conditioned media. Fig. 2.7D shows ISG20L2 expression for a representative group of HT6(6+8)/1-83 clones. Clones without ISG20L2 expression were selected for functional experiments described later (2.6). Control WT clones to compare with ISG20L2 KO lines were generated following the same proccess of two round electroporation but transfecting a CRISPR-Cas9 plasmid without sgRNAs.

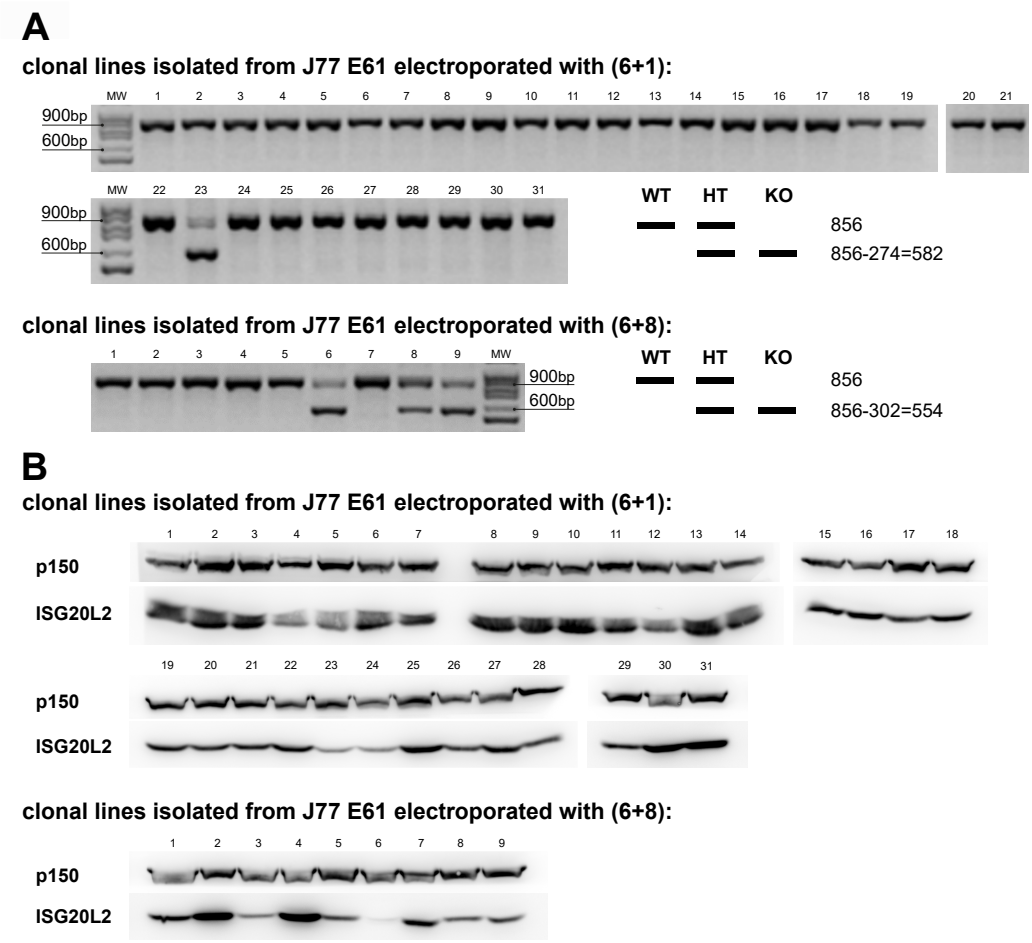

Figure 2.6. First round clonal cell lines genotyping and phenotyping.
A) Genotyping of clonal lines obtained after single cell sorting to a 96-well plate. Bands diagram specifies the size of WT and KO bands and expected for each targeting strategy. B) Analysis of ISG20L2 protein expression by western blot. p150 is included as a loading control.

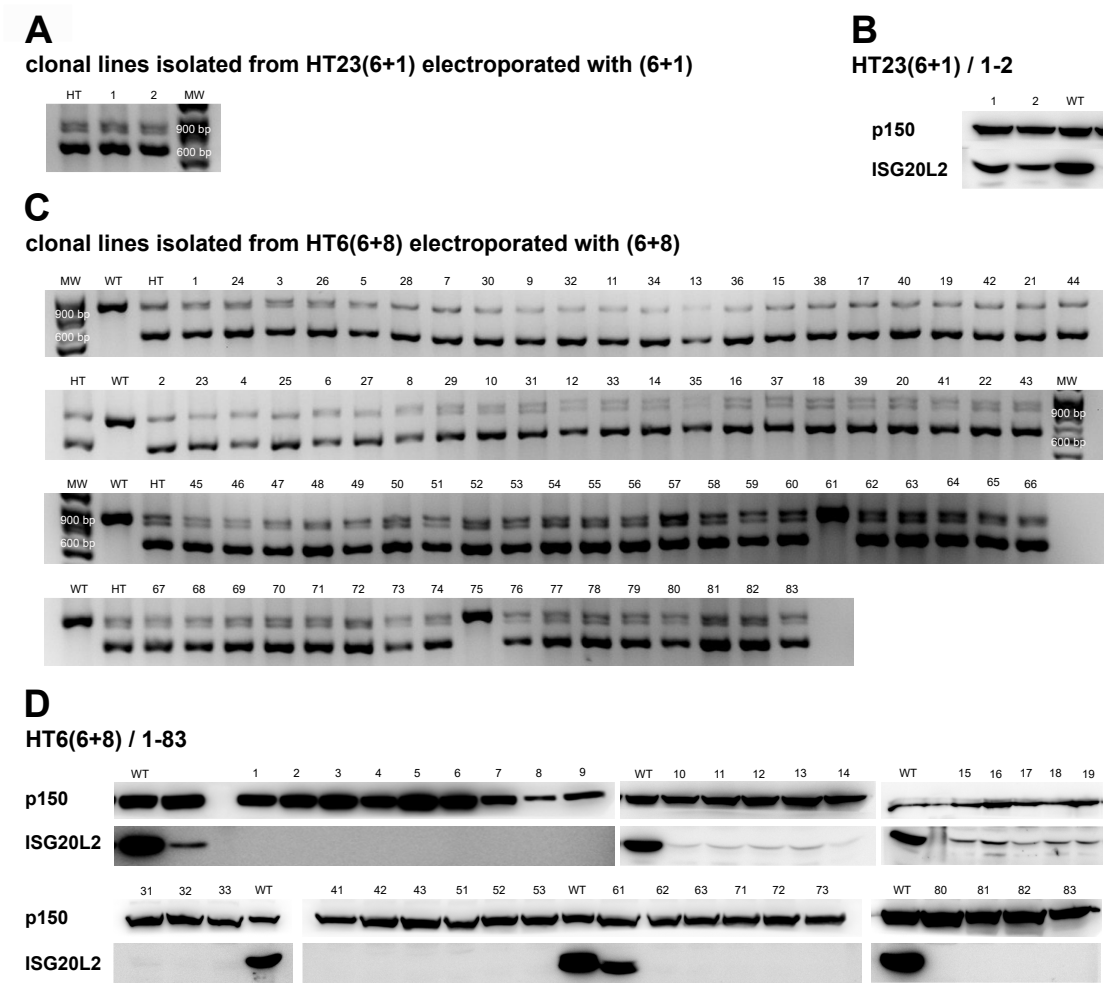

Figure 2.7. Second round clonal cell lines genotyping and phenotyping. A,C) Genotyping of clonal lines obtained after HT electroporation repeating the corresponding initial targeting strategy. B,D) Analysis of ISG20L2 protein expression by western blot. p150 is included as a loading control.

2.5. RNA and smallRNA changes upon ISG20L2 silencing

In order to gain an understanding of the substrates ISG20L2 may target in T cells, an NGS experiment was performed, expecting specific targets would be accumulated in the absence of the exoribonuclease. Considering the kinetics of ISG20L2 silencing upon electroporation of CRISPR-Cas9 plasmids with specific sgRNAs [Fig. 2.5C], 72 h was selected to compare RNA repertoire between control and knockdown samples [Fig. 2.8A]. A temporary silencing method was chosen to avoid potential compensations that may occur in established clones. Both smallRNA and mRNA were sequenced, in an attempt to cover a wider range of potential substrates.

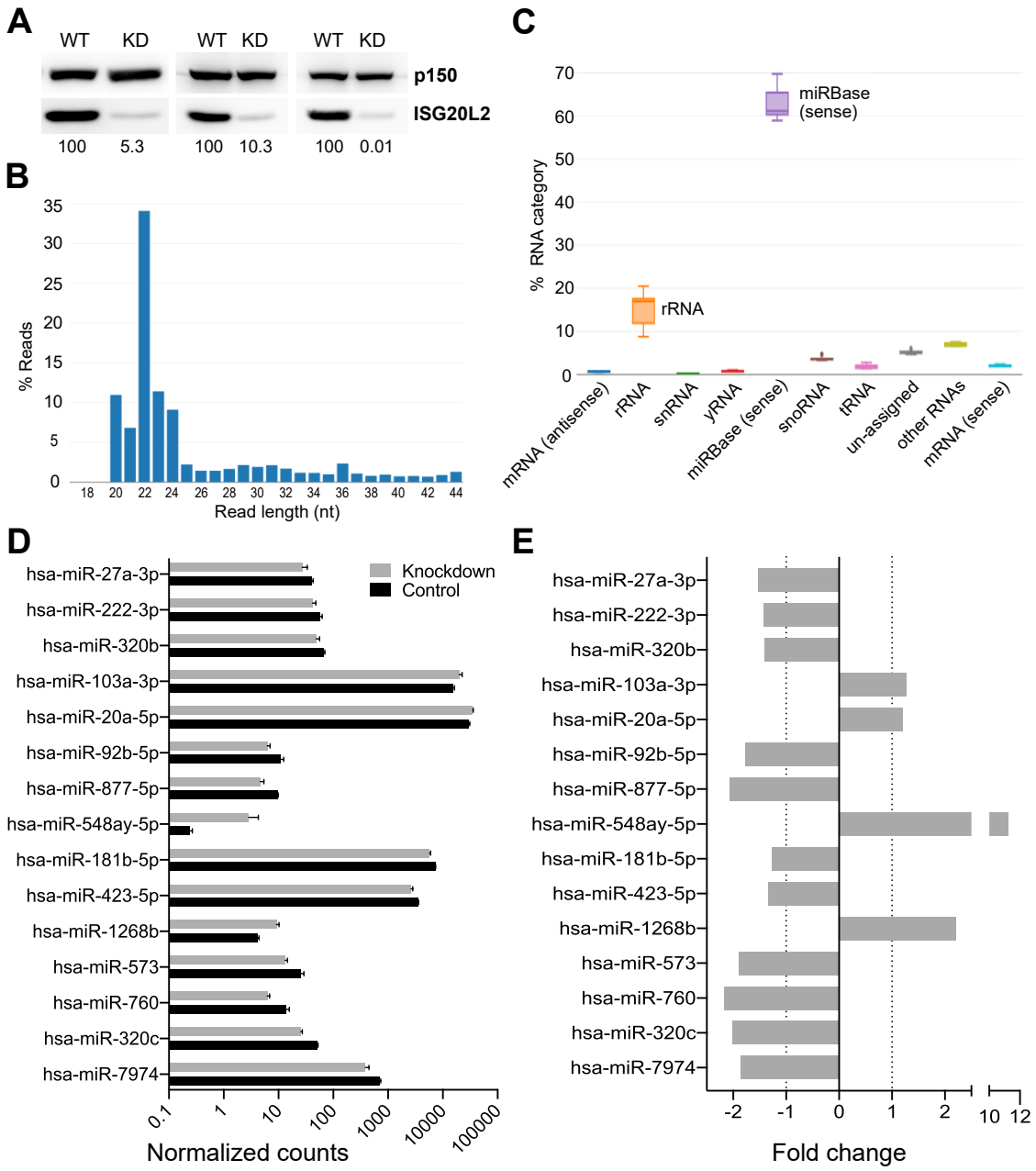

Figure 2.8. ISG20L2 silencing in J77 cells did not elicit a substantial change in miRNA expression.
A) ISG20L2 expression in sequenced samples. B) Read length distribution for a representative sample. C) Abundance of specific RNA types D) Normalized total counts (CPMs) detected for the 15 miRNAs with differential expression (log scale). E) Limma estimated fold change for the 4 miRNAs upregulated in ISG02L2 knockdown, and the 11 downregulated.

SmallRNAseq was performed preparing libraries with a larger size than usual for this kind of sequencing, with the aim of opening the possibility of detecting a differential expression in other small RNAs apart from miRNAs. For this reason, the read length detected varies between 20 and 44 nt, although it has a clear peak around the usual

miRNA size (22nt) [Fig. 2.8B]. In fact, the presence of other small RNAs was very limited [Fig. 2.8C]. A total of 597 miRNAs were detected in our samples, four of which: miR-92a-3p, miR-7-5p, miR-148a-3p and let-7f-5p accounted for almost 50% of the normalized counts (data not shown). 15 miRNAs were differentially expressed (adjusted p-value < 0,10): 4 upregulated and 11 downregulated in ISG20L2 knockdown samples [Fig. 2.8DE]. Five differentially expressed miRNAs were detected with CPMs over 500, while the other ten did not sum more than 70 CPM on average [Fig. 2.8D].

We wonder whether ISG20L2 could be modifying the landscape of miRNA post-transcriptional modifications, beyond its limited effect in miRNA expression. To assess this possibility PTMs were plotted for the total amount of detected miRNAs and for the upregulated and downregulated subsets [Fig. 2.9]. ISG20L2 knockdown does not seem to exert any effect in the miRNA PTMs profile.

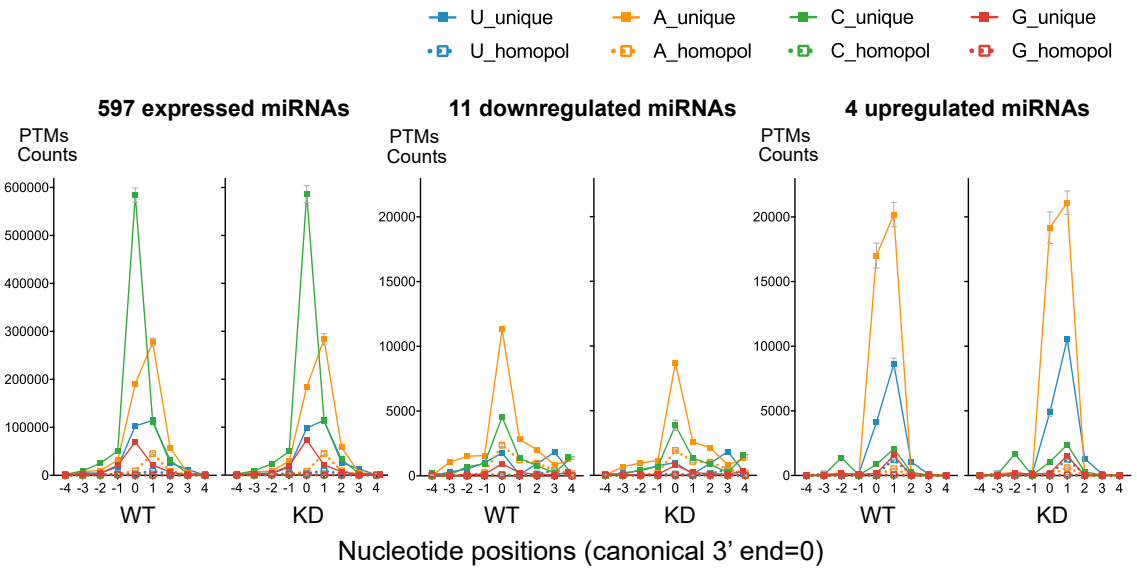

Figure 2.9. ISG20L2 does not alter miRNA PtMs profile.
PtMs profile generated by Chimira for all detected miRNAs (left), downregulated miRNAs (middle) and upregulated miRNAs (right). Plots included the most abundant PtMs (mono-additions: U, A, C, G; and oligo-additions: ≥UU, ≥AA, ≥CC, ≥GG) at positions -4 to 4 of '3p-end'. Mono-additions refer to the specific nucleotide on their own or followed by a different nucleotide, but not followed by the same nucleotide. Oligo-additions include PtMs with two or more equal nucleotides.

Differential expression analysis of NGS RNA sequenced revealed three genes with adjusted p-value <0.1: RPL22L1(fold change, -1,30X), EEF1A1 (1,10X) and the silenced ISG20L2 (-1,56x). Table A.6 (annexes) shows data for the 50 genes with lower p-values detected for differential expression. This list includes ribosomal proteins, several lncRNA (long non-coding RNAs), and interestingly a series of molecules related with immune response, such as CD69 (marker of activation and immunoregulator (150)), LEF1

(transcription factor which binds to the TCR enhancer (151)), RHOH (regulates integrin LFA-1 avidity (152,153)) or AQP3 (involved in T cell migration toward cytokines (154)).

Enriched 'canonical pathways', 'molecular and cellular functions' and 'physiological system development and function' predicted by IPA are presented in Fig. 2.10. This analysis was performed including molecules with an adjusted p-value<0.5, a total of 1499. Threshold p-values of 0.3 and 0.4 were also evaluated with a more limited number of molecules, 35 and 204, respectively. The most prominent difference was the effect on the EIF2 (eukaryotic initiation factor-2) signalling pathway, involved in translation initiation, which could be related with ISG20L2 role in ribosome biogenesis.

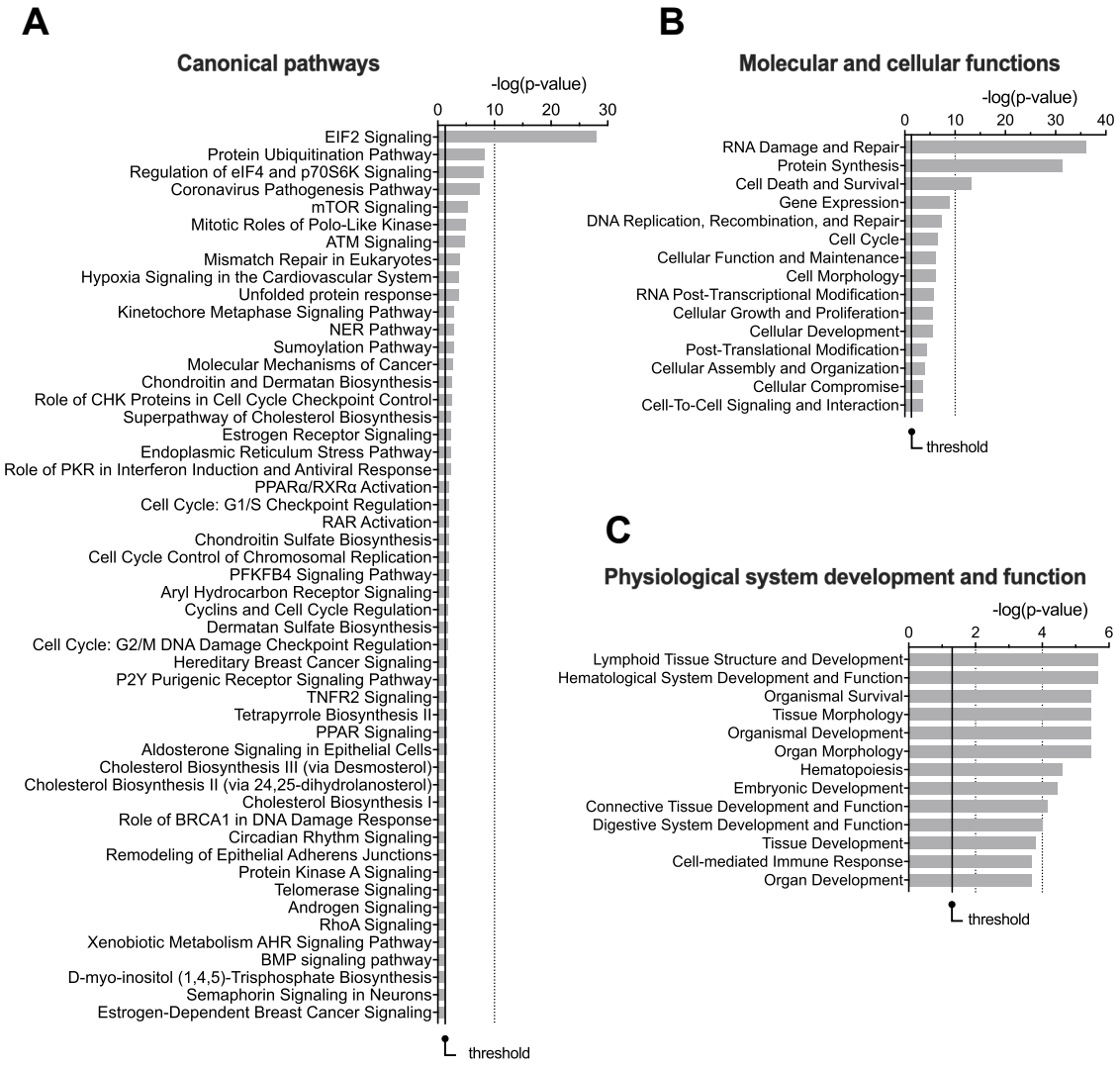

Figure 2.10. ISG20L2 mRNAseq IPA core analysis.
Ingenuity pathway analysis of mRNAseq molecules with a differential expression between control and ISG20L2 knockdown samples detected with an adjusted p-value<0.5 (p-value <0.05254), considering experimentally observed and predicted data, and direct and indirect relationships. A) Canonical pathways. B) Molecular and cellular functions. C) Physiological system development and function.

Molecules selected for qPCR analysis include some of those with lowest p-adjusted values for differential expression and molecules selected considering IPA enrichment functions analysis [Fig. 2.11]. Among the molecules with lowest p-values we could confirm ISG20L2 silencing, H2AX downregulation and CD69 upregulation [Fig. 2.11AB]. RPL22L1 downregulation and EEF1A1 upregulation were not significant by qPCR [Fig. 2.11A]. Several lncRNA were analysed among those with lowest p-value or higher fold change for differential expression, without finding significant differences [Fig. 2.11C]. However, upregulation of several immunoregulatory molecules (AHR, NKG2D, CTLA4, CD137, TIM3 and PD-L1) besides CD69, was detected in ISG20L2 knockdown samples [Fig. 2.11B]. This list of molecules was gathered after IPA analysis pointed to an upstream role of the immune regulatory molecules NKG2D (with target molecules in dataset with adj. p-values<0.30: CD69, LEF1) and CTLA4 (targets with adj. p-value<0.30: CD69, TENT5C). In addition, AHR (Aryl hydrocarbon receptor) signalling was one of the canonical pathways predicted to be dysregulated [Fig 2.10A]. AHR, NKG2D, CTLA4 and CD137 had been excluded from the RNAseq differential expression analysis because their expression was not detected over the established threshold (1 CPM in at least 3 samples). TIM3 accumulated 1,14 CPM in control and 0,90 CPM in knockdown samples; and PD-L1 1,35 and 1,35 CPM, respectively. Most likely, RNAseq sensitivity, lower than qPCR one, is not enough to detect the changes in these molecules at the level they are expressed in this context.

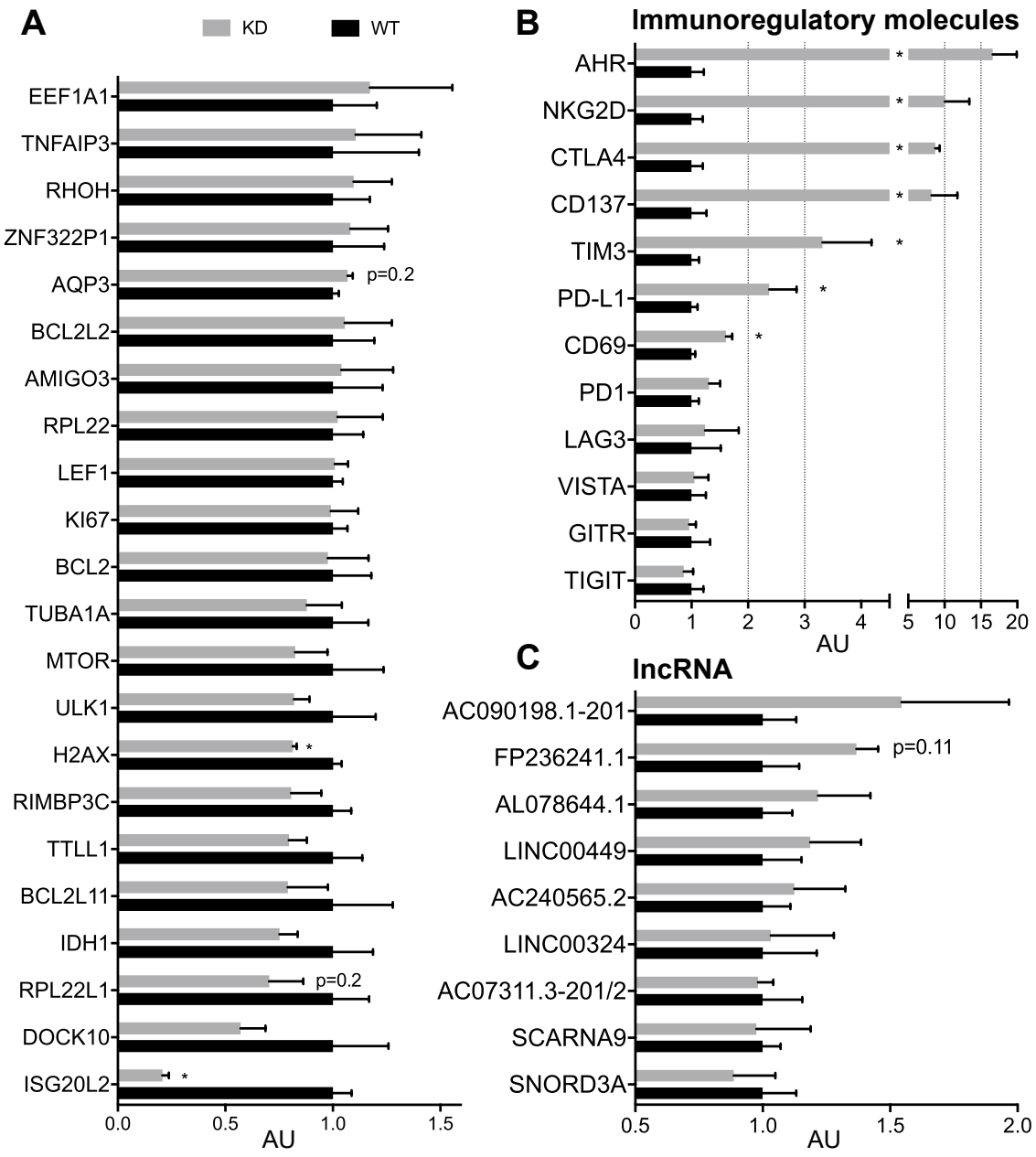

Figure 2.11. ISG20L2 silencing upregulates a set of immunoregulatory molecules.
qPCR performed in control and ISG20L2 samples from four independent experiments. A) RNAseq molecules with low p-adjusted values for differential expression and molecules selected after consideration of IPA results on enriched functions. B) Immunoregulatory molecules detected to be upregulated by RNAseq (CD69), relevant in IPA analysis (AHR, NKG2D, CTLA4) and others. C) LncRNA detected by RNAseq to be differentially expressed with low p-values and/or higher fold changes.

2.6. ISG20L2 function in T cells

In order to gain an understanding of ISG20L2 function in T cell activation, a series of experiments were performed evaluating clonal ISG20L2 KO J77 T cell lines (generated as detailed in 2.4). ISG20L2 KO clones were co-cultured with Raji cells (a B lymphocyte line able to act as APC for J77) in the presence or absence of SEE. Cell proliferation was assessed following the decrease of Cell Violet staining up to seven days and measuring Ki67 intracellular staining after activation. Cell Violet geometric Mean Fluorescence Intensity (gMFI) did not present any significant changes up to day 3, while at day 4 ISG20L2 KO showed a slight delay compared with control cells, observed as a

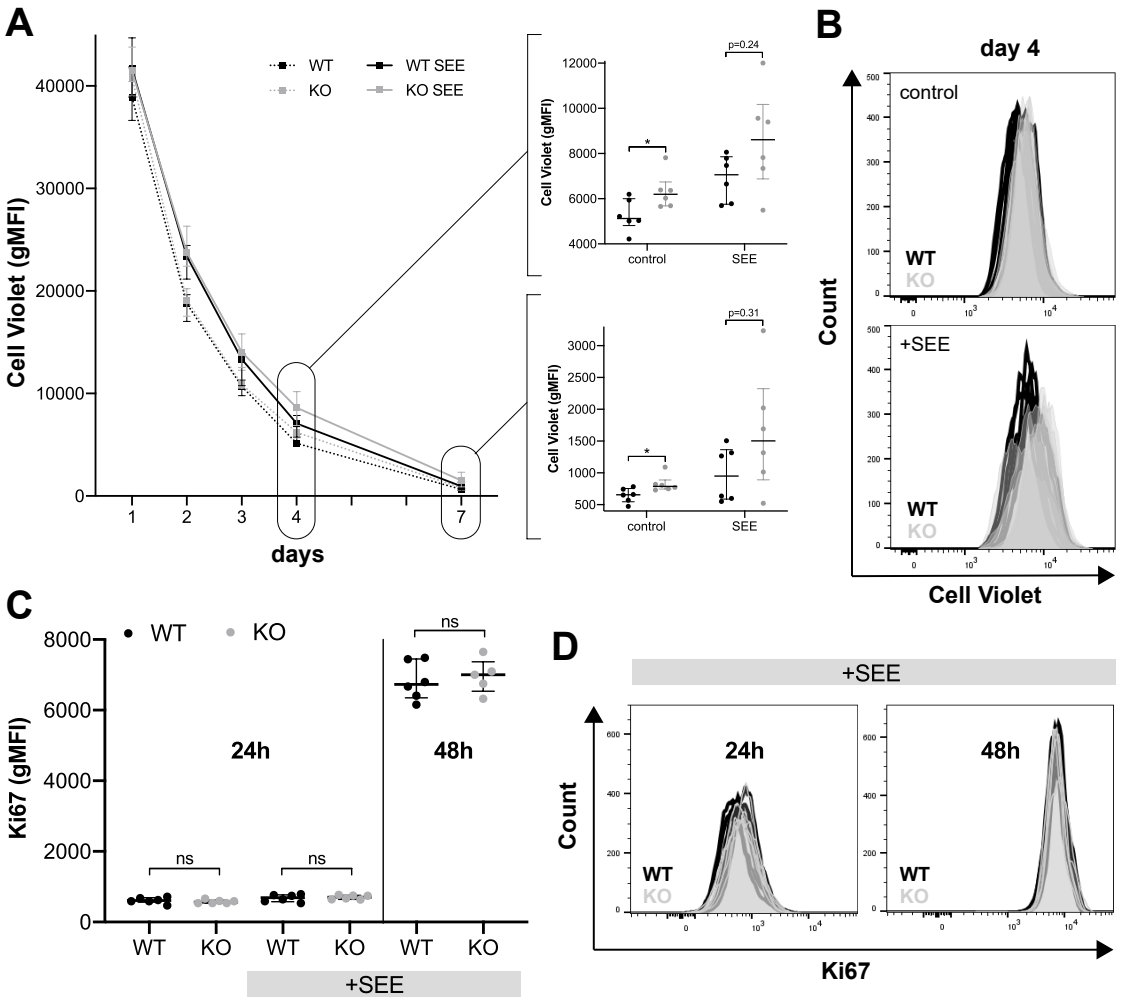

Figure 2.12. ISG20L2 absence does not impair T cell proliferation.
Raji cells and WT or ISG20L2 KO T cell clones were cultured with and without SEE. A) Cell Violet geometric Mean Fluorescence Intensity (gMFI) with scatter dot plot included at days were significant differences were detected. B) Cell Violet plots at day 4: KO samples are represented with gray colouring and gray contour and WT samples with black thick contour. C) Ki67 gMFI at 24h for unstimulated T cells and at 24 and 48 h for cell cultures with SEE. Dead cells were discarded with TO-PRO-3. T cells were gated as cell violet positive cells (A,B) or CD19 PerCP-Cy5.5 negative cells (C,D).

trend with high dispersion in SEE cultures [Fig. 2.12A]. However, this small difference was barely observable [Fig. 2.12B]. In addition, both control and KO cells presented similar Ki67 (expressed in proliferating cells (155)) basal levels, which were increased at 48 h after stimulation [Fig. 2.12CD]].

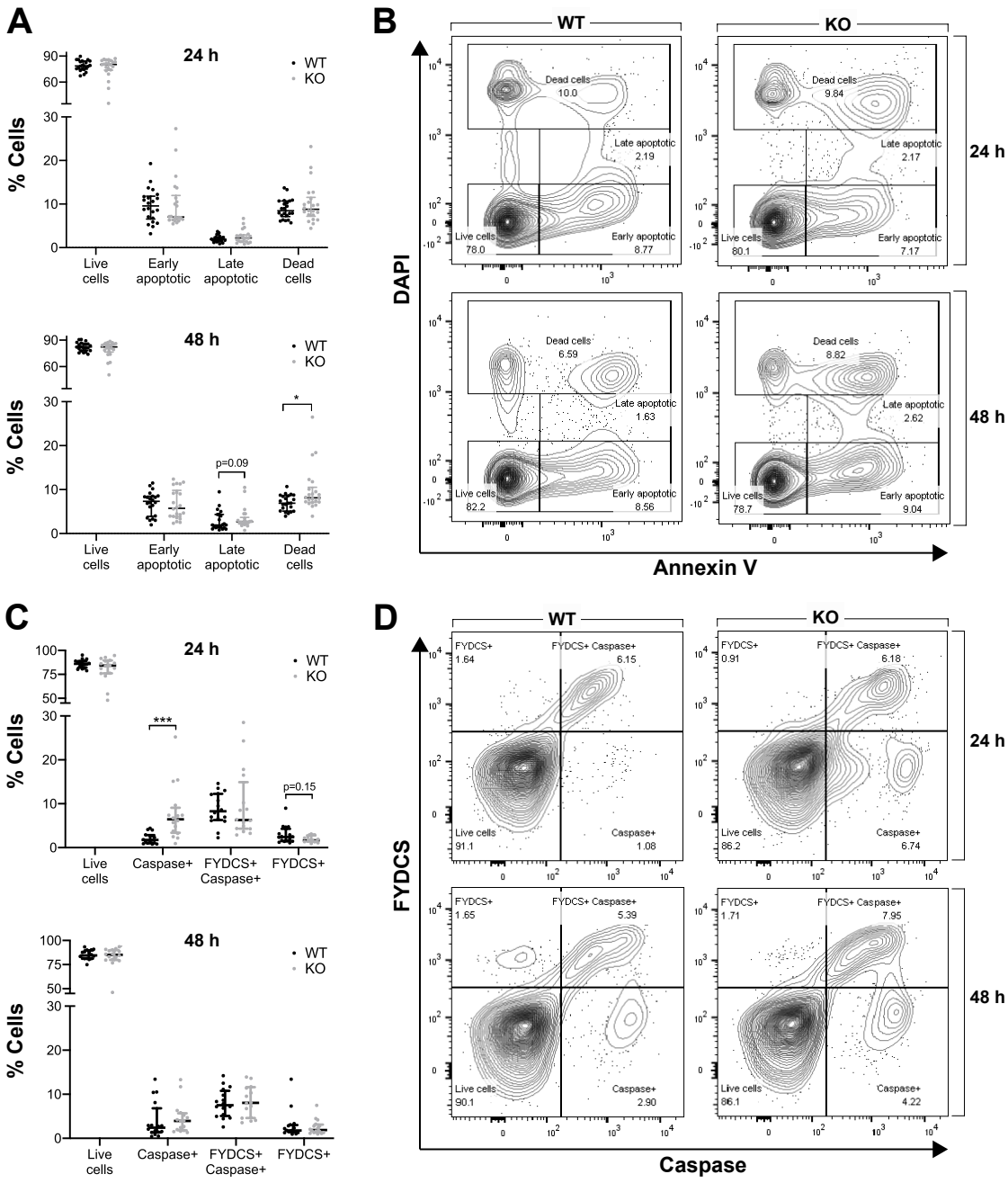

Figure 2.13. ISG20L2 absence does not substantially affect cell viability. WT or ISG20L2 KO T cell clones were cultured with PMA and ionomycin for 24h and 48 h. A,B) DAPI (cell viability dye) and Annexin V staining. C,D) FYDCS (Fixable Yellow Dead Cell Stain) and Cleaved Caspase-3 intracellular staining. All plots show whole flow cytometry recorded events after a unique gating step excluding debris with very low side and forward scatter.

To test specifically whether ISG20L2 had an effect on cell viability and apoptosis, Annexin V staining and Cleaved Caspase-3 expression (as markers of apoptotic cells (156,157)) were evaluated upon PMA and ionomycin stimulation. ISG20L2 KO cells presented a higher percentage of apoptotic cells in caspase staining, but no differences were observed in Annexin V at the same time. ISG20L2 KO percentage of dead cells was higher at 48h in Annexin V staining, while the same data was not found for caspase. ISG20L2 deficiency could have a detrimental role in cell viability, but it does not seem an essential factor for cell survival.

Surface markers of activation CD69 and CD25 were also evaluated by flow cytometry [Fig 2.14]. CD69 was detected in RNAseq and qPCR as a mRNA upregulated upon ISG20L2 silencing. Consistently, ISG20L2 KO clones present higher CD69 surface expression, both in percentage of CD69+ T cells [Fig. 2.14AC] and abundance of CD69 per cell [Fig. 2.14B]. However, both WT and KO clones are able to upregulate CD69 upon activation at similar levels. CD25 was monitored as an additional surface marker expressed upon T cell activation. ISG20L2 KO cells showed a reduced CD25 expression both in basal and activation conditions, at population and single cell levels [Fig. 2.14, CDE]. Cells were tested at 24 and 48 h in J77:Raji cell culture ratio 1:1, while at 20h, ratio was 1:10. This reduced ratio was tested as a method to reduce Raji 'contamination' for subsequent qPCRs experiments and here we can observe these cells were activated at comparable levels.

To evaluate whether synaptic contacts between T and B cells were occurring with KO ISG20L2 T cells in a similar way than with control cells, these co-cultures were analysed by immunofluorescence. B cells were previously stained with CMAC, and co-cultured with T cells during 30 min. Conjugated T cells were quantified as T cells presenting an actin accumulation towards the contact site with B cells [Fig. 2.15AB]. The proportion of T cells forming synaptic contacts was similar for WT and KO clones, with and without SEE [Fig. 2.15B]. CD3ε, a 20kDa subunit of the TCR complex (T cell receptor includes: two CD3ε, CD3γ, CD3δ, CD3ζ and a heterodimer of α/β or γ/δ chains) is accumulated at the immune synapse (IS) [Fig. 2.15A]. CD3ε accumulation ratio at IS in ISG20L2 KO cells was 2.7, while WT cells doubled this number [Fig. 2.15C]. Fig. 2.15A shows a representative image with accumulation of CD3ε in KO cells at values very close to median population, and a diverse range of WT CD3ε increments at IS.

Distance of synaptic T cell MTOC (Microtubule-organizing centre) to the surface of Raji cell (modelled with Imaris software [Fig. 2.15D]) was also quantified [Fig. 2.15E]. Here, ISG20L2 KO cells showed a slight increase in MTOC-APC distance [Fig. 2.15E].

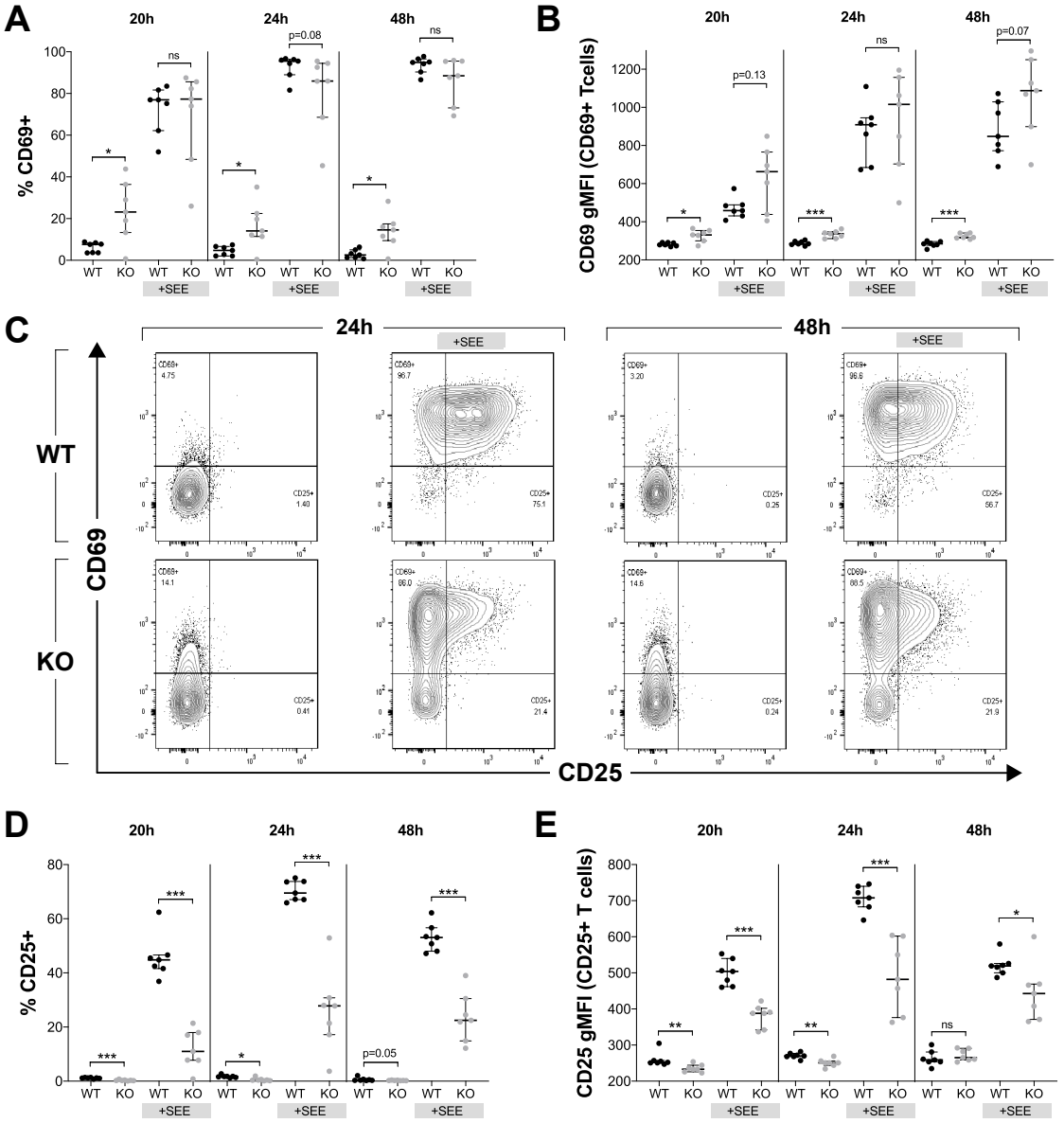

Figure 2.14. ISG20L2 regulates CD69 and CD25 expression.
WT or ISG20L2 KO T cell clones were cultured with Raji cells at 1:1 ratio (24 and 48h) and 10:1 (20h). Propidium Iodide was used to remove death cells, and CD19 to exclude B cells. A) Percentage of CD69+ T cells at 20, 24, and 48 h, cultured with or without SEE. B) Geometric Mean Fluorescence Intensity (gMFI) CD69+ T cells. C) Representative WT and KO plots. D) Percentage of CD25+ T cells at 20, 24, and 48 h, cultured with or without SEE. E) gMFI of CD25+ T cells.

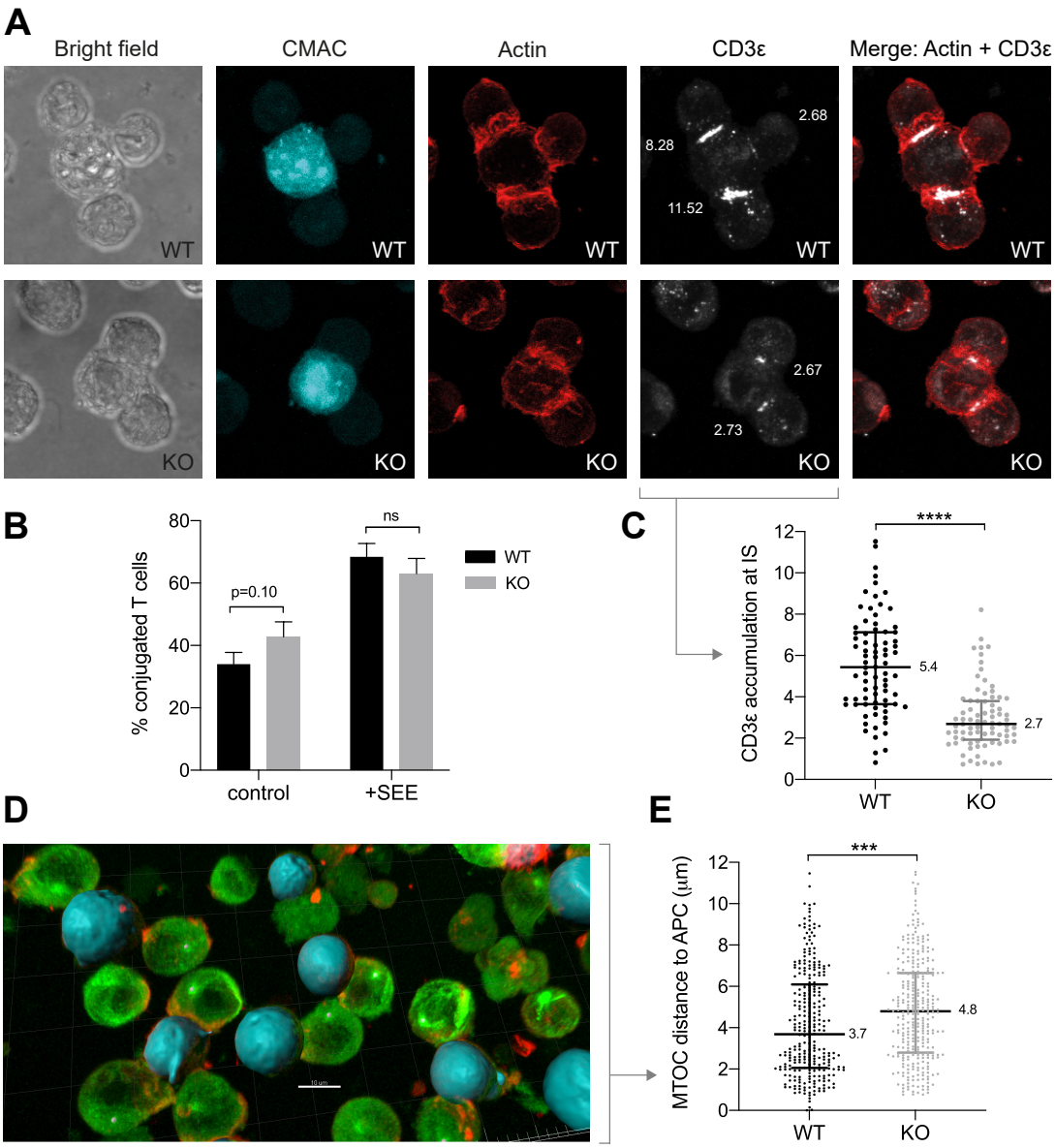

Figure 2.15. ISG20L2 is involved in CD3 accumulation at IS.
A) Representative Bright field, CMAC, Actin, CD3ε and merge (Actin+CD3ε) for WT and ISG20L2 KO T cells incubated with Raji (CMAC+) in the presence of SEE. B) Percentage of conjugated T cells quantified as T cells in contact with B cells presenting enriched actin staining towards the B cell. C) CD3ε accumulation at immune synapse (IS) quantified for WT and KO T cells in synaptic contact. CD3ε was not quantified in SEE absence, since it was not accumulated in contact areas. D) Representative image for MTOC locations and Raji (APC) surfaces modelled with Imaris software. E) MTOC distance to APC measured in μm.

Since a significant upregulation of immunoregulatory molecules (AHR, NKG2D, CTLA4, CD137, TIM3, PD-L1 and CD69) was previously detected in J77 cells 72 h after electroporation with CRISPR-Cas9 plasmid, qPCR analysis was performed in co-culture samples to evaluate the expression of these molecules in clones and the effect of activation. A trend towards higher level of AHR, CD137, TIM3, PD-L1, CD69 and GITR

(p-values <0.3) was detected in KO clones in the absence of SEE [Fig. 2.16]. Strikingly, NKG2D, CTLA4 and PD-1 molecules seem to display a reduced expression in activated established clones (p-values: 0.05-0.14) [Fig. 2.16]. Although CD69 protein overexpression in KO clones was significant when evaluated in flow cytometry, at mRNA level showed an increase supported only by a p=0.21 value [Fig. 2.16].

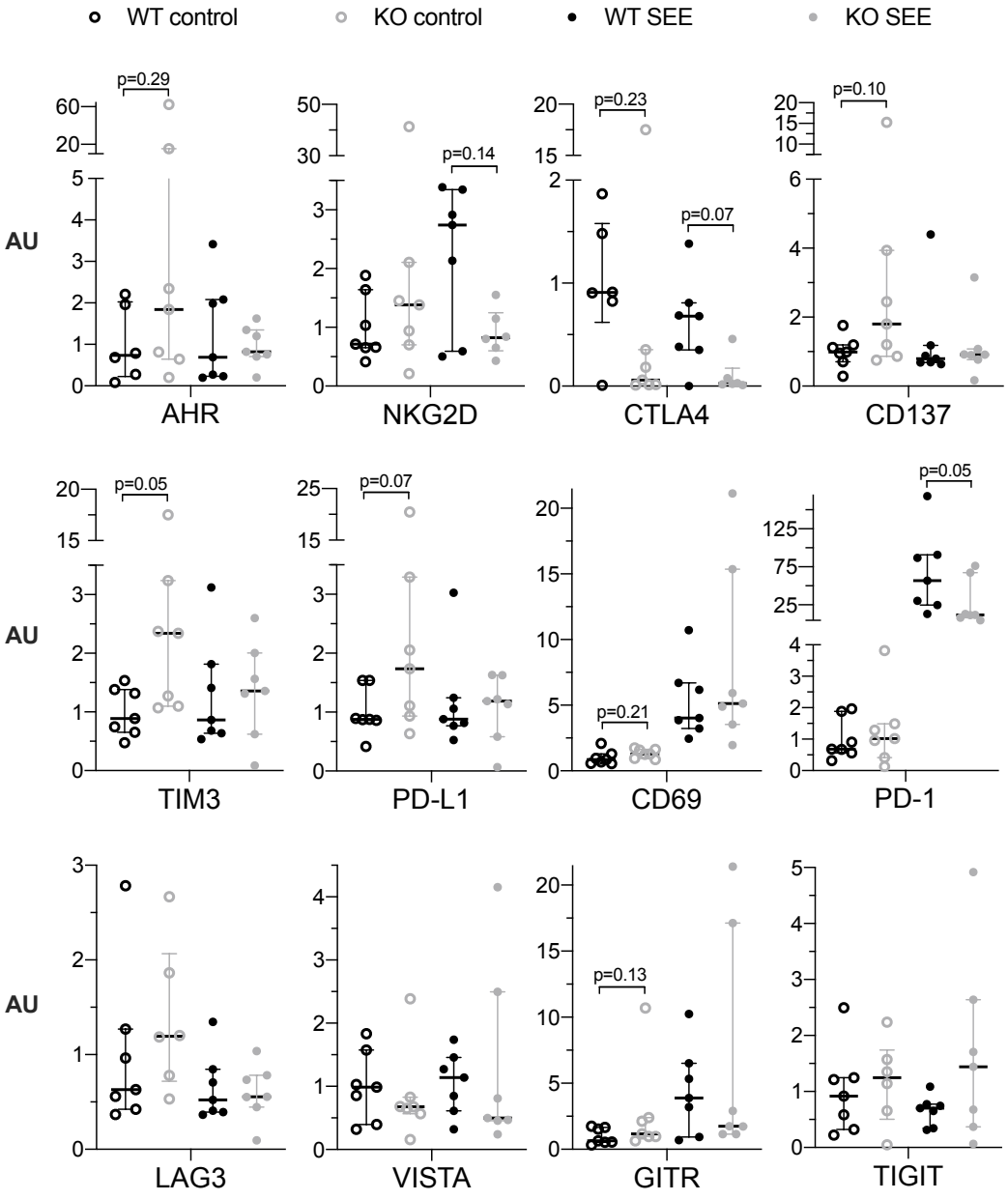

Figure 2.16. Immunoregulatory molecules expression in ISG20L2 KO clones. mRNA expression of indicated molecules in Raji:T cell clones (ratio 1:10) co-cultures, performed after 5 h incubation in absence (control) or presence of SEE. Data belong to a representative experiment including 7 WT clones and 7 KO clones. Mann-whitney test, indicated in text: p-values<0.30.

Other molecules where also tested by qPCR: H2AX, AQP3, LEF1, BCL2L2 (selected from RNAseq), BCL2, BIM, Ki67 (involved in survival and proliferation), CD25, IL2 and IFN (as markers of T cell function) [Fig. 2.17]. AQP3 showed a trend towards an increase in ISG20L2 KO, observed previously in RNAseq data. LEF1 was upregulated in ISG20L2KO stimulated samples. Consistently with flow cytometry results, CD25 mRNA was also down-regulated in KO clones. Interestingly, IL2 mRNA shows higher

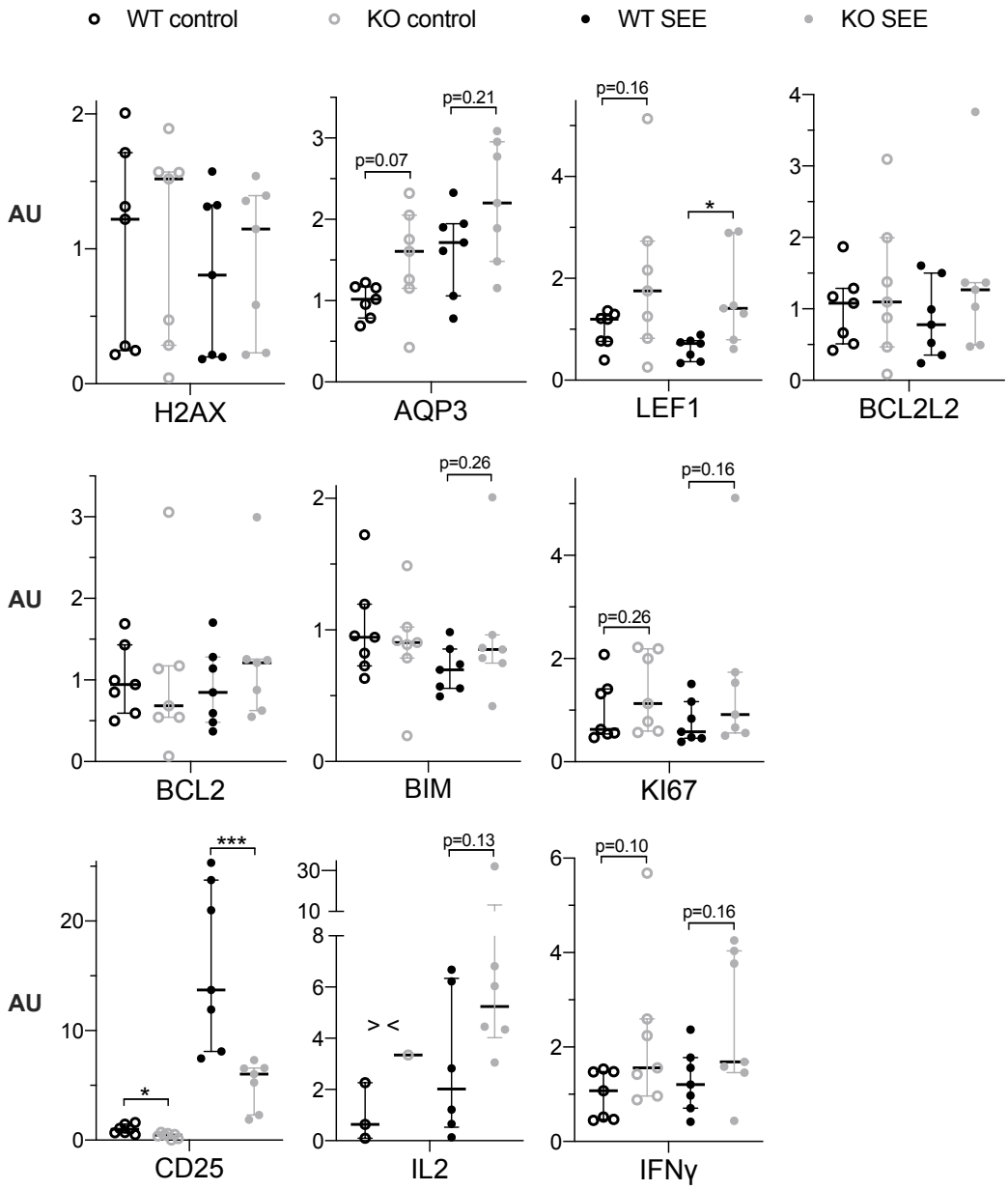

Figure 2.17. Essential molecules in T cell activation are dysregulated in ISG20L2 KO clones.
mRNA expression of indicated molecules in Raji:T cell clones (ratio 1:10) co-cultures, performed after 5 h incubation in absence (control) or presence of SEE. Data belongs to representative experiment including 7 WT clones and 7 KO clones.
>< (statistical analysis not performed since IL2 was only detected in 1 KO sample)
Mann-whitney test, indicated in text: p-values<0.30.

median values (although not significant) in ISG20L2 KO co-cultures.

IL2 production of clones was stimulated with PMA and ionomycin, and measured through ELISA [Fig. 2.18]. Since we detected a higher IL2 expression in KO clones [Fig. 2.18A], we analysed again the mRNAseq data performed upon ISG20L2 silencing searching for potential factors involved in IL2 expression. Within the list of potential candidates, Jun and Egr-1, transcription factors involved in IL2 production, may account for the IL2 upregulation in knockdown samples [Fig. 2.18B].

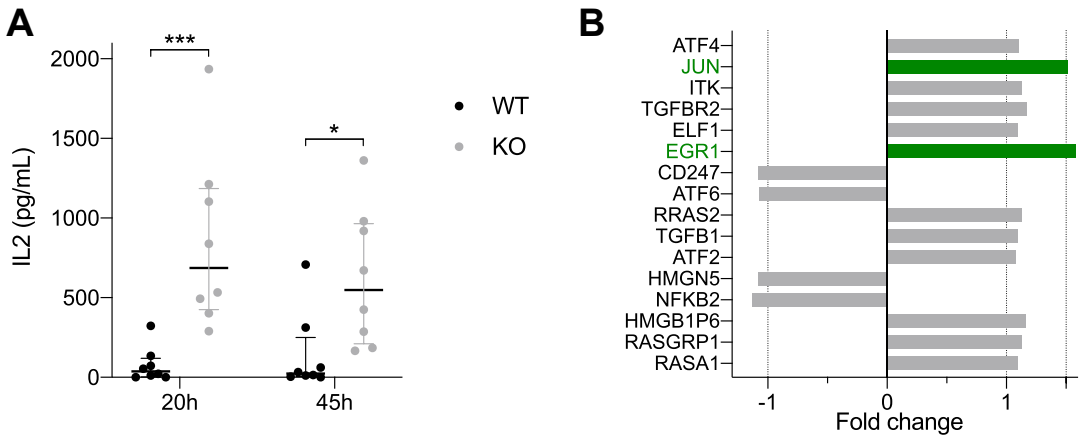

Figure 2.18. ISG20L2 impairs IL2 production.
A) IL2 expression at 24 or 48 h of PMA and ionomycin in WT and ISG20L2 KO clones. B) Molecules detected in mRNAseq as differentially expressed upon ISG20L2 silencing (adj. p-value<0.5, molecules with lower p-values are at the top of the graph) which could be involved in regulation of IL2 expression. Green corresponds with molecules of a Fold change > 1.5 in knockdown compared to control samples.

Discussion

Discussion

1. MiRNA and RNA enzymes expression upon T cell stimulation

A high number of miRNAs not previously linked with T cell stimulation were significantly down or up-regulated in response to αCD3αCD28. Two miRNAs could be highlighted for their differentiated behaviour: miRNA-1281 showed a high upregulation at early time points (3-6 h), and miRNA-4455 reached at 24 h a 122-fold increase, while no other upregulated miRNA surpassed 24-fold. MiRNA-1281 suppresses proliferation and migration in pulmonary artery smooth muscle cells, likely through targeting histone deacetylase 4 (HDAC4) (158). In osteosarcoma, miR-1281 (induced by the tumour suppressor p53) promoted apoptosis (159). MiR-4455 also exerts a tumour suppressive effect, described in gastric cancer probably due to inhibition of ADGRD1 (Adhesion G protein-coupled receptor D1) (160). ADGRD1 appears upregulated in a mouse model of gastrointestinal stromal tumour (161) and inversely correlates with patient survival in acute myeloid leukaemia (162) and glioblastoma (163). It also plays an essential role in glioblastoma growth (163,164). Consistently, miR-4455 increased apoptosis and reduced proliferation, invasion and migration in a gastric cancer cell line (MGC-803) (165). MiR-4455 targets VASP 3'-UTR and a decrease in VASP levels results in PI3K/AKT inhibition (165). VASP is a key mediator of actin cytoskeleton remodelling, polarization and cell migration (166,167). Ena/VASP proteins are part of a complex that connects signalling from TCR receptor to actin remodelling (168). A previous study used a double knock out mouse to demonstrate that EVL (Ena-VASP-like) and VASP are involved in activated T-cell trafficking into inflammation sites and secondary lymphoid tissues, particularly promoting diapedesis (169).

To our knowledge, no other study has evaluated miRNA changes in human primary T cells stimulated with type I IFN. A recent review gathered data available on IFN I regulated microRNAs, mainly in the liver cell line Huh7 and human glioma (170). Out of 36 miRNAs identified, 7 were described in two or more studies, indicating certain overlapping but also a great diversity across cell types regarding their response to IFN I (170). In fact, only one of these 36 miRNAs (miR-212) has been found as differentially expressed in our samples. Two prior studies had used immune cells: PBMCs and NK cells. MiRNAs involved in the anti-viral response against Hepatitis C virus (miR-1, miR-30, miR-128, miR-196 and miR-296) were induced in peripheral blood mononuclear cells (PBMCs) upon IFN-α treatment (171). In human NK Cells, miRNA-30e and miRNA-378

were downregulated by IFN I (172). Our study provides a novel dataset of IFN I regulated miRNAs in human primary CD4+ T cells, which comprises 24 miRNAs that are upregulated and 33 that are downregulated. Of the 57 genes modulated by IFN-I, 37 are also regulated by αCD3αCD28 stimulation. Interestingly, many miRNAs significantly upregulated in our samples, such as miR-1246 (173,174), miR-1261 (175), miR-1290 (173), miR-3196 (176), miR-3614-5p (177), miR-4301 (177), miR-4448 (178) or miR-4488 (179), also appear increased in cells infected with Dengue, RSV (Respiratory Syncytial Virus), Hepatitis C virus (HCV), Legionella pneumophila or BCG (Mycobacterium bovis Bacillus Calmette–Guerin).

IPA assessment of IFN-I and αCD3αCD28 regulated miRNAs indicates their involvement in cellular development, growth, proliferation and movement. These processes are indeed essential for activated T cells to perform their function, which includes their differentiation to effector and/or memory phenotypes to combat infection short- and long-term, respectively. In this regard, activated T cells undergo intense cellular reprogramming with an increase in mRNA and protein expression. Accordingly, activated T cells would need to control inhibitory safeguards that prevent abnormal activation that could produce autoimmunity. MiRNA regulation may act as a negative regulator of gene expression, which would need to be withdrawn, at least partially. Several studies support this hypothesis. For instance, mRNAs undergo 3' UTR shortening upon T lymphocyte activation, thereby reducing the pool of potential target sites for miRNA binding (180). Moreover, T cell activation promotes a rapid global miRNA downregulation and degradation of Argonaute proteins, which are key effectors of the RISC complex (54). We postulate that a selective active mechanism of miRNA degradation underlies the intense miRNA downregulation observed only a few hours after T cell activation. For this reason, we evaluated the expression of Eri1 and Dis3L2. Both exoribonucleases display a clear preference for uridylated RNA substrates (115,116,122); also, Eri1-deficient NK cells and T cells showed increased overall miRNAs levels (76). Here we detected a marked upregulation of both enzymes following T cell activation. Consistently, TUT4 and TUT7, which are specifically regulated by αCD3αCD28 stimulation, could be uridylating substrates for subsequent degradation by Eri1 or Dis3l2. Nevertheless, T cells still require certain miRNAs to remain stable even in generally degradative conditions. PtMs could control miRNA stability, promoting degradation but also protecting specific miRNAs.

2. MiRNA PtMs are associated to differential expression

The global PtMs profile of our samples reveals that modification processes were focused on the 3' end of most miRNAs. While uridylation and adenylation have been the best characterized 3' end modifications described across animal miRNAs (103–107), cytosylation was highly represented in our samples. Cytosine was specifically found at position 0 (3' end nucleotide). At this position, A and C modifications were similarly represented, much more frequently than U and G. Upregulated miRNAs were characterized by a strong presence of mono-A at 1 and oligo-A at 0 and 1. Consistent with previous studies from our laboratory, which had indicated that uridylation is a miRNA degradation signal in T cells (121), higher levels of U additions were found in αCD3αCD28downregulated miRNAs. A similar pattern can be observed in IFN I stimulation, although differences are milder, which may be due to a less dynamic miRNA environment; the number of differentially expressed miRNAs was roughly half of those quantified in cells treated with αCD3αCD28.

Although most studies evaluating PtMs have found guanosine and cytosine additions to be barely represented, mono-addition of cytosine was the second most abundant 3' modification after mono-uridylation, in mouse primordial germ cells and gonadal somatic cells at various embryonic stages (181). The presence of 'non-templated cytosylation' has been described in Arabidopsis, which prompted the hypothesis of the existence of a nucleotidyl transferase with a preference for cytosine as substrate (182). Cytosine additions could be relevant for miRNA in very specific developmental or differentiation stages.

In summary, our results offer a novel dataset of differentially regulated miRNAs at early time points of human primary CD4+ T cell activation. Most importantly, we also describe the kinetics of post-transcriptional modifications and the potential effect of these modifications in miRNA stability in the context of T cell activation. Our data also indicate that RNA degrading enzymes Eri1 and Dis3L2 are upregulated upon activation, which could be part of an active mechanism of miRNA degradation guided by uridylation. Indeed, higher uridylation was found in downregulated miRNAs. Upregulated miRNAs, which manage to multiply their levels in this adverse environment, point towards 3' adenine addition as a protective signal.

3. A new exoribonuclease with 3' end specificity: ISG20L2

When considering the following steps to gain a further insight in the enzymatic activities behind miRNA regulation during T cell activation, we decided to pursue the search of a potential enzyme responsible for the decreased expression of uridylated miRNAs upon stimulation. A better understanding of the nucleotide transferase activities is an essential missing piece of knowledge, particularly, characterizing the unexpected potential C-tailing enzyme. However, we have not found so far a way to approach this scientific problem. In the case of the potential U-degrading enzyme, at least we had a bait to start with. We thought of presenting uridylated miRNA to a lysate of activated T cells. The most important challenge for this experiment was that it attempts to catch an enzyme with a substrate that could be degraded within seconds under physiological conditions. In some preliminary experiments (data not included), a RNAse inhibitor of recombinant origin was added to the lysis buffer. No nuclease was found in these early attempts; possibly due to a non-accessible substrate binding region, occupied by the RNAse inhibitor itself. Later, our experiments end up relying on handling our samples on ice and at 4ºC, using EDTA to substrate free divalent cations (required by catalytic activity of many nuclease families) and crosslinking with UV radiation to fix RNA-protein interactions.

After the first unsuccessful attempts, it was unexpected to find the 3' to 5' exoribonuclease ISG20L2 (145) could stabilize an interaction with miRNAs due to the presence of only two additional uridines at the 3' end. Other factors apart from uridylation seem to be involved, since a different pattern of interaction was found comparing miR-25 and miR-151. Besides the preference towards uridylated forms, ISG20L2 presents more affinity towards miR-151-AA than for its canonical form, while it interacts similarly with miR-25 with or without adenylation. Likewise, Dis3L2, a previously introduced exonuclease which preferentially degrades uridylated substrates, interacts with miR-25 forms in a similar way to ISG20L2, while it does not bind miR-151.

The limitations of this pull-down approach involve missing relevant enzymes due to the reduced probability of identifying those whose catalytic activity is not inhibited in the experimental conditions or whose interaction with the substrate is not retained. In addition, we work with whole lysates, missing the cellular context that may will be crucial for RNA and RNA-binding proteins interactions. In this regard, many ribosomal, ribonucleoproteins and other RNA binding proteins were detected to bind differentially to miRNAs with different PTMs and poly(U) and poly(A) stretches. The 3' end catalytic specificity could be guided by and RNA-binding protein. In these cases, finding a specific nuclease activity with this method would have the additional complication of retaining an

interaction between the nuclease and the partner protein which specifically recognize the miRNA edge.

For instance, hnRNPM, a poly(U) and poly(G) interacting ribonucleoprotein (142), was detected bound to poly(U) beads, and more abundant in uridylated miRNAs compared to their canonical forms in human samples. ISG20L2 specificity for RNA substrates could come from the enzyme itself or a result from interacting with a partner such as hnRNPM. Although additional ISG20L2 immunoprecipitation experiments are still on-going, it is worthy to point here that hnRNPM has also been found by mass spectrometry as a potential ISG20L2 interactor.

To test whether ISG20L2 is able to degrade miRNAs and evaluate whether this preferential interaction for uridylated substrates translates into a differential enzymatic activity, miRNA degradation experiments were performed with WT ISG20L2 and two catalytic mutants. While bacterial expression of mutants did not present major problems, expressing ISG20L2 WT was extremely difficult, due to specific bacterial degradation of this form. Overexpressing ISG20L2 WT in J77 T cells has also been highly challenging, achieving a very low percentage of positively electroporated cells (data not shown). In fact, Zhou et al. analysing whether ISG20L2 and ISG20L1 shared ISG20 antiviral capacities, reported they did not succeed generating a Huh7.5 cell culture stably expressing ISG20L2 (183). Therefore, ISG20L2 could be highly toxic for bacterial and mammalian cells expressed in large amounts or during long periods of time.

Degradation assays probed miRNAs are susceptible to ISG20L2 catalytic activity. MiR-151-UU and miR-151-AA were degraded at similar rates; but poly(U) stretches, more efficiently than poly(A). The favoured interaction with uridylated miRNA compared to adenylated, may influence catalytic efficiency, but possibly, we cannot distinguish a functional effect in our working conditions comparing just a two uridine addition with two adenines. However, two uridine additions increased degradation compared to its absence and to cytosylation (which was protective towards ISG20L2). Amino acids D267, D183 and E185 seem to be involved in catalysis, since point mutations introducing alanine in these positions reduced the ribonucleolytic activity. This enzymatic capacity was inhibited by EDTA, consistently with a dependence on divalent cations (147,148).

4. Searching RNA targets

After observing this selective effect on miRNA degradation, we set to obtain an in-deep analysis of potential RNA substrates altered in ISG20L2 absence *in vivo*. We expected to find a clear series of up-regulated RNA, mainly miRNA, that would be

accumulated in the absence of ISG20L2 degradation capacity. However, we obtained a more complex and difficult to interpret dataset. A total of 15 miRNAs were detected as differentially expressed: 4 upregulated and 11 downregulated. Most of them with a modest fold change (|1.2-2.2|x), except for miR-548ay-5p (11.2x) which was barely detected in control samples. To our knowledge no function or experimental target has been described yet for this miRNA. Beyond miRNA expression, ISG20L2 does not seem to bias the miRNA post-transcriptional profile. Future research may elucidate whether the observed miRNA expression changes are direct consequences of ISG20L2 action, or a compensatory mechanism secondary to other effects of ISG20L2 silencing. This uncertainty of whether what we are observing is a direct or indirect consequence of ISG20L2 absence extends also to mRNAseq studies. In this regard, performing RNAseq after ISG20L2 immunoprecipitation could be of great interest to better define ISG20L2 substrates. Another limitation of our RNAseq experiment is that ISG20L2 is induced upon T cell activation, and our sequencing experiments have been performed in a non-stimulated J77 T cell line context, where we may be missing key partners or physiological conditions only present in T cell stimulation.

In the generated mRNA dataset, we also found few mRNA differentially expressed with low adjusted p-values, among which only ISG20L2, H2AX (a histone involved in DNA repair (184,185), and CD69 were finally confirmed as differentially expressed by qPCR. The CD69 finding together with Ingenuity Pathway Analysis (pointing towards NKG2D and CTLA4 as potential upstream regulators of changes detected in our dataset and to dysregulation of AHR signalling), lead us to evaluate mRNA levels of a set of immunoregulatory molecules. Strikingly, AHR, NKG2D, CTLA4, CD137, TIM3 and PD-L1 were upregulated upon ISG20L2 silencing while PD1, LAG3, VISTA, GITR and TIGIT maintained similar expression levels. This is suggestive that ISG20L2 downregulation could increase T cell immunomodulatory capacity.

It is important to bear in mind this RNAseq was not performed in a T cell activation context, where ISG20L2 most probably exerts its function, since we have observed it is strongly upregulated upon T cell activation. For instance, LEF1 (Lymphoid Enhancer binding Factor, a transcription factor which binds to the TCR enhancer (151) detected as potentially upregulated by RNA seq, but not confirmed by qPCR, was clearly upregulated in ISG20L2 KO clones activated with Raji cells and SEE.

Immunoregulatory molecules were also analysed in clones in basal and activation conditions, obtaining unexpected results for many of them. AHR, CD137, TIM3 and PD-L1 upregulation in KO at basal conditions were conserved as trends possibly due to compensatory effects generated during long term ISG20L2 absence. In fact, H2AX differential expression was lost when comparing established clones. It could be

speculated that outliers, only found in KO clones presenting high mRNA values in AHR, NKG2D, CTLA4, CD137 and PD-L1 may have maintained the initial overexpression observed in transient silencing. Many expression differences were diluted even more under activation conditions. However, the two clearest changes in activation were unexpectedly CTLA4 (p=0.07) and PD-1 (p=0.05) downregulation in KO clones' activation, which have been before detected as up-regulated or non-affected in temporal silencing.

CTLA-4, PD-1, LAG3, VISTA,TIM3, GITR, TIGIT and other immunoregulatory molecules have been studied in the last decades as immune checkpoints with a high therapeutic interest for their role downregulating T cell activation (186–188). Antibodies can target these immune receptors preventing ligand interaction and the subsequent inhibition of immune responses. In fact, anti-PD-1/PD-L1 and anti-CTLA4 are used as antitumoral treatments (186,189–191). Both CTLA-4 and PD-1 function as inhibitors of TCR activation, blocking TCR signalling and antigen-independent costimulatory signal, which is essential for cytokine secretion, effector function and clonal expansion. As a result of interaction with ligands PD-L1 (widely expressed and possibly involved in maintenance of peripheral tolerance) and PD-L2 (on APCs), PD-1 recruits phosphatases able to dephosphorylate TCR signalling intermediates (192,193). While PD-1 is located at the plasma membrane, CTLA-4 is translocated there only upon activation (194). Once at the membrane, CTLA-4 competes for CD80 and CD86 ligands with CD28, but eliciting a detrimental effect on T cell stimulation (195–197). CTLA4 diminishes TCR signalling through recruitment of the phosphatases SHP2 (dephosphorylates CD3ζ) (198,199) and PP2AA (leads to downstream decreased AKT phosphorylation) (200,201). CTLA4 and PD-1 downregulation of KO clones could be directly related with a more activated T cell phenotype producing more IL2. Future studies will need to better characterize the dynamics of these and others immunoregulatory molecules in primary mouse and human cells, both in basal and activated contexts.

A small description of the immune significance of those most likely to undergo ISG20L2 modulation according to our study, but not described before in this text is included in the next lines. AHR (Aryl Hydrocarbon Receptor), the mRNA most strongly upregulated with ISG20L2 silencing, is a ligand-activated transcription factor. Although first described as a receptor of polycyclic aromatic hydrocarbon contaminants (202,203), currently is known to respond to natural ligands (present in the diet or generated by host cells or microbiota) and regulate physiological condition in response to endogenous and environmental signals. AHR, now regarded as a potential therapeutic target, regulates both innate and adaptive immune responses (204–206). CD4+ T cells are particularly

sensitive to AHR, which modulates in a ligand-specific manner differentiation of naïve cells into Th1, Th2, Treg and Th17 subsets (207–211).

NKG2D, also upregulated upon ISG20L2 silencing, is an activating receptor mostly expressed on NK cells, CD8+ T cells, and γδ T cells, $NK1.1^+$ T cells. It recognizes ligands expressed on infected, transformed or stressed cells (212). NKG2D triggers NK cell cytokine production and cytolytic capacity, and serves as a co-stimulatory signal for T cell activation (212–214). In mouse, naïve T cells do not express NKG2D, which is induced upon activation in CD8+ but not in CD4+ T cells (215,216). However, in pathological conditions NKG2D has been detected in mouse(217,218) and human (219–221) CD4+ T cells.

CD137, a member of TNFR (TNF-receptor) family upregulated in silenced samples and almost significantly overexpressed (p=0.10) in KO clones, is expressed on activated T cells and NK cells (222). Upon interaction with its ligand CD137L provides T-cell costimulation (223) through TRAFs (TNFR-Associated-Factors) signalling (224), providing antiapoptotic signals and promoting IL2 production and T cell proliferation (225).

CD69, upregulated with ISG20L2 silencing in 'basal conditions' and in resting KO clones, is a surface receptor well known as an early marker of T cell activation, which regulates T cell differentiation and function (150). Growing evidence, associates CD69 with immunosuppression for its ability to limit Th17 differentiation (226,227) and promote Treg development and function (228–230). In addition, CD69 may also be implicated in T cell effector function and cytokine production, modulation of mTOR signalling and AHR responses (231).

In summary, a series of immunoregulatory molecules seem so far the targets most clearly affected by ISG0L2 absence: CD69, AHR, NKG2D, CTLA4, CD137, TIM3 and PD-L1 upregulation in silenced samples; and CTLA4 and PD-1 downregulation in activated KO clones. Further research will be required to better understand how ISG20L2 may modulate these immunoregulatory molecules which are critical for T cell differentiation and function.

5. ISG20L2, an insight in T cell function

ISG20L2 KO clones did not present any major viability or proliferation deficiencies, challenging the role of ISG20L2 as an enzyme whose primary function is ribosome biogenesis. Rather than a global effect on protein expression caused by a possibly defective ribosome translation machinery, ISG20L2 KO clones showed a specific

regulation of selected molecules, such as upregulation of CD69 in resting conditions. When clones were activated with Raji cells and SEE, KO cells upregulated CD69 up to almost WT levels, while their CD25 overexpression was clearly impaired. Other parameters found affected in KO clones were a reduction in CD3ε accumulation at immune synapse, a slightly higher MTOC distance to Raji cells and an increased IL2 expression.

Regulation of IL2 and CD25 could occur at a transcriptional level, since corresponding mRNAs are upregulated and downregulated, respectively, in activated ISG20L2 KO clones. IL2 expression is the result of a complex interaction between transcription factors which bind to the IL2 promoter region upon TCR stimulation. NFAT, AP-1, NF-kB, Sp1/Egr-1 are some of the involved factors (232,233). In response to TCR antigen interaction, NFAT (Nuclear factor of activated T cells) is translocated to the nucleous upon dephosphorylation by calcineurin phosphatase (234–237). TCR signaling also leads to AP-1 (Activator Protein-1) formation, which is comprised of a dimeric combination of proteins which belong to the Jun, Fos, Maf and ATF families (238,239). IL-2 promoter counts with two binding sites which can be occupied by different NF-kB family members (NFKB1, a repressor (240,241); NFKB2; RelA, not essential for IL2 production (242); RelB and c-Rel, requiered for IL2 expression (243)) at different time points eliciting various regulatory signals (232,244). Sp1 and Egr-1 share a binding site within the IL2 promoter, which is occupied by Sp1 in unstimulated cells and replaced upon activation by Egr-1 which interacts with NFAT and drives IL-2 transcription (245,246). Contrary to the IL-2 positive regulators Egr-1 and AP-1 (formed by Jun and others), FOXP3 forms a complex with NFAT which inhibits IL-2 expression while induces CTLA4 and CD25 (247). CD25 (IL-2Rα, IL-2 receptor α chain) transcription is regulated also by NF-kB, NFAT, AP-1, but also by other transcription factors as Elf1 and Stat5, all of them bind to positive regulatory regions (232,233).

Interestingly, Jun (AP-1 component) and Egr-1 which could be promoting IL2 expression in ISG20L2 KO clones were upregulated in ISG20L2 silenced J77 cells mRNAseq. In addition, other molecules involved in IL2 production seem to be slightly affected, maybe leading to a synergistic final effect. By analysing mRNAseq data, we did not find a dysregulated molecule that could justify CD25 diminished mRNA expression. However, is essential to remind that mRNAseq was performed in non-activated samples. We will keep exploring regulation of transcription factors which could be involved with IL-2 and CD25 dysregulated expression in T cell activation.

In spite of CD25 decreased expression, KO clones seem functional regarding CD69 and IL2, which are triggered even with a diminished TCR presence at synaptic contacts. Reduced TCR accumulation at immune synapse (CD3ε ratio) could be due to a

decreased expression of CD3ε in KO cells, or to an impaired capacity of rapid concentration at the immune synapse. TCR accumulation at the synapsis depends on the available TCR pool at the plasma membrane, but also on vesicular trafficking (248). In fact, a correct MTOC translocation towards immune synapse has been related to an adequate supply of molecules in intracellular pools to synapse (249). Therefore, a MTOC more distant to APC in ISG20L2 KO, could be related with a decrease TCR concentration. Future research would need to evaluate a potential deficiency in CD3ε expression, CD3 ε dynamics at synaptic contacts along a wider range of interacting times, and its signalling consequences.

To conclude, ISG20L2 seems to regulate key aspects of T cell function. However, we are only at the very beginning of understanding the involved mechanisms and potential consequences. Associating ISG20L2 absence in activation with CTLA4 and PD-1 downregulation, and IL2 overproduction lead us to hypothesize a potential role of ISG20L2 to limit T cell responses.

6. Beyond ribosome biogenesis and clues to enlighten future research

ISG20L2 was first identified in proteomics analyses of human nucleoli, the main site of ribosome biogenesis, and characterized as a 3' to 5' exoribonuclease involved in the processing of 12 S precursor rRNA, a component of 5.8 S rRNA (145). This function is consistent with the enrichment of 60S ribosomal proteins in a type of human pre-ribosomal complexes where ISG20L2 has also been localized (250). ISG20L2, could be involved in regulatory roles beyond its function as 12 S precursor rRNA processing, either in interaction with ribosomal components or in other locations. The evaluation of ISG20L2 interaction partners found many ribosomal proteins and proteins involved in ribosome biogenesis, consistently with the original role postulated for ISG20L2 (145). Nevertheless, other unexpected partners involved in mRNA splicing, exporting or trafficking were also identified: hnRNP A1, hnRNP A2/B1, SRp20 and ASF/SF2. Due to these findings, a potential additional role in mRNA metabolism was already suggested for ISG20L2 by Couté and co-workers (145). Data presented in this thesis work supports ISG20L2 as a new immune regulator involved in key functions for T cell activity. In the new discovery path towards a detail understanding of ISG20L2 function in the immune system, we can learn important lessons from previous research on ribosome regulatory capacity and look towards ribosomal proteins as potential key interactors of ISG20L2 function. In addition, previous research on Eri1 (another exoribonuclease involved in

ribosome biogenesis, with already known role in immune responses) and Regnase-1 (an endoribonuclease, tightly regulated upon immune cell activation which regulates specific set of mRNAs key for immune function) could help designing future ISG20L2 studies.

First described as an inhibitor of RNA interference (251), Eri1 roles have been later extended to 3' end formation in 5.8S rRNA processing (252,253) and degradation of oligouridylated histone mRNA (122,254). Eri1 is abundantly expressed in mouse spleen and thymus, pointing to a role in the immune system (253). Eri1 knockout animals showed a reduced NK cell population in spleen, while other lymphocyte populations were found at normal numbers (76). Interestingly, WT Ly49H NK cells increased Eri1 expression upon MCMV infection, which is consistent with our data on human CD4+ T cells upregulating Eri1 upon activation. Ly49H NK cells lacking Eri1 underwent inefficient expansion, consistent with higher viral titres and reduced splenomegaly in Eri1$^{-/-}$ chimeras. On the other side, knockout T cells were able to proliferate and show activation markers during infection. However, T cell antigen specific responses to MCMV were decreased: CD4+ and CD8+ IFNɣ producing cells upon stimulation with a MCMV peptide were reduced in Eri1 deficient mice. Importantly, Eri1$^{-/-}$ NK cells miRNA expression showed on average a 2-fold increase compared to WT cells from littermate controls. Also, a modest increase in miRNA abundance was found in Eri1 deficient CD4+ T cells. Hence, Eri1 seems to be involved in regulating global miRNA homeostasis in a sequence-independent manner (no specific miRNA targets were identified) and to specifically modulate immune responses beyond its role in ribosome biogenesis (76).

Regnase-1 (MCPIP1) belongs to a CCH-Zinc Finger protein family (MCPIP1-4, encoded by four genes: *Zc3h12a-d*) transcriptionally induced in human monocytes by MCP-1 (255) and in mouse macrophages by LPS (256,257). However, at the protein level, a rapid degradation of Regnase-1 occurs upon TLR-induction due to IKK complex, through phosphorylation and subsequent ubiquitination (258). A similar mechanism works in T cells where Malt-1 cleaves Regnase-1 upon TCR stimulation (259). Regnase-1 deficient mice develop severe autoimmunity (257), pointing to its critical role in maintaining immune homeostasis and the relevance of its tight regulation. Knockout mice showed increased white blood cells and platelets, hypergammaglobulinemia, antinuclear and anti-dsDNA antibodies (257) and specific deficiency in CD4+ T cells promoted spontaneous generation of effector cells (259). Regnase-1 endonuclease activity downregulates a set of mRNAs (either through direct recognition of specific structures on 3'-UTR or with the aid of other RBPs), such as: *IL-6*, *IL12b*, IL1b, IL2, Rel and Ox40 (257–260). Regnase-1 capacity to restrain immune responses has been

regarded as a potential clinical target. For instance, Regnase-1 deficiency in CD8+ T cells increased adoptive cell therapy efficiency against various cancers (261).

7. Current work and future perspectives

We have just recently known that ISG20L2 KO mice are not viable, with no KO detected already among 9.5 day-old embryos. Consequently, we are now working to understand whether there is any functional difference between WT and HT mouse lymphocytes, while awaiting an on-going generation of a conditional ISG20L2 KO mouse succeeds soon. In addition, we want to assess whether the data obtained in T cell lines about immunoregulatory molecules is also consistent in human primary T cells and to gain a more detailed understanding of the mechanisms behind the observed CD3ε, CD25 and IL2 dysregulation upon T cell activation.

Conclusions

Conclusions

1. αCD3αCD28 and IFN I T cell activation elicit miRNA remodelling within few hours of human CD4+ T cell stimulation. SmallRNAseq analysis provided a new unbiased miRNA dataset, brand new for the unexplored IFN I field, and completing previous TCR activation studies performed using microarrays, northern and qPCR approaches.

2. Human CD4+ T cell miRNAs present a highly post-transcriptionally modified 3' end. MiRNAs downregulated upon stimulation show higher uridylation at 3' end than those upregulated. MiRNA increasing their levels with activation are characterized by high adenine levels at +1 position.

3. Human CD4+ T cell activation leads to upregulation of the Terminal Uridyl Transferases TUT4 and TUT7, and of the uridylated miRNA exoribonucleases Dis3L2 and Eri1.

4. The 3' to 5' exoribonuclease ISG20L2, detected in activated T cell lysates, interacts preferentially with 3' uridylated miRNAs.

5. ISG20L2 degradation activity is able to distinguish specific nucleotides at miRNA 3' edge. Double uridine or adenine addition favoured degradation, compared to canonical or cytosylated substrates. ISG20L2 degraded 3' poly(U) edges more rapidly than those of poly(A) stretches. Residues D267, D183 and E185 are implicated in ISG20L2 catalytic activity.

6. In human primary CD4+ T cells, ISG20L2 is upregulated early upon αCD3αCD28 and IFN I stimulation.

7. ISG20L2 silencing in J77 cells did not elicit a substantial remodelling in miRNA levels or miRNA post-transcriptional modifications. However, knock down samples revealed an increase in immunoregulatory molecules: AHR, NKG2D, CTLA4, CD137, TIM3, PD-L1 and CD69.

8. ISG20L2 seems to be involved in regulation of specific key molecules for T cell function such as CD69, CD3ε, CD25 and IL2.

Conclusiones

Conclusiones

1. La activación de células T CD4+ humanas mediante αCD3αCD28 o IFN I reestructura en pocas horas el repertorio de microARNs. Los datos obtenidos gracias a secuenciación de ARN de pequeño tamaño ofrecen una lista no-sesgada de microARNs relacionados con activación T, totalmente nueva para IFN I y que en el caso de αCD3αCD28 completa estudios anteriores que habían utilizado microarrays, nothern blot, y qPCR.

2. Los microARNs en células T CD4+ humanas presentan un extremo 3' altamente susceptible a modificaciones post-transcripcionales. Se detecta una mayor uridilación en microARNs cuyos niveles disminuyen con la activación. Los microARNs que incrementan su expresión, presentan una posición 3' +1 altamente adenilada.

3. La activación de células T CD4+ humanas induce un aumento de la expresión de las transferasas terminales de uridina TUT4 y TUT7; y de las enzimas Dis3L2 y Eri1, previamente descritas por su capacidad de degradar preferentemente ARN uridilado.

4. La exonucleasa de tipo 3' a 5', ISG20L2, identificada en lisados de células T activadas, es capaz de interaccionar preferentemente con microARNs uridilados.

5. La actividad catalítica de ISG20L2 distingue nucleótidos específicos en el extremo 3'. La presencia de dos adeninas o uridinas en 3' favorece la degradación por parte de ISG20L2, en comparación con el microARN canónico o la forma citosilada. ISG20L2 degrada más rápidamente los extremos 3' de secuencias poli(U) que los de secuencias poli(A). Los aminoácidos D267, D183 y E185 están implicados en la actividad catalítica de ISG20L2.

6. Al activar células T CD4+ humanas con αCD3αCD28 o IFN I, ISG20L2 aumenta su expresión.

7. Al analizar por secuenciación muestras de células J77 en las que se había silenciado ISG20L2, no se encontraron grandes cambios en el repertorio de microARNs ni en las modificaciones post-transcripcionales de los mismos. En cambio, al silenciar ISG20L2

varias moléculas inmunoreguladoras aumentaron su expresión: AHR, NKG2D, CTLA4, CD137, TIM3, PD-L1 y CD69.

8. ISG20L2 parece estar involucrada en la regulación de moléculas esenciales para la función de células T: CD69, CD3ε, CD25 y IL2.

References

References

1. Huppa JB, Davis MM. T-cell-antigen recognition and the immunological synapse. Vol. 3, Nature Reviews Immunology. European Association for Cardio-Thoracic Surgery; 2003. p. 973–83.
2. Dustin ML. The immunological synapse. Vol. 2, Cancer immunology research. NIH Public Access; 2014. p. 1023–33.
3. Monks CRF, Freiberg BA, Kupfer H, Sciaky N, Kupfer A. Three-dimensional segregation of supramolecular activation clusters in T cells. Nature. 1998 Sep 3;395(6697):82–6.
4. Schamel WW, Alarcon B, Minguet S. The TCR is an allosterically regulated macromolecular machinery changing its conformation while working. Immunol Rev. 2019 Sep 12;291(1):8–25.
5. Gil D, Schamel WWA, Montoya M, Sánchez-Madrid F, Alarcón B. Recruitment of Nck by CD3ε reveals a ligand-induced conformational change essential for T cell receptor signaling and synapse formation. Cell. 2002 Jun 28;109(7):901–12.
6. Tsoukas CD, Landgraf B, Bentin J, Valentine M, Lotz M, Vaughan JH, et al. Activation of resting T lymphocytes by anti-CD3 (T3) antibodies in the absence of monocytes. J Immunol. 1985;135(3):1719–23.
7. Trickett A, Kwan YL. T cell stimulation and expansion using anti-CD3/CD28 beads. J Immunol Methods. 2003 Apr;275(1–2):251–5.
8. Fleischer B, Schrezenmeier H. T cell stimulation by staphylococcal enterotoxins: Clonally variable response and requirement for major histocompatibility complex class II molecules on accessory or target cells. J Exp Med. 1988 May 1;167(5):1697–707.
9. Roumier A, Olivo-Marin JC, Arpin M, Michel F, Martin M, Mangeat P, et al. The membrane-microfilament linker ezrin is involved in the formation of the immunological synapse and in T cell activation. Immunity. 2001 Nov 1;15(5):715–28.
10. Bustos-Morán E, Blas-Rus N, Martín-Cófreces NB, Sánchez-Madrid F. Orchestrating Lymphocyte Polarity in Cognate Immune Cell–Cell Interactions. In: International Review of Cell and Molecular Biology. Elsevier Inc.; 2016. p. 195–261.
11. Smith-Garvin JE, Koretzky GA, Jordan MS. T cell activation. Vol. 27, Annual

Review of Immunology. Annu Rev Immunol; 2009. p. 591–619.

12. Balagopalan L, Coussens NP, Sherman E, Samelson LE, Sommers CL. The LAT story: a tale of cooperativity, coordination, and choreography. Vol. 2, Cold Spring Harbor perspectives in biology. Cold Spring Harb Perspect Biol; 2010.
13. Kummerow C, Junker C, Kruse K, Rieger H, Quintana A, Hoth M. The immunological synapse controls local and global calcium signals in T lymphocytes. Immunol Rev. 2009 Sep;231(1):132–47.
14. Matthews SA, Navarro MN, Sinclair L V., Emslie E, Feijoo-Carnero C, Cantrell DA. Unique functions for protein kinase D1 and protein kinase D2 in mammalian cells. Biochem J. 2010;432(1):153–63.
15. Navarro MN, Sinclair L V., Feijoo-Carnero C, Clarke R, Matthews SA, Cantrell DA. Protein kinase D2 has a restricted but critical role in T-cell antigen receptor signalling in mature T-cells. Biochem J. 2012 Mar 15;442(3):649–59.
16. Quann EJ, Merino E, Furuta T, Huse M. Localized diacylglycerol drives the polarization of the microtubule-organizing center in T cells. Nat Immunol. 2009;10(6):627–35.
17. Kupfer A, Dennert G. Reorientation of the microtubule-organizing center and the Golgi apparatus in cloned cytotoxic lymphocytes triggered by binding to lysable target cells. J Immunol. 1984;133(5).
18. Huse M, Lillemeier BF, Kuhns MS, Chen DS, Davis MM. T cells use two directionally distinct pathways for cytokine secretion. Nat Immunol. 2006 Mar;7(3):247–55.
19. Griffiths GM, Tsun A, Stinchcombe JC. The immunological synapse: A focal point for endocytosis and exocytosis. Vol. 189, Journal of Cell Biology. The Rockefeller University Press; 2010. p. 399–406.
20. Weiss A, Imboden JB. Cell Surface Molecules and Early Events Involved in Human T Lymphocyte Activation. Adv Immunol. 1987 Jan 1;41(C):1–38.
21. Read KA, Powell MD, Sreekumar BK, Oestreich KJ. In vitro differentiation of effector CD4+ T helper cell subsets. In: Methods in Molecular Biology. Humana Press Inc.; 2019. p. 75–84.
22. Mosmann TR, Cherwinski H, Bond MW, Giedlin MA, Coffman RL. Two types of murine helper T cell clone. I. Definition according to profiles of lymphokine activities and secreted proteins. J Immunol. 1986;136(7):2348–57.
23. Bartel DP. MicroRNAs: Genomics, Biogenesis, Mechanism, and Function. Cell. 2004;116(2):281–97.
24. Griffiths-Jones S, Saini HK, van Dongen S, Enright AJ. miRBase: tools for microRNA genomics. Nucleic Acids Res. 2008 Jan;36(Database issue):D154-8.

25. Londin E, Loher P, Telonis AG, Quann K, Clark P, Jing Y, et al. Analysis of 13 cell types reveals evidence for the expression of numerous novel primate- and tissue-specific microRNAs. Proc Natl Acad Sci. 2015;112(10):E1106–15.
26. Friedman RC, Farh KKH, Burge CB, Bartel DP. Most mammalian mRNAs are conserved targets of microRNAs. Genome Res. 2009;19(1):92–105.
27. Bernstein E, Caudy AA, Hammond SM, Hannon GJ. Role for bidentate ribnuclease in the initiation site of RNA interference. Nature. 2001;409(1997):363–6.
28. Hutvagner G. A Cellular Function for the RNA-Interference Enzyme Dicer in the Maturation of the let-7 Small Temporal RNA. Science (80-). 2001 Aug 3;293(5531):834–8.
29. Grishok A, Pasquinelli AE, Conte D, Li N, Parrish S, Ha I, et al. Genes and mechanisms related to RNA interference regulate expression of the small temporal RNAs that control C. elegans developmental timing. Cell. 2001 Jul 13;106(1):23–34.
30. Bernstein E, Kim SY, Carmell MA, Murchison EP, Alcorn H, Li MZ, et al. Dicer is essential for mouse development. Nat Genet. 2003 Nov 5;35(3):215–7.
31. Marcais A, Blevins R, Graumann J, Feytout A, Dharmalingam G, Carroll T, et al. microRNA-mediated regulation of mTOR complex components facilitates discrimination between activation and anergy in CD4 T cells. J Exp Med. 2014;211(11):2281–95.
32. Muljo SA, Ansel KM, Kanellopoulou C, Livingston DM, Rao A, Rajewsky K. Aberrant T cell differentiation in the absence of Dicer. J Exp Med. 2005 Jul 18;202(2):261–9.
33. Chong MMW, Rasmussen JP, Rudensky AY, Littman DR. The RNAseIII enzyme Drosha is critical in T cells for preventing lethal inflammatory disease. J Exp Med. 2008 Sep 1;205(9):2005–17.
34. Steiner DF, Thomas MF, Hu JK, Yang Z, Babiarz JE, Allen CDC, et al. MicroRNA-29 Regulates T-Box Transcription Factors and Interferon-γ Production in Helper T Cells. Immunity. 2011 Aug;35(2):169–81.
35. Kroesen B-J, Teteloshvili N, Smigielska-Czepiel K, Brouwer E, Boots AMH, van den Berg A, et al. Immuno-miRs: critical regulators of T-cell development, function and ageing. Immunology. 2015 Jan;144(1):1–10.
36. Jeker LT, Bluestone JA. MicroRNA regulation of T-cell differentiation and function. Immunol Rev. 2013 May;253(1):65–81.
37. Liu J, Wu C-P, Lu B-F, Jiang J-T. Mechanism of T cell regulation by microRNAs. Cancer Biol Med. 2013;10(3):131–7.

38. Baumjohann D, Ansel KM. MicroRNA-mediated regulation of T helper cell differentiation and plasticity. Nat Rev Immunol. 2013 Sep;13(9):666–78.
39. Podshivalova K, Salomon DR. MicroRNA regulation of T-lymphocyte immunity: modulation of molecular networks responsible for T-cell activation, differentiation, and development. Crit Rev Immunol. 2013;33(5):435–76.
40. Cobb BS, Hertweck A, Smith J, O'Connor E, Graf D, Cook T, et al. A role for Dicer in immune regulation. J Exp Med. 2006 Oct 30;203(11):2519–27.
41. Liston A, Lu L-F, O'Carroll D, Tarakhovsky A, Rudensky AY. Dicer-dependent microRNA pathway safeguards regulatory T cell function. J Exp Med. 2008 Sep 1;205(9):1993–2004.
42. Zhou X, Jeker LT, Fife BT, Zhu S, Anderson MS, McManus MT, et al. Selective miRNA disruption in T reg cells leads to uncontrolled autoimmunity. J Exp Med. 2008 Sep 1;205(9):1983–91.
43. Zhang N, Bevan MJ. Dicer controls CD8+ T-cell activation, migration, and survival. Proc Natl Acad Sci. 2010 Dec 14;107(50):21629–34.
44. Boldin MP, Taganov KD, Rao DS, Yang L, Zhao JL, Kalwani M, et al. miR-146a is a significant brake on autoimmunity, myeloproliferation, and cancer in mice. J Exp Med. 2011 Jun 6;208(6):1189–201.
45. Yang L, Boldin MP, Yu Y, Liu CS, Ea C-K, Ramakrishnan P, et al. miR-146a controls the resolution of T cell responses in mice. J Exp Med. 2012 Aug 27;209(9):1655–70.
46. Rossi RL, Rossetti G, Wenandy L, Curti S, Ripamonti A, Bonnal RJP, et al. Distinct microRNA signatures in human lymphocyte subsets and enforcement of the naive state in CD4+ T cells by the microRNA miR-125b. Nat Immunol. 2011 Jun 26;12(8):796–803.
47. Sun Y, Oravecz-Wilson K, Mathewson N, Wang Y, McEachin R, Liu C, et al. Mature T cell responses are controlled by microRNA-142. J Clin Invest. 2015 Jul 1;125(7):2825–40.
48. Mildner A, Chapnik E, Varol D, Aychek T, Lampl N, Rivkin N, et al. MicroRNA-142 controls thymocyte proliferation. Eur J Immunol. 2017 Jul 1;47(7):1142–52.
49. Rodriguez A, Vigorito E, Clare S, Warren M V, Couttet P, Soond DR, et al. Requirement of bic/microRNA-155 for Normal Immune Function. Science (80-). 2007 Apr 27;316(5824):608–11.
50. Jiang S, Li C, Olive V, Lykken E, Feng F, Sevilla J, et al. Molecular dissection of the miR-17-92 cluster's critical dual roles in promoting Th1 responses and preventing inducible Treg differentiation. Blood. 2011 Nov 17;118(20):5487–97.
51. Mehta A, Baltimore D. MicroRNAs as regulatory elements in immune system logic.

Vol. 16, Nature Reviews Immunology. Nature Publishing Group; 2016. p. 279–94.

52. Gracias DT, Katsikis PD. MicroRNAs: Key components of immune regulation. In: Advances in Experimental Medicine and Biology. Adv Exp Med Biol; 2011. p. 15–26.
53. Lindsay MA. microRNAs and the immune response. Vol. 29, Trends in Immunology. Elsevier; 2008. p. 343–51.
54. Bronevetsky Y, Villarino A V, Eisley CJ, Barbeau R, Barczak AJ, Heinz GA, et al. T cell activation induces proteasomal degradation of Argonaute and rapid remodeling of the microRNA repertoire. J Exp Med. 2013 Feb 11;210(2):417–32.
55. Gutiérrez-Vázquez C, Rodríguez-Galán A, Fernández-Alfara M, Mittelbrunn M, Sánchez-Cabo F, Martínez-Herrera DJ, et al. miRNA profiling during antigen-dependent T cell activation: A role for miR-132-3p. Sci Rep. 2017 Jun 14;7(1):3508.
56. Jindra PT, Bagley J, Godwin JG, Iacomini J. Costimulation-Dependent Expression of MicroRNA-214 Increases the Ability of T Cells To Proliferate by Targeting Pten. J Immunol. 2010 Jul 15;185(2):990–7.
57. Wu H, Neilson JR, Kumar P, Manocha M, Shankar P, Sharp PA, et al. miRNA Profiling of Naïve, Effector and Memory CD8 T Cells. Califano A, editor. PLoS One. 2007 Oct 10;2(10):e1020.
58. Grigoryev YA, Kurian SM, Hart T, Nakorchevsky AA, Chen C, Campbell D, et al. MicroRNA Regulation of Molecular Networks Mapped by Global MicroRNA, mRNA, and Protein Expression in Activated T Lymphocytes. J Immunol. 2011;187(5).
59. Sousa IG, do Almo MM, Simi KCR, Bezerra MAG, Andrade RV, Maranhão AQ, et al. MicroRNA expression profiles in human CD3+ T cells following stimulation with anti-human CD3 antibodies. BMC Res Notes. 2017 Mar 14;10(1):124.
60. Teteloshvili N, Smigielska-Czepiel K, Kroesen B-J, Brouwer E, Kluiver J, Boots A, et al. T-cell Activation Induces Dynamic Changes in miRNA Expression Patterns in CD4 and CD8 T-cell Subsets. MicroRNA. 2015 Oct 7;4(2):117–22.
61. Lee Y, Kim M, Han J, Yeom KH, Lee S, Baek SH, et al. MicroRNA genes are transcribed by RNA polymerase II. EMBO J. 2004 Oct 13;23(20):4051–60.
62. Cai X, Hagedorn CH, Cullen BR. Human microRNAs are processed from capped, polyadenylated transcripts that can also function as mRNAs. RNA. 2004 Dec;10(12):1957–66.
63. Ha M, Kim VN. Regulation of microRNA biogenesis. Vol. 15, Nature Reviews Molecular Cell Biology. Nature Publishing Group; 2014. p. 509–24.
64. Michlewski G, Cáceres JF. Post-transcriptional control of miRNA biogenesis.

RNA. 2019 Jan 1;25(1):1–16.

65. Diederichs S, Haber DA. Dual Role for Argonautes in MicroRNA Processing and Posttranscriptional Regulation of MicroRNA Expression. Cell. 2007 Dec 14;131(6):1097–108.
66. Duchaine TF, Fabian MR. Mechanistic insights into microrna-mediated gene silencing. Cold Spring Harb Perspect Biol. 2019 Mar 1;11(3).
67. Gebert LFR, MacRae IJ. Regulation of microRNA function in animals. Vol. 20, Nature Reviews Molecular Cell Biology. Nature Publishing Group; 2019. p. 21–37.
68. Upton JP, Wang L, Han D, Wang ES, Huskey NE, Lim L, et al. IRE1α cleaves select microRNAs during ER stress to derepress translation of proapoptotic caspase-2. Science (80-). 2012 Nov 9;338(6108):818–22.
69. Suzuki HI, Arase M, Matsuyama H, Choi YL, Ueno T, Mano H, et al. MCPIP1 ribonuclease antagonizes dicer and terminates microRNA biogenesis through precursor microRNA degradation. Mol Cell. 2011 Nov 4;44(3):424–36.
70. Gu SQ, Gallego-Perez D, McClory SP, Shi J, Han J, Lee LJ, et al. The human PMR1 endonuclease stimulates cell motility by down regulating miR-200 family microRNAs. Nucleic Acids Res. 2016 Jul 8;44(12):5811–9.
71. Ameres SL, Horwich MD, Hung JH, Xu J, Ghildiyal M, Weng Z, et al. Target RNA-directed trimming and tailing of small silencing RNAs. Science (80-). 2010 Jun 18;328(5985):1534–9.
72. la Mata M, Gaidatzis D, Vitanescu M, Stadler MB, Wentzel C, Scheiffele P, et al. Potent degradation of neuronal mi RNA s induced by highly complementary targets . EMBO Rep. 2015 Apr;16(4):500–11.
73. Marzi MJ, Ghini F, Cerruti B, de Pretis S, Bonetti P, Giacomelli C, et al. Degradation dynamics of microRNAs revealed by a novel pulse-chase approach. Genome Res. 2016 Jan 28;
74. Nicassio F. Killing miR-softly: new clues to miRNA degradation by RNA targets. Non-coding RNA Investig. 2019 Jan;3:5–5.
75. Sheu-Gruttadauria J, Pawlica P, Klum SM, Wang S, Yario TA, Schirle Oakdale NT, et al. Structural Basis for Target-Directed MicroRNA Degradation. Mol Cell. 2019 Sep 19;75(6):1243-1255.e7.
76. Thomas MF, Abdul-Wajid S, Panduro M, Babiarz JE, Rajaram M, Woodruff P, et al. Eri1 regulates microRNA homeostasis and mouse lymphocyte development and antiviral function. Blood. 2012 Jul 5;120(1):130–42.
77. Ramachandran V, Chen X. Degradation of microRNAs by a family of exoribonucleases in Arabidopsis. Science. 2008 Sep 12;321(5895):1490–2.

78. Chatterjee S, Großhans H. Active turnover modulates mature microRNA activity in Caenorhabditis elegans. Nature. 2009 Sep 24;461(7263):546–9.
79. Chatterjee S, Fasler M, Büssing I, Großhans H. Target-Mediated Protection of Endogenous MicroRNAs in C. elegans. Dev Cell. 2011 Mar 15;20(3):388–96.
80. Bail S, Swerdel M, Liu H, Jiao X, Goff LA, Hart RP, et al. Differential regulation of microRNA stability. RNA. 2010 May;16(5):1032–9.
81. Das SK, Sokhi UK, Bhutia SK, Azab B, Su Z-Z, Sarkar D, et al. Human polynucleotide phosphorylase selectively and preferentially degrades microRNA-221 in human melanoma cells. Proc Natl Acad Sci U S A. 2010 Jun 29;107(26):11948–53.
82. Elbarbary RA, Miyoshi K, Myers JR, Du P, Ashton JM, Tian B, et al. Tudor-SN-mediated endonucleolytic decay of human cell microRNAs promotes G1/S phase transition. Science (80-). 2017 May 26;356(6340):859–62.
83. Ebhardt HA, Tsang HH, Dai DC, Liu Y, Bostan B, Fahlman RP. Meta-analysis of small RNA-sequencing errors reveals ubiquitous post-transcriptional RNA modifications. Nucleic Acids Res. 2009 May;37(8):2461–70.
84. Lee LW, Zhang S, Etheridge A, Ma L, Martin D, Galas D, et al. Complexity of the microRNA repertoire revealed by next-generation sequencing. RNA. 2010 Nov;16(11):2170–80.
85. Neilsen CT, Goodall GJ, Bracken CP. IsomiRs--the overlooked repertoire in the dynamic microRNAome. Trends Genet. 2012 Nov;28(11):544–9.
86. de Sousa MC, Gjorgjieva M, Dolicka D, Sobolewski C, Foti M. Deciphering miRNAs' action through miRNA editing. Vol. 20, International Journal of Molecular Sciences. MDPI AG; 2019.
87. Wu H, Ye C, Ramirez D, Manjunath N. Alternative processing of primary microRNA transcripts by Drosha generates 5′ end variation of mature microRNA. PLoS One. 2009 Oct 27;4(10).
88. Starega-Roslan J, Krol J, Koscianska E, Kozlowski P, Szlachcic WJ, Sobczak K, et al. Structural basis of microRNA length variety. Nucleic Acids Res. 2011 Jan;39(1):257–68.
89. Zhou H, Arcila ML, Li Z, Lee EJ, Henzler C, Liu J, et al. Deep annotation of mouse iso-miR and iso-moR variation. Nucleic Acids Res. 2012;40(13):5864–75.
90. Gu S, Jin L, Zhang Y, Huang Y, Zhang F, Valdmanis PN, et al. The loop position of shRNAs and pre-miRNAs is critical for the accuracy of dicer processing in vivo. Cell. 2012 Nov 9;151(4):900–11.
91. Kim B, Jeong K, Kim VN. Genome-wide Mapping of DROSHA Cleavage Sites on Primary MicroRNAs and Noncanonical Substrates. Mol Cell. 2017 Apr

20;66(2):258-269.e5.

92. Zhu L, Kandasamy SK, Fukunaga R. Dicer partner protein tunes the length of miRNAs using base-mismatch in the pre-miRNA stem. Nucleic Acids Res. 2018 Apr 20;46(7):3726–41.
93. Kwon SC, Baek SC, Choi YG, Yang J, Lee Y suk, Woo JS, et al. Molecular Basis for the Single-Nucleotide Precision of Primary microRNA Processing. Mol Cell. 2019 Feb 7;73(3):505-518.e5.
94. Yang W, Chendrimada TP, Wang Q, Higuchi M, Seeburg PH, Shiekhattar R, et al. Modulation of microRNA processing and expression through RNA editing by ADAR deaminases. Nat Struct Mol Biol. 2006 Jan;13(1):13–21.
95. Bazak L, Haviv A, Barak M, Jacob-Hirsch J, Deng P, Zhang R, et al. A-to-I RNA editing occurs at over a hundred million genomic sites, located in a majority of human genes. Genome Res. 2014;24(3):365–76.
96. Nishikura K. A-to-I editing of coding and non-coding RNAs by ADARs. Vol. 17, Nature Reviews Molecular Cell Biology. Nature Publishing Group; 2016. p. 83–96.
97. Tan MH, Li Q, Shanmugam R, Piskol R, Kohler J, Young AN, et al. Dynamic landscape and regulation of RNA editing in mammals. Nature. 2017 Oct 11;550(7675):249–54.
98. Blanc V, Davidson NO. APOBEC-1-mediated RNA editing. Wiley Interdiscip Rev Syst Biol Med. 2010 Sep;2(5):594–602.
99. Rosenberg BR, Hamilton CE, Mwangi MM, Dewell S, Papavasiliou FN, Struct N, et al. Transcriptome-wide sequencing reveals numerous APOBEC1 mRNA editing targets in transcript 3′ UTRs HHS Public Access Author manuscript. Nat Struct Mol Biol. 2011;18(2):230–6.
100. Li L, Song Y, Shi X, Liu J, Xiong S, Chen W, et al. The landscape of miRNA editing in animals and its impact on miRNA biogenesis and targeting. Genome Res. 2018 Jan 1;28(1):132–43.
101. Wang Y, Liang H. When MicroRNAs Meet RNA Editing in Cancer: A Nucleotide Change Can Make a Difference. Vol. 40, BioEssays. John Wiley and Sons Inc.; 2018.
102. Warkocki Z, Liudkovska V, Gewartowska O, Mroczek S, Dziembowski A. Terminal nucleotidyl transferases (TENTs) in mammalian RNA metabolism. Vol. 373, Philosophical Transactions of the Royal Society B: Biological Sciences. Royal Society Publishing; 2018.
103. Landgraf P, Rusu M, Sheridan R, Sewer A, Iovino N, Aravin A, et al. A Mammalian microRNA Expression Atlas Based on Small RNA Library Sequencing. Cell. 2007

Jun 29;129(7):1401–14.

104. Chiang HR, Schoenfeld LW, Ruby JG, Auyeung VC, Spies N, Baek D, et al. Mammalian microRNAs: Experimental evaluation of novel and previously annotated genes. Genes Dev. 2010 May 15;24(10):992–1009.
105. Burroughs AM, Ando Y, de Hoon MJL, Tomaru Y, Nishibu T, Ukekawa R, et al. A comprehensive survey of 3' animal miRNA modification events and a possible role for 3' adenylation in modulating miRNA targeting effectiveness. Genome Res. 2010 Oct 1;20(10):1398–410.
106. Wyman SK, Knouf EC, Parkin RK, Fritz BR, Lin DW, Dennis LM, et al. Post-transcriptional generation of miRNA variants by multiple nucleotidyl transferases contributes to miRNA transcriptome complexity. Genome Res. 2011 Sep;21(9):1450–61.
107. Muller H, Marzi MJ, Nicassio F. IsomiRage: From Functional Classification to Differential Expression of miRNA Isoforms. Front Bioeng Biotechnol. 2014 Sep 29;2(SEP):38.
108. D'Ambrogio A, Gu W, Udagawa T, Mello CC, Richter JD. Specific miRNA Stabilization by Gld2-Catalyzed Monoadenylation. Cell Rep. 2012 Dec 27;2(6):1537–45.
109. Katoh T, Sakaguchi Y, Miyauchi K, Suzuki T, Suzuki T, Kashiwabara SI, et al. Selective stabilization of mammalian microRNAs by 3' adenylation mediated by the cytoplasmic poly(A) polymerase GLD-2. Genes Dev. 2009 Feb 15;23(4):433–8.
110. Yang Q, Lin J, Liu M, Li R, Tian B, Zhang X, et al. Highly sensitive sequencing reveals dynamic modifications and activities of small RNAs in mouse oocytes and early embryos. Sci Adv. 2016 Jun 1;2(6):e1501482.
111. Boele J, Persson H, Shin JW, Ishizu Y, Newie IS, Søkilde R, et al. PAPD5-mediated 3′ adenylation and subsequent degradation of miR-21 is disrupted in proliferative disease. Proc Natl Acad Sci U S A. 2014 Aug 5;111(31):11467–72.
112. Heo I, Joo C, Kim Y-K, Ha M, Yoon M-J, Cho J, et al. TUT4 in concert with Lin28 suppresses microRNA biogenesis through pre-microRNA uridylation. Cell. 2009 Aug 21;138(4):696–708.
113. Thornton JE, Chang HM, Piskounova E, Gregory RI. Lin28-mediated control of let-7 microRNA expression by alternative TUTases Zcchc11 (TUT4) and Zcchc6 (TUT7). RNA. 2012 Oct;18(10):1875–85.
114. Heo I, Joo C, Cho J, Ha M, Han J, Kim VN. Lin28 mediates the terminal uridylation of let-7 precursor MicroRNA. Mol Cell. 2008 Oct 24;32(2):276–84.
115. Ustianenko D, Hrossova D, Potesil D, Chalupnikova K, Hrazdilova K, Pachernik

J, et al. Mammalian DIS3L2 exoribonuclease targets the uridylated precursors of let-7 miRNAs. RNA. 2013 Dec;19(12):1632–8.

116. Chang H-M, Triboulet R, Thornton JE, Gregory RI. A role for the Perlman syndrome exonuclease Dis3l2 in the Lin28-let-7 pathway. Nature. 2013 May 9;497(7448):244–8.
117. Heo I, Ha M, Lim J, Yoon MJ, Park JE, Kwon SC, et al. Mono-uridylation of pre-microRNA as a key step in the biogenesis of group II let-7 microRNAs. Cell. 2012 Oct 26;151(3):521–32.
118. Büssing I, Slack FJ, Großhans H. let-7 microRNAs in development, stem cells and cancer. Vol. 14, Trends in Molecular Medicine. Trends Mol Med; 2008. p. 400–9.
119. Jones MR, Quinton LJ, Blahna MT, Neilson JR, Fu S, Ivanov AR, et al. Zcchc11-dependent uridylation of microRNA directs cytokine expression. Nat Cell Biol. 2009 Sep;11(9):1157–63.
120. Yang A, Shao TJ, Bofill-De Ros X, Lian C, Villanueva P, Dai L, et al. AGO-bound mature miRNAs are oligouridylated by TUTs and subsequently degraded by DIS3L2. Nat Commun. 2020 Dec 1;11(1).
121. Gutiérrez-Vázquez C, Enright AJ, Rodríguez-Galán A, Pérez-García A, Collier P, Jones MR, et al. 3' Uridylation controls mature microRNA turnover during CD4 T-cell activation. RNA. 2017 Jun 1;23(6):882–91.
122. Hoefig KP, Rath N, Heinz GA, Wolf C, Dameris J, Schepers A, et al. Eri1 degrades the stem-loop of oligouridylated histone mRNAs to induce replication-dependent decay. Nat Struct Mol Biol. 2013 Jan 2;20(1):73–81.
123. Martin M. Cutadapt removes adapter sequences from high-throughput sequencing reads. EMBnet.journal. 2011 May 2;17(1):10–2.
124. Li B, Dewey CN. RSEM: Accurate transcript quantification from RNA-Seq data with or without a reference genome. BMC Bioinformatics. 2011 Aug 4;12:323.
125. Ritchie ME, Phipson B, Wu D, Hu Y, Law CW, Shi W, et al. limma powers differential expression analyses for RNA-sequencing and microarray studies. Nucleic Acids Res. 2015 Apr 20;43(7):e47–e47.
126. Sturn A, Quackenbush J, Trajanoski Z. Genesis: cluster analysis of microarray data. Bioinformatics. 2002 Jan 1;18(1):207–8.
127. Vitsios DM, Enright AJ. Chimira: analysis of small RNA sequencing data and microRNA modifications. Bioinformatics. 2015 Oct 15;31(20):3365–7.
128. Fan Y, Xia J. miRNet—Functional analysis and visual exploration of miRNA–target interactions in a network context. In: Methods in Molecular Biology. Humana Press Inc.; 2018. p. 215–33.
129. Bonzon-Kulichenko E, Pérez-Hernández D, Núñez E, Martínez-Acedo P, Navarro

P, Trevisan-Herraz M, et al. A Robust Method for Quantitative High-throughput Analysis of Proteomes by 18 O Labeling. Mol Cell Proteomics. 2011 Jan 1;10(1):M110.003335.

130. Martínez-Bartolomé S, Navarro P, Martín-Maroto F, López-Ferrer D, Ramos-Fernández A, Villar M, et al. Properties of average score distributions of SEQUEST: The probability ratio method. Mol Cell Proteomics. 2008 Jun;7(6):1135–45.
131. Navarro P, Vazquez J. A refined method to calculate false discovery rates for peptide identification using decoy databases. J Proteome Res. 2009 Apr 3;8(4):1792–6.
132. Ran FA, Hsu PD, Wright J, Agarwala V, Scott DA, Zhang F. Genome engineering using the CRISPR-Cas9 system. Nat Protoc. 2013 Oct 24;8(11):2281–308.
133. Labun K, Montague TG, Gagnon JA, Thyme SB, Valen E. CHOPCHOP v2: a web tool for the next generation of CRISPR genome engineering. Nucleic Acids Res. 2016 Jul 8;44(W1):W272–6.
134. Labun K, Montague TG, Krause M, Torres Cleuren YN, Tjeldnes H, Valen E. CHOPCHOP v3: Expanding the CRISPR web toolbox beyond genome editing. Nucleic Acids Res. 2019 Jul 1;47(W1):W171–4.
135. Calabia-Linares C, Robles-Valero J, De La Fuente H, Perez-Martinez M, Martín-Cofreces N, Alfonso-Pérez M, et al. Endosomal clathrin drives actin accumulation at the immunological synapse. J Cell Sci. 2011 Mar 1;124(5):820–30.
136. Blas-Rus N, Bustos-Morán E, Sánchez-Madrid F, Martín-Cófreces NB. Analysis of microtubules and microtubule-organizing center at the immune synapse. In: Methods in Molecular Biology. Humana Press Inc.; 2017. p. 31–49.
137. Rodríguez-Galán A, Fernández-Messina L, Sánchez-Madrid F. Control of Immunoregulatory Molecules by miRNAs in T Cell Activation. Front Immunol. 2018;9(September):1–10.
138. Stefano JE. Purified lupus antigen la recognizes an oligouridylate stretch common to the 3′ termini of RNA polymerase III transcripts. Cell. 1984;36(1):145–54.
139. Maraia RJ, Intine R V. La protein and its associated small nuclear and nucleolar precursor RNAs. Vol. 10, Gene Expression. Cognizant Communication Corporation; 2002. p. 41–57.
140. Topfer F, Gordon T, McCluskey J. Characterization of the mouse autoantigen La (SS-B): Identification of conserved RNA-binding motifs, a putative ATP binding site and reactivity of recombinant protein with poly(U) and human autoantibodies. J Immunol. 1993;150(7):3091–100.
141. Maraia RJ, Mattijssen S, Cruz-Gallardo I, Conte MR. The La and related RNA-

binding proteins (LARPs): structures, functions, and evolving perspectives. Vol. 8, Wiley Interdisciplinary Reviews: RNA. Blackwell Publishing Ltd; 2017.

142. Datar K V, Dreyfuss1 G, Swanson MS. The human hnRNP M proteins: identification of a methionine/arginine-rich repeat motif in ribonucleoproteins. Vol. 21, Nucleic Acids Research. 1993.
143. Salton M, Elkon R, Borodina T, Davydov A, Yaspo ML, Halperin E, et al. Matrin 3 binds and stabilizes mRNA. PLoS One. 2011;6(8).
144. Ramesh N, Kour S, Anderson EN, Rajasundaram D, Pandey UB. RNA-recognition motif in Matrin-3 mediates neurodegeneration through interaction with hnRNPM. Acta Neuropathol Commun. 2020 Aug 18;8(1):138.
145. Couté Y, Kindbeiter K, Belin S, Dieckmann R, Duret L, Bezin L, et al. ISG20L2, a novel vertebrate nucleolar exoribonuclease involved in ribosome biogenesis. Mol Cell Proteomics. 2008 Mar;7(3):546–59.
146. Moser MJ, Holley WR, Chatterjee A, Saira Mian I. The proofreading domain of Escherichia coli DNA polymerase I and other DNA and/or RNA exonuclease domains. Vol. 25, Nucleic Acids Research. Oxford University Press; 1997.
147. Zuo Y, Deutscher MP. Exoribonuclease superfamilies: Structural analysis and phylogenetic distribution. Nucleic Acids Res. 2001 Mar 1;29(5):1017–26.
148. Steitz TA, Steitz JA. A general two-metal-ion mechanism for catalytic RNA (phosphoryl transfer mechanism/ribozyme/group I splicing/spliceosome/group H splicing). Vol. 90, Proc. Natl. Acad. Sci. USA. 1993.
149. Montague TG, Cruz JM, Gagnon JA, Church GM, Valen E. CHOPCHOP: A CRISPR/Cas9 and TALEN web tool for genome editing. Nucleic Acids Res. 2014 Jul 1;42(W1):401–7.
150. Cibrián D, Sánchez-Madrid F. CD69: from activation marker to metabolic gatekeeper. Eur J Immunol. 2017;47(6):946–53.
151. Travis A, Amsterdam A, Belanger C, Grosschedl R. LEF-1, a gene encoding a lymphoid-specific with protein, an HMG domain, regulates T-cell receptor α enhancer function. Genes Dev. 1991 May 1;5(5):880–94.
152. Cherry LK, Li X, Schwab P, Lim B, Klickstein LB. RhoH is required to maintain the integrin LFA-1 in a nonadhesive state on lymphocytes. Nat Immunol. 2004 Sep 8;5(9):961–7.
153. Baker CM, Comrie WA, Hyun Y-M, Chung H-L, Fedorchuk CA, Lim K, et al. Opposing roles for RhoH GTPase during T-cell migration and activation. Proc Natl Acad Sci U S A. 2012 Jun 26;109(26):10474–9.
154. Hara-Chikuma M, Chikuma S, Sugiyama Y, Kabashima K, Verkman AS, Inoue S, et al. Chemokine-dependent T cell migration requires aquaporin-3-mediated

hydrogen peroxide uptake. J Exp Med. 2012 Sep;209(10):1743–52.

155. Sun X, Kaufman PD. Ki-67: more than a proliferation marker. Vol. 127, Chromosoma. Springer Science and Business Media Deutschland GmbH; 2018. p. 175–86.
156. Wlodkowic D, Telford W, Skommer J, Darzynkiewicz Z. Apoptosis and Beyond: Cytometry in Studies of Programmed Cell Death. Vol. 103, Methods in Cell Biology. NIH Public Access; 2011. 55–98 p.
157. Kabakov AE, Gabai VL. Cell death and survival assays. In: Methods in Molecular Biology. Humana Press Inc.; 2018. p. 107–27.
158. Li Y, Li L, Qian Z, Lin B, Chen J, Luo Y, et al. Phosphatidylinositol 3-kinase-DNA methyltransferase 1-miR-1281-histone deacetylase 4 regulatory axis mediates platelet-derived growth factor-induced proliferation and migration of pulmonary artery smooth muscle cells. J Am Heart Assoc. 2018 Mar 20;7(6).
159. Jiang J, Ma B, Li X, Jin W, Han C, Wang L, et al. MiR-1281, a p53-responsive microRNA, impairs the survival of human osteosarcoma cells upon ER stress via targeting USP39. Am J Cancer Res. 2018;8(9):1764–74.
160. Zhou LL, Jiao Y, Chen HM, Kang LH, Yang Q, Li J, et al. Differentially expressed long noncoding RNAs and regulatory mechanism of LINC02407 in human gastric adenocarcinoma. World J Gastroenterol. 2019 Oct 21;25(39):5973–90.
161. Gromova P, Ralea S, Lefort A, Libert F, Rubin BP, Erneux C, et al. Kit K641E oncogene up-regulates Sprouty homolog 4 and Trophoblast glycoprotein in interstitial cells of Cajal in a murine model of gastrointestinal stromal tumours. J Cell Mol Med. 2009 Aug;13(8 A):1536–48.
162. Yang J, Wu S, Alachkar H. Characterization of upregulated adhesion GPCRs in acute myeloid leukemia. Transl Res. 2019 Oct 1;212:26–35.
163. Bayin NS, Frenster JD, Kane JR, Rubenstein J, Modrek AS, Baitalmal R, et al. GPR133 (ADGRD1), an adhesion G-protein-coupled receptor, is necessary for glioblastoma growth. Oncogenesis. 2016 Oct 1;5(10):e263–e263.
164. Frenster JD, Inocencio JF, Xu Z, Dhaliwal J, Alghamdi A, Zagzag D, et al. GPR133 Promotes Glioblastoma Growth in Hypoxia. Neurosurgery. 2017;64(CN_suppl_1):177–81.
165. Chen H, Dai G, Cai Y, Gong Q, Wu W, Gao M, et al. Vasodilator-stimulated phosphoprotein (VASP), a novel target of miR-4455, promotes gastric cancer cell proliferation, migration, and invasion, through activating the PI3K/AKT signaling pathway. Cancer Cell Int. 2018;18:97.
166. Krause M, Dent EW, Bear JE, Loureiro JJ, Gertler FB. Ena/VASP Proteins: Regulators of the Actin Cytoskeleton and Cell Migration. Annu Rev Cell Dev Biol.

2003 Nov 28;19(1):541–64.

167. Bailly M. Ena/VASP family: New partners, bigger enigma. Vol. 7, Developmental Cell. Elsevier; 2004. p. 462–3.
168. Krause M, Sechi AS, Konradt M, Monner D, Gertler FB, Wehland J. Fyn-binding protein (Fyb)/SLP-76-associated protein (SLAP), ena/vasodilator-stimulated phosphoprotein (VASP) proteins and the Arp2/3 complex link T cell receptor (TCR) signaling to the actin cytoskeleton. J Cell Biol. 2000 Apr 3;149(1):181–94.
169. Estin ML, Thompson SB, Traxinger B, Fisher MH, Friedman RS, Jacobelli J. Ena/VASP proteins regulate activated T-cell trafficking by promoting diapedesis during transendothelial migration. Proc Natl Acad Sci. 2017 Apr 4;114(14):E2901–10.
170. Forster SC, Tate MD, Hertzog PJ. MicroRNA as Type I Interferon-Regulated Transcripts and Modulators of the Innate Immune Response. Front Immunol. 2015 Jul 8;6(JUN):1.
171. Scagnolari C, Zingariello P, Vecchiet J, Selvaggi C, Racciatti D, Taliani G, et al. Differential expression of interferon-induced microRNAs in patients with chronic hepatitis C virus infection treated with pegylated interferon alpha. Virol J. 2010;7:311.
172. Wang P, Gu Y, Zhang Q, Han Y, Hou J, Lin L, et al. Identification of Resting and Type I IFN-Activated Human NK Cell miRNomes Reveals MicroRNA-378 and MicroRNA-30e as Negative Regulators of NK Cell Cytotoxicity. J Immunol. 2012 Jul 1;189(1):211–21.
173. Qi Y, Li Y, Zhang L, Huang J. MicroRNA expression profiling and bioinformatic analysis of dengue virus-infected peripheral blood mononuclear cells. Mol Med Rep. 2013 Mar 1;7(3):791–8.
174. Li Q, Lowey B, Sodroski C, Krishnamurthy S, Alao H, Cha H, et al. Cellular microRNA networks regulate host dependency of hepatitis C virus infection. Nat Commun. 2017 Dec 1;8(1).
175. Martins S de T, Kuczera D, Lötvall J, Bordignon J, Alves LR. Characterization of dendritic cell-derived extracellular vesicles during dengue virus infection. Front Microbiol. 2018 Aug 6;9(AUG).
176. Herkt CE, Caffrey BE, Surmann K, Blankenburg S, Salazar MG, Jung AL, et al. A microRNA network controls legionella pneumophila replication in human macrophages via LGALS8 and MX1. MBio. 2020 Mar 1;11(2).
177. Diosa-Toro M, Echavarría-Consuegra L, Flipse J, Fernández GJ, Kluiver J, van den Berg A, et al. MicroRNA profiling of human primary macrophages exposed to dengue virus identifies miRNA-3614-5p as antiviral and regulator of ADAR1

expression. PLoS Negl Trop Dis. 2017 Oct 18;11(10).

178. Baños-Lara MDR, Zabaleta J, Garai J, Baddoo M, Guerrero-Plata A. Comparative analysis of miRNA profile in human dendritic cells infected with respiratory syncytial virus and human metapneumovirus. BMC Res Notes. 2018 Jul 3;11(1).
179. Alipoor SD, Mortaz E, Tabarsi P, Farnia P, Mirsaeidi M, Garssen J, et al. Bovis Bacillus Calmette-Guerin (BCG) infection induces exosomal miRNA release by human macrophages. J Transl Med. 2017 May 12;15(1):105.
180. Sandberg R, Neilson JR, Sarma A, Sharp PA, Burge CB. Proliferating Cells Express mRNAs with Shortened 3' Untranslated Regions and Fewer MicroRNA Target Sites. Science (80-). 2008 Jun 20;320(5883):1643–7.
181. Darnell RB, Ke S, Darnell JE. Protein–RNA interactions: structural characteristics and hotspot amino acids. Rna. 2018;24:1457–65.
182. Chou M-T, Han BW, Hsiao C-P, Zamore PD, Weng Z, Hung J-H. Tailor: a computational framework for detecting non-templated tailing of small silencing RNAs. Nucleic Acids Res. 2015;43(17):109.
183. Zhou Z, Wang N, Woodson SE, Dong Q, Wang J, Liang Y, et al. Antiviral activities of ISG20 in positive-strand RNA virus infections. Virology. 2011 Jan 20;409(2):175–88.
184. Dickey JS, Redon CE, Nakamura AJ, Baird BJ, Sedelnikova OA, Bonner WM. H2AX: Functional roles and potential applications. Vol. 118, Chromosoma. NIH Public Access; 2009. p. 683–92.
185. Chen Q, Bian C, Wang X, Liu X, Ahmad Kassab M, Yu Y, et al. ADP-ribosylation of histone variant H2AX promotes base excision repair. EMBO J. 2020 Dec 2;
186. He X, Xu C. Immune checkpoint signaling and cancer immunotherapy. Vol. 30, Cell Research. Springer Nature; 2020. p. 660–9.
187. Nirschl CJ, Drake CG. Molecular pathways: Coexpression of immune checkpoint molecules: Signaling pathways and implications for cancer immunotherapy. Clin Cancer Res. 2013 Sep 15;19(18):4917–24.
188. Qin S, Xu L, Yi M, Yu S, Wu K, Luo S. Novel immune checkpoint targets: Moving beyond PD-1 and CTLA-4. Vol. 18, Molecular Cancer. BioMed Central Ltd.; 2019. p. 1–14.
189. Ribas A, Wolchok JD. Cancer immunotherapy using checkpoint blockade. Vol. 359, Science. American Association for the Advancement of Science; 2018. p. 1350–5.
190. Sanmamed MF, Chen L. A Paradigm Shift in Cancer Immunotherapy: From Enhancement to Normalization. Vol. 175, Cell. Cell Press; 2018. p. 313–26.
191. Riley RS, June CH, Langer R, Mitchell MJ. Delivery technologies for cancer

immunotherapy. Vol. 18, Nature Reviews Drug Discovery. Nature Publishing Group; 2019. p. 175–96.

192. Keir ME, Butte MJ, Freeman GJ, Sharpe AH. PD-1 and its ligands in tolerance and immunity. Vol. 26, Annual Review of Immunology. Annu Rev Immunol; 2008. p. 677–704.
193. Riley JL. PD-1 signaling in primary T cells. Vol. 229, Immunological Reviews. NIH Public Access; 2009. p. 114–25.
194. Linsley PS, Bradshaw J, Greene JA, Peach R, Bennett KL, Mittler RS. Intracellular trafficking of CTLA-4 and focal localization towards sites of TCR engagement. Immunity. 1996;4(6):535–43.
195. Walunas TL, Lenschow DJ, Bakker CY, Linsley PS, Freeman GJ, Green JM, et al. CTLA-4 can function as a negative regulator of T cell activation. Immunity. 1994;1(5):405–13.
196. Krummel MF, Allison JP. CD28 and CTLA-4 have opposing effects on the response of T ceils to stimulation. J Exp Med. 1995 Aug 1;182(2):459–65.
197. Walunas TL, Bakker CY, Bluestone JA. CTLA-4 ligation blocks CD28-dependent T cell activation. J Exp Med. 1996 Jun 1;183(6):2541–50.
198. Marengère LEM, Waterhouse P, Duncan GS, Mittrücker HW, Feng GS, Mak TW. Regulation of T cell receptor signaling by tyrosine phosphatase SYP association with CTLA-4. Science (80-). 1996 May 24;272(5265):1170–3.
199. Lee KM, Chuang E, Griffin M, Khattri R, Hong DK, Zhang W, et al. Molecular basis of T cell inactivation by CTLA-4. Science (80-). 1998 Dec 18;282(5397):2263–6.
200. Chuang E, Fisher TS, Morgan RW, Robbins MD, Duerr JM, Vander Heiden MG, et al. The CD28 and CTLA-4 receptors associate with the serine/threonine phosphatase PP2A. Immunity. 2000;13(3):313–22.
201. Parry R V., Chemnitz JM, Frauwirth KA, Lanfranco AR, Braunstein I, Kobayashi S V., et al. CTLA-4 and PD-1 Receptors Inhibit T-Cell Activation by Distinct Mechanisms. Mol Cell Biol. 2005 Nov 1;25(21):9543–53.
202. Poland A, Glover E, Kende AS. Stereospecific, high affinity binding of 2,3,7,8 tetrachlorodibenzo p dioxin by hepatic cytosol. Evidence that the binding species is receptor for induction of aryl hydrocarbon hydroxylase. J Biol Chem. 1976;251(16):4936–46.
203. Poland A, Knutson JC. 2,3,7,8-tetrachlorodibenzo-p-dioxin and related halogenated aromatic hydrocarbons: examination of the mechanism of toxicity. Vol. 22, Annual review of pharmacology and toxicology. Annual Reviews 4139 El Camino Way, P.O. Box 10139, Palo Alto, CA 94303-0139, USA; 1982. p. 517–54.
204. Quintana FJ, Sherr DH. Aryl hydrocarbon receptor control of adaptive immunity.

Vol. 65, Pharmacological Reviews. American Society for Pharmacology and Experimental Therapeutics; 2013. p. 1148–61.

205. Gutiérrez-Vázquez C, Quintana FJ. Regulation of the Immune Response by the Aryl Hydrocarbon Receptor. Vol. 48, Immunity. Cell Press; 2018. p. 19–33.
206. Wang XS, Cao F, Zhang Y, Pan HF. Therapeutic potential of aryl hydrocarbon receptor in autoimmunity. Vol. 28, Inflammopharmacology. Springer; 2020. p. 63–81.
207. Quintana FJ, Basso AS, Iglesias AH, Korn T, Farez MF, Bettelli E, et al. Control of Treg and TH17 cell differentiation by the aryl hydrocarbon receptor. Nature. 2008 May 1;453(7191):65–71.
208. Kimura A, Naka T, Nohara K, Fujii-Kuriyama Y, Kishimoto T. Aryl hydrocarbon receptor regulates Stat1 activation and participates in the development of Th17 cells. Proc Natl Acad Sci U S A. 2008 Jul 15;105(28):9721–6.
209. Veldhoen M, Hirota K, Westendorf AM, Buer J, Dumoutier L, Renauld JC, et al. The aryl hydrocarbon receptor links TH17-cell-mediated autoimmunity to environmental toxins. Nature. 2008 May 1;453(7191):106–9.
210. Marshall NB, Kerkvliet NI. Dioxin and immune regulation: Emerging role of aryl hydrocarbon receptor in the generation of regulatory T cells. Vol. 1183, Annals of the New York Academy of Sciences. Blackwell Publishing Inc.; 2010. p. 25–37.
211. Hwang YJ, Yun MO, Jeong KT, Park JH. Uremic toxin indoxyl 3-sulfate regulates the differentiation of Th2 but not of Th1 cells to lessen allergic asthma. Toxicol Lett. 2014 Feb 10;225(1):130–8.
212. Raulet DH. Roles of the NKG2D immunoreceptor and its ligands. Vol. 3, Nature Reviews Immunology. European Association for Cardio-Thoracic Surgery; 2003. p. 781–90.
213. Groh V, Rhinehart R, Randolph-Habecker J, Topp MS, Riddell SR, Spies T. Costimulation of CD8αβ T cell by NKG2D via engagement by MIC induced on virus-infected cells. Nat Immunol. 2001 Mar;2(3):255–60.
214. Wensveen FM, Jelenčić V, Polić B. NKG2D: A master regulator of immune cell responsiveness. Vol. 9, Frontiers in Immunology. Frontiers Media S.A.; 2018. p. 441.
215. Diefenbach A, Jamieson AM, Liu SD, Shastri N, Raulet DH. Ligands for the murine NKG2D receptor: Expression by tumor cells and activation of NK cells and macrophages. Nat Immunol. 2000;1(2):119–26.
216. Jamieson AM, Diefenbach A, McMahon CW, Xiong N, Carlyle JR, Raulet DH. The role of the NKG2D immunoreceptor in immune cell activation and natural killing. Immunity. 2002 Jul 1;17(1):19–29.

217. Ito Y, Kanai T, Totsuka T, Okamoto R, Tsuchiya K, Nemoto Y, et al. Blockade of NKG2D signaling prevents the development of murine CD4 + T cell-mediated colitis. Am J Physiol - Gastrointest Liver Physiol. 2007;294(1).
218. Andersson AK, Sumariwalla PF, McCann FE, Amjadi P, Chang C, McNamee K, et al. Blockade of NKG2D ameliorates disease in mice with collagen-induced arthritis: A potential pathogenic role in chronic inflammatory arthritis. Arthritis Rheum. 2011 Sep;63(9):2617–29.
219. Sáez-Borderías A, Gumá M, Angulo A, Bellosillo B, Pende D, López-Botet M. Expression and function of NKG2D in CD4+ T cells specific for human cytomegalovirus. Eur J Immunol. 2006 Dec 1;36(12):3198–206.
220. Allez M, Tieng V, Nakazawa A, Treton X, Pacault V, Dulphy N, et al. CD4+NKG2D+ T Cells in Crohn's Disease Mediate Inflammatory and Cytotoxic Responses Through MICA Interactions. Gastroenterology. 2007;132(7):2346–58.
221. Dai Z, Turtle CJ, Booth GC, Riddell SR, Gooley TA, Stevens AM, et al. Normally occurring NKG2D +CD4 + T cells are immunosuppressive and inversely correlated with disease activity in juvenileonset lupus. J Exp Med. 2009 Apr 13;206(4):793–805.
222. Sanchez-Paulete AR, Labiano S, Rodriguez-Ruiz ME, Azpilikueta A, Etxeberria I, Bolaños E, et al. Deciphering CD137 (4-1BB) signaling in T-cell costimulation for translation into successful cancer immunotherapy. Eur J Immunol. 2016 Mar 1;46(3):513–22.
223. DeBenedette MA, Randall Chu N, Pollok KE, Hurtado J, Wade WF, Kwon BS, et al. Role of 4-1BB ligand in costimulation of T lymphocyte growth and its upregulation on M12 B lymphomas by camp. J Exp Med. 1995 Mar 1;181(3):985–92.
224. Zapata JM, Perez-Chacon G, Carr-Baena P, Martinez-Forero I, Azpilikueta A, Otano I, et al. CD137 (4-1BB) signalosome: Complexity is a matter of TRAFs. Vol. 9, Frontiers in Immunology. Frontiers Media S.A.; 2018.
225. Lee H-W, Park S-J, Choi BK, Kim HH, Nam K-O, Kwon BS. 4-1BB Promotes the Survival of CD8 + T Lymphocytes by Increasing Expression of Bcl-x L and Bfl-1 . J Immunol. 2002 Nov 1;169(9):4882–8.
226. Martin P, Gomez M, Lamana A, Cruz-Adalia A, Ramirez-Huesca M, Ursa MA, et al. CD69 association with Jak3/Stat5 proteins regulates Th17 cell differentiation. Mol Cell Biol. 2010/08/11. 2010;30(20):4877–89.
227. Martín P, Sánchez-Madrid F. CD69: An unexpected regulator of TH17 cell-driven inflammatory responses. Vol. 4, Science Signaling. Sci Signal; 2011.
228. Radulovic K, Manta C, Rossini V, Holzmann K, Kestler HA, Wegenka UM, et al.

CD69 Regulates Type I IFN-Induced Tolerogenic Signals to Mucosal CD4 T Cells That Attenuate Their Colitogenic Potential. J Immunol. 2012 Feb 15;188(4):2001–13.

229. Cortés JR, Sánchez-Díaz R, Bovolenta ER, Barreiro O, Lasarte S, Matesanz-Marín A, et al. Maintenance of immune tolerance by Foxp3+ regulatory T cells requires CD69 expression. J Autoimmun. 2014 Dec 1;55(1):51–62.
230. Yu L, Yang F, Zhang F, Guo D, Li L, Wang X, et al. CD69 enhances immunosuppressive function of regulatory T-cells and attenuates colitis by prompting IL-10 production. Cell Death Dis. 2018 Sep 1;9(9).
231. Cibrian D, Saiz ML, De La Fuente H, Sánchez-Díaz R, Moreno-Gonzalo O, Jorge I, et al. CD69 controls the uptake of L-tryptophan through LAT1-CD98 and AhR-dependent secretion of IL-22 in psoriasis. Nat Immunol. 2016 Jul 19;17(8):985–96.
232. Kim HP, Imbert J, Leonard WJ. Both integrated and differential regulation of components of the IL-2/IL-2 receptor system. Vol. 17, Cytokine and Growth Factor Reviews. Pergamon; 2006. p. 349–66.
233. Spolski R, Li P, Leonard WJ. Biology and regulation of IL-2: from molecular mechanisms to human therapy. Vol. 18, Nature Reviews Immunology. Nature Publishing Group; 2018. p. 648–59.
234. Jain J, McCafffrey PG, Miner Z, Kerppola TK, Lambert JN, Verdine GL, et al. The T-cell transcription factor NFATp is a substrate for calcineurin and interacts with Fos and Jun. Nature. 1993;365(6444):352–5.
235. McCaffrey PG, Luo C, Kerppola TK, Jain J, Badalian TM, Ho AM, et al. Isolation of the cyclosporin-sensitive T cell transcription factor NFATp. Science (80-). 1993;262(5134):750–4.
236. Flanagan WM, Corthésy B, Bram RJ, Crabtree GR. Nuclear association of a T-cell transcription factor blocked by FK-506 and cyclosporin A. Nature. 1991;352(6338):803–7.
237. Müller MR, Rao A. NFAT, immunity and cancer: A transcription factor comes of age. Vol. 10, Nature Reviews Immunology. Nature Publishing Group; 2010. p. 645–56.
238. Shaulian E, Karin M. AP-1 as a regulator of cell life and death. Vol. 4, Nature Cell Biology. Nat Cell Biol; 2002. p. E131–6.
239. Jain J, McCaffrey PG, Valge-Archer VE, Rao A. Nuclear factor of activated T cells contains Fos and Jun. Nature. 1992;356(6372):801–4.
240. Yang L, Cohn L, Zhang DH, Homer R, Ray A, Ray P. Essential role of nuclear factor κB in the induction of eosinophilia in allergic airway inflammation. J Exp

Med. 1998 Nov 2;188(9):1739–50.

241. Kang SM, Tran AC, Grilli M, Lenardo MJ. NF-κB subunit regulation in nontransformed CD4+ T lymphocytes. Science (80-). 1992 Jun 5;256(5062):1452–6.
242. Doi TS, Takahashi T, Taguchi O, Azuma T, Obata Y. NF-κB RelA-deficient lymphocytes: Normal development of T cells and B cells, impaired production of IgA and IgG1 and reduced proliferative responses. J Exp Med. 1997;185(5):953–61.
243. Köntgen F, Grumont RJ, Strasser A, Metcalf D, Li R, Tarlinton D, et al. Mice lacking the c-rel proto-oncogene exhibit defects in lymphocyte proliferation, humoral immunity, and interleukin-2 expression. Genes Dev. 1995 Aug 15;9(16):1965–77.
244. Ghosh S, May MJ, Kopp EB. NF-κB and rel proteins: Evolutionarily conserved mediators of immune responses. Vol. 16, Annual Review of Immunology. Annu Rev Immunol; 1998. p. 225–60.
245. Skerka C, Decker EL, Zipfel PF. A regulatory element in the human interleukin 2 gene promoter is a binding site for the zinc finger proteins sp1 and EGR-1. J Biol Chem. 1995;270(38):22500–6.
246. Decker EL, Skerka C, Zipfel PF. The early growth response protein (EGR-1) regulates interleukin-2 transcription by synergistic interaction with the nuclear factor of activated T cells. J Biol Chem. 1998 Oct 9;273(41):26923–30.
247. Wu Y, Borde M, Heissmeyer V, Feuerer M, Lapan AD, Stroud JC, et al. FOXP3 Controls Regulatory T Cell Function through Cooperation with NFAT. Cell. 2006 Jul 28;126(2):375–87.
248. Onnis A, Baldari CT. Orchestration of Immunological Synapse Assembly by Vesicular Trafficking. Vol. 7, Frontiers in Cell and Developmental Biology. Frontiers Media S.A.; 2019. p. 110.
249. Martín-Cófreces NB, Robles-Valero J, Cabrero JR, Mittelbrunn M, Gordón-Alonso M, Sung CH, et al. MTOC translocation modulates IS formation and controls sustained T cell signaling. J Cell Biol. 2008 Sep 8;182(5):951–62.
250. Simabuco FM, Morello LG, Zambon A, Aragã B, Franco A, Leme P, et al. Proteomic Characterization of the Human FTSJ3 Preribosomal Complexes. 2012;
251. Kennedy S, Wang D, Ruvkun G. A conserved siRNA-degrading RNase negatively regulates RNA interference in C. elegans. Nature. 2004 Feb 12;427(6975):645–9.
252. Gabel HW, Ruvkun G, Struct Mol Biol Author manuscript N. The exonuclease ERI-1 has a conserved dual role in 5.8S rRNA processing and RNAi. Nat Struct Mol

Biol. 2008;15(5):531–3.

253. Ansel KM, Pastor WA, Rath N, Lapan AD, Glasmacher E, Wolf C, et al. Mouse Eri1 interacts with the ribosome and catalyzes 5.8S rRNA processing. Nat Struct Mol Biol. 2008;15(5):523.
254. Hoefig KP, Heissmeyer V. Degradation of oligouridylated histone mRNAs: see UUUUU and goodbye. Wiley Interdiscip Rev RNA. 2014 Jul 1;5(4):577–89.
255. Zhou L, Azfer A, Niu J, Graham S, Choudhury M, Adamski FM, et al. Monocyte chemoattractant protein-1 induces a novel transcription factor that causes cardiac myocyte apoptosis and ventricular dysfunction. Circ Res. 2006 May 12;98(9):1177–85.
256. Liang J, Wang J, Azfer A, Song W, Tromp G, Kolattukudy PE, et al. A novel CCCH-zinc finger protein family regulates proinflammatory activation of macrophages. J Biol Chem. 2008 Mar 7;283(10):6337–46.
257. Matsushita K, Takeuchi O, Standley DM, Kumagai Y, Kawagoe T, Miyake T, et al. Zc3h12a is an RNase essential for controlling immune responses by regulating mRNA decay. Nature. 2009 Apr 30;458(7242):1185–90.
258. Iwasaki H, Takeuchi O, Teraguchi S, Matsushita K, Uehata T, Kuniyoshi K, et al. The IκB kinase complex regulates the stability of cytokine-encoding mRNA induced by TLR-IL-1R by controlling degradation of regnase-1. Nat Immunol. 2011 Dec;12(12):1167–75.
259. Uehata T, Iwasaki H, Vandenbon A, Matsushita K, Hernandez-Cuellar E, Kuniyoshi K, et al. Malt1-induced cleavage of Regnase-1 in CD4+ Helper T cells regulates immune activation. Cell. 2013 May 23;153(5):1036.
260. Li M, Cao W, Liu H, Zhang W, Liu X, Cai Z, et al. MCPIP1 Down-Regulates IL-2 Expression through an ARE-Independent Pathway. Stoecklin G, editor. PLoS One. 2012 Nov 21;7(11):e49841.
261. Wei J, Long L, Zheng W, Dhungana Y, Lim SA, Guy C, et al. Targeting REGNASE-1 programs long-lived effector T cells for cancer therapy. Nature. 2019 Dec 11;576(7787):471–6.

Annexes

ID	CPMs (hours after αCD3αCD28 stimulation) 0	3	6	24
hsa-miR-150-5p	83691,60			65981,98
hsa-miR-92a-3p	32931,55		40921,39	60620,04
hsa-miR-155-5p	6125,68		9312,52	54913,26
hsa-miR-30d-5p	15844,38			13505,79
hsa-miR-1260a	6938,74	4282,38	3713,64	1611,18
hsa-miR-27a-3p	5962,95			4672,93
hsa-miR-140-3p	2831,81			2279,21
hsa-miR-20a-5p	1443,44			3005,39
hsa-miR-101-3p	2202,82			1395,30
hsa-miR-221-3p	1311,92			1870,99
hsa-miR-378a-3p	1379,14			1788,88
hsa-miR-142-5p	1593,51			848,28
hsa-miR-30e-5p	1313,83			934,59
hsa-miR-192-5p	1111,00			815,64
hsa-miR-150-3p	1128,14			579,62
hsa-miR-1275	1114,97			590,43
hsa-miR-197-3p	844,40			650,70
hsa-miR-27a-5p	757,82		346,88	326,04
hsa-miR-17-5p	385,79			937,66
hsa-miR-484	457,65			544,07
hsa-miR-98-5p	343,93			573,90
hsa-miR-93-5p	372,89			481,54
hsa-miR-5701	467,73			304,71
hsa-miR-769-5p	419,84			340,35
hsa-miR-339-3p	429,59			316,47
hsa-miR-92a-1-5p	75,21		152,31	367,80
hsa-miR-16-2-3p	149,43	89,02	75,72	75,50
hsa-miR-425-5p	216,54			159,97
hsa-miR-1246	59,24			289,43
hsa-miR-625-3p	167,81			140,26
hsa-miR-181a-3p	136,47			110,64
hsa-miR-339-5p	152,28			89,66
hsa-miR-29c-3p	143,89			89,97
hsa-miR-501-3p	127,11			98,43
hsa-miR-1261	81,59			142,01
hsa-miR-671-3p	88,51			122,83
hsa-miR-92b-3p	58,60			133,61
hsa-miR-1290	29,56		54,73	92,48
hsa-miR-132-5p	18,93	42,00	53,57	41,87
hsa-miR-4791	90,31			58,14
hsa-miR-1307-5p	59,92		37,09	38,19
hsa-miR-132-3p	23,06		45,08	65,16
hsa-miR-1268a	41,22			90,10
hsa-miR-20b-5p	50,13			77,99
hsa-miR-4488	32,97		74,55	
hsa-miR-766-3p	56,27			42,89
hsa-miR-106a-5p	36,16			50,92
hsa-miR-29b-1-5p	23,15			62,76
hsa-miR-30b-3p	50,02			35,64
hsa-miR-21-3p	26,47			57,38
hsa-miR-4455	0,69			78,94
hsa-miR-4485-3p	41,48	13,61	9,74	3,82
hsa-miR-212-5p	8,99		20,87	27,51
hsa-miR-18a-3p	18,35			36,41
hsa-miR-4451	3,30	14,72	14,17	22,11
hsa-miR-335-5p	31,76			19,70
hsa-miR-25-5p	26,87			14,34
hsa-miR-12136	23,37			11,89
hsa-miR-3173-5p	13,91		21,32	
hsa-miR-4448	2,38	6,29	9,07	17,38

Table A.1. Differential miRNA expression 3h, 6h and 24h after αCD3αCD28 stimulation of human primary CD4+ T cells (continued, 1/2). Total CPMs (3 donors average) for miRNA differentially expressed at indicated time points vs time 0h.
Continued in next page.

ID	CPMs (hours after αCD3αCD28 stimulation) 0	3	6	24
hsa-miR-12135	22,56		9,80	
hsa-miR-9-5p	10,43			19,19
hsa-miR-191-3p	3,36	8,47	8,00	8,91
hsa-miR-193a-5p	10,60			18,03
hsa-miR-331-5p	11,99			15,21
hsa-miR-1306-5p	15,27			10,72
hsa-miR-4301	3,25		8,16	13,78
hsa-miR-4695-3p	14,28		7,51	3,11
hsa-miR-1291	10,45		6,06	6,21
hsa-miR-421	12,23			8,19
hsa-miR-18a-5p	2,78		5,67	10,73
hsa-miR-23a-5p	13,85			5,14
hsa-miR-296-5p	11,49			7,31
hsa-miR-5193	11,86			6,64
hsa-miR-331-3p	10,70			6,96
hsa-miR-766-5p	9,61			6,75
hsa-miR-190b-5p	6,12			10,03
hsa-miR-6803-3p	8,35			5,76
hsa-let-7g-3p	8,66			4,90
hsa-miR-7974	0,66			11,11
hsa-miR-4661-5p	7,19		4,35	
hsa-miR-222-5p	0,29	1,60	2,26	6,51
hsa-miR-1281	0,64	4,83	4,84	
hsa-miR-1180-3p	2,42			7,88
hsa-miR-582-3p	7,27			2,75
hsa-miR-3195	0,70		4,98	4,28
hsa-miR-203a-3p	6,70			3,11
hsa-miR-219a-1-3p	3,72			5,94
hsa-miR-550a-5p	4,62		2,51	2,52
hsa-miR-27b-5p	6,40		2,69	
hsa-miR-23b-5p	3,24			5,68
hsa-miR-877-3p	1,74			6,76
hsa-miR-223-3p	5,17			2,39
hsa-miR-1304-3p	2,46			4,91
hsa-miR-1268b	1,73			4,20
hsa-miR-5585-3p	3,50			1,63
hsa-miR-155-3p	0,22			4,25
hsa-miR-365a-5p	0,85		3,10	
hsa-miR-2355-3p	2,47			1,18
hsa-miR-127-3p	2,20			1,16
hsa-miR-19b-1-5p	0,53			2,74
hsa-miR-6873-3p	0,38			2,71
hsa-miR-139-3p	2,33			0,83
hsa-miR-4521	0,19			2,86
hsa-miR-942-3p	0,91			1,89
hsa-miR-33b-3p	0,63			1,84
hsa-miR-4639-5p	0,43		1,48	
hsa-miR-1226-5p	0,32			1,43
hsa-miR-375-3p	0,35			1,35
hsa-miR-1303	0,33			1,23
hsa-miR-12130	0,31			1,22
hsa-miR-548h-3p	0,97			0,42
hsa-miR-548z	0,97			0,42
hsa-miR-6755-5p	0,42			0,95
hsa-miR-548s	0,36			0,93
hsa-miR-663a	0,18		0,93	
hsa-miR-6743-3p	0,20		0,88	
hsa-miR-570-3p	0,69			0,21
hsa-miR-5588-5p	0,59			0,18
hsa-miR-369-3p	0,45			0,15

Table A.1. Differential miRNA expression 3h, 6h and 24h after αCD3αCD28 stimulation of human primary CD4+ T cells (continued, 2/2). Total CPMs (3 donors average) for miRNA differentially expressed at indicated time points vs time 0h.

ID	CPMs (hours after IFN I stimulation)			
	0	3	6	24
hsa-miR-92a-3p	32931,55			43025,14
hsa-miR-1260a	6938,739	5008,144	3934,446	1872,082
hsa-miR-27a-3p	5962,949			4493,788
hsa-miR-148a-3p	4932,086			3662,717
hsa-miR-7-5p	4054,489			2247,008
hsa-miR-192-5p	1111,001			867,7856
hsa-miR-27a-5p	757,8247	223,2073	127,5912	55,06303
hsa-miR-339-3p	429,5853			354,6546
hsa-miR-7704	250,0201			360,5319
hsa-miR-1246	59,23732		101,4326	251,8901
hsa-miR-1261	81,58511		155,6308	158,3131
hsa-miR-16-2-3p	149,4283	78,02162	77,36553	61,96279
hsa-miR-339-5p	152,2837			103,0051
hsa-miR-181a-3p	136,474			100,2256
hsa-miR-1290	29,55987		56,49406	97,01349
hsa-miR-4488	32,96871	64,62691	72,48496	
hsa-miR-4791	90,31223			60,34051
hsa-miR-10400-5p	41,26733	79,79322		
hsa-miR-30c-1-3p	63,42033			48,4404
hsa-miR-1307-5p	59,92336			39,30146
hsa-miR-30b-3p	50,01581			36,80907
hsa-miR-4485-3p	41,48062	16,40789	10,66798	3,391186
hsa-miR-335-3p	45,08055			25,71605
hsa-miR-148a-5p	30,33599			21,03367
hsa-miR-25-5p	26,86908			17,39277
hsa-miR-21-3p	26,46691			17,12903
hsa-miR-4451	3,297546	11,79294	13,6752	9,376463
hsa-miR-12136	23,36863			13,29612
hsa-miR-3173-5p	13,91446			22,40708
hsa-miR-4301	3,251752	6,290716	9,122942	12,04313
hsa-miR-12135	22,56015			6,642223
hsa-miR-193a-5p	10,60382			17,19358
hsa-miR-3614-5p	1,482233	3,548004	7,279818	11,93282
hsa-miR-4695-3p	14,28375		6,888898	2,742154
hsa-miR-23a-5p	13,85023		4,806445	2,836494
hsa-miR-4448	2,377959		6,397818	9,80948
hsa-miR-191-3p	3,363855	7,85347	6,587458	
hsa-miR-193b-3p	9,59176			6,101913
hsa-let-7f-2-3p	10,79944			3,915205
hsa-miR-1281	0,640733	5,225725	4,280072	
hsa-miR-582-3p	7,269388			1,777215
hsa-miR-27b-5p	6,399186			2,58302
hsa-miR-3196	1,985931	4,559296		
hsa-miR-4286	3,974405			1,980258
hsa-miR-3195	0,703802		5,245471	
hsa-miR-3912-3p	4,013393			1,90221
hsa-miR-5585-3p	3,501862			1,564764
hsa-miR-3917	1,108136			3,222077
hsa-miR-503-5p	1,059646			3,054687
hsa-miR-127-3p	2,204662		0,807335	
hsa-miR-589-3p	0,563664			1,607033
hsa-miR-4498	0,576901	1,380379		
hsa-miR-663a	0,184898	0,757733		0,741033
hsa-miR-4510	0,341734			0,996013
hsa-miR-3180-3p	0,970996	0,196829		
hsa-miR-212-3p	0,718196			0,22054
hsa-miR-6743-3p	0,204116			0,696794

Table A.2.Differential miRNA expression 3h, 6h and 24h after IFN I stimulation of human primary CD4+ T cells.
Total CPMs (3 donors average) for miRNA differentially expressed at indicated time points vs time 0h.

Accession	Protein name	Beads	miRNA-25	miRNA-25-UU	miRNA-25-AA	miRNA-151	miRNA-151-UU	miRNA-151-AA	Poly(U)	Poly(A)
P05455	Lupus La protein		1	12	1	1	5	1	17	1
P52272	Heterogeneous nuclear ribonucleoprotein M	5	13	22	13	12	19	20	69	5
P43243	Matrin-3		8	20	16	2			34	
P46778	60S ribosomal protein L21	1	8	11	7	5	11	11	12	9
P27635	60S ribosomal protein L10	3	8	12	7	6	13	10	14	11
P61353	60S ribosomal protein L27	2	4	8	6	3	9	8	9	10
P11940	Polyadenylate-binding protein 1		13	15	12	5	10	16	23	27
O76021	Ribosomal L1 domain-containing protein 1		9	11	7	2	7	8	14	2
P46777	60S ribosomal protein L5		1	5	2	1	3	4	4	1
Q96ME7	Zinc finger protein 512			2	3		4	4	11	3
P18621	60S ribosomal protein L17	3	8	11	9	8	13	12	13	13
O60832	H/ACA ribonucleoprotein complex subunit 4		4	8	3	3	4	3	12	2
Q13823	Nucleolar GTP-binding protein 2	2	5	10	6	7	9	9	9	5
Q9HB58	Sp110 nuclear body protein		1	4	4	3	5	2	2	
P62910	60S ribosomal protein L32	2	9	11	7	7	11	13	15	10
P14923	Junction plakoglobin	3	3	9	5	3	4	4	4	4
Q02878	60S ribosomal protein L6	1	5	7	7	3	6	10	9	5
P40429	60S ribosomal protein L13a		6	6	5	2	6	7	8	6
O43143	Pre-mRNA-splicing factor ATP-dependent RNA helicase DHX15		4	5	14	6	9	7	13	20
Q9UJV9	Probable ATP-dependent RNA helicase DDX41	1	6	9	6	7	9	10	8	8
Q9BUJ2	Heterogeneous nuclear ribonucleoprotein U-like protein 1		2	5	1	1	2	2	21	15
P29508	Serpin B3	1		2			3	2	3	
Q71U36	Tubulin alpha-1A chain	3	4	6	2	1	6	4	1	1
P17026	Zinc finger protein 22		1	3	1		2	4	5	3
P05387	60S acidic ribosomal protein P2			3	5	1	2	3	1	
P62280	40S ribosomal protein S11	3	9	11	11	9	13	12	14	13
P46779	60S ribosomal protein L28	4	7	9	8	6	11	10	9	11
P62424	60S ribosomal protein L7a	2	15	13	11	8	15	16	9	9
P08708	40S ribosomal protein S17		2	2	3	2	5	5	4	5
P23396	40S ribosomal protein S3	3	4	7	5	6	9	5	9	5
P83881	60S ribosomal protein L36a	1	8	7	5	4	9	8	5	7
P61513	60S ribosomal protein L37a	1	4	4	4	3	7	5	3	5
P62906	60S ribosomal protein L10a	1	6	6	5	1	5	5	5	1
P62888	60S ribosomal protein L30		3	5	5	1	2	4	3	1
P49711	Transcriptional repressor CTCF			2			1	1	7	3
Q4G0J3	La-related protein 7		6	7	2		2	3	11	
Q9NXF1	Testis-expressed protein 10		3	3	6	2	5	4		
O95478	Ribosome biogenesis protein NSA2 homolog		2	1	4		4	4	1	2
Q9H6W3	Bifunctional lysine-specific demethylase and histidyl-hydroxylase NO66	1	2	4	3	2	4	3		
Q8IYB7	DIS3-like exonuclease 2			3					14	

Table A.3. Proteins differentially detected interacting with uridylated miRNAs in human lymphoblasts pull-down experiments (continued, 1/3).
Proteins with a sum of at least two peptides more detected in uridylated miRNAs in comparison to canonical forms and subtracting non-specific binding. Colour legend (blue: ribosomal proteins, green: ribonucleoproteins, yellow: exonucleases). Continued in next page.

Accession	Protein name	Beads	miRNA-25	miRNA-25-UU	miRNA-25-AA	miRNA-151	miRNA-151-UU	miRNA-151-AA	Poly(U)	Poly(A)
O95625	Zinc finger and BTB domain-containing protein 11		2	3	1	1	3		5	2
Q9Y3B7	39S ribosomal protein L11, mitochondrial		2	4	4		1	2	1	
Q9UGY1	Nucleolar protein 12			2		1	2	2	1	1
Q9BQ48	39S ribosomal protein L34, mitochondrial			1	1		2	1		1
P39023	60S ribosomal protein L3	1	10	14	10	8	7	13	12	10
Q07020	60S ribosomal protein L18	1	6	8	7	5	6	6	8	5
P50914	60S ribosomal protein L14	1	6	7	7	3	5	7	6	6
P46776	60S ribosomal protein L27a	3	5	8	4	5	7	6	8	7
Q92522	Histone H1x	1	5	6	4	3	5	5	4	5
P62851	40S ribosomal protein S25	2	2	4	4	2	4	5	3	2
P62244	40S ribosomal protein S15a	2	5	6	5	4	7	5	4	2
P62899	60S ribosomal protein L31	1	3	6	3	4	4	6	2	1
Q9Y3U8	60S ribosomal protein L36	1	4	6	5	4	5	9	5	5
P63173	60S ribosomal protein L38	1	1	3	2	2	3	2	3	3
Q14103	Heterogeneous nuclear ribonucleoprotein D0			1	2	1	2	1	19	2
Q15717	ELAV-like protein 1		1	3	2	1	1	3	19	
Q9UKM9	RNA-binding protein Raly	1	2	5	5	2	2	5	9	
P05109	Protein S100-A8		1	2			1	2	1	2
B2RXH8	Heterogeneous nuclear ribonucleoprotein C-like 2		3	4	1	3	4	4	5	
Q9BV38	WD repeat-containing protein 18	2	2	5	2	3	4	3	1	1
P18077	60S ribosomal protein L35a		4	3	5	1	4	5	1	1
Q96P63	Serpin B12	1		3				2		
P05089	Arginase-1			2						1
Q13509	Tubulin beta-3 chain		2	3	3	1	2	3	2	2
Q59GN2	Putative 60S ribosomal protein L39-like 5		1	1			2	1	1	1
Q99848	Probable rRNA-processing protein EBP2		1	3	4	1	1	2	1	
Q9NUL3	Double-stranded RNA-binding protein Staufen homolog 2			2	1			2	4	12
Q92901	60S ribosomal protein L3-like			1	1	1	2		1	2
Q8NEJ9	Neuroguidin	2	1	3	1	2	4	2		1
O95758	Polypyrimidine tract-binding protein 3		1	4	2	1			4	
Q5SY16	Polynucleotide 5'-hydroxyl-kinase NOL9		1	2			1	2	1	1
Q9NY93	Probable ATP-dependent RNA helicase DDX56			1	1		1	1		
P51398	28S ribosomal protein S29, mitochondrial						2	2	2	
Q9NY61	Protein AATF			1	1	1	2	1		1
Q5JTW2	Centrosomal protein of 78 kDa				1		2	1	2	1
A0A0U1RQF3	Uncharacterized protein			1	1		1	1	1	1
Q5H9U9	Probable ATP-dependent RNA helicase DDX60-like			2	1					2
O75182	Paired amphipathic helix protein Sin3b			1			1	1	1	1
P52815	39S ribosomal protein L12, mitochondrial			2	2					

Table A.3. Proteins differentially detected interacting with uridylated miRNAs in human lymphoblasts pull-down experiments (continued, 2/3).
Proteins with a sum of at least two peptides more detected in uridylated miRNAs in comparison to canonical forms and subtracting non-specific binding. Colour legend (blue: ribosomal proteins, green: ribonucleoproteins, yellow: exonucleases). Continued in next page.

Accession	Protein name	Beads	miRNA-25	miRNA-25-UU	miRNA-25-AA	miRNA-151	miRNA-151-UU	miRNA-151-AA	Poly(U)	Poly(A)
Q8TAA3	Proteasome subunit alpha type-7-like			1	1		1			1
F5GZ99	Lysine-specific demethylase 5A (Fragment)			1			1		1	
Q9H9J2	39S ribosomal protein L44, mitochondrial			2	1					
Q9H9L3	Interferon-stimulated 20 kDa exonuclease-like 2			1			1	1		

Table A.3. Proteins differentially detected interacting with uridylated miRNAs in human lymphoblasts pull-down experiments (Continued, 3/3).
Proteins with a sum of at least two peptides more detected in uridylated miRNAs in comparison to canonical forms and subtracting non-specific binding. Colour legend (blue: ribosomal proteins, green: ribonucleoproteins, yellow: exonucleases).

Accession	Protein name	Beads	miRNA-25	miRNA-25-UU	miRNA-25-AA	miRNA-151	miRNA-151-UU	miRNA-151-AA	Poly(U)	Poly(A)
Q9H0J9	Poly [ADP-ribose] polymerase 12									19
O75152	Zinc finger CCCH domain-containing protein 11A									9
Q96BK5	PIN2/TERF1-interacting telomerase inhibitor 1				2				1	8
Q8N5A5	Zinc finger CCCH-type with G patch domain-containing protein									7
Q02543	60S ribosomal protein L18a		8	9	7	5	5	8	7	11
Q96SI9	Spermatid perinuclear RNA-binding protein									4
Q9UPY3	Endoribonuclease Dicer									4
Q6PKG0	La-related protein 1		5	3	3	2	3	2	4	8
Q92843-2	Isoform 3 of Bcl-2-like protein 2								1	4
P18583	Protein SON	2	7	4	11	9	11	5	3	8
P05090	Apolipoprotein D							1		2
O95793	Double-stranded RNA-binding protein Staufen homolog 1									2
Q15633	RISC-loading complex subunit TARBP2									2
Q8IWR0	Zinc finger CCCH domain-containing protein 7A									2

Table A.4. Proteins differentially detected interacting with poly(A) in human lymphoblasts pull-down experiments.
Proteins with a sum of at least two peptides more detected in poly(A) sample in comparison to poly(U). Colour legend (blue: ribosomal proteins, green: ribonucleoproteins, yellow: exonucleases).

Accession	Protein name	Beads	miRNA-25	miRNA-25-UU	miRNA-25-AA	miRNA-151	miRNA-151-UU	miRNA-151-AA	Poly(U)	Poly(A)
P07814	Bifunctional glutamate/proline--tRNA ligase					1			33	
Q9NR30	Nucleolar RNA helicase 2		5	4	2	3		4	29	
Q00839	Heterogeneous nuclear ribonucleoprotein U		2	1		1	1	5	29	1
P42704	Leucine-rich PPR motif-containing protein, mitochondrial								27	
Q15046	Lysine--tRNA ligase								25	
Q92945	Far upstream element-binding protein 2								25	
P14868	Aspartate--tRNA ligase, cytoplasmic								23	
O75533	Splicing factor 3B subunit 1			1	1	1			24	2
Q96AE4	Far upstream element-binding protein 1								22	
P54136	Arginine--tRNA ligase, cytoplasmic								20	
Q14690	Protein RRP5 homolog								20	
P19338	Nucleolin		5	7	3	3	2	3	19	
Q96I24	Far upstream element-binding protein 3								19	
Q15393	Splicing factor 3B subunit 3		2	1		1	2	2	19	1
P42285	Superkiller viralicidic activity 2-like 2								17	
Q92900	Regulator of nonsense transcripts 1		11	6	7	2	5	12	17	
P41252	Isoleucine--tRNA ligase, cytoplasmic								16	
Q13435	Splicing factor 3B subunit 2								15	
Q6NZY4	Zinc finger CCHC domain-containing protein 8								15	
P67809	Nuclease-sensitive element-binding protein 1		11	7	9	5	9	8	15	1
O14979	Heterogeneous nuclear ribonucleoprotein D-like								14	
P22626	Heterogeneous nuclear ribonucleoproteins A2/B1		2			1		3	14	
P47897	Glutamine--tRNA ligase								13	
Q6P2Q9	Pre-mRNA-processing-splicing factor 8		1	1		1		1	13	
O75643	U5 small nuclear ribonucleoprotein 200 kDa helicase		1	1	1	1		1	13	
Q1KMD3	Heterogeneous nuclear ribonucleoprotein U-like protein 2				1	2			13	
P26599	Polypyrimidine tract-binding protein 1		1	2	2				11	
Q12904	Aminoacyl tRNA synthase complex-interacting multifunctional protein 1								11	
P38919	Eukaryotic initiation factor 4A-III		2	1	2	1	1	3	11	
Q12906	Interleukin enhancer-binding factor 3		1						18	7
Q9NW13	RNA-binding protein 28	1	1	2	2		1	1	11	
O95319	CUGBP Elav-like family member 2								10	
P31483	Nucleolysin TIA-1 isoform p40								10	
P42696	RNA-binding protein 34		1	2	4	5	3	7	10	
P35637	RNA-binding protein FUS		1			1			10	
P56192	Methionine--tRNA ligase, cytoplasmic								9	

Table A.5. Proteins differentially detected interacting with poly(U) in human lymphoblasts pull-down experiments (not included in Table A.3) (continued, 1/3).

Proteins with a sum of at least four peptides more detected in poly(U) sample in comparison to poly(A). Colour legend (blue: ribosomal proteins, green: ribonucleoproteins, yellow: exonucleases). Continued in next page.

Accession	Protein name	Beads	miRNA-25	miRNA-25-UU	miRNA-25-AA	miRNA-151	miRNA-151-UU	miRNA-151-AA	Poly(U)	Poly(A)
Q15029	116 kDa U5 small nuclear ribonucleoprotein component		2	2		3	2	4	9	
Q8IX01	SURP and G-patch domain-containing protein 2			1	2				8	
P62701	40S ribosomal protein S4, X isoform	2	7	8	5	6	7	5	16	6
Q99729	Heterogeneous nuclear ribonucleoprotein A/B								8	
Q9HCS7	Pre-mRNA-splicing factor SYF1								8	
Q15459	Splicing factor 3A subunit 1								8	
Q8TDD1	ATP-dependent RNA helicase DDX54				1				8	
Q9HCE1	Putative helicase MOV-10		5	2		1	1	3	8	
O43390	Heterogeneous nuclear ribonucleoprotein R								13	6
O60506	Heterogeneous nuclear ribonucleoprotein Q							1	13	6
O60306	Intron-binding protein aquarius								7	
Q13573	SNW domain-containing protein 1								7	
Q05048	Cleavage stimulation factor subunit 1								7	
Q13151	Heterogeneous nuclear ribonucleoprotein A0								7	
Q01081	Splicing factor U2AF 35 kDa subunit					1			7	
Q96PK6	RNA-binding protein 14		2	2	2		1		6	
Q14498	RNA-binding protein 39			1				1	6	
Q8IY37	Probable ATP-dependent RNA helicase DHX37				1			1	7	1
Q9BYK8	Helicase with zinc finger domain 2								6	
Q5VYS8	Terminal uridylyltransferase 7								6	
Q86XP3	ATP-dependent RNA helicase DDX42								6	
P07910	Heterogeneous nuclear ribonucleoproteins C1/C2		4	2	2	2	3	2	7	1
P09661	U2 small nuclear ribonucleoprotein A'		1		2	1	1		6	
P14866	Heterogeneous nuclear ribonucleoprotein L				1	2	1	2	6	
Q9BQ39	ATP-dependent RNA helicase DDX50					2			6	
P61326	Protein mago nashi homolog		1			1			6	
Q99575	Ribonucleases P/MRP protein subunit POP1			2	2	2	1	2	6	1
Q9P2J5	Leucine--tRNA ligase, cytoplasmic								5	
P51991	Heterogeneous nuclear ribonucleoprotein A3								5	
Q01085	Nucleolysin TIAR								5	
Q2TAY7	WD40 repeat-containing protein SMU1								5	
Q9Y4Z0	U6 snRNA-associated Sm-like protein LSm4								5	
Q96QD9	UAP56-interacting factor								6	1
Q9H2U1	ATP-dependent RNA helicase DHX36								5	
Q13263	Transcription intermediary factor 1-beta								5	
Q96LT9	RNA-binding protein 40								5	
Q9Y2R9	28S ribosomal protein S7, mitochondrial								5	

Table A.5. Proteins differentially detected interacting with poly(U) in human lymphoblasts pull-down experiments (not included in Table A.3) (continued, 2/3).
Proteins with a sum of at least four peptides more detected in poly(U) sample in comparison to poly(A). Colour legend (blue: ribosomal proteins, green: ribonucleoproteins, yellow: exonucleases). Continued in next page.

Accession	Protein name	Beads	miRNA-25	miRNA-25-UU	miRNA-25-AA	miRNA-151	miRNA-151-UU	miRNA-151-AA	Poly(U)	Poly(A)
Q9Y580	RNA-binding protein 7								5	
P15880	40S ribosomal protein S2	2	3	4	5	3	3	4	15	8
Q9UMS4	Pre-mRNA-processing factor 19				1	2			6	1
P62316	Small nuclear ribonucleoprotein Sm D2		2		1	2	2		5	
Q9BZE4	Nucleolar GTP-binding protein 1		2	3	5	2	2	2	4	
P62312	U6 snRNA-associated Sm-like protein LSm6								4	
Q12996	Cleavage stimulation factor subunit 3								4	
Q99729-2	Isoform 2 of Heterogeneous nuclear ribonucleoprotein A/B								4	
Q9Y3Y2	Chromatin target of PRMT1 protein								5	1
P98179	RNA-binding protein 3								4	
Q9BZJ0	Crooked neck-like protein 1								4	
P26368	Splicing factor U2AF 65 kDa subunit								4	
Q86TB9	Protein PAT1 homolog 1								4	
Q9H0D6	5'-3' exoribonuclease 2				1				4	
Q9HC16	DNA dC->dU-editing enzyme APOBEC-3G								4	
Q15233	Non-POU domain-containing octamer-binding protein					1			4	
P11142	Heat shock cognate 71 kDa protein	1	6	7	7	6	4	6	10	5
Q92841	Probable ATP-dependent RNA helicase DDX17		1			1		1	4	
O00148	ATP-dependent RNA helicase DDX39A		2		1	2	1	2	5	1

Table A.5. Proteins differentially detected interacting with poly(U) in human lymphoblasts pull-down experiments (not included in Table A.3) (continued, 3/3).
Proteins with a sum of at least four peptides more detected in poly(U) sample in comparison to poly(A). Colour legend (blue: ribosomal proteins, green: ribonucleoproteins, yellow: exonucleases).

ID	CTM WT	CTM KD	logFC	P.Value	adjusted P.Value	Fold change	Symbol	Description
ENSG00000143319	**75,42**	**48,20**	**-0,64**	**0,000**	**0,008**	**-1,56**	**ISG20L2**	**interferon stimulated exonuclease gene 20 like 2**
ENSG00000163584	**81,00**	**62,45**	**-0,38**	**0,000**	**0,017**	**-1,30**	**RPL22L1**	**ribosomal protein L22 like 1**
ENSG00000156508	**9680,58**	**10662,04**	**0,14**	**0,000**	**0,079**	**1,10**	**EEF1A1**	**eukaryotic translation elongation factor 1 alpha 1**
ENSG00000168421	130,66	159,65	0,29	0,000	0,118	1,22	RHOH	ras homolog family member H
ENSG00000284048	4,18	0,35	-5,19	0,000	0,123	-36,45	lncRNA	AC073111.3-201/2
ENSG00000188801	0,29	2,84	4,23	0,000	0,227	18,80	ZNF322P1	zinc finger protein 322 pseudogene 1
ENSG00000138413	51,63	42,13	-0,29	0,000	0,227	-1,22	IDH1	isocitrate dehydrogenase (NADP(+)) 1, cytosolic
ENSG00000228144	13,55	9,83	-0,46	0,000	0,227	-1,38		uncharacterized protein
ENSG00000254911	1,94	7,06	1,80	0,000	0,227	3,47	SCARNA9	small Cajal body-specific RNA 9
ENSG00000249884	4,13	7,77	0,93	0,000	0,227	1,90	RNF103-CHMP3	RNF103-CHMP3 readthrough
ENSG00000023330	55,49	65,52	0,24	0,000	0,227	1,18	ALAS1	5'-aminolevulinate synthase 1
ENSG00000214562	7,75	5,08	-0,62	0,000	0,227	-1,54	NUTM2D	NUT family member 2D
ENSG00000167552	192,45	161,57	-0,25	0,000	0,227	-1,19	TUBA1A	tubulin alpha 1a
ENSG00000114805	12,42	16,62	0,42	0,000	0,227	1,33	PLCH1	phospholipase C eta 1
ENSG00000232573	53,10	42,81	-0,31	0,000	0,227	-1,24	RPL3P4	ribosomal protein L3 pseudogene 4
ENSG00000116199	95,26	81,48	-0,23	0,000	0,247	-1,17	FAM20B	FAM20B, glycosaminoglycan xylosylkinase
ENSG00000165272	53,59	63,11	0,24	0,000	0,247	1,18	AQP3	aquaporin 3 (Gill blood group)
ENSG00000183508	92,41	78,53	-0,23	0,000	0,247	-1,17	FAM46C	family with sequence similarity 46 member C
ENSG00000263934	1,89	4,33	1,18	0,000	0,247	2,27	SNORD3A	small nucleolar RNA, C/D box 3A
ENSG00000197816	2,50	4,45	0,89	0,000	0,247	1,85	CCDC180	coiled-coil domain containing 180
ENSG00000103226	132,05	112,13	-0,23	0,000	0,247	-1,18	NOMO3	NODAL modulator 3
ENSG00000110848	8,25	12,94	0,63	0,000	0,247	1,55	CD69	CD69 molecule
ENSG00000138795	621,78	705,34	0,18	0,000	0,247	1,13	LEF1	lymphoid enhancer binding factor 1
ENSG00000188486	101,65	88,14	-0,21	0,000	0,247	-1,15	H2AFX	H2A histone family member X
ENSG00000184923	2,11	3,72	0,85	0,000	0,247	1,81	NUTM2A	NUT family member 2A
ENSG00000080644	31,04	36,95	0,25	0,000	0,247	1,19	CHRNA3	cholinergic receptor nicotinic alpha 3 subunit
ENSG00000177169	87,14	76,15	-0,19	0,000	0,247	-1,14	ULK1	unc-51 like autophagy activating kinase 1
ENSG00000253106	1,61	0,79	-1,01	0,001	0,247	-2,01	lnc-RNF139-1	AC090198.1 (novel transcript, antisense to TATDN1)
ENSG00000204568	69,74	81,37	0,22	0,001	0,247	1,17	MRPS18B	mitochondrial ribosomal protein S18B
ENSG00000157429	2,83	4,45	0,66	0,001	0,247	1,58	ZNF19	zinc finger protein 19
ENSG00000135905	58,96	68,02	0,21	0,001	0,247	1,15	DOCK10	dedicator of cytokinesis 10
ENSG00000279277	2,56	1,37	-0,91	0,001	0,247	-1,88	lnc-CD47-1	AC012020.1
ENSG00000224003	1,45	0,68	-1,11	0,001	0,247	-2,15	YES1P1	YES1 pseudogene 1
ENSG00000273167	0,59	2,22	3,94	0,001	0,247	15,30		uncharacterized protein
ENSG00000203441	0,64	1,45	1,32	0,001	0,262	2,50	LINC00449	long intergenic non-protein coding RNA 449
ENSG00000277053	56,09	65,36	0,22	0,001	0,301	1,17	GTF2IP1	general transcription factor IIi pseudogene 1
ENSG00000100271	14,91	11,63	-0,35	0,001	0,301	-1,28	TTLL1	tubulin tyrosine ligase like 1
ENSG00000264668	3,12	0,73	-4,50	0,001	0,303	-22,71		Zinc Finger Protein 41 Homolog
ENSG00000118503	29,73	37,19	0,33	0,001	0,309	1,26	TNFAIP3	TNF alpha induced protein 3
ENSG00000129473	3,72	2,40	-0,63	0,001	0,309	-1,55	BCL2L2	BCL2 like 2
ENSG00000136295	58,91	50,50	-0,22	0,001	0,309	-1,17	TTYH3	tweety family member 3
ENSG00000241945	51,01	59,25	0,22	0,001	0,309	1,16	PWP2	PWP2, small subunit processome component
ENSG00000260916	2,29	3,58	0,65	0,001	0,309	1,57	CCPG1	cell cycle progression 1
ENSG00000143314	58,99	49,62	-0,25	0,001	0,309	-1,19	MRPL24	mitochondrial ribosomal protein L24
ENSG00000243364	8,50	6,13	-0,46	0,001	0,309	-1,38	EFNA4	ephrin A4
ENSG00000176124	30,39	35,85	0,24	0,001	0,309	1,18	DLEU1	deleted in lymphocytic leukemia 1 (non-protein coding)
ENSG00000177410	64,99	76,83	0,25	0,001	0,309	1,19	ZFAS1	ZNFX1 antisense RNA 1
ENSG00000283709	2,56	1,45	-0,81	0,001	0,309	-1,75	FAM238C	family with sequence similarity 238 member C (non-protein coding)
ENSG00000178977	1,22	0,54	-1,30	0,001	0,309	-2,46	LINC00324	long intergenic non-protein coding RNA 324
ENSG00000162607	371,76	419,51	0,18	0,001	0,309	1,13	USP1	ubiquitin specific peptidase 1

Table A.6. mRNAseq ISG20L2 knockdown vs control samples.
Molecules included were detected with the 50 lowest p-values for differential expression. Colour legend (blue: ribosomal proteins, green: lncRNA).

Publications

1. Publications related with this work (attached those published/accepted):

I. Gutiérrez-Vázquez C, Enright AJ, **Rodríguez-Galán A**, Pérez-García A, Collier P, Jones MR, et al. 3' Uridylation controls mature microRNA turnover during CD4+ T-cell activation. RNA. 2017 Jun 1;23(6):882–91.

II. Gutiérrez-Vázquez C, **Rodríguez-Galán A**, Fernández-Alfara M, Mittelbrunn M, Sánchez-Cabo F, Martínez-Herrera DJ, et al. miRNA profiling during antigen-dependent T cell activation: A role for miR-132-3p. Sci Rep. 2017 Jun 14;7(1):3508.

III. **Rodríguez-Galán A**, Fernández-Messina L, Sánchez-Madrid F. Control of Immunoregulatory Molecules by miRNAs in T Cell Activation. Front Immunol. 2018;9(September):1–10.

IV. **Rodríguez-Galán A**, Dosil S G, Gómez M J, Fernández-Delgado I, Fernández-Messina L, Sánchez-Cabo F, Sánchez-Madrid F. MiRNA post-transcriptional modification dynamics in T cell activation, iScience 2021 Jun; 24, 102530.

V. ISG20L2: an RNA enzyme regulating T cell activation // in preparation

2. Other publications (not included):

I. Nielsen CM, White MJ, Bottomley C, Lusa C, **Rodríguez-Galán A**, Turner SEG, et al. Impaired NK Cell Responses to Pertussis and H1N1 Influenza Vaccine Antigens in Human Cytomegalovirus-Infected Individuals. J Immunol. 2015 May 15;194(10):4657–67.

II. Goodier MR, Lusa C, Sherratt S, **Rodriguez-Galan A**, Behrens R, Riley EM. Sustained Immune Complex-Mediated Reduction in CD16 Expression after Vaccination Regulates NK Cell Function. Front Immunol. 2016 Sep 26;7:384.

III. Goodier MR, **Rodriguez-Galan A**, Lusa C, Nielsen CM, Darboe A, Moldoveanu AL, et al. Influenza Vaccination Generates Cytokine-Induced Memory-like NK Cells: Impact of Human Cytomegalovirus Infection. J Immunol. 2016 Jul 1;197(1):313–25.

IV. **Rodríguez-Galán A**, Salman AM, Bowyer G, Collins KA, Longley RJ, Brod F, et al. An in vitro assay to measure antibody-mediated inhibition of P. berghei sporozoite invasion against P. falciparum antigens. Sci Rep. 2017;7(1).

V. Fernández-Messina L, **Rodríguez-Galán A**, de Yébenes VG, Gutiérrez-Vázquez C, Tenreiro S, Seabra MC, et al. Transfer of extracellular vesicle-microRNA controls germinal center reaction and antibody production. EMBO Rep. 2020 Feb 19;e48925.

REPORT

3′ Uridylation controls mature microRNA turnover during CD4 T-cell activation

CRISTINA GUTIÉRREZ-VÁZQUEZ,[1,2] ANTON J. ENRIGHT,[3] ANA RODRÍGUEZ-GALÁN,[1,2] ARANTXA PÉREZ-GARCÍA,[2] PAUL COLLIER,[4] MATTHEW R. JONES,[5] VLADIMIR BENES,[4] JOSEPH P. MIZGERD,[5] MARÍA MITTELBRUNN,[2] ALMUDENA R. RAMIRO,[2] and FRANCISCO SÁNCHEZ-MADRID[1,2,6]

[1]Instituto de Investigación Sanitaria Princesa, Hospital Universitario de la Princesa, Universidad Autónoma de Madrid, Madrid 28006, Spain
[2]Centro Nacional de Investigaciones Cardiovasculares Carlos III (CNIC), Madrid 28029, Spain
[3]European Bioinformatics Institute, Wellcome Trust Genome Campus, Hinxton, Cambridge CB10 1SD, United Kingdom
[4]European Molecular Biology Laboratory (EMBL), Core Facilities and Services, Heidelberg 69117, Germany
[5]Pulmonary Center, Boston University School of Medicine, Boston, Massachusetts 02118, USA
[6]CIBER: Centro Investigación en Red Cardiovascular, Madrid 28029, Spain

ABSTRACT

Activation of T lymphocytes requires a tight regulation of microRNA (miRNA) expression. Terminal uridyltransferases (TUTases) catalyze 3′ nontemplated nucleotide addition (3′NTA) to miRNAs, which may influence miRNA stability and function. Here, we investigated 3′NTA to mature miRNA in CD4 T lymphocytes by deep sequencing. Upon T-cell activation, miRNA sequences bearing terminal uridines are specifically decreased, concomitantly with down-regulation of TUT4 and TUT7 enzymes. Analyzing TUT4-deficient T lymphocytes, we proved that this terminal uridyltransferase is essential for the maintenance of miRNA uridylation in the steady state of T lymphocytes. Analysis of synthetic uridylated miRNAs shows that 3′ addition of uridine promotes degradation of these uridylated miRNAs after T-cell activation. Our data underline post-transcriptional uridylation as a mechanism to fine-tune miRNA levels during T-cell activation.

Keywords: 3′ nontemplated nucleotides addition (3′NTA); CD4 T lymphocytes; microRNAs; uridylation; Zcchc11 (TUT4); Zcchc6 (TUT7); isomiRs

INTRODUCTION

MicroRNAs (miRNAs) are short (~22 nt) noncoding RNAs involved in the control of gene expression in many biological processes (Filipowicz et al. 2008). To fulfill their function, their levels need to be tightly regulated, and dysregulated levels of miRNAs are associated with many diseases (Chang and Mendell 2007). MiRNA turnover is controlled through the precise regulation of both biogenesis and degradation (Filipowicz et al. 2008). The control of miRNA levels through transcriptional and processing mechanisms is well established, but regulation of miRNA degradation is still poorly understood, particularly in mammals. MiRNA stability has been shown to be affected by the cellular physiological status (Hwang et al. 2007; Krol et al. 2010) and the presence of mRNA targets (Ameres et al. 2010; Chatterjee et al. 2011). Moreover, the fate of mature miRNAs is determined by post-transcriptional modifications such as methylation (Li et al. 2005) and nucleotide additions (Landgraf et al. 2007).

In recent years, next-generation sequencing analysis has revealed variability in the individual mature miRNA sequences derived from the same precursor (pre-miRNA), giving rise to the term "isomiRs" (Ameres and Zamore 2013). This sequence diversification in mature miRNAs can be produced through a variety of mechanisms, including imprecise or alternative cropping of the precursor, post-transcriptional A-to-I editing mediated by the enzyme ADAR (adenosine deaminase acting on RNA), terminal trimming of nucleotides, or nontemplated nucleotide additions (NTA). These mechanisms increase the repertoire of cellular regulatory miRNAs and therefore provide additional flexibility to miRNA-mediated regulation of gene expression (Ameres and Zamore 2013).

The most common modification of mature miRNAs is the NTA of uridines and adenosines at the 3′ end (3′NTA) (Landgraf et al. 2007). Several noncanonical poly(A)

Corresponding author: fsmadrid@salud.madrid.org
Article is online at http://www.rnajournal.org/cgi/doi/10.1261/rna.060095.116.

polymerases (PAP) have been shown to add ribonucleotides to the 3′ end of pre-miRNAs and mature miRNAs in a template-independent manner. These enzymes are able to utilize not only adenine triphosphate (ATP) but also uridine triphosphate (UTP); hence, they are called terminal uridyltransferases (TUTases) (Heo et al. 2009, 2012). The identified nucleotidyl transferases in mammals are MTPAP, GLD2, PAPD5, PAPD7 (POLS), U6TUT, ZCCHC11 (TUT4), and ZCCHC6 (TUT7) (Wyman et al. 2011; Norbury 2013). Among these enzymes, TUT4 and TUT7 have been shown to preferentially uridylate mature miRNAs (Minoda et al. 2006; Jones et al. 2009, 2012; Thornton et al. 2015).

MiRNAs are tightly regulated during the activation of T lymphocytes (Monticelli et al. 2005; Cobb et al. 2006; Baumjohann and Ansel 2013). T cells are activated upon encounter with a specific antigen on the surface of an antigen presenting cell. Signaling through the T-cell receptor (TCR) and costimulatory molecules initiates an array of signaling programs that prepare the cell for differentiation, proliferation, and effector function, leading to profound changes in their metabolism and protein and RNA content. Recent studies link the T-cell activation process to a global down-regulation of miRNAs (Bronevetsky et al. 2013), although the specific regulatory mechanisms remain unknown.

In this study, we have investigated NTA to the 3′ of mature miRNAs during T-lymphocyte activation. Mature miRNA 3′ uridylation is predominantly observed in steady state ("naïve") T cells, while T-cell activation promotes both the down-regulation of TUT4 and TUT7 enzymes and the degradation of uridylated microRNAs. Moreover, we have identified TUT4 to be essential for the maintenance of miRNA uridylation.

RESULTS

Uridylated miRNAs are decreased upon T-cell activation

To assess the dynamics of NTA during T-cell activation, we performed a deep-sequencing analysis on small RNAs from mouse $CD4^+$ T cells in naïve conditions ($CD25^-$, $CD62L^+$) and upon stimulation with anti-CD3 and anti-CD28 antibodies. The homogeneity of the replicates for each condition was confirmed by their proximity on the principal components analysis (PCA) (Supplemental Fig. S1A). T-cell activation was confirmed by staining of the activation markers CD25 and CD69 (Supplemental Fig. S1B). Moreover, a global down-regulation of miRNA was detected between naïve and activated samples when miRNA count distributions were analyzed with the Kolmogorov–Smirnov test ($P \leq 4.66 \times 10^{-12}$).

MiRNA modifications were classified according to the number of nucleotides added, i.e., mono addition (one nucleotide) and oligo addition (two or more nucleotides). The relative modification levels from miRNA to miRNA independent of their total expression levels was first examined (Fig. 1A). Uridylation and adenylation were the two most common modifications of CD4 T-cell miRNAs (Fig. 1A). A significant reduction of miRNA uridylation, both mono and oligo additions, was observed in activated T cells upon global examination of the data (Fig. 1B). Individual examination of each miRNA confirmed this observation (Fig. 1C; Supplemental Table S1). In contrast, adenylation seemed to be increased after activation when miRNAs were analyzed globally (Fig. 1A,B), but this was not confirmed in the individual analysis (Fig. 1D). This apparent contradiction is due to a highly expressed adenylated miRNA that must be dominating the global analysis but that does not reflect the general behavior of adenylated miRNAs that is better defined in the individual analysis (Fig. 1D).

Abundance profiles corresponding to each 3′ NTA and the canonical (unmodified) sequence of example miRNAs are shown in Figure 1E. The fraction of counts that correspond to the uridylated forms decreases in activated samples as illustrated also in Supplemental Table S1. Moreover, the five example miRNAs with lower uridylation in activated samples (Fig. 1E) illustrate also that total counts of the miRNA can be either higher, lower, or not changing between naïve and activated conditions (Supplemental Fig. S2). Thus, these data indicate that in CD4 T cells uridylated miRNAs are decreased upon activation.

TUT4 and TUT7 are down-regulated during T-cell activation

To investigate the molecular mechanism underlying the post-transcriptional modification of miRNAs during T-cell activation, we studied the regulation of terminal uridyl transferases (TUTases) during this process. The mRNA transcript levels of MTPAP, GLD2 (TUT2), PAPD5, TUT4 (ZCCHC11), POLS, and TUT7 (ZCCHC6) in CD4 T cells were determined before and after polyclonal stimulation with anti-CD3 and anti-CD28 antibodies for 48 h. TUT4 and TUT7, the two enzymes mainly responsible for uridylation, were decreased upon T-cell activation, whereas MTPAP and POLS were up-regulated, and GLD2 and PAPD5 remained unaltered (Fig. 2A). The reduction of TUT4 mRNA levels was confirmed in human T lymphoblasts stimulated in a polyclonal manner (Fig. 2B) and in antigen-specific experiments in which CD4 T cells from transgenic OT-II mice were co-cultured with bone marrow-derived dendritic cells loaded with OVA peptide (Fig. 2C). TUT4 mRNA was decreased after 24 h of stimulation and remained low at 96 h (Fig. 2D). Western blot analysis of TUT4 protein showed a decrease at 24 h after activation with anti-CD3 and anti-CD28 antibodies and upon treatment with concanavalin A, followed by expansion with recombinant interleukin 2 (an equivalent activating stimulus), where a maximal decrease was observed after 72 h of stimulation (Fig. 2E). Immunofluorescence and subcellular fractionation experiments showed a predominant cytoplasmic confinement of TUT4, and T-cell activation did not elicit any significant subcellular redistribution (Supplemental Fig. S3A,B).

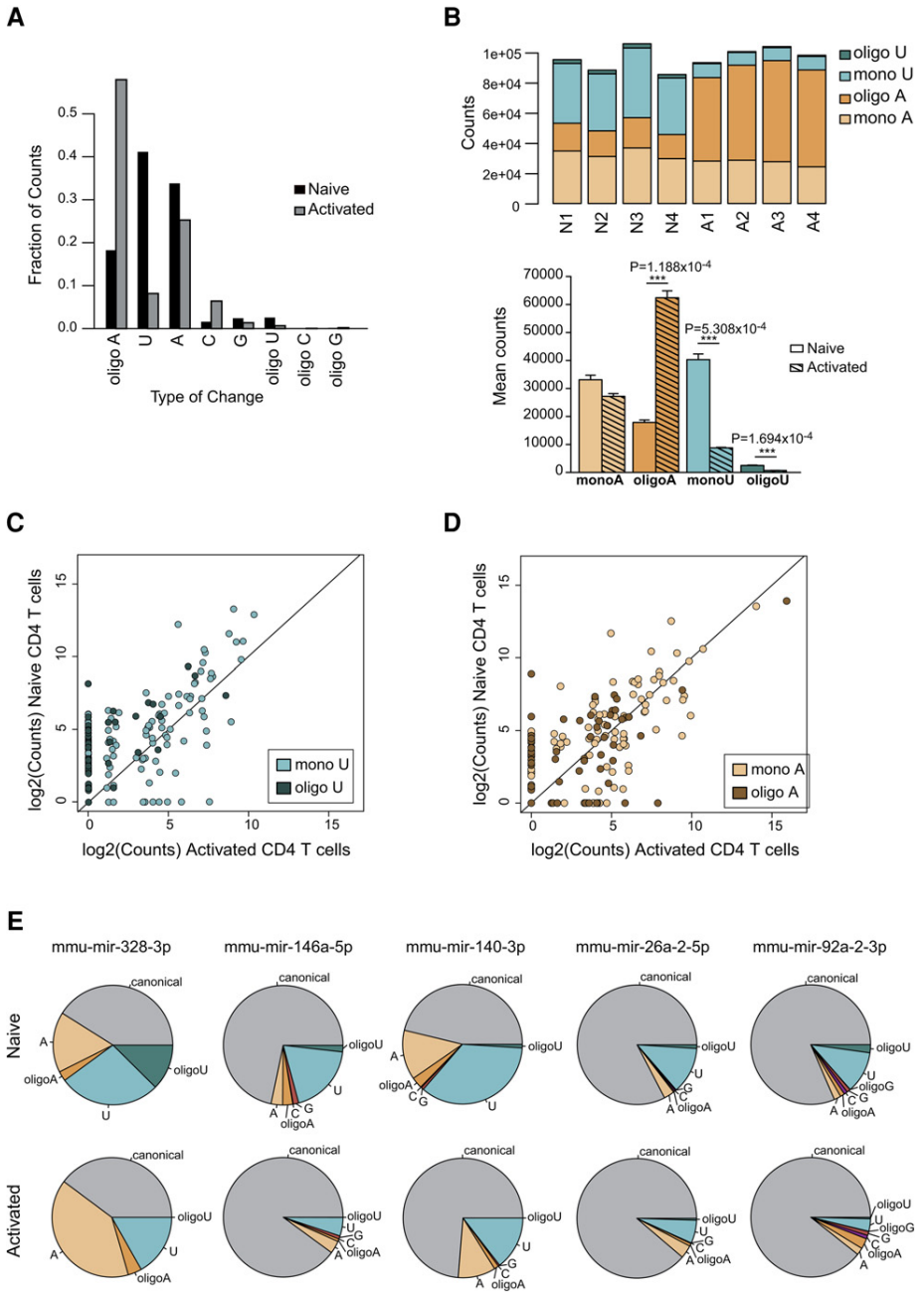

FIGURE 1. Uridylated miRNAs are decreased upon T-cell activation. Deep-sequencing libraries were generated from naïve CD4 T cells or cells activated for 48 h with anti-CD3 and anti-CD28 ($n = 4$). (*A*) 3′ NTAs to all mature miRNAs in naive and activation conditions. The fraction of modified reads that fall into one of eight categories was computed for each miRNA providing the normalized relative levels of modification. These were averaged across all miRNAs observed for both conditions. (*B*) Total normalized (raw) counts for uridylation and adenylation modifications observed across each sample (N: naïve; A: activated CD3/CD28) (*upper* panel) and averaged across replicates (*lower* panel). Error bars indicate the standard error between samples and *P*-values are computed using a Welch's two-sample *t*-test. (*C*,*D*) Comparison of the relative abundance of 3′ mono-uridine and oligo-uridines (*C*) and of 3′ mono-adenine or oligo-adenines (*D*) in individual miRNAs from naïve and activated CD4 T cells. Each dot represents an individual miRNA with the corresponding type of modification. (*E*) Pie charts for selected miRNAs depict the fraction of counts for each type of 3′NTA-modified and canonical miRNA detected. (A) Adenine, (C) cytosine, (G) guanine, and (U) uracil.

The levels of TUT7 protein were also decreased after stimulation with anti-CD3 and anti-CD28 antibodies, albeit with a slower kinetic profile compared to TUT4 (Fig. 2F). These data indicate that T-cell activation triggers a decrease in the cellular levels of TUT4 and TUT7, the main TUTases accounting for miRNA uridylation. The conjoined down-

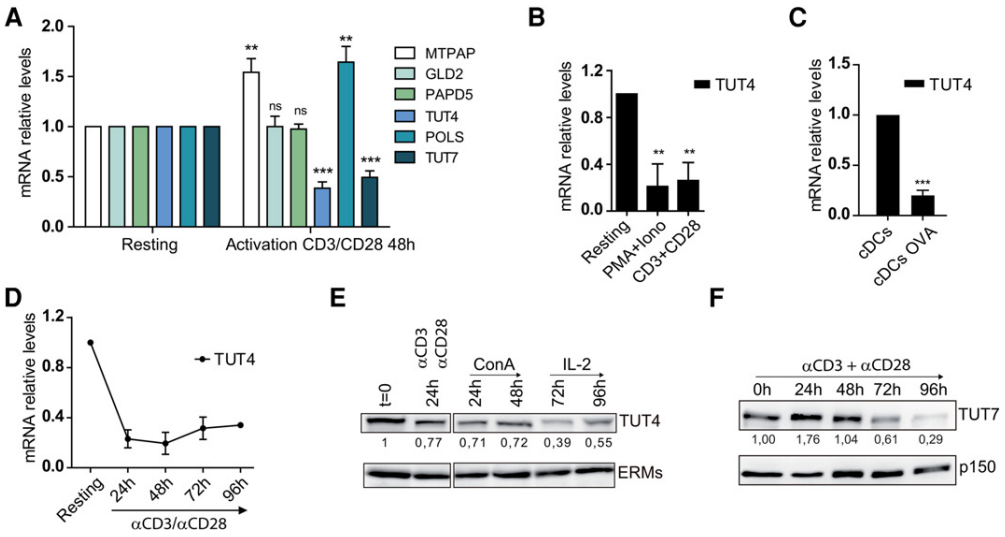

FIGURE 2. TUT4 and TUT7 expression is down-regulated after T-cell activation: (*A*) RNA levels of MTPAP, GLD2, PAPD5, TUT4, POLS, and TUT7 were assessed by RT-qPCR in freshly isolated mouse naïve CD4 T cells or cells activated with anti-CD3 and anti-CD28 for 48 h. mRNA levels were normalized to β-actin and Yhwaz housekeeping genes and are presented in arbitrary units ($n = 7$). (*B*) TUT4 mRNA levels in human T lymphoblasts measured by RT-qPCR after two different activation stimuli: phorbol myristate acetate (PMA) with ionomycin and anti-CD3 plus anti-CD28 ($n = 3$). (*C*) Mouse naïve CD4 T cells from OT-II mice specific to ovalbumin peptide were co-cultured with dendritic cells in the absence or presence of the peptide. TUT4 mRNA levels were determined by RT-qPCR as in *A* ($n = 5$). (*D*) Long-term time course of TUT4 mRNA levels in activated mouse CD4 T cells ($n = 3$). (*E*) Western blot analysis of TUT4 protein content in CD4 T cells after activation with anti-CD3 plus anti-CD28 or with concanavalin A (ConA) followed by expansion with interleukin 2 (IL-2). Representative immunoblots ($n = 3$). ERMs were included as a loading control. (*F*) Western blot analysis of TUT7 protein at different time points after antibody activation of CD4 T cells. Representative immunoblots ($n = 3$). p150 was included as a loading control. Numbers *below* blots show normalized densitometry values relative to naïve T cells. Error bars in *A–C* represent standard deviation; (***) $P < 0.001$; (**) $P < 0.05$; ns, nonsignificant.

regulation of these enzymes, concomitant with the decrease in miRNA uridylation, suggests that the decrease of uridylated miRNA plays an important role during T-cell activation.

TUT4-dependent uridylation of mature microRNA

To assess the role of TUT4 in the uridylation of mature miRNAs in T lymphocytes, we examined CD4 T cells of TUT4-deficient mice in steady state. The lymphoid organs of these mice presented no significant alteration in the percentage of CD4 and CD8 T lymphocytes in thymus (Supplemental Fig. S4A), and CD4 and CD8 T lymphocytes as well as B lymphocytes in spleen or peripheral lymph nodes (Supplemental Fig. S4B,C). Levels of miRNA mono- and oligo-uridylation were lower in naive TUT4-deficient CD4 T cells compared with wild-type cells (Fig. 3A,B). Interestingly, miRNA mono- and oligo-adenylation were higher in TUT4-deficient T cells (Fig. 3C,D). Putative miRNA targets of TUT4 were identified in T cells. We considered as targets both mono-uridylated and oligo-uridylated species that were significantly less uridylated in TUT4-deficient CD4 T cells compared with wild-type cells (Supplemental Table S2A,B). Moreover, miR-seq data showed no significant differences in the levels of canonical miRNAs corresponding to TUT4 targets between TUT4-deficient and wild-type CD4 T cells (Fig. 3E) in accordance with previous reports (Jones et al. 2012; Thornton et al. 2015). Interestingly, analysis of these identified putative targets of TUT4 during T-cell activation of wild-type T cells revealed that the majority of these uridylated miRNAs were down-regulated (Fig. 3F; Supplemental Tables S3, S4). Thus, our data reveal that putative TUT4 targets account for a substantial proportion of the uridylated miRNAs down-regulated upon T-cell activation. These results indicate that TUT4 contributes to the turnover control of a specific set of modified miRNAs during T-cell activation.

Although uridylated miRNAs are clearly less abundant in TUT4-deficient CD4 T cells, we could still detect some miRNAs with 3′ nontemplated uridines. This may reflect the activity of TUT7, which can uridylate miRNAs (Thornton et al. 2015). TUT4-deficient T cells showed no compensatory increase in the levels of TUT7 or any other TUTase (Supplemental Fig. S5A,B), but given the presence of TUT7 protein, it is likely that the remaining miRNA uridylation in TUT4-deficient mice is attributable to this enzyme.

Uridylation directs mature miRNA to activation-dependent degradation

Uridylation of mRNA is associated with both stabilization [when 1 or 2 nt are added to histone mRNAs and poly(A) RNAs] (Lackey et al. 2016; Scheer et al. 2016; Zuber et al. 2016) and decay (Shen and Goodman 2004; Mullen and Marzluff 2008; Schmidt et al. 2011; Lim et al. 2014). To investigate whether uridylation targets mature miRNAs for

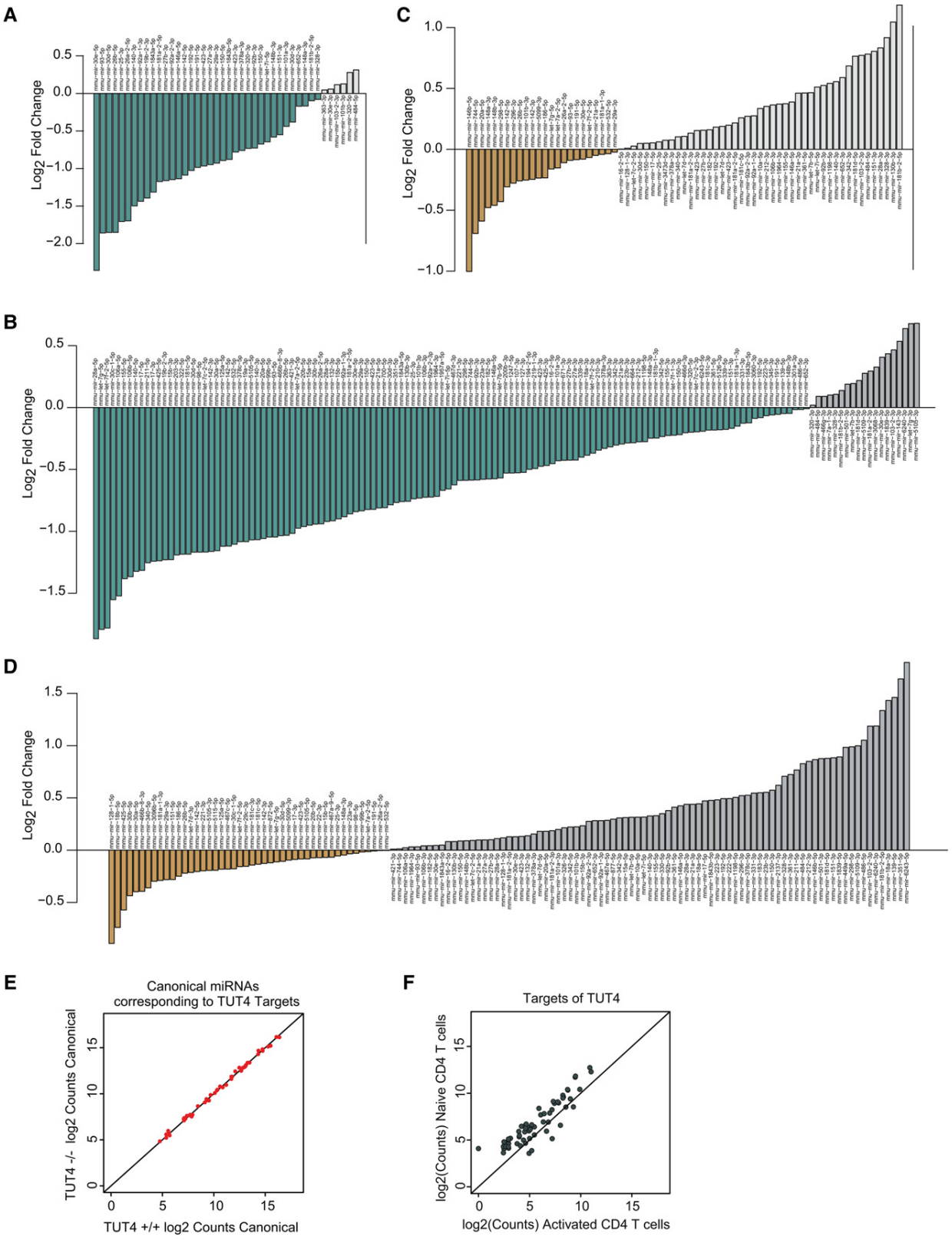

FIGURE 3. (Legend on next page)

degradation during T-cell activation, we transfected naïve CD4 T cells with synthetic RNAs (miR-151-3p and miR-25-3p) corresponding to canonical or di-uridylated miRNA sequences. The cells were subsequently either activated with anti-CD3 and anti-CD28 or maintained in resting conditions with IL-7 to prevent naïve T-cell apoptosis. Levels of the synthetic miRNAs were measured with a variation of miQPCR (Fig. 4A, and see Materials and Methods; Benes et al. 2015), which distinguishes single-nucleotide changes in the miRNA sequence. The levels of synthetic di-uridylated forms of both miR-151-3p and miR-25-3p dropped sharply in activated T cells, whereas the levels of their canonical (unmodified) counterparts remained much more stable (Fig. 4B), indicating that uridylated miRNAs are declined faster than the unmodified miRNAs, specifically upon T-cell activation. Moreover, these results suggest that the decay of uridylated miRNAs comprises total degradation of the molecule rather than the trimming of merely the U tail since there is no increase of canonical synthetic miRNA after activation. That would only occur if the U tail had been removed from the synthetic di-uridylated miRNA while preserving the rest of the molecule. Finally, it is worth mentioning that the synthetic ssRNAs that we are using might not be behaving exactly as endogenous miRNAs in terms of their incorporation to the RISC complex, a process that could affect their decay, Nevertheless, these data indicate that miRNA uridine tailing is an important mechanism to target a specific set of miRNAs for degradation, and that this process is tightly regulated upon T-cell activation.

DISCUSSION

The present study demonstrates that miRNA 3′ NTA are modifications tightly regulated that can modulate the stability of these small RNA species. Our data indicate that the enzymes responsible for miRNA uridylation as well as uridylated miRNAs themselves are regulated during T-cell activation. We further report TUT4 as an enzyme responsible for uridylation of mature miRNA in T cells, and show that the stability of uridylated miRNAs differs in T cells between naïve and activated conditions. The proposed mechanism for the post-transcriptional regulation of miRNAs during T-cell activation is illustrated in the scheme (Fig. 4C).

The addition of poly(U) tails to the 3′ ends of pre-miRNAs has been reported to trigger their degradation in stem cells (Heo et al. 2009), while in somatic cells lacking Lin28, TUT-mediated mono-uridylation of pre-miRNAs facilitates their processing (Heo et al. 2012). The impact of 3′ NTA on mature miRNAs varies depending on the organism and the miRNA examined (Katoh et al. 2009; Lu et al. 2009; Burroughs et al. 2010). Uridylation of miRNAs leads to degradation in *Chlamydomonas* (Ibrahim et al. 2010) and plants, where it prevents their methylation (Zhao et al. 2012). In mammals, uridylation of mature miRNA has been shown to specifically reduce the functionality of miR-26a, miR-126-5p, and miR-379 (Jones et al. 2009, 2012). Our data demonstrate that the stability of mature miRNAs is decreased in the context of T-cell activation when they bear uracils added to their 3′ end. This is supported by the fact that synthetic di-uridylated miRNAs are decreased more rapidly than the corresponding synthetic canonical miRNAs, but only when T cells are activated. Nevertheless, since these conclusions arise from exogenously added miRNAs, we cannot undoubtedly predict that the exact same process is happening for endogenous uridylated miRNAs.

Our data are consistent with a decrease in the uridylation of miRNA due to a reduction in the levels of the uridyl transferases TUT4 and TUT7 during T-cell activation. Additionally, a specific subset of uridylated miRNAs has been identified as targets of TUT4. In this regard, it is important to mention that TUT4-deficient T cells still contain low levels of uridylated miRNAs that are likely to be substrates of other TUTases, e.g., TUT7.

According to data from previous work (Jones et al. 2009, 2012) and the present study, it is conceivable that uridylation changes the targeting specificity of the miRNA, its functionality, and/or labels miRNAs for degradation. Thus, the degradation of a defined set of uridylated miRNAs specifically during T-cell activation may represent an additional mechanism for the cell to eliminate certain miRNAs at this specific stage. However, our data do not allow us to rule out additional mechanisms of miRNA biogenesis, like their transcription and processing, accounting for miRNA levels' regulation and the imbalance of the 3′ uridylated miRNA pool during T-cell activation.

A key outstanding question about miRNA decay is the identity of the enzymes that catalyze the degradation of these small RNAs during T-cell activation. Several mammalian exoribonucleases related to miRNAs have been described that show a certain substrate specificity (Ruegger and Grosshans 2012). Further research will be needed to identify the specific exoribonucleases that mediate the specific degradation of uridylated miRNAs observed after T-cell activation. Defining the mechanisms and purpose of miRNA 3′ nucleotide additions will be important for understanding the post-transcriptional regulation of miRNA function and turnover,

FIGURE 3. TUT4-dependent uridylation of mature microRNA. Small RNAs from naïve wild-type or TUT4-deficient CD4 T cells were analyzed by deep sequencing. (*A–D*) Fold changes between wild-type and TUT4−/− CD4 T cells calculated from oligo- (*A*) and mono-uridylated miRNAs (*B*) as well as mono- (*C*) and oligo-adenylated miRNA counts (*D*). Only modified miRNAs whose expression level is above $\log_2 > 2$ are presented. A negative fold change indicates lower levels in TUT4-deficient compared to wild-type. (*E*) Comparison of the levels of the individual canonical miRNAs corresponding to the identified TUT4 uridylation targets between wild-type and TUT4-deficient CD4 T cells. (*F*) Comparison of the levels of individual uridylated miRNAs identified as TUT4 targets between naïve and activated wild-type CD4 T cells.

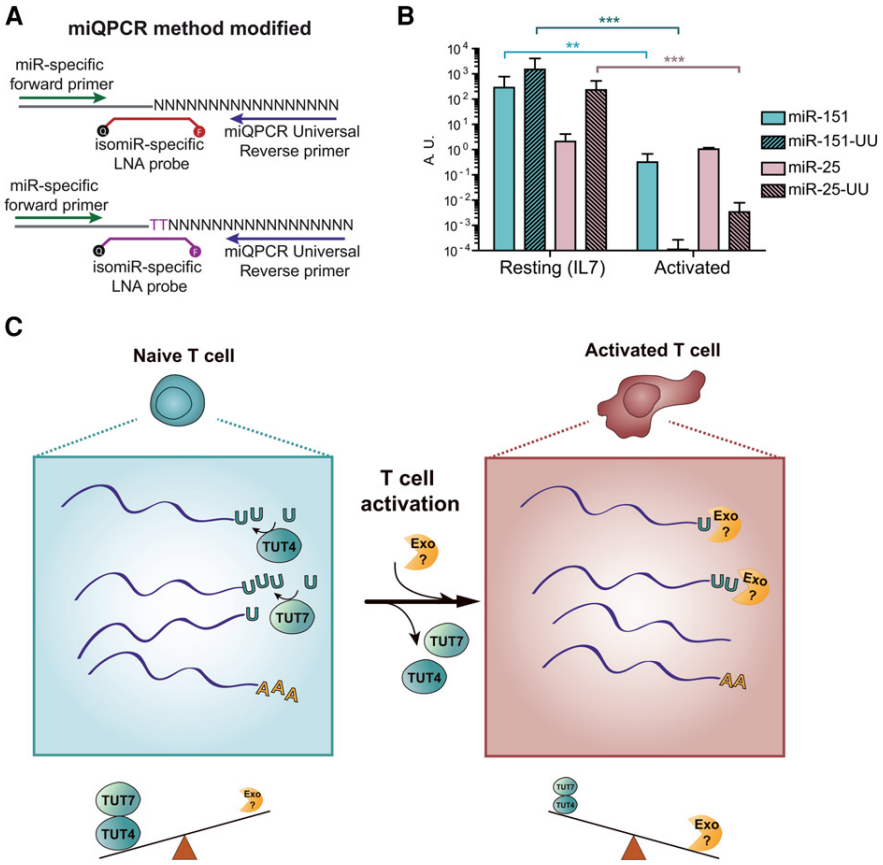

FIGURE 4. Uridylation of mature miRNAs determines their turnover during T-cell activation. (*A*) Diagram representing the qPCR method used to distinguish between di-uridylated synthetic miRNAs and unmodified ones. After a linker ligation and reverse transcription, custom probes specific for the 3′ end were used in combination with reverse and forward primers for the miRNA. (*B*) Synthetic miRNAs were nucleofected into naïve CD4 T cells, which were then activated with anti-CD3 and anti-CD28 or left resting in the presence of IL-7. Levels of the synthetic miRNAs were analyzed by a variation of MiQPCR. Synthetic RNA levels were normalized to endogenous controls snoRNA 420 and snoRNA 412 and are presented in arbitrary units ($n = 3$). (*C*) Scheme of the proposed mechanism of miRNA post-transcriptional regulation during T-cell activation. Naïve cells under steady-state contain basal levels of uridylated miRNAs that are down-regulated after T-cell activation. This decrease is accompanied by the down-regulation of uridyltransferases TUT4 and TUT7. Additionally, we hypothesize that a putative exonuclease might be induced in activated T cells responsible for uridylated miRNAs degradation.

and could also inform strategies for therapeutic modulation of miRNA activity.

MATERIALS AND METHODS

Mice

C57BL/6 and OT-II mice and C57BL/6 Zcchc11-/+ mice (TUT4-deficient mice) were bred under specific pathogen-free conditions according to European Commission recommendations. The TUT4-deficient strain was maintained in heterozygosis as described previously (Jones et al. 2012).

T-cell isolation, culture, and activation

Naïve $CD4^+$ T cells were obtained from cell suspensions of lymph nodes or spleen. Cell suspensions were incubated with biotinylated antibodies against CD8, CD19, CD25, CD11b, CD45R, major histocompatibility complex (MHC) class II (I-Ab), DX5, IgM, Gr-1, and F4/80 and subsequently with streptavidin microbeads (MACS; Miltenyi Biotec). $CD4^+$ T cells were negatively selected in autoMACS Pro Separator (Miltenyi Biotec) according to the manufacturer's instructions. The cells were then labeled with antibodies to CD4, CD62L, and CD25 (BD Biosciences) and analyzed by flow cytometry to confirm their purity and naïve status (data not shown). Naïve CD4+ T cells (10^6 cells mL^{-1}) were either directly lysed or cultured in RPMI 1640 medium supplemented with 10% fetal bovine serum, 100 U mL^{-1} of penicillin and streptomycin, 10 mM Hepes, 50 µM 2-mercaptoethanol, and 1 mM sodium pyruvate and 2 µg mL^{-1} of anti-CD28 on plates previously coated with 10 µg mL^{-1} of anti-CD3 (BD Biosciences). Alternatively, cells were maintained in the naïve state in the presence of 4 ng mL^{-1} of interleukin 7 (Peprotech). The activation status of CD4 T cells was assessed at the indicated time points by flow cytometry after staining with antibodies against CD4, CD25, and CD69 (BD Biosciences). Data were acquired and analyzed with a FACSFortessa flow cytometer and FACSDiva (BD Biosciences) or FlowJo software.

Antigen-specific T-cell stimulation

When indicated, dendritic cells (DCs) were used to stimulate OT-II CD4 T cells. DCs were derived from wild-type bone marrow cell suspensions after culture on nontreated 150-mm Petri dishes in complete RPMI 1640 medium supplemented with 10% FCS, 2 mM L-glutamine, 100 U mL^{-1} penicillin and streptomycin, 50 µM 2-mercaptoethanol and 20 ng mL^{-1} recombinant GM-CSF (Peprotech). Cells were collected on day 9 and subsequently stimulated with 100 ng mL^{-1} LPS from *Escherichia coli* (Sigma). At this point, DC preparations were characterized as CD11c+ MHCII+ Ly6G−. OT-II CD4 T cells were co-cultured with DCs (8:1 T-cell/DC ratio) in the presence of ovalbumin (OVA) peptide for 18 h. Cells were stained for CD4 and MHCII for subsequent sorting of the CD4 T-cell fraction on a FACSAria flow cytometer (BD Biosciences).

Human T lymphoblasts

Human T lymphoblasts were obtained as previously described (Mittelbrunn et al. 2011). Briefly, peripheral blood mononuclear cells were isolated from buffy coats from healthy donors. Isolated nonadherent cells were cultured for 2 d in the presence of phytohemagglutinin (5 µg mL^{-1}) and subsequently interleukin 2 (50 U mL^{-1}) was added to the medium every 2 d for a period of 8 d. T lymphoblasts were later stimulated either with anti-CD3 and anti-CD28 coated beads (Gibco) or with phorbol myristate acetate (PMA) and ionomycin.

RNA isolation

Total RNA was extracted with QIAzol lysis reagent (Qiagen) and the miRNeasy mini kit (Qiagen). Purity and concentration were measured in a Nanodrop-1000 spectrophotometer (Thermo Scientific), and RNA integrity was assessed using the Agilent 2100 Bioanalyzer.

Small RNA cloning and sequencing (miR-seq library preparation, sequencing, and generation of FastQ files)

Total RNA (1 µg) was used to generate barcoded miR-seq libraries using the TruSeq Small RNA Sample Preparation Kit (Illumina). Briefly, 3′ and 5′ adapters were first ligated to the RNA sample. Next, reverse transcription followed by PCR amplification was used to enrich cDNA fragments with adapters at both ends. Adapter-ligated cDNA fragments from different samples were pooled and run on a 6% polyacrylamide gel. The band between 147 and 180 base pairs, corresponding to the pooled miRNA libraries including slightly longer fragments (potential IsomiRs with 3′NTAs), was purified from the gel. Finally, the quantity and quality of the pooled miR-seq libraries were determined using the Agilent 2100 Bioanalyzer High Sensitivity DNA chip. Libraries were sequenced on a Genome Analyzer IIx (Illumina). FastQ files for each sample were obtained using CASAVA v1.8 (Illumina). Library preparation and sequencing was performed by the CNIC genomic unit.

Next-generation sequencing analysis and statistics

Raw FASTQ files were trimmed for adapter contamination using REAPER from the Kraken package (Davis et al. 2013). All reads were mapped against miRNA precursors obtained from miRBase release 21 (Kozomara and Griffiths-Jones 2014) using BLASTn. A custom pipeline interrogated each read to determine which miRNAs originated from which precursor and which arm (either 5′ or 3′). Extra nucleotides that could not be explained by the associated miRNA precursor sequence were flagged as noncanonical 5′ or 3′ extensions. Count data for canonical matches and noncanonical extensions were stored for each sample in the tabular form. Count data were normalized and analyzed using R/BioConductor with the DeSeq2 package. DESeq2 automatically excludes outliers using a Cook′s distance for all genes.

Changes to either global miRNA levels or individual miRNA modifications were viewed as significant if they had an absolute log fold-change >0.5 and an adjusted *P*-value <0.05. miRNAs were considered into DE analysis when having a mean expression level of $\log_2 > 2$.

All data and scripts used are available. NGS analysis data have been deposited in European Nucleotide Archive and are accessible through ENA accession number PRJEB15528.

mRNA reverse transcription and quantitative real-time PCR

cDNA was synthesized using the High Capacity cDNA Reverse Transcription Kit (Applied Biosystems). Expression analysis by quantitative PCR was performed with SYBRgreen PCR master mix (Applied Biosystems), and the corresponding primers are listed in Supplemental Table S5. Data were acquired and analyzed using the ABI Prism 7900HT Sequence Detection System (Applied Biosystems) and Biogazelle QBasePlus software (Biogazelle). B-actin and Yhwaz (tyrosine 3-monooxygenase/tryptophan 5-monooxygenase activation protein, ζ) genes were used as endogenous controls for presentation of relative mRNA levels.

Reverse transcription and RT-qPCR of mature canonical miRNA

cDNA was synthesized and mature miRNAs were quantified by miRCURY LNA Universal RT microRNA PCR (Exiqon), using miRNA LNA primers (Exiqon) and SYBRgreen PCR master mix (Applied Biosystems). Quantitative miRNA expression data were acquired and analyzed using the ABI Prism 7900HT Sequence Detection System (Applied Biosystems). Data were further analyzed using BiogazelleQBasePlus software (Biogazelle). RNU1A1 and RNU5G RNAs were used as endogenous controls and results are expressed in arbitrary units.

Nucleofection of synthetic RNAs

Synthetic RNAs that correspond to canonical or di-uridylated miRNAs (Integrated DNA Technologies) were nucleofected into freshly isolated naïve CD4 T cells using the Amaxa Mouse T-cell Nucleofector Kit and Amaxa Nucleofector II (Lonza) according to the manufacturer's instructions.

Reverse transcription and qPCR of synthetic miRS and isomirs

Levels of the synthetic miRNAs previously nucleofected into T cells were analyzed by a variation of the miQPCR method (Benes et al.

2015). In brief, 60 ng of total RNA were ligated to an oligonucleotide adapter (miLINKER) followed by retrotranscription to cDNA. Quantitative PCR was then performed with Taqman PCR master mix (Applied Biosystems) using both specific primers and LNA Taqman probes. Quantitative data of synthetic RNA levels were acquired and analyzed using the ABI Prism 7900HT Sequence Detection System (Applied Biosystems). Data were further analyzed using BiogazelleQBasePlus software (Biogazelle). snoRNA 420 and snoRNA 412 were used as endogenous controls for normalization and results are expressed in arbitrary units.

Immunofluorescence

Cells were plated onto slides coated with poly-L-lysine (50 µg mL^{-1}), incubated for 30 min, fixed, blocked, and stained with anti-tubulin-FITC (Sigma-Aldrich) and rabbit polyclonal anti-Zcchc11 (TUT4) (Proteintech) (5 µg mL^{-1}) followed by Rhodamine Red X-labeled secondary antibody (5 µg mL^{-1}) (Life Technologies). Samples were examined with a Leica SP5 confocal microscope (Leica) fitted with a ×63 objective, and images were processed and assembled using Leica software.

Immunoblotting

Cells were lysed in lysis buffer (50 mM Tris pH 7.5, 150 mM NaCl, 2 mM MgCl2, 1%NP-40, 5 mM EDTA) containing a protease inhibitor cocktail (Complete, Roche). Proteins were separated on 8% acrylamide/bisacrylamide gels and transferred to a nitrocellulose membrane. Membranes were incubated with specific primary antibodies (5 µg mL^{-1}) and peroxidase-conjugated secondary antibodies (5 µg mL^{-1}), and chemoluminescence was measured with LAS-3000 (Fujifilm). The following antibodies were used: rabbit polyclonal anti-Zcchc11 (TUT4), rabbit polyclonal anti-Zcchc6 (TUT7) (Proteintech), goat polyclonal anit-Zcchc11 (ProSci), anti-p150glued (BD Transduction Laboratories), monoclonal anti-EZH2 (Cell Signaling), polyclonal anti ezrin/moesin (ERMs) (90/3) (provided by Heinz Furthmayr, Stanford University, Stanford, CA). Secondary antibodies were goat anti-mouse peroxidase (31446, Thermo Scientific) (1:5,000) and goat anti-rabbit peroxidase (37460, Thermo Scientific) (1: 10,000). Band intensities were quantified with Image Gauge (Fujifilm). The Proteo Extract subcellular proteome extraction kit (Calbiochem) was used for subcellular fractionation of proteins followed by Western blot.

SUPPLEMENTAL MATERIAL

Supplemental material is available for this article.

ACKNOWLEDGMENTS

We appreciate help from Carolina Villarroya-Beltri and Marta Ramirez-Huesca. We also thank the CNIC Genomics and Cellomics Units for technical support, Simon Bartlett for help with English editing, and Salvador Iborra, David Sancho, and Miguel Vicente Manzanares for helpful discussions. This work was supported by grants SAF2014-55579R from the Ministerio de Economía y Competitividad-Spain, ERC-2011-AdG 294340-GENTRIS, COST-Action BN1202, CIBERCV (Instituto de Salud Carlos III) PIE-13-00041, and INDISNET S2011-BMD-2332 (F.S.-M.). This research has been cofinanced by FEDER. The Centro Nacional de Investigaciones Cardiovasculares (CNIC, Spain) is supported by the Ministerio de Economía y Competitividad-Spain and the Pro-CNIC Foundation. A.R.R. was funded by research grants SAF2013-42767-R and SAF2016-75511-R (Plan Estatal de Investigación Científica y Técnica y de Innovación 2013-2016 Programa Estatal de I+D+i Orientada a los Retos de la Sociedad Retos Investigación: Proyectos I+D+i 2016, Ministerio de Economía, Industria y Competitividad) and cofunded by Fondo Europeo de Desarrollo Regional (FEDER). M.M. is supported by grant MS14/00219 from the Instituto de Salud Carlos III. A.R.-G. is supported by the FPU program (Spanish Ministry of Education).

Received November 23, 2016; accepted March 23, 2017.

REFERENCES

Ameres SL, Zamore PD. 2013. Diversifying microRNA sequence and function. *Nat Rev Mol Cell Biol* **14:** 475–488.

Ameres SL, Horwich MD, Hung JH, Xu J, Ghildiyal M, Weng Z, Zamore PD. 2010. Target RNA-directed trimming and tailing of small silencing RNAs. *Science* **328:** 1534–1539.

Baumjohann D, Ansel KM. 2013. MicroRNA-mediated regulation of T helper cell differentiation and plasticity. *Nat Rev Immunol* **13:** 666–678.

Benes V, Collier P, Kordes C, Stolte J, Rausch T, Muckentaler MU, Haussinger D, Castoldi M. 2015. Identification of cytokine-induced modulation of microRNA expression and secretion as measured by a novel microRNA specific qPCR assay. *Sci Rep* **5:** 11590.

Bronevetsky Y, Villarino AV, Eisley CJ, Barbeau R, Barczak AJ, Heinz GA, Kremmer E, Heissmeyer V, McManus MT, Erle DJ, et al. 2013. T cell activation induces proteasomal degradation of Argonaute and rapid remodeling of the microRNA repertoire. *J Exp Med* **210:** 417–432.

Burroughs AM, Ando Y, de Hoon MJ, Tomaru Y, Nishibu T, Ukekawa R, Funakoshi T, Kurokawa T, Suzuki H, Hayashizaki Y, et al. 2010. A comprehensive survey of 3′ animal miRNA modification events and a possible role for 3′ adenylation in modulating miRNA targeting effectiveness. *Genome Res* **20:** 1398–1410.

Chang TC, Mendell JT. 2007. microRNAs in vertebrate physiology and human disease. *Annu Rev Genomics Hum Genet* **8:** 215–239.

Chatterjee S, Fasler M, Bussing I, Grosshans H. 2011. Target-mediated protection of endogenous microRNAs in *C. elegans*. *Dev Cell* **20:** 388–396.

Cobb BS, Hertweck A, Smith J, O'Connor E, Graf D, Cook T, Smale ST, Sakaguchi S, Livesey FJ, Fisher AG, et al. 2006. A role for Dicer in immune regulation. *J Exp Med* **203:** 2519–2527.

Davis MP, van Dongen S, Abreu-Goodger C, Bartonicek N, Enright AJ. 2013. Kraken: a set of tools for quality control and analysis of high-throughput sequence data. *Methods* **63:** 41–49.

Filipowicz W, Bhattacharyya SN, Sonenberg N. 2008. Mechanisms of post-transcriptional regulation by microRNAs: are the answers in sight? *Nat Rev Genet* **9:** 102–114.

Heo I, Joo C, Kim YK, Ha M, Yoon MJ, Cho J, Yeom KH, Han J, Kim VN. 2009. TUT4 in concert with Lin28 suppresses microRNA biogenesis through pre-microRNA uridylation. *Cell* **138:** 696–708.

Heo I, Ha M, Lim J, Yoon MJ, Park JE, Kwon SC, Chang H, Kim VN. 2012. Mono-uridylation of pre-microRNA as a key step in the biogenesis of group II let-7 microRNAs. *Cell* **151:** 521–532.

Hwang HW, Wentzel EA, Mendell JT. 2007. A hexanucleotide element directs microRNA nuclear import. *Science* **315:** 97–100.

Ibrahim F, Rymarquis LA, Kim EJ, Becker J, Balassa E, Green PJ, Cerutti H. 2010. Uridylation of mature miRNAs and siRNAs by the MUT68 nucleotidyltransferase promotes their degradation in *Chlamydomonas*. *Proc Natl Acad Sci* **107:** 3906–3911.

Jones MR, Quinton LJ, Blahna MT, Neilson JR, Fu S, Ivanov AR, Wolf DA, Mizgerd JP. 2009. Zcchc11-dependent uridylation of microRNA directs cytokine expression. *Nat Cell Biol* **11:** 1157–1163.

Jones MR, Blahna MT, Kozlowski E, Matsuura KY, Ferrari JD, Morris SA, Powers JT, Daley GQ, Quinton LJ, Mizgerd JP. 2012. Zcchc11 uridylates mature miRNAs to enhance neonatal IGF-1 expression, growth, and survival. *PLoS Genet* **8:** e1003105.

Katoh T, Sakaguchi Y, Miyauchi K, Suzuki T, Kashiwabara S, Baba T. 2009. Selective stabilization of mammalian microRNAs by 3′ adenylation mediated by the cytoplasmic poly(A) polymerase GLD-2. *Genes Dev* **23:** 433–438.

Kozomara A, Griffiths-Jones S. 2014. miRBase: annotating high confidence microRNAs using deep sequencing data. *Nucleic Acids Res* **42:** D68–D73.

Krol J, Busskamp V, Markiewicz I, Stadler MB, Ribi S, Richter J, Duebel J, Bicker S, Fehling HJ, Schubeler D, et al. 2010. Characterizing light-regulated retinal microRNAs reveals rapid turnover as a common property of neuronal microRNAs. *Cell* **141:** 618–631.

Lackey PE, Welch JD, Marzluff WF. 2016. TUT7 catalyzes the uridylation of the 3′ end for rapid degradation of histone mRNA. *RNA* **22:** 1673–1688.

Landgraf P, Rusu M, Sheridan R, Sewer A, Iovino N, Aravin A, Pfeffer S, Rice A, Kamphorst AO, Landthaler M, et al. 2007. A mammalian microRNA expression atlas based on small RNA library sequencing. *Cell* **129:** 1401–1414.

Li J, Yang Z, Yu B, Liu J, Chen X. 2005. Methylation protects miRNAs and siRNAs from a 3′-end uridylation activity in *Arabidopsis*. *Curr Biol* **15:** 1501–1507.

Lim J, Ha M, Chang H, Kwon SC, Simanshu DK, Patel DJ, Kim VN. 2014. Uridylation by TUT4 and TUT7 marks mRNA for degradation. *Cell* **159:** 1365–1376.

Lu S, Sun YH, Chiang VL. 2009. Adenylation of plant miRNAs. *Nucleic Acids Res* **37:** 1878–1885.

Minoda Y, Saeki K, Aki D, Takaki H, Sanada T, Koga K, Kobayashi T, Takaesu G, Yoshimura A. 2006. A novel Zinc finger protein, ZCCHC11, interacts with TIFA and modulates TLR signaling. *Biochem Biophys Res Commun* **344:** 1023–1030.

Mittelbrunn M, Gutierrez-Vazquez C, Villarroya-Beltri C, Gonzalez S, Sanchez-Cabo F, Gonzalez MA, Bernad A, Sanchez-Madrid F. 2011. Unidirectional transfer of microRNA-loaded exosomes from T cells to antigen-presenting cells. *Nat Commun* **2:** 282.

Monticelli S, Ansel KM, Xiao C, Socci ND, Krichevsky AM, Thai TH, Rajewsky N, Marks DS, Sander C, Rajewsky K, et al. 2005. MicroRNA profiling of the murine hematopoietic system. *Genome Biol* **6:** R71.

Mullen TE, Marzluff WF. 2008. Degradation of histone mRNA requires oligouridylation followed by decapping and simultaneous degradation of the mRNA both 5′ to 3′ and 3′ to 5′. *Genes Dev* **22:** 50–65.

Norbury CJ. 2013. Cytoplasmic RNA: a case of the tail wagging the dog. *Nat Rev Mol Cell Biol* **14:** 643–653.

Ruegger S, Grosshans H. 2012. MicroRNA turnover: when, how, and why. *Trends Biochem Sci* **37:** 436–446.

Scheer H, Zuber H, De Almeida C, Gagliardi D. 2016. Uridylation earmarks mRNAs for degradation…and more. *Trends Genet* **32:** 607–619.

Schmidt MJ, West S, Norbury CJ. 2011. The human cytoplasmic RNA terminal U-transferase ZCCHC11 targets histone mRNAs for degradation. *RNA* **17:** 39–44.

Shen B, Goodman HM. 2004. Uridine addition after microRNA-directed cleavage. *Science* **306:** 997.

Thornton JE, Du P, Jing L, Sjekloca L, Lin S, Grossi E, Sliz P, Zon LI, Gregory RI. 2015. Selective microRNA uridylation by Zcchc6 (TUT7) and Zcchc11 (TUT4). *Nucleic Acids Res* **42:** 11777–11791.

Wyman SK, Knouf EC, Parkin RK, Fritz BR, Lin DW, Dennis LM, Krouse MA, Webster PJ, Tewari M. 2011. Post-transcriptional generation of miRNA variants by multiple nucleotidyl transferases contributes to miRNA transcriptome complexity. *Genome Res* **21:** 1450–1461.

Zhao Y, Yu Y, Zhai J, Ramachandran V, Dinh TT, Meyers BC, Mo B, Chen X. 2012. The *Arabidopsis* nucleotidyl transferase HESO1 uridylates unmethylated small RNAs to trigger their degradation. *Curr Biol* **22:** 689–694.

Zuber H, Scheer H, Ferrier E, Sement FM, Mercier P, Stupfler B, Gagliardi D. 2016. Uridylation and PABP cooperate to repair mRNA deadenylated ends in *Arabidopsis*. *Cell Rep* **14:** 2707–2717.

3′ Uridylation controls mature microRNA turnover during CD4 T-cell activation

Cristina Gutiérrez-Vázquez, Anton J. Enright, Ana Rodríguez-Galán, et al.

RNA 2017 23: 882-891 originally published online March 28, 2017
Access the most recent version at doi:10.1261/rna.060095.116

SCIENTIFIC REPORTS

OPEN

miRNA profiling during antigen-dependent T cell activation: A role for miR-132-3p

Received: 22 December 2016
Accepted: 4 May 2017
Published online: 14 June 2017

Cristina Gutiérrez-Vázquez[1,2], Ana Rodríguez-Galán[1,2], Marcos Fernández-Alfara[2], María Mittelbrunn[2], Fátima Sánchez-Cabo[2], Dannys Jorge Martínez-Herrera[3], Marta Ramírez-Huesca[2], Alberto Pascual-Montano[3] & Francisco Sánchez-Madrid[1,2,4]

microRNAs (miRNAs) are tightly regulated during T lymphocyte activation to enable the establishment of precise immune responses. Here, we analyzed the changes of the miRNA profiles of T cells in response to activation by cognate interaction with dendritic cells. We also studied mRNA targets common to miRNAs regulated in T cell activation. *pik3r1* gene, which encodes the regulatory subunits of PI3K p50, p55 and p85, was identified as target of miRNAs upregulated after T cell activation. Using 3′UTR luciferase reporter-based and biochemical assays, we showed the inhibitory relationship between miR-132-3p upregulation and expression of the *pik3r1* gene. Our results indicate that specific miRNAs whose expression is modulated during T cell activation might regulate PI3K signaling in T cells.

T cells display specific miRNA profiles compared to other cell types of the immune system. These profiles show specific changes in response to activation by CD3 and CD28 antibody stimulation and T helper (Th) cell *in vitro* polarization[1–3]. Studies using mice deficient for genes involved in the miRNA biogenesis pathway, e.g. Dicer and Drosha, established the central role of miRNAs in the regulation of development and homeostasis of the immune system, and specifically Th cell differentiation[4–6].

miR-132-3p has been mainly described in the nervous system, with only a few recent emerging examples in the immune system, e.g. regulation of hematopoietic stem cell function[7]. miR-132-3p facilitates viral infection both in innate immune cells[8] and CD4 T cells[9]. Moreover, the miR-132/212 cluster has been described in the interphase between nervous and immune systems since it is related to resistance to experimental autoimmune encephalomyelitis (EAE). Hence, miR-132/212 cluster induces a cholinergic anti-inflammatory effect on EAE by targeting acetylcholinesterase upon aryl hydrocarbon receptor activation by its exogenous ligand TCDD[10–12]. Recently, the miR-132/212 cluster has been involved in B cell development when it is induced in response to B cell receptor and targets Sox4[13]. However none of these works studied the role of miR-132-3p in CD4 T cell activation.

Here we used a miRNA microarray approach to study the miRNA profile of T cells after their encounter with professional antigen-presenting cells (APC) bearing specific antigen. We then studied *in silico* the mRNAs predicted to be targeted by the combination of the miRNAs upregulated after T cell activation. We observed that the mRNA and protein levels of the *pik3r1* gene displayed a negative correlation with specific miRNAs upregulated during T cell activation. Finally we established the direct inhibition of *pik3r1* by miR-132-3p, one of the miRNAs upregulated after T cell activation.

Results and Discussion

miRNA profile of CD4+ T cells after cognate interactions with antigen-loaded dendritic cells. To analyze the miRNA profile of CD4 T cells after their encounter with an APC, we co-cultured freshly isolated CD4 T cells from OT-II transgenic mice with *in vitro* derived conventional dendritic cells (cDCs) in the presence or absence of chicken ovalbumin (OVA) 323–339 peptide. CD4 T cells from OT-II mice express a T cell receptor that is specific for OVA peptide in the context of I-A b. After 18 h of co-culture, CD69 and CD25 activation markers were upregulated in T cells after co-culture with cDCs in the presence of OVA but not in its absence (Supplementary Figure S1A). The effect was similar to the one observed using antigen-independent stimulation

[1]Instituto de Investigación Sanitaria Princesa, Hospital Universitario de la Princesa, Universidad Autónoma de Madrid, Madrid, Spain. [2]Fundación Centro Nacional de Investigaciones Cardiovasculares Carlos III (CNIC), Madrid, Spain. [3]Centro Nacional de Biotecnología-CSIC, Madrid, Spain. [4]CIBER Cardiovascular, Madrid, Spain. Correspondence and requests for materials should be addressed to F.S. (email: fsmadrid@salud.madrid.org)

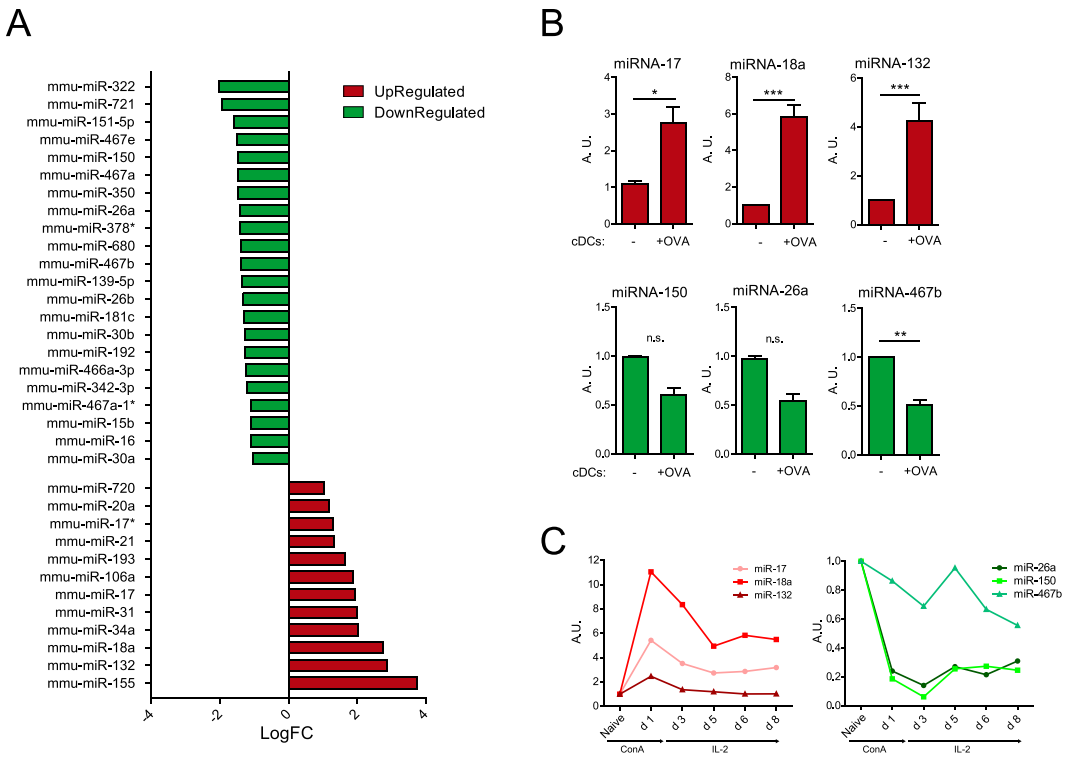

Figure 1. microRNA profile of CD4 T cells activated by cognate interaction with cDCs. CD4 T cells from OT-II mice were cocultured with cDCs in the presence or absence of OVA peptide for 18 h and their miRNA analyzed by miRNA microarray. **(A)** Comparison of miRNAs expression on T cells after stimulation by cDCs loaded or not with OVA peptide. **(B)** Selected miR-17-5p, miR-18a-5p, miR-132-3p, miR-26a-5p, miR-150-5p and miR-467b-5p miRNAs were validated by RT-qPCR. miRNAs that were detected by microarrays to be upregulated or downregulated are depicted in red and green respectively. (n = 8) **(C)** miRNA levels were assessed by RT-qPCR in freshly isolated mouse naive CD4 T cells in different time points of activation with ConA followed by IL-2. (Plots are representative of two independent experiments). RNU1A1 and RNU5G were used as endogenous controls and data are presented in arbitrary units (A.U.). ***$P < 0.001$; **$P < 0.05$; ns, non-significant.

with antibodies against CD3 and CD28 (Supplementary Figure 1B). CD4+ T cells were subsequently sorted from the coculture by flow cytometry and their miRNA profile analyzed using Agilent microarrays. We found 34 miRNAs differentially expressed in T cells activated by cDCs-OVA compared to those co-cultured in the absence of OVA (Fig. 1A). Our microarray data agree with previous studies on miRNA profile changes on T cells after activation with CD3 and CD28 antibodies assessed by different techniques, from Northern blot to microarrays[3,14–16]. Our study adds information regarding the modulation of the T cell miRNA profile using a more physiological trigger, i.e. antigen-loaded professional APC. This is likely to better represent an *in vivo* scenario of T cell activation.

We next performed spot-check validation of some of the observed miRNA found in the microarray data by RT-qPCR. We chose miRNAs previously known to be implicated in T cell activation like miR-17-5p, miR-18a-5p and miR-150-5p as well as others not previously described to be related to this process (miR-132-3p, miR-467b-5p and miR-26a-5p). miR-17-5p, miR-18a-5p and miR-132-3p were significantly upregulated in T cells upon contact with OVA-loaded cDC (Fig. 1B). They were also upregulated, albeit to a lower extent, when T cells were stimulated with OVA-loaded plasmacytoid DCs (pDC) (Supplementary Figure S2). miR-467b-5p was significantly downregulated in T cells upon contact with OVA-loaded cDC (Fig. 1B). miR-26a-5p and miR-150-5p also exhibited lower levels when pulsed with OVA-loaded cDCs and pDCs (Fig. 1B and Supplementary Figure S2).

The expression levels of the identified miRNAs were also assessed in CD4 T cells treated with the polyclonal activator concanavalin-A (ConA) followed by expansion with recombinant interleukin 2 (IL-2). A clear upregulation of miR-17-5p, miR-18a-5p and miR-132-3p was detected. The three miRNAs were maximally expressed at 24 h post stimulation. Interestingly, the levels of miR-132-3p were back to the baseline after approximately 96 h. Conversely, the levels of miR-17-5p and miR-18a-5p remained elevated after eight days (Fig. 1C). Similar behaviors were observed in those miRNA that became downregulated in response to ConA. For example, miR-26a and miR-150 decreased sharply their levels only 24 h post stimulation, reaching a lowest value after 72 h and remaining low up to eight days. Conversely, miR-467b-5p displayed a minor decrease after 72 h, and its levels fluctuated afterwards (Fig. 1C). Overall, these data indicate that there is a specific profile of miRNAs regulated after T cell activation. Also, we found similarities of the miRNA profiles changes triggered by antigen-loaded cDC and the mitogen ConA.

Gen	Number of miRNAs	Combined Prediction SCORE
Tnrc6b	12	0.80847
Eif4g2	11	0.73535
Tnrc6a	11	0.68594
Sox5	11	0.66711
Pik3r1	**11**	**0.65147**
Tbc1d2b	11	0.59698
Tbxas1	11	0.57699
Syncrip	11	0.56623
Gsk3b	11	0.56402
Neo1	11	0.56114
Zfp664	11	0.54515
Rdx	11	0.53015

Table 1. Targets of upregulated miRNAs in CD4 T cell activation. Prediction of the targets of the miRNAs upregulated in CD4 T cells from OT-II mice after stimulation with cDCs loaded with OVA peptide. Prediction was performed with a combinatorial method of different available prediction tools. Higher combined prediction score denotes more confidence in the prediction.

miRNA	logFC	adjpv
mmu-miR-155-5p	3,746	0,003
mmu-miR-132-3p	2,865	0,031
mmu-miR-18a-5p	2,752	0,025
mmu-miR-34a-5p	2,041	0,012
mmu-miR-31-5p	2,012	0,042
mmu-miR-17-5p	1,928	0,008
mmu-miR-106a-5p	1,867	0,018
mmu-miR-193a-3p	1,661	0,018
mmu-miR-21a-5p	1,330	0,042
mmu-miR-17-3p	1,307	0,039
mmu-miR-20a-5p	1,190	0,031
mmu-miR-146a-5p	0,936	0,048

Table 2. miRNAs upregulated in CD4 T cell activation. A total of 11 out of the 12 miRNAs upregulated after CD4 T cell stimulation by cDC-OVA are predicted to be targeting pik3r1. The only miRNA not predicted to target is presented in gray.

PIK3R1 is a target of the miRNAs upregulated during T cell activation. As a first approach to identify the possible common mRNA targets of the miRNAs that were regulated after T cell activation, we used a customized program which combines several prediction algorithms as well as databases for experimentally validated targets making its prediction more reliable[17]. Interestingly, several target genes of the miRNAs upregulated after T cell activation, were related to the establishment of the immune response (Supplementary Figure S3). We focused our attention on those mRNA targets that have the higher number of predicted miRNAs modulating them, particularly those interactions that have not been experimentally validated yet. Table 1 shows some of these genes and the combined prediction score of our prediction tool.

We focused in the *pik3r1* (Phosphoinositide-3-Kinase, Regulatory Subunit 1 Alpha) gene among those predicted targets of the miRNAs upregulated after T cell activation since it is implicated in important signaling pathways of this process. Interestingly, *pik3r1* was predicted to be inhibited by 11 out of the 12 miRNAs upregulated in T cells after cognate interaction with cDCs (Table 1). The specific list of these miRNAs and their logFoldChange of cDC- vs cDC-OVA stimulated CD4 T cells is presented in Table 2.

Pik3r1 encodes for the proteins p50α, p55α and p85α, which are the regulatory subunits of Class IA phosphatidylinositol 3-kinases (PI3K). PI3K signaling pathway is one of the signaling pathways that arise from TCR and co-receptors engagement during T cell activation. The main role of the regulatory subunits of I_A PI3K is to bind and stabilize the catalytic subunit p110, inhibiting its activity in basal conditions[18,19]. They also recruit the PI3K complex to phosphotyrosine residues in receptors and adaptor molecules, which relieve the inhibitory contact with the catalytic subunits and will bring them in contact with their lipid substrates in the membrane[20].

The expression of the corresponding proteins and mRNA of *pik3r1* gene were studied during T cell activation. p85 and p50 proteins, and the mRNA levels of the two corresponding alternative transcripts, decreased over time in CD4 T cells stimulated with anti CD3 and anti CD28 for 7 d (Fig. 2A,B and C). On the other hand, miR-17-5p, miR-18a-5p and miR-132-3p, which are predicted to target *pik3r1*, were inversely regulated (Fig. 2D). These data indicate that the regulator of PI3K, *pik3r1*, might be directly modulated by miRNAs induced during T cell activation.

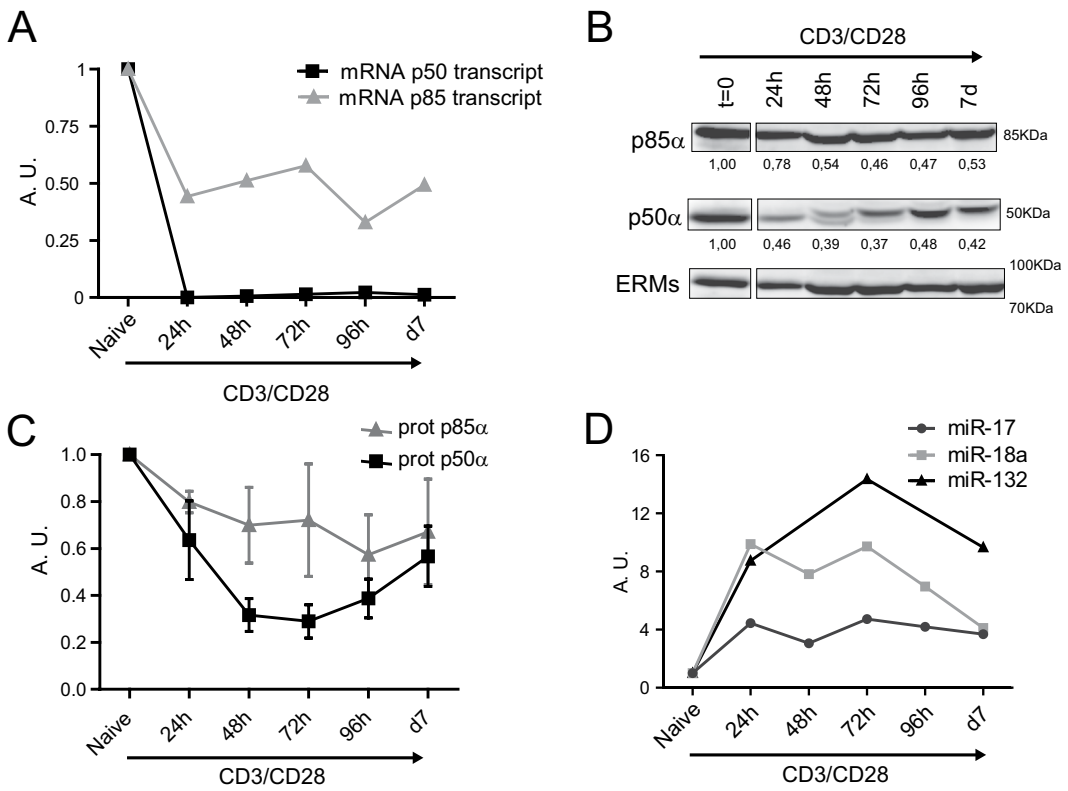

Figure 2. pik3r1 is downregulated during T cell activation. **(A)** mRNA relative levels of the two main transcripts of *pik3r1* were measured by qPCR. Levels were normalized to Yhwaz and β-actin housekeeping genes (n = 2). **(B)** Western blot analysis of p85α and p50α protein content in CD4 T cells after activation with anti-CD3 plus anti-CD28. Representative Immunoblots (n = 3); protein bands were cropped from the same gel. ERMs were included as a loading control. **(C)** Protein levels of p85α and p50α in (B) normalized to ERMs. **(D)** miRNA levels in CD4 T cells after activation with anti-CD3 plus anti-CD28. Levels are normalized to RNU1A1 and RNU5G and presented in arbitrary units (n = 2).

miR-132-3p targets *pik3r1*. Next, we used a combination of prediction programs to analyze the predicted miRNA binding sites on the 3′UTR of *pik3r1* (Supplementary Table S1). We identified ten canonical binding sites and two unusual sites for miRNAs upregulated during T cell activation in the 3′UTR of *pik3r1*. We focused on the interaction of miR-132-3p with *pik3r1* because the prediction algorithms projected two different binding sites for miR-132-3p in the 3′UTR of the gene; also, because the role of this miRNA in the context of T cell activation had not been previously reported. We generated luciferase reporter vectors of the two regions of the 3′UTR of *pik3r1* containing the two predicted target sites of miR-132-3p. For Site 1, we used the 71-362 fragment; Site 2 contained the 2957-3162 fragment (Fig. 3A). We co-transfected the reporter plasmids into HEK cells either with a control plasmid or a plasmid driving the overexpression of miR-132-3p co-expressing GFP. GFP-positive cells were sorted by flow cytometry and overexpression of miRNA-132 was monitored by RT-qPCR (Fig. 3B). Luciferase signal analysis revealed that both predicted sites are targeted by miR-132-3p, since luciferase levels were lower in cells co-transfected with miR-132-3p plasmid compared to the control plasmid (Fig. 3C). To further assess the functional relationship between miR-132-3p and *pik3r1* gene in T cells, we next transfected miR-132-3p mimics into Jurkat T cells and evaluated the levels of *pik3r1* gene products, the proteins p85α, p55α and p50α that are expressed in this cell line. After 48 h post transfection, miR-132-3p was overexpressed in these cells, significantly reducing p55α and p50α protein levels (Fig. 3D–F). The overexpression by transfection of miR132-3p mimic resulted in levels of the miRNA greater than the endogenous levels of activated T cells. However, the reduction of the protein levels was not so dramatic. Indeed, p85α protein levels were lower in miR-132-3p overexpressing cells although the decrease was milder compared to the other isoforms probably due to the higher stability of this specific isoform. Thus, our data experimentally demonstrate that miR-132-3p inhibits the expression of the products of the *pik3r1* gene in T lymphocytes.

The prediction algorithms that we used projected that the different pik3r1 transcripts would be targeted by 11 of the 12 miRNAs upregulated after T cell activation. Moreover, we detected a downregulation of both its protein products and mRNA transcripts at different time points after initial T cell activation. The specific loss of p85α (with the other regulatory subunits unaltered like p50α) has been previously shown to inhibit the activation of Akt under conditions promoting the differentiation of Th1, Th2 and Th17 cells, but only Th17 differentiation was affected[21]. A recent study described that patients with mutations on PIK3R1 undergo excessive lymphoproliferation and exhibit hyperactive PI3K signaling as a result of the abnormally low level of expression of the

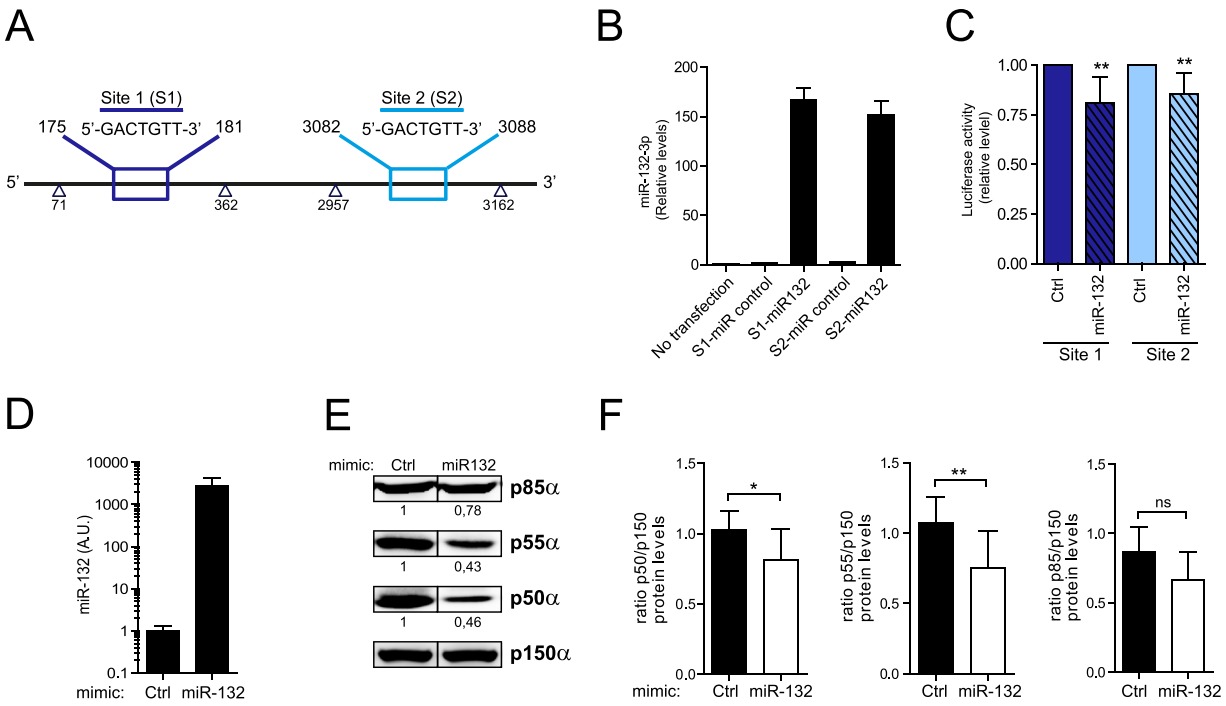

Figure 3. miR-132-3p targets pik3r1. **(A)** 3′UTR of *pik3r1* cloning strategy. Fragments from 71 to 362 bp and from 2957 to 3162 bp containing the two binding sites predicted for miR-132-3p were cloned into the psiCheck2 vector. **(B)** miR-132-3p levels in HEK cells after transfection. Levels were normalized to RNU1A1 and RNU5G. **(C)** HEK cells were transfected with indicated plasmids (Control empty vector or miR-132 expressing vector), GFP+ cells sorted and Renilla and Firefly luciferase signal measured. Data are presented in Renilla Luciferase signal relative to Firefly (n = 5). T-test **P < 0.05. **(D)** miR-132-3p expression in Jurkat cells 48 h post transfection with either negative Control-Dy547 or mmu-miR-132-3p miRNA Mimics. **(E)** Western blot analysis of p85α, p55α and p50α isoforms in Jurkat cells after 48 h of transfection with the control or miR-132-3p mimics as in (**D**). A representative blot of one experiment out of five is shown; protein bands were cropped from the same gel. **(F)** Protein relative levels of p85α, p55α and p50α as in (**E**) after normalization to p150 (n = 5) T-test **P < 0.05; *P < 0.01.

mutant p85α[22]. We hypothesize that the decreased expression of *pik3r1* after T cell activation might be regulated by a combination of miRNAs that control that PI3K signaling is precisely dosed during T cell activation. In this context, miR-132-3p would have a cooperative role in T cell activation. It is worth mentioning that signaling downstream pik3r1 was not significantly changed by the overexpression of miR-132-3p (data not shown) further supporting the idea of miR-132-3p cooperative role with other miRNAs. However, our experimental data only provide information about this specific miRNA. In summary, we propose that the modulation of the observed group of miRNAs during T cell activation, including miR-132-3p, finely tunes the availability of gene products to promote the proper activation of T cells.

Methods

Mice. C57BL/6 and OT-II mice were bred under specific pathogen-free conditions according to European Commission recommendations at Centro Nacional de Investigaciones Cardiovasculares (CNIC) animal facility. All experimental methods and protocols were approved by CNIC and Comunidad Autónoma de Madrid and followed European Commission guidelines and regulations.

Cell lines culture and transfection. HEK-293T were cultured in DMEM Medium (SIGMA) supplemented with 10% Fetal Bovine Serum (FBS) (Invitrogen). Cells were co-transfected with Psicheck2 reporter plasmids for *pik3r1* 3′UTR fragments and control GFP plasmid or a miR-132-3p-GFP plasmid (ABM) with Lipofectamine-2000 (Invitrogen) according to manufacturer's instructions. GFP+ cells were sorted at FACSAria flow cytometer (BD Biosciences) before downstream analysis. Jurkat cells were cultured in RPMI (Sigma) containing 10% FBS (Invitrogen). Jurkat cells were transfected with either miRIDIAN miRNA Mimic negative Control-Dy547 or miRIDIAN miRNA Mimic mmu-miR-132-3p (Dharmacon) by electroporation. Cells were resuspended in Opti-MEM (GIBCO) with 1 μM of mimic and electroporated with Gene Pulser Xcell (Bio-Rad) at 1200 μFa, 240 mV during 30 ms.

Primary cells isolation, culture and activation. Mouse primary cells were cultured in RPMI 1640 medium supplemented with 10% fetal bovine serum, 50 μM 2-mercaptoethanol and 1 mM sodium pyruvate.

Mouse naive CD4+ T cells were isolated from cell suspensions of lymph nodes or spleen that were incubated with biotinylated antibodies (BD Biosciences) against CD8, CD19, CD25, CD11b, CD11c, CD45R, MHC-II (I-Ab), DX5, IgM, Gr-1 and F4/80, subsequently with streptavidin microbeads and negatively selected in auto-MACS Pro Separator (Miltenyi Biotec) according to the manufacturer's instructions. Wild type bone marrow cell suspensions were either cultured to obtain conventional DCs or both pDCs and cDCs as described[23,24]. When indicated, OT-II CD4 T cells were cocultured with the corresponding subset of DCs (8:1T cell/DC ratio) in the presence or absence of chicken ovalbumin (OVA) 323–339 peptide. Polyclonal activation of CD4 T cells was performed with 10 $\mu g\,ml^{-1}$ of anti-CD3 plate bound and 2 $\mu g\,ml^{-1}$ of anti-CD28 (BD Biosciences).

Flow cytometry analysis and sorting. Cell samples were analyzed with a BD FACS Canto or BD LSR Fortessa flow cytometers and FACSDiva software (BD Biosciences) and FlowJo software. For mouse CD4 T cells phenotyping to check purity and activation the following antibodies were used against: CD4, CD69, CD62L, CD25, and CD8 coupled with the appropriate fluorophore (BD Biosciences). Cells were sorted on a FACSAria flow cytometer (BD Biosciences). CD4+ T cells from the coculture with DCs were discriminated by staining of MHC-II and CD4 plus CD69.

Cloning. The two fragments of the 3′UTR of *pik3r1* (sequence from 71 to 362 bp and from 2957 to 3162 (Fig. 3A) were cloned into psiCHECK2 vector (Promega). Fragments were amplified from genomic DNA using Q5 High-Fidelity DNA Polymerase (New England BioLabs) and the corresponding primers (Supplementary Table S1). Each amplified DNA fragment was ligated to the psiCHECK2 vector after digestion with PmeI restriction enzyme (NEB) using the *Gibson Assembly* Master Mix[25] (NEB) following manufacturer's instructions.

Immunoblotting. Total cell extracts were prepared in RIPA lysis buffer and analyzed by Western blotting. The following antibodies were used: anti-alpha Tubulin (DM1A, Sigma), anti-$p150^{glued}$ (BD Transduction Laboratories), rabbit anti-p85a (Millipore), anti ezrin/moesin (ERMs) (90/3) (provided by Heinz Furthmayr, Stanford University, CA). Full immunoblots are provided in Supplementary Figure S4.

Luciferase UTR reporter assays. HEK cells were lysed after 24 h postransfection and the ratio of Renilla and Firefly luciferase activities was measured by the dual luciferase assay (Promega). Psicheck2 dual luciferase reporter vector comprises the gene of Firefly luciferase as a normalizing gene and the luciferease *Renilla reniformis* gene downstream of the cloning site.

RNA isolation. Total RNA was extracted with the miRNeasy mini kit (Qiagen). Purity and concentration were measured in a Nanodrop-1000 spectrophotometer (Thermo Scientific) and RNA integrity using the Agilent 2100 Bioanalyzer.

microRNA microarrays and analysis. Agilent Mouse miRNA V2 (4 × 44 K) microarray was performed on RNA preparations. miRNA data were normalized based on the VSN-invariant method[26,27] using the GeneView files extracted from the Agilent Feature Extraction suite. This method preserves the biological characteristics of the data while stabilizing the variance across all the intensity range based on a fit to some invariant miRNAs (113 in this case). After normalization, only those probes present in at least two samples and with average expression over the 20th percentile of all average expressions were considered for further analysis (198 miRNAs). We used linear models[28] as implemented in the limma Bioconductor package.

The microarray data have been deposited in NCBI's Gene Expression Omnibus and are accessible through GEO Series accession number GSE85363.

Bioinformatic analysis of miRNA target and miRNA seed sequence on 3′UTRs. The targets of the murine microRNAs upregulated after T cell activation were predicted using the Weighted Scoring by Precision (WSP) method[17]. Briefly, the method searches nine databases of predicted interactions for the putative targets of the object miRNAs and finds which of these interactions are among four databases of experimentally validated interactions. Thus, the reliability and precision of each interaction in each database is calculated. An integrated score is calculated for each interaction as the sum of each individual database score multiplied by the precision of that interaction in the specific database.

The sequences of the 3′-UTR of murine pik3r1 gene and those of mature miRNAs upregulated after T cell activation were retrieved from the Ensembl database (release 72, June 2013) and the miRBase database (release 19, August 2012), respectively. Predictions were made using the algorithms miRanda[29], PITA[30], FindTar v3.11.12[31], RNAHybrid[32], and TargetScan v6[33] using parameter default values. The sequences of six, seven and eight nucleotides of each miRNA 5′ end were considered as seeds, starting from the first, second or third nucleotide. Mismatches were not allowed in the canonical seeds but noncanonical seed-matches were also searched.

RT-qPCR of mature miRNA and messenger RNA. cDNA was synthesized and mature miRNAs were quantified by miRCURY LNA Universal RT microRNA PCR (Exiqon), using miRNA LNA primers (Exiqon) and SYBRgreen PCR master mix (Applied Biosystems). cDNA for mRNA quantification was synthesized using the High Capacity cDNA Reverse Transcription Kit (Applied Biosystems) and quantitative PCR was performed with SYBRgreen PCR master mix (Applied Biosystems) and corresponding primers (Supplementary Table S2). Quantitative miRNA or mRNA expression data were acquired on ABI Prism 7900HT SDS (Applied Biosystems) and further analyzed using BiogazelleQBasePlus software (Biogazelle). Results are expressed in arbitrary units (A.U.) relative to endogenous controls, RNU1A1 and RNU5G RNAs for miRNAs and B-actin and Yhwaz for mRNAs.

References

1. Kuchen, S. *et al*. Regulation of microRNA expression and abundance during lymphopoiesis. *Immunity* **32**, 828–839, doi:10.1016/j.immuni.2010.05.009 (2010).
2. Landgraf, P. *et al*. A mammalian microRNA expression atlas based on small RNA library sequencing. *Cell* **129**, 1401–1414, doi:10.1016/j.cell.2007.04.040 (2007).
3. Monticelli, S. *et al*. MicroRNA profiling of the murine hematopoietic system. *Genome Biol* **6**, R71, doi:10.1186/gb-2005-6-8-r71 (2005).
4. Chong, M. M., Rasmussen, J. P., Rudensky, A. Y. & Littman, D. R. The RNAseIII enzyme Drosha is critical in T cells for preventing lethal inflammatory disease. *The Journal of experimental medicine* **205**, 2005–2017, doi:10.1084/jem.20081219 (2008).
5. Cobb, B. S. *et al*. A role for Dicer in immune regulation. *The Journal of experimental medicine* **203**, 2519–2527, doi:10.1084/jem.20061692 (2006).
6. Muljo, S. A. *et al*. Aberrant T cell differentiation in the absence of Dicer. *The Journal of experimental medicine* **202**, 261–269, doi:10.1084/jem.20050678 (2005).
7. Mehta, A. *et al*. The MicroRNA-132 and MicroRNA-212 Cluster Regulates Hematopoietic Stem Cell Maintenance and Survival with Age by Buffering FOXO3 Expression. *Immunity* **42**, 1021–1032, doi:10.1016/j.immuni.2015.05.017 (2015).
8. Lagos, D. *et al*. miR-132 regulates antiviral innate immunity through suppression of the p300 transcriptional co-activator. *Nature cell biology* **12**, 513–519, doi:10.1038/ncb2054 (2010).
9. Chiang, K., Liu, H. & Rice, A. P. miR-132 enhances HIV-1 replication. *Virology* **438**, 1–4, doi:10.1016/j.virol.2012.12.016 (2013).
10. Hanieh, H. & Alzahrani, A. MicroRNA-132 suppresses autoimmune encephalomyelitis by inducing cholinergic anti-inflammation: a new Ahr-based exploration. *European journal of immunology* **43**, 2771–2782, doi:10.1002/eji.201343486 (2013).
11. Nakahama, T. *et al*. Aryl hydrocarbon receptor-mediated induction of the microRNA-132/212 cluster promotes interleukin-17-producing T-helper cell differentiation. *Proceedings of the National Academy of Sciences of the United States of America* **110**, 11964–11969, doi:10.1073/pnas.1311087110 (2013).
12. Shaked, I. *et al*. MicroRNA-132 potentiates cholinergic anti-inflammatory signaling by targeting acetylcholinesterase. *Immunity* **31**, 965–973, doi:10.1016/j.immuni.2009.09.019 (2009).
13. Mehta, A. *et al*. The microRNA-212/132 cluster regulates B cell development by targeting Sox4. *The Journal of experimental medicine*. doi:10.1084/jem.20150489 (2015).
14. Bronevetsky, Y. *et al*. T cell activation induces proteasomal degradation of Argonaute and rapid remodeling of the microRNA repertoire. *The Journal of experimental medicine* **210**, 417–432, doi:10.1084/jem.20111717 (2013).
15. Grigoryev, Y. A. *et al*. MicroRNA regulation of molecular networks mapped by global microRNA, mRNA, and protein expression in activated T lymphocytes. *Journal of immunology* **187**, 2233–2243, doi:10.4049/jimmunol.1101233 (2011).
16. Jindra, P. T., Bagley, J., Godwin, J. G. & Iacomini, J. Costimulation-dependent expression of microRNA-214 increases the ability of T cells to proliferate by targeting Pten. *Journal of immunology* **185**, 990–997, doi:10.4049/jimmunol.1000793 (2010).
17. Tabas-Madrid, D. *et al*. Improving miRNA-mRNA interaction predictions. *BMC Genomics* **15**(Suppl 10), S2, doi:10.1186/1471-2164-15-S10-S2 (2014).
18. Burke, J. E. *et al*. Dynamics of the phosphoinositide 3-kinase p110delta interaction with p85alpha and membranes reveals aspects of regulation distinct from p110alpha. *Structure* **19**, 1127–1137, doi:10.1016/j.str.2011.06.003 (2011).
19. Conley, M. E. *et al*. Agammaglobulinemia and absent B lineage cells in a patient lacking the p85alpha subunit of PI3K. *The Journal of experimental medicine* **209**, 463–470, doi:10.1084/jem.20112533 (2012).
20. Vanhaesebroeck, B., Guillermet-Guibert, J., Graupera, M. & Bilanges, B. The emerging mechanisms of isoform-specific PI3K signalling. *Nature reviews, molecular cell biology* **11**, 329–341, doi:10.1038/nrm2882 (2010).
21. Kurebayashi, Y. *et al*. PI3K-Akt-mTORC1-S6K1/2 axis controls Th17 differentiation by regulating Gfi1 expression and nuclear translocation of RORgamma. *Cell Rep* **1**, 360–373, doi:10.1016/j.celrep.2012.02.007 (2012).
22. Lucas, C. L. *et al*. Heterozygous splice mutation in PIK3R1 causes human immunodeficiency with lymphoproliferation due to dominant activation of PI3K. *The Journal of experimental medicine* **211**, 2537–2547, doi:10.1084/jem.20141759 (2014).
23. Martinez del Hoyo, G. *et al*. CD81 controls immunity to Listeria infection through rac-dependent inhibition of proinflammatory mediator release and activation of cytotoxic T cells. *Journal of immunology* **194**, 6090–6101, doi:10.4049/jimmunol.1402957 (2015).
24. Mittelbrunn, M. *et al*. Imaging of plasmacytoid dendritic cell interactions with T cells. *Blood* **113**, 75–84, doi:10.1182/blood-2008-02-139865 (2009).
25. Gibson, D. G. *et al*. Enzymatic assembly of DNA molecules up to several hundred kilobases. *Nat Methods* **6**, 343–345, doi:10.1038/nmeth.1318 (2009).
26. Huber, W., von Heydebreck, A., Sultmann, H., Poustka, A. & Vingron, M. Variance stabilization applied to microarray data calibration and to the quantification of differential expression. *Bioinformatics* **18**(Suppl 1), S96–104 (2002).
27. Pradervand, S. *et al*. Impact of normalization on miRNA microarray expression profiling. *RNA* **15**, 493–501, doi:10.1261/rna.1295509 (2009).
28. Smyth, G. K. Linear models and empirical bayes methods for assessing differential expression in microarray experiments. *Statistical applications in genetics and molecular biology* **3**, Article3, doi:10.2202/1544-6115.1027 (2004).
29. Enright, A. J. *et al*. MicroRNA targets in Drosophila. *Genome Biol* **5**, R1, doi:10.1186/gb-2003-5-1-r1 (2003).
30. Kertesz, M., Iovino, N., Unnerstall, U., Gaul, U. & Segal, E. The role of site accessibility in microRNA target recognition. *Nat Genet* **39**, 1278–1284, doi:10.1038/ng2135 (2007).
31. Ye, W. *et al*. The effect of central loops in miRNA:MRE duplexes on the efficiency of miRNA-mediated gene regulation. *PLoS One* **3**, e1719, doi:10.1371/journal.pone.0001719 (2008).
32. Rehmsmeier, M., Steffen, P., Hochsmann, M. & Giegerich, R. Fast and effective prediction of microRNA/target duplexes. *RNA* **10**, 1507–1517, doi:10.1261/rna.5248604 (2004).
33. Lewis, B. P., Shih, I. H., Jones-Rhoades, M. W., Bartel, D. P. & Burge, C. B. Prediction of mammalian microRNA targets. *Cell* **115**, 787–798 (2003).

Acknowledgements

We thank Miguel Vicente-Manzanares for help with English editing and Almudena R. Ramiro for helpful discussions. We appreciate help from Gloria Martinez del Hoyo on DCs experiments set up. We also thank the CNIC Genomics, Bioinformatics and Cellomics Units for technical support. This work was supported by grants SAF2014-55579R from Ministerio de Economía y Competitividad-Spain, ERC-2011-AdG 294340-GENTRIS, CIBER CARDIOVASCULAR (FEDER and Instituto de Salud Carlos III), PIE-13-00041 and INDISNET S2011-BMD-2332 (F. S. M.). The Centro Nacional de Investigaciones Cardiovasculares (CNIC, Spain) is supported by the Ministerio de Economía y Competitividad-Spain and the Pro-CNIC Foundation.

Author Contributions

C.G.-V., M.M. and F.S.-M. conceived the study. Experiments were performed by C.G.-V., M.F.-A., M.R-H. and A.R.-G. Microarray data analysis and target prediction were performed by F.S.-C., DJ.M.-H. and A.P.-M. Planning of the study, interpretation of data and manuscript writing were performed by C.G.-V., and F.S.-M.

Additional Information

Supplementary information accompanies this paper at doi:10.1038/s41598-017-03689-7

Competing Interests: The authors declare that they have no competing interests.

Accession Codes: The microarray data have been deposited in NCBI's GEO with accession number GSE85363.

Publisher's note: Springer Nature remains neutral with regard to jurisdictional claims in published maps and institutional affiliations.

frontiers in Immunology

REVIEW
published: 25 September 2018
doi: 10.3389/fimmu.2018.02148

Control of Immunoregulatory Molecules by miRNAs in T Cell Activation

Ana Rodríguez-Galán[1,2], *Lola Fernández-Messina*[1,2] *and Francisco Sánchez-Madrid*[1,2,3]*

[1] *Servicio de Inmunología, Instituto de Investigación Sanitaria Princesa (IP), Hospital Universitario de la Princesa, Universidad Autónoma de Madrid, Madrid, Spain,* [2] *Centro Nacional de Investigaciones Cardiovasculares, Madrid, Spain,* [3] *Centro de Investigación Biomédica en Red de Enfermedades Cardiovasculares, Madrid, Spain*

MiRNA targeting of key immunoregulatory molecules fine-tunes the immune response. This mechanism boosts or dampens immune functions to preserve homeostasis while supporting the full development of effector functions. MiRNA expression changes during T cell activation, highlighting that their function is constrained by a specific spatiotemporal frame related to the signals that induce T cell-based effector functions. Here, we update the state of the art regarding the miRNAs that are differentially expressed during T cell stimulation. We also revisit the existing data on miRNA function in T cell activation, with a special focus on the modulation of the most relevant immunoregulatory molecules.

Keywords: T cell activation, microRNAs (miRNAs), immunoregulatory molecules, miRNA signature, CD4, CD8, T lymphocyte

OPEN ACCESS

Edited by:
Alexandre M. Carmo, i3S, Instituto de Investigação e Inovação em Saúde, Portugal

Reviewed by:
Isabel Castro, i3S, Instituto de Investigação e Inovação em Saúde, Portugal
Cosima T. Baldari, Università degli Studi di Siena, Italy

***Correspondence:**
Francisco Sánchez-Madrid
fsmadrid@salud.madrid.org

Specialty section:
This article was submitted to T Cell Biology, a section of the journal Frontiers in Immunology

Received: *18 July 2018*
Accepted: *30 August 2018*
Published: *25 September 2018*

Citation:
Rodríguez-Galán A, Fernández-Messina L and Sánchez-Madrid F (2018) Control of Immunoregulatory Molecules by miRNAs in T Cell Activation. Front. Immunol. 9:2148. doi: 10.3389/fimmu.2018.02148

INTRODUCTION

MiRNAs are small (∼19–24 nucleotides) single-stranded non-coding RNA species that act as post-transcriptional modulators; they control gene expression, either by promoting mRNAs degradation or repressing their translation (1). More than 2,500 human mature miRNA sequences have been already listed in MirBase (2) although the total amount of miRNAs is likely up to 10 times higher (3). Friedman et al. (4) estimated that miRNAs could modulate around 60% of protein-coding genes, indicating the relevance of these regulatory pathways in gene expression.

The miRNA repertoire changes upon T cell activation (5–11). **Figure 1** summarizes miRNA species described to be either upregulated or downregulated upon T cell stimulation. Different studies have yielded data that may appear contradictory, likely due to T cell subset differences, the origin of the sample (murine or human) and the strategy of stimulation. Additional differences stem from the strategy used to evaluate miRNA expression, being arrays the most commonly employed technique, together with RT-qPCR and Northern Blot.

Despite variability, some trends are very consistent, including downregulation of miR-26a, miR-26b, miR-150, miR-181a, miR-223, and miR-342-3p; and upregulation of miR-155 and the miR-17∼92 cluster (particularly miR-17-5p, miR-18a-5p, and miR-19b). MiR-146a was downregulated in mouse T cells, but upregulated in human upon activation, while miR-31 behaved in the opposite way, suggesting the existence of species-specific regulatory mechanisms.

In addition to variations in miRNA expression, it would be essential to consider the total abundance of each miRNA in the cell. Interestingly, only 7 miRNAs accounted for around 60% of the total sequencing reads in $CD8^+$ T cells (8).

Beyond individual miRNA changes, it is important to highlight that miRNAs undergo a global downregulation upon stimulation. In this regard, almost three times higher total miRNA array

hybridization signal has been detected in mouse $CD8^+$ naive T cells compared to activated cells (8); similarly, an independent study found a significant downregulation of the total amount of miRNA in stimulated mouse and human $CD4^+$ T cells compared to non-stimulated controls (5).

LESSONS FROM MIRNA-DEFICIENT MODELS

Dicer is an RNase III endonuclease that controls miRNA biogenesis. It processes precursor miRNA (pre-miRNA) into mature miRNA forms (12–14). Constitutive Dicer KO mice display embryonic lethality (15), indicating the relevance of this enzyme in development. Lineage-specific Dicer-deficient models were therefore required to study the consequences of reduced miRNA function in a tissue-specific manner.

Dicer-deficient $CD4^+$ T cells were hyper-responsive to TCR stimulation and produced IL-2 in the absence of co-stimulation (16). After activation, $CD4^+$ Dicer-deficient mice showed reduced proliferation, higher levels of apoptosis and a bias towards Th1 differentiation and IFN-γ release (17). In Th1 differentiation, IFN-γ production and a decline in IL-2 secretion occurred earlier in Dicer-deficient than in wild-type $CD4^+$ T cells (17). Th2 cells presented reduced levels of GATA3 mRNA and failed to suppress IFN-γ expression (17). Consistently, similar phenotypes were observed in T cells lacking Drosha or its RNA-binding cofactor DGCR8, which form a complex responsible for primary miRNA transcript processing. Drosha-deficient naïve $CD4^+$ T cells differentiated into Th1 and Th2, but expressed higher levels of IFN-γ than control cells (18). Similarly, DGCR8-deficient T lymphocytes showed reduced proliferation and an increase in IFN-γ secretion (19). A number of very comprehensive reports have addressed the role of miRNAs in T cell differentiation (20–24). In this review, immunoregulatory molecules responsible for differentiation have been discussed when closely related to T cell activation events.

CD4-specific Dicer deficiency also affects the regulatory T cell compartment, impairing Tregs development in the thymus and reducing their numbers in peripheral lymphoid organs (25). In addition, deficient naïve $CD4^+$ T cells activated in the presence of TGF-β expressed significantly less FOXP3 than control cells (25). Besides, several studies have demonstrated that miRNA disruption in Treg cells leads to autoimmune diseases (18, 26, 27).

Dicer-deficient $CD8^+$ T lymphocytes responded more rapidly to activation *in vitro*, as indicated by faster CD69 up-regulation and an earlier proliferative response, although their survival was reduced after 2 days (28). $CD8^+$ Dicer KO cells also showed a delay in CD69 down-regulation after removal of the TCR-activating stimulus, suggesting a sustained activation of cytotoxic lymphocytes in the absence of miRNAs (28). Furthermore, $CD8^+$ Dicer-deficient cells failed to produce an efficient *in vivo* effector response, including lower proliferation and impaired cytokine production (IFN-γ and TNF-α) (28).

Models with impaired miRNA synthesis machinery highlight the importance of miRNAs as positive (booster) and/or negative (brake) regulators of T cell development and function, which is a major focus of this review (**Figure 2**).

MiR-146a mainly acts as a "brake" miRNA, as miR-146a-deficient mice develop chronic inflammation and autoimmunity (29). $CD4^+$ and $CD8^+$ T cells from miR-146a deficient mice display less apoptosis and increased proliferation, expression of activation markers (CD25 and CD69) and effector cytokines (IL2, IFN-γ, and IL-17A) (30). Likewise, miR-125b is another negative regulator of T cell function, contributing to the maintenance of the naïve state in human $CD4^+$ T cells, in which it appears at high levels (31). This effect is at least partly achieved via targeting key molecules for T cell activation, e.g., BLIMP-1, IL-2Rβ, IL-10Rα, and IFN-γ (31). Conversely, other miRNAs boost the immune response. For instance, miR-142-deficient mouse T cells showed reduced proliferation, deregulated cytokine expression and decreased secretion of pro-inflammatory cytokines such as IFN-γ, IL-17, and IL2 in response to activation (32, 33). Other examples of enhancer miRNAs are miR-155 and miR-17∼92; miR-155-depleted mice are immunodeficient (34), whereas miR-17∼92-deficient T cells exhibited reduced antitumoral responses (35).

IMMUNOREGULATORY MOLECULES AS MIRNA TARGETS

T cell activation requires that the TCR recognizes a specific antigen bound to the MHC on the surface of an APC in the presence of co-stimulation. PI3K, AKT and mTOR are crucial mediators of T cell activation. Their positive signaling, downstream the TCR, is counter-balanced by negative regulators such as PTEN and BIM. Costimulatory signals are provided by surface receptors expressed on T lymphocytes that interact with specific ligands on APCs, and can be either activating (such as CD28 and ICOS) or inhibitory (like CTLA-4 and PD-1). These activating and inhibitory events are integrated into a net response that triggers the activation and/or repression of transcription factors (NFAT, AP-1, NF-κB, and others). Their nuclear localization promotes the synthesis of immune effector molecules, e.g., cytokines. MiRNAs also control the activation and integration of these pathways to support T cell effector functions while maintaining immune homeostasis. Herein, we review the miRNA-mediated regulation of key molecules involved in T cell activation.

Cell Survival and Signaling Molecules

BIM

The balance between BIM and BCL-2 molecules is essential for the fate of T lymphocytes, and their expression is tightly regulated by miRNAs, promoting either apoptosis or survival. BIM is a pro-apoptotic regulator and tumor suppressor downstream

Abbreviations: AKT3, v-akt murine thymoma viral oncogene homolog 3; APC, antigen-presenting cell; BIM, B-cell lymphoma 2 (Bcl-2) interacting mediator of cell death; CTLA-4, Cytotoxic T lymphocyte-associated antigen 4; GVHD, Graft versus host disease; IL, Interleukin; PD-1, Programmed Death 1; PI(3,4,5)P3, phosphatidylinositol-(3,4,5)-triphosphate; PI(4,5)P2, phosphatidylinositol-(4,5)-biphosphate; PTEN, phosphatase and tensin homolog; TCR, T-cell receptor; Tfh, T follicular helper; TGF-β, Transforming Growth Factor- β; Treg, regulatory T cell; tTreg, Thymic-derived regulatory T cells; UTR, untranslated region.

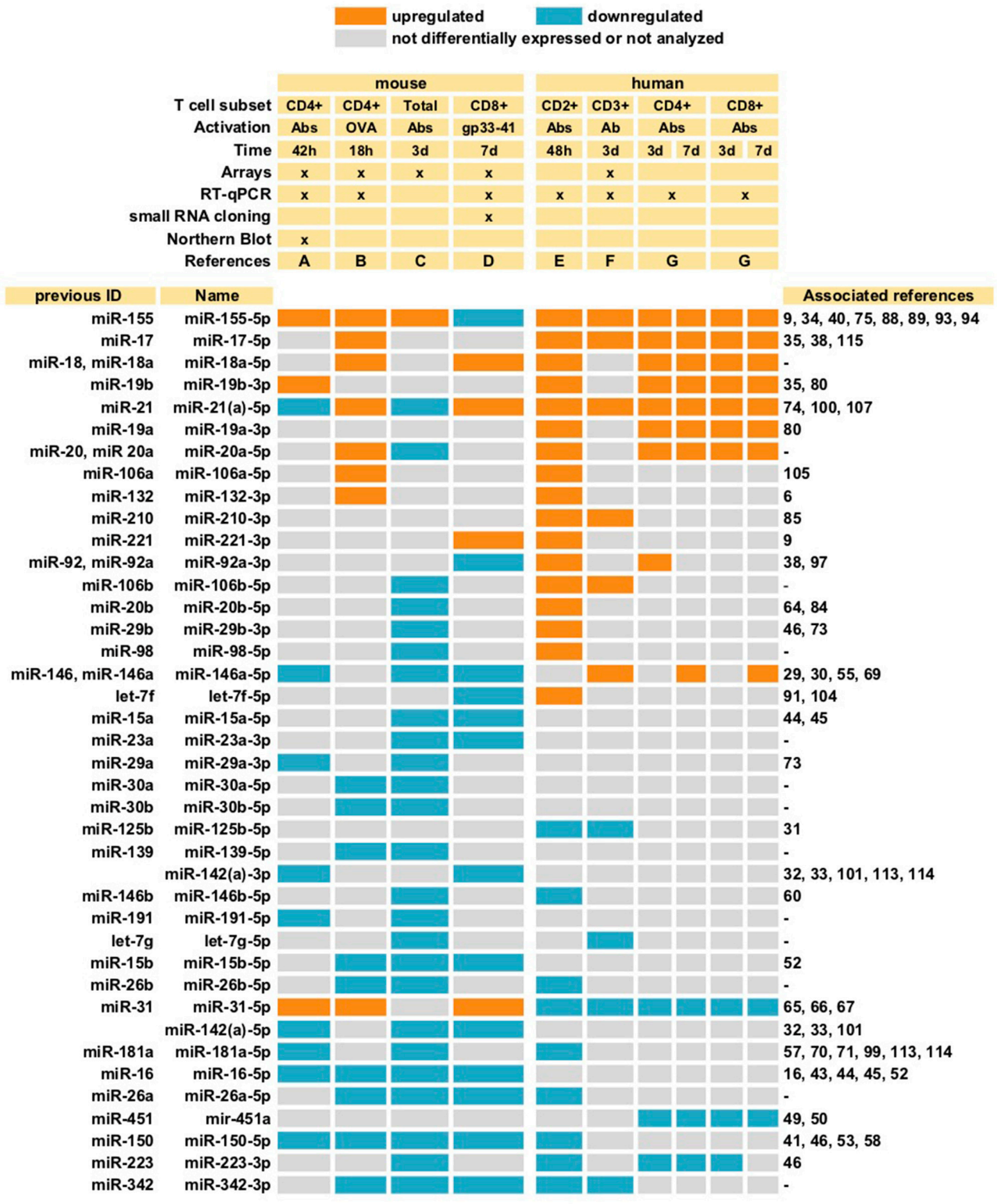

FIGURE 1 | MiRNAs differentially expressed upon T cell stimulation. MiRNAs described in at least two different studies are summarized. Different subsets of T cells (both mouse and human) were activated with either antibodies against CD3 alone (Ab), or together with antibody against CD28 (Abs), or with specific peptides (OVA or gp33-41). Cells were stimulated during different lengths of time ranging from 18 h (18 h) to 7 days (7 d). The studies included in the table are: A (5), B (6), C (7), D (8), E (9), F (10), G (11). Whenever more than one detection method was used, only consistent data obtained with at least two techniques was selected (8). Most studies evaluated miRNA expression with miRNAs arrays, some together with RT-qPCR and Northern Blot, as indicated (x).

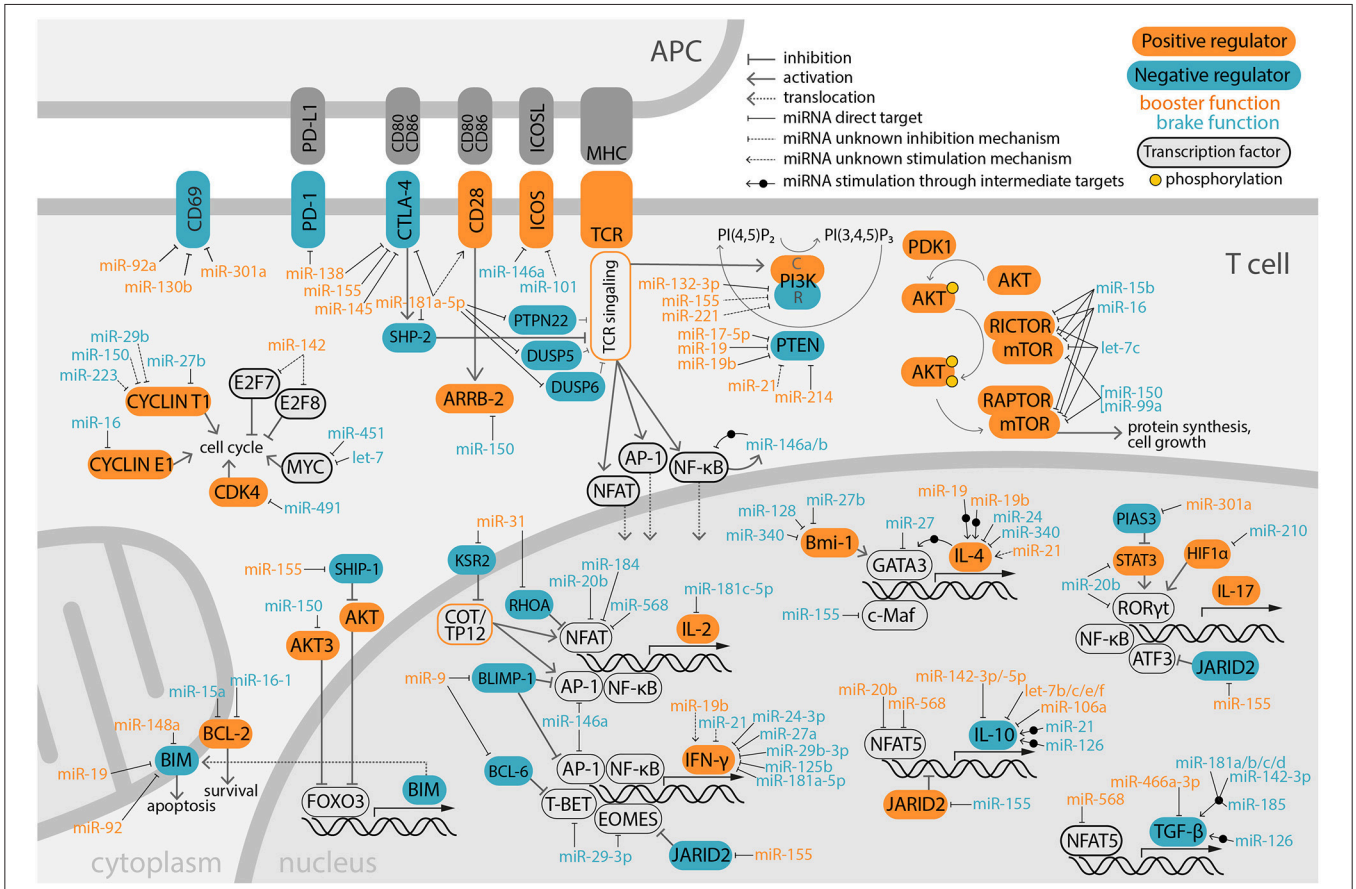

FIGURE 2 | Overview of miRNA modulation on positive and negative immune-regulator molecules. Signaling coming from TCR and costimulatory molecules is integrated by the T lymphocyte promoting cell survival, proliferation and production of effector molecules, such as cytokines. This complex network is fine-tuned by miRNAs that target key immunoregulatory molecules, supporting either T cell activation (booster) or inhibition (brake). MiRNAs exert their function by targeting the mRNA 3′UTR in the cytoplasm, although for simplicity sake some have been depicted in the nucleus, close to their targeted immunoregulators. In PI3K, C and R designated the catalytic and regulatory subunits, respectively.

of AKT3, an important mediator of TCR signaling (36, 37). It destabilizes mitochondrial membrane, inducing CASPASE-9 activation and apoptosis. Within the miR-17∼92 cluster, miR-19 and miR-92 target BIM 3′UTR mRNA (38). MiR-148a is upregulated in mouse Th1 cells after sustained activation (39). It also targets BIM, promoting cell survival (39). MiR-155 indirectly regulates BIM by targeting SHIP-1, which is a phosphatase that reduces AKT activity (40). In turn, AKT represses FOXO3, which is a transcription factor that promotes BIM expression, thus miR-155 limits BIM expression (40). Conversely, miR-150 promotes apoptosis by downregulating AKT3, which induces the accumulation of BIM (41). Human $CD4^+$ T cells with high levels of miR-150 display reduced proliferation, increased apoptosis and lower T cell activation (41).

BCL-2

BCL-2 is an anti-apoptotic protein that antagonizes BIM, stabilizing the mitochondrial membrane and preventing its permeabilization (42). Treatment of mice with experimental autoimmune encephalomyelitis with 3,3′-Diindolylmethane (a plant-derived anti-inflammatory compound), induced the upregulation of miR-16 in brain $CD4^+$ T cells and suppressed BCL-2; consistently, miR-16 overexpression in mouse $CD4^+$ T cells downregulated BCL-2 (43). Interestingly, $CD4^+$ T cells from relapsing-remitting multiple sclerosis patients (an autoimmune disease elicited by activated autoreactive T lymphocytes) displayed lower levels of miR-15a and miR-16, correlating with higher levels of their validated target BCL-2 mRNA (44, 45).

Cell Cycle Regulators

Molecules involved in cell cycle progression are essential mediators of T cell proliferation. miR-142-null T cells displayed gross cell cycle alterations, with cells differentially arrested in S and G_2/M phases (32). Cell-cycle defects were associated to the transcription factors E2F7 and E2F8, which are putative targets for miR-142. MiR-142 is likely responsible of maintaining low levels of both molecules in resting T-cells and limiting their increase upon activation. Treatment of mice with miR-142 antagomir markedly increased survival and reduced clinical

symptoms in a murine GVHD model, suggesting a potential new therapeutic strategy (32).

Cyclins are also directly targeted by miRNAs. Several miRNAs (miR-27b, miR-29b, miR-150, and miR-223) promote CYCLIN T1 downregulation in human resting $CD4^+$ T cells. The levels of these miRNAs decrease upon activation, correlating with an upregulation of CYCLIN T1 (46). MiR-16 downregulates CYCLIN E1 in mouse $CD4^+$ T cells (43). Another molecule involved in cell cycle progression is CDK4, a target of miR-491 in mouse $CD8^+$ T cells (47). MYC is a transcription factor involved in cell cycle and proliferation, is targeted by let-7 in mouse $CD8^+$ T cells (48) and by miR-451 in both mouse (49) and human (50) $CD4^+$ T cells.

mTOR

Mammalian Target Of Rapamycin (mTOR) is a metabolic regulator that promotes protein synthesis and cell growth during the onset of T lymphocyte function (51). mTOR kinase and Raptor are part of the complex mTORC1, while mTORC2 includes mTOR and Rictor. Both miR-16 and let-7c target the 3′UTR of mTOR and RICTOR (16). Elevated mTOR activity in Dicer-deficient $CD4^+$ T cells and the subsequently increased AKT phosphorylation is associated with a lower activation threshold, overcoming the need of co-stimulation. MiRNA-mediated mTOR down-regulation contributes to the correct discrimination of activating and anergic stimuli and prevents co-stimulation independent IL-2, IFN-γ and TNF-α overproduction (16). mTOR signaling suppression is relevant for Treg induction. In this regard, miR-16 and miR-15b, which are abundantly expressed in Tregs, target RICTOR and mTOR mRNAs (52). Furthermore, miR-150 and miR-99a cooperatively target mTOR, promoting Treg induction (53).

Co-stimulatory Molecules

Membrane Receptors: ICOS and CD28

Inducible co-stimulatory (ICOS) molecule and CD28 are surface receptors expressed on T cells that recognize specific ligands on APCs, acting as TCR signaling positive regulators (54). In germinal center responses, miR-146a upregulation in Tfh cells downregulates ICOS by interacting with its ligand on germinal center B cells, facilitating the termination of the immune response (55). MiR-101 is highly represented in human naïve $CD4^+$ T cells and its transfection into the EL4 murine T cell line downregulates ICOS (56). Regarding CD28, miR-181a-5p overexpression in mouse T cells increases its levels (57), whereas miR-150 limits CD28 co-stimulation by targeting the arrestin β-2 protein (ARRB-2), with a subsequent increase in cAMP levels and inhibition of LCK, PI3K and AKT (58).

Cytokines

MiRNA regulation of cytokine expression can be due to direct cytokine mRNA targeting or targeting of transcription factors such as NF-κB, NFAT, or AP-1 or their regulators, often affecting multiple cytokines. For example, miR-146a is induced in mouse $CD4^+$ and $CD8^+$ T cells upon TCR engagement through NF-κB (30). This miRNA provides negative feedback regulation, downregulating NF-κB by targeting TRAF6 and IRAK1 (30, 59). Compared to wild-type cells, both $CD4^+$ and $CD8^+$ mouse T cells lacking miR-146a exhibited a higher induction of genes regulated by NF-κB, e.g., BCL-2, CD25, CD69, IL-2, IFN-γ, and IL-17A (30). TRAF6 is also targeted by miR-146b in mouse Tregs (60).

IL-2

IL-2 is one of the main signatures of T cell activation. MiRNA-based IL-2 regulation relies on the inhibition of translation by miR-181c-5p (downregulated during T cell activation), which binds to the 3′UTR of IL-2 mRNA (61). It also depends on the miRNA-based downregulation of transcription factors such as NFAT or BLIMP-1. MiR-184 inhibits NFAT1 translation in human $CD4^+$ T cells. This is particularly relevant in cells isolated from umbilical cord blood (62). MiR-568 transfection into human $CD4^+$ T cells inhibited IL-2 expression after activation, through NFAT5 downregulation (63). MiR-20b also downregulated IL-2 through NFAT5 targeting (64). MiR-31 upregulates IL-2 by inhibiting RHOA, a small GTPase which suppresses NFAT (65, 66). It also targets the kinase suppressor of RAS2 (KSR2), which inhibits the COT/TPI2 signaling pathway (enhancer of IL-2 expression through NFAT and AP-1) (67). MiR-9 (upregulated in activated human $CD4^+$ T cells) targets BLIMP-1, de-repressing IL-2 transcription (68). MiR-146a is upregulated around 8 days after stimulation in human $CD4^+$ and $CD8^+$ T cells, impairing IL-2 production, by targeting AP-1 (69).

IFN-γ

IFN-γ release orchestrates Th1 immune responses by activating different cell lineages, e.g., dendritic cells, macrophages or NK cells. MiR-125b maintains T cell naïve state by targeting *IFN-γ* among other genes (31). Several miRNAs repress IFN-γ: miR-24-3p (70) and miR-181a-5p in human $CD4^+$ T cells (70, 71); miR-24 and miR-27a in activated human $CD8^+$ T cells (72); and miR-29 directly (73) and indirectly, by downregulating T-BET and EOMES, in mouse $CD4^+$ T cells (19). On the other hand, miR-19b is required for normal IFN-γ production, restoring IFN-γ expression in miR-17∼92-deficient mouse Th1 cells (35). MiR-9 suppresses BLIMP-1 and BCL-6 (repressors of AP-1 and T-BET, respectively), increasing IFN-γ secretion in activated human $CD4^+$ T cells (68). Murine miR-21 KO $CD4^+$ T cells re-stimulated *in vitro* produced more IFN-γ (74). Moreover, IFN-γ responsiveness is regulated by miR-155, which targets IFN-γRα in activated mouse $CD4^+$ T cells, contributing to Th1 differentiation (75).

IL-4

T cell activation stimulates the production of IL-4, leading to Th2 responses (76, 77). Its release is controlled directly by miR-24 [78] and miR-340 (78), or through the targeting of specific transcription factors and kinases/phosphatases. IL-4 triggers the upregulation of GATA3 dependent STAT6, repressing Th1 differentiation and inducing IL-4 production in a positive feedback loop. Conversely, MiR-27 targets the transcription factor GATA3 (79). BMI1 binds to GATA3, preventing its degradation. $CD4^+$ T cells from MS patients display increased expression of miR-27b, miR-128 and miR-340 (78). These

miRNAs inhibited Th2 development by targeting BMI1 (78). MiR-155 targets the 3′UTR of c-MAF mRNA, which is another transcription factor involved in IL-4 expression (34). MiR-21 contributes to IL-4 expression, since *in vitro* re-stimulated miR-21-null mouse $CD4^+$ T cells produced less IL-4 than wild-type cells (74). Both miR-19a and miR-19b rescued IL-4 production in miR-17∼92 cluster-deficient cells by targeting PTEN, SOCS1 and A20 (80).

IL-17

TCR signaling promotes expression of the proinflammatory cytokine IL-17 (81–83). IL-17 expression depends on the transcription factor RORγt downstream of STAT3. miR-20b targets both molecules in mouse $CD4^+$ T cells (84). RORγt transcription is promoted by HIF-1α, which is targeted by miR-210 (85). In turn, STAT3 is inhibited by the E3 SUMO-protein ligase PIAS3, a target of miR-301a that increases IL-17 secretion (86). MiR-212 targets BCL-6 3′UTR, which is a repressor of Th17 differentiation (87). JARID2, a chromatin-binding protein, recruits the polycomb repressive complex 2 (PRC2) and silences transcription of IL22, IL10, ATF3, TBX21, or EOMES through histone methylation (88). MiR-155 inhibits JARID2, releasing the repression of ATF3, which promotes IL-17 (88). ETS-1, a transcription factor that inhibits Th17 differentiation, is a target of miR-155 (89) and miR-326 (90). Li et al. (91) reported IL-17 downregulation due to IL-23R inhibition by let-7f.

Inhibitory Molecules

Membrane Receptors: CTLA-4, PD-1, CD69

CTLA-4 and PD-1 are both co-inhibitory receptors that repress TCR signaling via binding to co-stimulators expressed by APCs (54). CTLA-4 (a target of miR-145) is very abundant in human peripheral blood Tregs, in which miR-145 is downregulated (92). MiR-155 also targeted CTLA-4 in mouse (93) and human (94) $CD4^+$ T cells. MiR-155 overexpression in human $CD4^+$ T cells promoted proliferation, and could underlie chronic inflammation in atopic dermatitis, in which it is highly expressed also by $CD4^+$ T cells present in skin lesions (94). MiR-138 targets CTLA-4 and PD-1, promoting tumor-regression by inhibiting tumor-infiltrating Tregs (95). MiR-181a-5p overexpression in mouse T cells decreased CTLA-4 expression, while increasing CD28 levels (57).

CD69 is an early surface marker of lymphocyte activation (96). Dicer KO $CD8^+$ T cells up-regulated CD69 more rapidly upon stimulation and retained the expression longer after stimuli removal (28), indicating a potential miRNA-based repression of CD69 in naïve stages that restrains activation. MiR-130b and miR-301a increased their levels during $CD8^+$ T cell activation and downregulated CD69 (28). MiR-92, which is downregulated in lamina propria leukocytes from rhesus macaques with chronic simian immunodeficiency virus infection, also targets the 3′UTR of CD69 mRNA (97).

Kinases and Phosphatases

TCR signaling is mediated by downstream kinases and phosphatases, which undergo a tight regulation that ensures functional activation while avoiding hyperreactivity.

PI3K regulatory subunits

Upon TCR and co-receptors engagement, PI3K phosphorylates $PI(4,5)P_2$. *PIK3R1* gene encodes the regulatory subunits p85, p50, and p55 (98). MiRNAs upregulated in $CD4^+$ activated human T cells, e.g., miR-155 and miR-221 downregulate PIK3R1 (9). MiR-132-3p is upregulated in mouse dendritic cell-activated $CD4^+$ T lymphocytes, targeting PIK3R1 mRNA (6).

TCR Inhibitory phosphatases

Phosphatases downstream the TCR pathway counteract signaling by dephosphorylation. Downregulation of some of these phosphatases by miR-181a-5p generates high levels of phosphorylated intermediates in steady-state (57). MiR-181a-5p targets the phosphatases PTPN22, DUSP5 and DUSP6, which dephosphorylate LCK, ZAP70, and ERK1/2; and SHP-2, which mediates negative costimulatory signals from CTLA-4 (57). Therefore, the expression of this miRNA contributes to reduce the activation threshold, increasing the strength and sensitivity of the T cell to peptides with lower affinity (57). In elderly individuals, reduced expression of miR-181a in $CD4^+$ naïve T cells is a cause of the declined T cell responsiveness associated with age (99).

PTEN

PTEN dephosphorylates $PI(3,4,5)P_3$, antagonizing PI3K. As such, PTEN curbs T cell activation, preserving self-tolerance. Transgenic mice overexpressing miR-17∼92 cluster developed lymphoproliferative and autoimmune pathologies associated to the reduced expression of PTEN and BIM (38). PTEN is downregulated by several miRNAs that are increased upon T cell activation: miR-21 (100), miR-214 (7) and the miR-17∼92 cluster [miR-17-5p (38), miR-19 (38), and miR-19b (35)]. Consistently, miR-21 and miR-214 expression increased T cell proliferation (7, 100).

Cytokines

IL-10

IL-10 is an important anti-inflammatory cytokine mainly produced by Th2 and Tregs. It counteracts CD28 signaling and suppresses the expression of IFN-γ and IL-2. IL-10 is directly targeted by miR-142-3p, miR-142-5p (101), miR-let-7e (102), let-7c (103, 104), let-7b (104), let-7f (104), and miR-106a (105). MiRNAs further regulate IL-10 post-transcriptionally by modulating JARID2, NFAT5, p85-β or the programmed cell death protein 4 (PDCD4). JARID2 silences IL-10 and is a target of miR-155, which thus promotes IL-10 expression (88). MiR-568 (downregulated upon human $CD4^+$ T cell activation) reduced IL-10 by targeting NFAT5 (63). NFAT5 was also targeted by miR-20b (64). MiR-126 is highly increased after Treg stimulation and promotes IL-10 expression (106), and miR-126 targeting of p85-β and PI3K/AKT pathway modulation is responsible of IL-10 release (106). MiR-21 is upregulated in $CD4^+$ T cells from systemic lupus erythematosus patients, and its inhibition led to a decrease in IL-10 production (107). MiR-21 positive regulation of IL-10 secretion likely depends on its targeting of PDCD4, a translation inhibitor (107).

TGF-β

TGF-β is expressed in naïve T cells preventing T cell activation until sufficient TCR stimulation downregulates the TGF-β type 1 receptor (108–110). TGF-β induces FOXP3, a key transcription factor that promotes Treg differentiation (111). In addition to IL-10 modulation, miR-568 (63) and miR-126 (106) also regulate TGF-β release. In $CD4^+$ mouse T cells from draining lymph nodes, miR-466a-3p (upregulated in mice after skin allograft) targets TGF-β2, limiting Treg generation (112). MiRNAs also regulate TGF-β function at different levels by targeting upstream molecules involved in cytokine production, TGF-β receptors and effector molecules of the TGF-β signaling pathway. GARP is a transmembrane protein specifically expressed in Tregs that cleaves the precursor form of TGF-β1 (113). GARP is targeted by miRNAs which are less abundant in human Tregs than in T helper subsets, e.g., miR-142-3p, miR-185, and miR-181a/b/c/d (113, 114). MiR-17 targets TGFBR2 (TGF-β receptor II) in mouse and human $CD4^+$ T cells (35, 115). In addition, it has been found that a set of miRNAs upregulated in naïve $CD4^+$ T cells from multiple sclerosis patients target TGFBR1 and/or SMAD4 (both involved in the TGF-β signaling pathway) limiting differentiation into Tregs (116).

CONCLUDING REMARKS

MiRNA-mediated modulation of molecules involved in T cell activation remains far from being fully understood, although strides have been made in recent years. There is a need to advance towards a "network study" of miRNA function. Considering more than one miRNA in experimental designs increases its technical complication, but also enables models that simulate the complexity of the physiological scenarios, in which individual miRNAs interact with a set of targets and each target in turn can be regulated by several miRNAs, at different levels, either directly targeting the molecule or indirectly regulating its expression via targeting its receptor and/or transcription factors.

Finally, integrating basic and clinical research (e.g., cancer, autoimmunity, and GVHD) could help to achieve a better understanding of T cell immune-regulation to design new strategies for therapy in T cell related malignancies.

AUTHOR CONTRIBUTIONS

AR-G wrote the draft manuscript and designed the Figures. LF-M corrected and edited the manuscript. FS-M edited the manuscript. AR-G, LF-M, and FS-M discussed all the items in the manuscript.

ACKNOWLEDGMENTS

We thank Dr M. Vicente-Manzanares for critical reading of the manuscript and for assistance with English editing. This study was supported by the following grants from the Spanish Ministry of Economy and Competitiveness, (grant SAF2017-82886-R to FSM), CIBER CARDIOVASCULAR and PIE 13.0004-BIOIMID from the Instituto de Salud Carlos III (Fondo de Investigación Sanitaria del Instituto de Salud Carlos III with co-funding from the Fondo Europeo de Desarrollo Regional; FEDER), Programa de Actividades en Biomedicina de la Comunidad de Madrid-B2017/BMD-3671-INFLAMUNE to FS-M, and ERC-2011-AdG294340-GENTRIS to FS-M. The Centro Nacional de Investigaciones Cardiovasculares (CNIC) is supported by the Spanish Ministry of Economy and Competitiveness (MINECO) and the Pro-CNIC Foundation and is a Severo Ochoa Center of Excellence (MINECO award SEV-2015-0505). AR-G is supported by the FPU program (Spanish Ministry of Education). LF-M is funded by the CIBER CARDIOVASCULAR.

REFERENCES

1. Bartel DP. MicroRNAs: genomics, biogenesis, mechanism, and function. *Cell* (2004) 116:281–97. doi: 10.1016/S0092-8674(04)00045-5
2. Griffiths-Jones S, Saini HK, van Dongen S, Enright AJ. miRBase: tools for microRNA genomics. *Nucleic Acids Res.* (2008) 36:D154–8. doi: 10.1093/nar/gkm952
3. Londin E, Loher P, Telonis AG, Quann K, Clark P, Jing Y, et al. Analysis of 13 cell types reveals evidence for the expression of numerous novel primate- and tissue-specific microRNAs. *Proc Natl Acad Sci USA*. (2015) 112:E1106–15. doi: 10.1073/pnas.1420955112
4. Friedman RC, Farh KKH, Burge CB, Bartel DP. Most mammalian mRNAs are conserved targets of microRNAs. *Genome Res.* (2009) 19:92–105. doi: 10.1101/gr.082701.108
5. Bronevetsky Y, Villarino AV, Eisley CJ, Barbeau R, Barczak AJ, Heinz GA, et al. T cell activation induces proteasomal degradation of Argonaute and rapid remodeling of the microRNA repertoire. *J Exp Med.* (2013) 210:417–32. doi: 10.1084/jem.20111717
6. Gutiérrez-Vázquez C, Rodríguez-Galán A, Fernández-Alfara M, Mittelbrunn M, Sánchez-Cabo F, Martínez-Herrera DJ, et al. miRNA profiling during antigen-dependent T cell activation: a role for miR-132-3p. *Sci Rep*. (2017) 7:3508. doi: 10.1038/s41598-017-03689-7
7. Jindra PT, Bagley J, Godwin JG, Iacomini J. Costimulation-dependent expression of MicroRNA-214 increases the ability of T cells to proliferate by targeting Pten. *J Immunol*. (2010) 185:990–7. doi: 10.4049/jimmunol.1000793
8. Wu H, Neilson JR, Kumar P, Manocha M, Shankar P, Sharp PA, et al. miRNA Profiling of Naïve, Effector and Memory CD8 T Cells. *PLoS ONE* (2007) 2:e1020. doi: 10.1371/journal.pone.0001020
9. Grigoryev YA, Kurian SM, Hart T, Nakorchevsky AA, Chen C, Campbell D, et al. MicroRNA regulation of molecular networks mapped by global MicroRNA, mRNA, and Protein Expression in Activated T Lymphocytes. *J Immunol*. (2011) 187:2233–43. doi: 10.4049/jimmunol.1101233
10. Sousa IG, do Almo MM, Simi KCR, Bezerra MAG, Andrade RV, Maranhão AQ, et al. MicroRNA expression profiles in human CD3+ T cells following stimulation with anti-human CD3 antibodies. *BMC Res Notes* (2017) 10:124. doi: 10.1186/s13104-017-2442-y
11. Teteloshvili N, Smigielska-Czepiel K, Kroesen B-J, Brouwer E, Kluiver J, Boots A, et al. T-cell Activation Induces Dynamic Changes in miRNA Expression Patterns in CD4 and CD8 T-cell Subsets. *MicroRNA* (2015) 4:117–22. doi: 10.2174/2211536604666150819194636
12. Bernstein E, Caudy AA, Hammond SM, Hannon GJ. Role for bidentate ribnuclease in the initiation site of RNA interference. *Nature* (2001) 409:363–6. doi: 10.1038/35053110
13. Hutvagner G. A cellular function for the RNA-interference enzyme dicer in the maturation of the let-7 small temporal RNA. *Science (80-)* (2001) 293:834–8. doi: 10.1126/science.1062961

14. Grishok A, Pasquinelli AE, Conte D, Li N, Parrish S, Ha I, et al. Genes and mechanisms related to RNA interference regulate expression of the small temporal RNAs that control C. elegans developmental timing. *Cell*. (2001) 106:23–34. doi: 10.1016/S0092-8674(01)00431-7
15. Bernstein E, Kim SY, Carmell MA, Murchison EP, Alcorn H, Li MZ, et al. Dicer is essential for mouse development. *Nat Genet*. (2003) 35:215–7. doi: 10.1038/ng1253
16. Marcais A, Blevins R, Graumann J, Feytout A, Dharmalingam G, Carroll T, et al. microRNA-mediated regulation of mTOR complex components facilitates discrimination between activation and anergy in CD4 T cells. *J Exp Med*. (2014) 211:2281–95. doi: 10.1084/jem.20132059
17. Muljo SA, Ansel KM, Kanellopoulou C, Livingston DM, Rao A, Rajewsky K. Aberrant T cell differentiation in the absence of Dicer. *J Exp Med*. (2005) 202:261–9. doi: 10.1084/jem.20050678
18. Chong MMW, Rasmussen JP, Rudensky AY, Littman DR. The RNAseIII enzyme drosha is critical in T cells for preventing lethal inflammatory disease. *J Exp Med*. (2008) 205:2005–17. doi: 10.1084/jem.20071219090508c
19. Steiner DF, Thomas MF, Hu JK, Yang Z, Babiarz JE, Allen CDC, et al. MicroRNA-29 Regulates T-Box transcription factors and interferon-γ production in helper T cells. *Immunity* (2011) 35:169–81. doi: 10.1016/j.immuni.2011.07.009
20. Kroesen B-J, Teteloshvili N, Smigielska-Czepiel K, Brouwer E, Boots AMH, van den Berg A, et al. Immuno-miRs: critical regulators of T-cell development, function and ageing. *Immunology* (2015) 144:1–10. doi: 10.1111/imm.12367
21. Jeker LT, Bluestone JA. MicroRNA regulation of T-cell differentiation and function. *Immunol Rev*. (2013) 253:65–81. doi: 10.1111/imr.12061
22. Liu J, Wu C-P, Lu B-F, Jiang J-T. Mechanism of T cell regulation by microRNAs. Cancer *Biol Med*. (2013) 10:131–7. doi: 10.7497/j.issn.2095-3941.2013.03.002
23. Baumjohann D, Ansel KM. MicroRNA-mediated regulation of T helper cell differentiation and plasticity. *Nat Rev Immunol*. (2013) 13:666–78. doi: 10.1038/nri3494
24. Podshivalova K, Salomon DR. MicroRNA regulation of T-lymphocyte immunity: modulation of molecular networks responsible for T-cell activation, differentiation, and development. *Crit Rev Immunol*. (2013) 33:435–76. doi: 10.1615/CritRevImmunol.2013006858
25. Cobb BS, Hertweck A, Smith J, O'Connor E, Graf D, Cook T, et al. A role for Dicer in immune regulation. *J Exp Med*. (2006) 203:2519–27. doi: 10.1084/jem.20061692
26. Liston A, Lu L-F, O'Carroll D, Tarakhovsky A, Rudensky AY. Dicer-dependent microRNA pathway safeguards regulatory T cell function. *J Exp Med*. (2008) 205:1993–2004. doi: 10.1084/jem.20081062
27. Zhou X, Jeker LT, Fife BT, Zhu S, Anderson MS, McManus MT, et al. Selective miRNA disruption in T reg cells leads to uncontrolled autoimmunity. *J Exp Med*. (2008) 205:1983–91. doi: 10.1084/jem.20080707
28. Zhang N, Bevan MJ. Dicer controls CD8+ T-cell activation, migration, and survival. *Proc Natl Acad Sci USA*. (2010) 107:21629–34. doi: 10.1073/pnas.1016299107
29. Boldin MP, Taganov KD, Rao DS, Yang L, Zhao JL, Kalwani M, et al. miR-146a is a significant brake on autoimmunity, myeloproliferation, and cancer in mice. *J Exp Med*. (2011) 208:1189–201. doi: 10.1084/jem.20101823
30. Yang L, Boldin MP, Yu Y, Liu CS, Ea C-K, Ramakrishnan P, et al. miR-146a controls the resolution of T cell responses in mice. *J Exp Med*. (2012) 209:1655–70. doi: 10.1084/jem.20112218
31. Rossi RL, Rossetti G, Wenandy L, Curti S, Ripamonti A, Bonnal RJP, et al. Distinct microRNA signatures in human lymphocyte subsets and enforcement of the naive state in CD4+ T cells by the microRNA miR-125b. *Nat Immunol*. (2011) 12:796–803. doi: 10.1038/ni.2057
32. Sun Y, Oravecz-Wilson K, Mathewson N, Wang Y, McEachin R, Liu C, et al. Mature T cell responses are controlled by microRNA-142. *J Clin Invest*. (2015) 125:2825–40. doi: 10.1172/JCI78753
33. Mildner A, Chapnik E, Varol D, Aychek T, Lampl N, Rivkin N, et al. MicroRNA-142 controls thymocyte proliferation. *Eur J Immunol*. (2017) 47:1142–52. doi: 10.1002/eji.201746987
34. Rodriguez A, Vigorito E, Clare S, Warren M V, Couttet P, Soond DR, et al. Requirement of bic/microRNA-155 for normal immune function. *Science (80-)*. (2007) 316:608–11. doi: 10.1126/science.1139253
35. Jiang S, Li C, Olive V, Lykken E, Feng F, Sevilla J, et al. Molecular dissection of the miR-17-92 cluster's critical dual roles in promoting Th1 responses and preventing inducible Treg differentiation. *Blood* (2011) 118:5487–97. doi: 10.1182/blood-2011-05-355644
36. Hildeman DA, Zhu Y, Mitchell TC, Bouillet P, Strasser A, Kappler J, et al. Activated T cell death *in vivo* mediated by proapoptotic Bcl-2 family member Bim. *Immunity* (2002) 16:759–67. doi: 10.1016/S1074-7613(02)00322-9
37. Reynolds C, Roderick JE, LaBelle JL, Bird G, Mathieu R, Bodaar K, et al. Repression of BIM mediates survival signaling by MYC and AKT in high-risk T-cell acute lymphoblastic leukemia. *Leukemia* (2014) 28:1819–27. doi: 10.1038/leu.2014.78
38. Xiao C, Srinivasan L, Calado DP, Patterson HC, Zhang B, Wang J, et al. Lymphoproliferative disease and autoimmunity in mice with increased miR-17-92 expression in lymphocytes. *Nat Immunol*. (2008) 9:405–14. doi: 10.1038/ni1575
39. Haftmann C, Stittrich AB, Zimmermann J, Fang Z, Hradilkova K, Bardua M, et al. MiR-148a is upregulated by Twist1 and T-bet and promotes Th1-cell survival by regulating the proapoptotic gene Bim. *Eur J Immunol*. (2015) 45:1192–205. doi: 10.1002/eji.201444633
40. Rouquette-Jazdanian AK, Kortum RL, Li W, Merrill RK, Nguyen PH, Samelson LE, et al. miR-155 controls lymphoproliferation in LAT mutant mice by restraining T-cell apoptosis via SHIP-1/mTOR and PAK1/FOXO3/BIM pathways. *PLoS ONE* (2015) 10:1–27. doi: 10.1371/journal.pone.0131823
41. Sang W, Sun C, Zhang C, Zhang D, Wang Y, Xu L, et al. MicroRNA-150 negatively regulates the function of CD4+T cells through AKT3/Bim signaling pathway. *Cell Immunol*. (2016) 306–307:35–40. doi: 10.1016/j.cellimm.2016.05.007
42. Guerrero AD, Welschhans RL, Chen M, Wang J. Cleavage of Anti-Apoptotic Bcl-2 Family Members after TCR Stimulation Contributes to the Decision between T Cell Activation and Apoptosis. *J Immunol*. (2013) 190:168–73. doi: 10.4049/jimmunol.1201610
43. Rouse M, Rao R, Nagarkatti M, Nagarkatti PS. 3,3'-Diindolylmethane ameliorates experimental autoimmune encephalomyelitis by promoting cell cycle arrest and apoptosis in activated T cells through MicroRNA signaling pathways. *J Pharmacol Exp Ther*. (2014) 350:341–52. doi: 10.1124/jpet.114.214742
44. Lorenzi JCC, Brum DG, Zanette DL, de Paula Alves Souza A, Barbuzano FG, dos Santos AC, et al. miR-15a and 16-1 Are Downregulated in $CD4^+$ T Cells of Multiple Sclerosis Relapsing Patients. *Int J Neurosci*. (2012) 122:466–71. doi: 10.3109/00207454.2012.678444
45. Cimmino A, Calin GA, Fabbri M, Iorio M V., Ferracin M, Shimizu M, et al. miR-15 and miR-16 induce apoptosis by targeting BCL2. *Proc Natl Acad Sci USA*. (2005) 102:13944–9. doi: 10.1073/pnas.0506654102
46. Chiang K, Sung T-L, Rice AP. Regulation of Cyclin T1 and HIV-1 Replication by MicroRNAs in Resting $CD4^+$ T Lymphocytes. *J Virol*. (2012) 86:3244–52. doi: 10.1128/JVI.05065-11
47. Yu T, Zuo Q-F, Gong L, Wang L-N, Zou Q-M, Xiao B. MicroRNA-491 regulates the proliferation and apoptosis of $CD8^+$ T cells. *Sci Rep*. (2016) 6:30923. doi: 10.1038/srep30923
48. Wells AC, Daniels KA, Angelou CC, Fagerberg E, Burnside AS, Markstein M, et al. Modulation of let-7 miRNAs controls the differentiation of effector CD8 T cells. *Elife*. (2017) 6:e26398. doi: 10.7554/eLife.26398
49. Chapman LM, Ture SK, Field DJ, Morrell CN. miR-451 limits $CD4^+$ T cell proliferative responses to infection in mice. *Immunol Res*. (2017) 65:828–40. doi: 10.1007/s12026-017-8919-x
50. Zeng Z, Wang K, Li Y, Xia N, Nie S, Lv B, et al. Down-regulation of microRNA-451a facilitates the activation and proliferation of $CD4^+$ T cells by targeting Myc in patients with dilated cardiomyopathy. *J Biol Chem*. (2017) 292:6004–13. doi: 10.1074/jbc.M116.765107
51. Liu Y, Zhang D, Liu X. mTOR Signaling in T Cell Immunity and Autoimmunity. *Int Rev Immunol*. (2015) 34:50–66. doi: 10.3109/08830185.2014.933957
52. Singh Y, Garden OA, Lang F, Cobb BS. MicroRNA-15b/16 enhances the induction of regulatory T cells by regulating the expression of rictor and mTOR. *J Immunol*. (2015) 195:5667–77. doi: 10.4049/jimmunol.1401875

53. Warth SC, Hoefig KP, Hiekel A, Schallenberg S, Jovanovic K, Klein L, et al. Induced miR-99a expression represses Mtor cooperatively with miR-150 to promote regulatory T-cell differentiation. *Embo J*. (2015) 34:1195–213. doi: 10.15252/embj.201489589
54. Chen L, Flies DB. Molecular mechanisms of T cell co-stimulation and co-inhibition. *Nat Rev Immunol*. (2013) 13:227–42. doi: 10.1038/nri3405
55. Pratama A, Srivastava M, Williams NJ, Papa I, Lee SK, Dinh XT, et al. MicroRNA-146a regulates ICOS-ICOSL signalling to limit accumulation of T follicular helper cells and germinal centres. *Nat Commun*. (2015) 6:1–14. doi: 10.1038/ncomms7436
56. Di Yu, Tan AHM, Hu X, Athanasopoulos V, Simpson N, Silva DG, et al. Roquin represses autoimmunity by limiting inducible T-cell co-stimulator messenger RNA. *Nature* (2007) 450:299–303. doi: 10.1038/nature06253
57. Li Q-J, Chau J, Ebert PJR, Sylvester G, Min H, Liu G, et al. miR-181a Is an Intrinsic Modulator of T Cell Sensitivity and Selection. *Cell* (2007) 129:147–61. doi: 10.1016/j.cell.2007.03.008
58. Sang W, Wang Y, Zhang C, Zhang D, Sun C, Niu M, et al. MiR-150 impairs inflammatory cytokine production by targeting ARRB-2 after blocking CD28/B7 costimulatory pathway. *Immunol Lett*. (2016) 172:1–10. doi: 10.1016/j.imlet.2015.11.001
59. Taganov KD, Boldin MP, Chang K-J, Baltimore D. NF- B-dependent induction of microRNA miR-146, an inhibitor targeted to signaling proteins of innate immune responses. *Proc Natl Acad Sci. USA* (2006) 103:12481–6. doi: 10.1073/pnas.0605298103
60. Lu Y, Hippen KL, Lemire AL, Gu J, Wang W, Ni X, et al. miR-146b antagomir-treated human Tregs acquire increased GVHD inhibitory potency. *Blood*. (2016) 128:1424–35. doi: 10.1182/blood-2016-05-714535
61. Xue Q, Guo ZY, Li W, Wen WH, Meng YL, Jia LT, et al. Human activated $CD4^+$ T lymphocytes increase IL-2 expression by downregulating microRNA-181c. *Mol Immunol*. (2011) 48:592–9. doi: 10.1016/j.molimm.2010.10.021
62. Weitzel RP, Lesniewski ML, Haviernik P, Kadereit S, Leahy P, Greco NJ, et al. microRNA 184 regulates expression of NFAT1 in umbilical cord blood $CD4^+$ T cells. *Blood*. (2009) 113:6648–57. doi: 10.1182/blood-2008-09-181156
63. Li W, Kong L, Li J-T, Guo Z-Y, Xue Q, Yang T, et al. MiR-568 inhibits the activation and function of $CD4^+$ T cells and Treg cells by targeting NFAT5. *Int Immunol*. (2014) 26:269–81. doi: 10.1093/intimm/dxt065
64. Xin Y, Cai H, Lu T, Zhang Y, Yang Y, Cui Y. miR-20b Inhibits T cell proliferation and activation via NFAT Signaling Pathway in Thymoma-Associated Myasthenia Gravis. *Biomed Res Int*. (2016) 2016:9595718. doi: 10.1155/2016/9595718
65. Helms WS, Jeffrey JL, Holmes DA, Townsend MB, Clipstone NA, Su L. Modulation of NFAT-dependent gene expression by the RhoA signaling pathway in T cells. *J Leukoc Biol*. (2007) 82:361–9. doi: 10.1189/jlb.0206120
66. Fan W, Liang D, Tang Y, Qu B, Cui H, Luo X, et al. Identification of microRNA-31 as a novel regulator contributing to impaired interleukin-2 production in T cells from patients with systemic lupus erythematosus. *Arthritis Rheum*. (2012) 64:3715–25. doi: 10.1002/art.34596
67. Xue F, Li H, Zhang J, Lu J, Xia Y, Xia Q. MiR-31 regulates interleukin 2 and kinase suppressor of ras 2 during T cell activation. *Genes Immun*. (2013) 14:127–31. doi: 10.1038/gene.2012.58
68. Thiele S, Wittmann J, Jäck H-M, Pahl A. miR-9 enhances IL-2 production in activated human $CD4^+$ T cells by repressing Blimp-1. *Eur J Immunol*. (2012) 42:2100–8. doi: 10.1002/eji.201142203
69. Curtale G, Citarella F, Carissimi C, Goldoni M, Carucci N, Fulci V, et al. An emerging player in the adaptive immune response: microRNA-146a is a modulator of IL-2 expression and activation-induced cell death in T lymphocytes. *Blood* (2010) 115:265–73. doi: 10.1182/blood-2009-06-225987
70. Fayyad-Kazan H, Hamade E, Rouas R, Najar M, Fayyad-Kazan M, El Zein N, et al. Downregulation of microRNA-24 and−181 parallels the upregulation of IFN-γ secreted by activated human CD4 lymphocytes. *Hum Immunol*. (2014) 75:677–85. doi: 10.1016/j.humimm.2014.01.007
71. Sang W, Zhang C, Zhang D, Wang Y, Sun C, Niu M, et al. MicroRNA-181a, a potential diagnosis marker, alleviates acute graft versus host disease by regulating IFN-γ production. *Am J Hematol*. (2015) 90:998–1007. doi: 10.1002/ajh.24136
72. Chandran PA, Keller A, Weinmann L, Adel Seida A, Braun M, Andreev K, et al. The TGF-β-inducible miR-23a cluster attenuates IFN- levels and antigen-specific cytotoxicity in human $CD8^+$ T cells. *J Leukoc Biol*. (2014) 96:633–45. doi: 10.1189/jlb.3A0114-025R
73. Ma F, Xu S, Liu X, Zhang Q, Xu X, Liu M, et al. The microRNA miR-29 controls innate and adaptive immune responses to intracellular bacterial infection by targeting interferon-γ. *Nat Immunol*. (2011) 12:861–9. doi: 10.1038/ni.2073
74. Lu TX, Hartner J, Lim E-J, Fabry V, Mingler MK, Cole ET, et al. MicroRNA-21 limits *in vivo* immune response-mediated activation of the IL-12/IFN- Pathway, Th1 Polarization, and the severity of delayed-type hypersensitivity. *J Immunol*. (2011) 187:3362–73. doi: 10.4049/jimmunol.1101235
75. Banerjee A, Schambach F, DeJong CS, Hammond SM, Reiner SL. Micro-RNA-155 inhibits IFN-γ signaling in $CD4^+$ T cells. *Eur J Immunol*. (2009) 40:225–31. doi: 10.1002/eji.200939381
76. McAdam AJ, Chang TT, Lumelsky AE, Greenfield EA, Boussiotis VA, Duke-Cohan JS, et al. Mouse Inducible Costimulatory Molecule (ICOS) expression is enhanced by CD28 costimulation and regulates differentiation of $CD4^+$ T cells. *J Immunol*. (2000) 165:5035–40. doi: 10.4049/jimmunol.165.9.5035
77. Milner JD. TCR signaling abnormalities in human Th2-associated atopic disease. *Front Immunol*. (2018) 9:2–6. doi: 10.3389/fimmu.2018.00719
78. Guerau-De-Arellano M, Smith KM, Godlewski J, Liu Y, Winger R, Lawler SE, et al. Micro-RNA dysregulation in multiple sclerosis favours pro-inflammatory T-cell-mediated autoimmunity. *Brain* (2011) 134:3575–86. doi: 10.1093/brain/awr262
79. Cho S, Wu C-J, Yasuda T, Cruz LO, Khan AA, Lin L-L, et al. miR-23∼27∼24 clusters control effector T cell differentiation and function. *J Exp Med*. (2016) 213:235–49. doi: 10.1084/jem.20150990
80. Simpson LJ, Patel S, Bhakta NR, Choy DF, Brightbill HD, Ren X, et al. A microRNA upregulated in asthma airway T cells promotes TH2 cytokine production. *Nat Immunol*. (2014) 15:1162–70. doi: 10.1038/ni.3026
81. Chen Z, Tato CM, Muul L, Laurence A, O'Shea JJ. Distinct regulation of interleukin-17 in human T helper lymphocytes. *Arthritis Rheum*. (2007) 56:2936–46. doi: 10.1002/art.22866
82. Gomez-Rodriguez J, Sahu N, Handon R, Davidson TS, Anderson SM, Kirby MR, et al. Differential Expression of Interleukin-17A and−17F is coupled to T Cell Receptor Signaling via Inducible T Cell Kinase. *Immunity* (2009) 31:587–97. doi: 10.1016/j.immuni.2009.07.009
83. Purvis HA, Stoop JN, Mann J, Woods S, Kozijn AE, Hambleton S, et al. Low-strength T-cell activation promotes Th17 responses. *Blood* (2016) 116:4829–38. doi: 10.1182/blood-2010-03-272153
84. Zhu E, Wang X, Zheng B, Wang Q, Hao J, Chen S, et al. miR-20b Suppresses Th17 differentiation and the pathogenesis of experimental autoimmune encephalomyelitis by targeting ROR t and STAT3. *J Immunol*. (2014) 192:5599–609. doi: 10.4049/jimmunol.1303488
85. Wang H, Flach H, Onizawa M, Wei L, Mcmanus MT, Weiss A. Negative regulation of Hif1a expression and TH 17 differentiation by the hypoxia-regulated microRNA miR-210. *Nat Immunol*. (2014) 15:393–401. doi: 10.1038/ni.2846
86. Mycko MP, Cichalewska M, Machlanska A, Cwiklinska H, Mariasiewicz M, Selmaj KW. MicroRNA-301a regulation of a T-helper 17 immune response controls autoimmune demyelination. *Proc Natl Acad Sci USA*. (2012) 109:E1248–57. doi: 10.1073/pnas.1114325109
87. Nakahama T, Hanieh H, Nguyen NT, Chinen I, Ripley B, Millrine D, et al. Aryl hydrocarbon receptor-mediated induction of the microRNA-132/212 cluster promotes interleukin-17-producing T-helper cell differentiation. *Proc Natl Acad Sci USA*. (2013) 110:11964–9. doi: 10.1073/pnas.1311087110
88. Escobar TM, Kanellopoulou C, Kugler DG, Kilaru G, Nguyen CK, Nagarajan V, et al. miR-155 Activates Cytokine Gene Expression in Th17 Cells by Regulating the DNA-Binding Protein Jarid2 to Relieve Polycomb-Mediated Repression. *Immunity* (2014) 40:865–79. doi: 10.1016/j.immuni.2014.03.014
89. Hu R, Huffaker TB, Kagele DA, Runtsch MC, Bake E, Chaudhuri AA, et al. MicroRNA-155 confers encephalogenic potential to Th17 cells by promoting effector gene expression. *J Immunol*. (2013) 190:5972–80. doi: 10.4049/jimmunol.1300351
90. Du C, Liu C, Kang J, Zhao G, Ye Z, Huang S, et al. MicroRNA miR-326 regulates TH-17 differentiation and is associated with the pathogenesis of multiple sclerosis. *Nat Immunol*. (2009) 10:1252–9. doi: 10.1038/ni.1798

91. Li Z, Wu F, Brant SR, Kwon JH. IL-23 receptor regulation by Let-7f in human $CD4^+$ memory T cells. *J Immunol.* (2011) 186:6182–90. doi: 10.4049/jimmunol.1000917
92. Fayyad-Kazan H, Rouas R, Fayyad-Kazan M, Badran R, El Zein N, Lewalle P, et al. MicroRNA profile of circulating CD4-positive regulatory T cells in human adults and impact of differentially expressed microRNAs on expression of two genes essential to their function. *J Biol Chem.* (2012) 287:9910–22. doi: 10.1074/jbc.M111.337154
93. Zhang Y, Sun E, Li X, Zhang M, Tang Z, He L, et al. miR-155 contributes to Df1-induced asthma by increasing the proliferative response of Th cells via CTLA-4 downregulation. *Cell Immunol.* (2017) 314:1–9. doi: 10.1016/j.cellimm.2017.01.005
94. Sonkoly E, Janson P, Majuri M-L, Savinko T, Fyhrquist N, Eidsmo L, et al. MiR-155 is overexpressed in patients with atopic dermatitis and modulates T-cell proliferative responses by targeting cytotoxic T lymphocyte–associated antigen 4. *J Allergy Clin Immunol.* (2010) 126:581–589.e20. doi: 10.1016/j.jaci.2010.05.045
95. Wei J, Nduom EK, Kong LY, Hashimoto Y, Xu S, Gabrusiewicz K, et al. MiR-138 exerts anti-glioma efficacy by targeting immune checkpoints. *Neuro Oncol.* (2016) 18:639–48. doi: 10.1093/neuonc/nov292
96. Cibrián D, Sánchez-Madrid F. CD69: from activation marker to metabolic gatekeeper. *Eur J Immunol.* (2017) 47:946–53. doi: 10.1002/eji.201646837
97. Kumar V, Torben W, Kenway CS, Schiro FR, Mohan M. Longitudinal examination of the intestinal lamina propria cellular compartment of simian immunodeficiency virus-infected rhesus macaques provides broader and deeper insights into the link between aberrant MicroRNA expression and persistent immune activati. *J Virol.* (2016) 90:5003–19. doi: 10.1128/JVI.00189-16
98. Jean S, Kiger AA. Classes of phosphoinositide 3-kinases at a glance. *J Cell Sci.* (2014) 127:923–8. doi: 10.1242/jcs.093773
99. Li G, Yu M, Lee WW, Tsang M, Krishnan E, Weyand CM, et al. Decline in miR-181a expression with age impairs T cell receptor sensitivity by increasing DUSP6 activity. *Nat Med.* (2012) 18:1518–24. doi: 10.1038/nm.2963
100. He W, Wang C, Mu R, Liang P, Huang Z, Zhang J, et al. MiR-21 is required for anti-tumor immune response in mice: an implication for its bi-directional roles. *Oncogene* (2017) 36:4212–23. doi: 10.1038/onc.2017.62
101. Ding S, Liang Y, Zhao M, Liang G, Long H, Zhao S, et al. Decreased microRNA-142-3p/5p expression causes $CD4^+$ T cell activation and B cell hyperstimulation in systemic lupus erythematosus. *Arthritis Rheum.* (2012) 64:2953–63. doi: 10.1002/art.34505
102. Guan H, Fan D, Mrelashvili D, Hao H, Singh NP, Singh UP, et al. MicroRNA let-7e is associated with the pathogenesis of experimental autoimmune encephalomyelitis. *Eur J Immunol.* (2013) 43:104–14. doi: 10.1002/eji.201242702
103. Jiang L, Cheng Z, Qiu S, Que Z, Bao W, Jiang C, et al. Altered let-7 expression in Myasthenia gravis and let-7c mediated regulation of IL-10 by directly targeting IL-10 in Jurkat cells. *Int Immunopharmacol.* (2012) 14:217–23. doi: 10.1016/j.intimp.2012.07.003
104. Swaminathan S, Suzuki K, Seddiki N, Kaplan W, Cowley MJ, Hood CL, et al. Differential regulation of the Let-7 family of MicroRNAs in $CD4^+$ T cells alters IL-10 expression. *J Immunol.* (2012) 188:6238–46. doi: 10.4049/jimmunol.1101196
105. Sharma A, Kumar M, Aich J, Hariharan M, Brahmachari SK, Agrawal A, et al. Posttranscriptional regulation of interleukin-10 expression by hsa-miR-106a. *Proc Natl Acad Sci USA.* (2009) 106:5761–6. doi: 10.1073/pnas.0808743106
106. Qin A, Wen Z, Zhou Y, Li Y, Li Y, Luo J, et al. MicroRNA-126 regulates the induction and function of $CD4^+$ $Foxp3^+$ regulatory T cells through PI3K/AKT pathway. *J Cell Mol Med.* (2013) 17:252–64. doi: 10.1111/jcmm.12003
107. Stagakis E, Bertsias G, Verginis P, Nakou M, Hatziapostolou M, Kritikos H, et al. Identification of novel microRNA signatures linked to human lupus disease activity and pathogenesis: MiR-21 regulates aberrant T cell responses through regulation of PDCD4 expression. *Ann Rheum Dis.* (2011) 70:1496–506. doi: 10.1136/ard.2010.139857
108. Chen CH, Seguin-Devaux C, Burke NA, Oriss TB, Watkins SC, Clipstone N, et al. Transforming growth factor beta blocks Tec kinase phosphorylation, $Ca2^+$ influx, and NFATc translocation causing inhibition of T cell differentiation. *J Exp Med.* (2003) 197:1689–99. doi: 10.1084/jem.20021170
109. Li MO, Sanjabi S, Flavell RA. Transforming growth factor-β controls development, homeostasis, and tolerance of T cells by regulatory T cell-dependent and -independent mechanisms. *Immunity* (2006) 25:455–71. doi: 10.1016/j.immuni.2006.07.011
110. Tu E, Chia CPZ, Chen W, Zhang D, Park SA, Jin W, et al. T cell receptor-regulated TGF-β Type I receptor expression determines T cell quiescence and activation. *Immunity* (2018) 48:745–759.e6. doi: 10.1016/j.immuni.2018.03.025
111. Li MO, Flavell RA. TGF-β: a master of all T cell trades. *Cell* (2008) 134:392–404. doi: 10.1016/j.cell.2008.07.025
112. Becker W, Nagarkatti M, Nagarkatti PS. miR-466a targeting of TGF-β2 contributes to $FoxP3^+$regulatory T cell differentiation in a murine model of allogeneic transplantation. *Front Immunol.* (2018) 9:688. doi: 10.3389/fimmu.2018.00688
113. Gauthy E, Cuende J, Stockis J, Huygens C, Lethé B, Collet JF, et al. GARP is regulated by miRNAs and controls latent TGF-β1 production by human regulatory T cells. *PLoS ONE* (2013) 8:e76186. doi: 10.1371/journal.pone.0076186
114. Zhou Q, Haupt S, Prots I, Thummler K, Kremmer E, Lipsky PE, et al. miR-142-3p Is involved in CD25+ CD4 T cell proliferation by targeting the expression of glycoprotein A repetitions predominant. *J Immunol.* (2013) 190:6579–88. doi: 10.4049/jimmunol.1202993
115. Meira M, Sievers C, Hoffmann F, Rasenack M, Kuhle J, Derfuss T, et al. Unraveling natalizumab effects on deregulated miR-17 expression in $CD4^+$ T cells of patients with relapsing-remitting multiple sclerosis. *J Immunol Res.* (2014) 2014:897249. doi: 10.1155/2014/897249
116. Severin ME, Lee PW, Liu Y, Selhorst AJ, Gormley MG, Pei W, et al. MicroRNAs targeting TGFb signalling underlie the regulatory T cell defect in multiple sclerosis. *Brain* (2016) 139:1747–61. doi: 10.1093/brain/aww084

Conflict of Interest Statement: The authors declare that the research was conducted in the absence of any commercial or financial relationships that could be construed as a potential conflict of interest.

iScience

CellPress
OPEN ACCESS

Article

MiRNA post-transcriptional modification dynamics in T cell activation

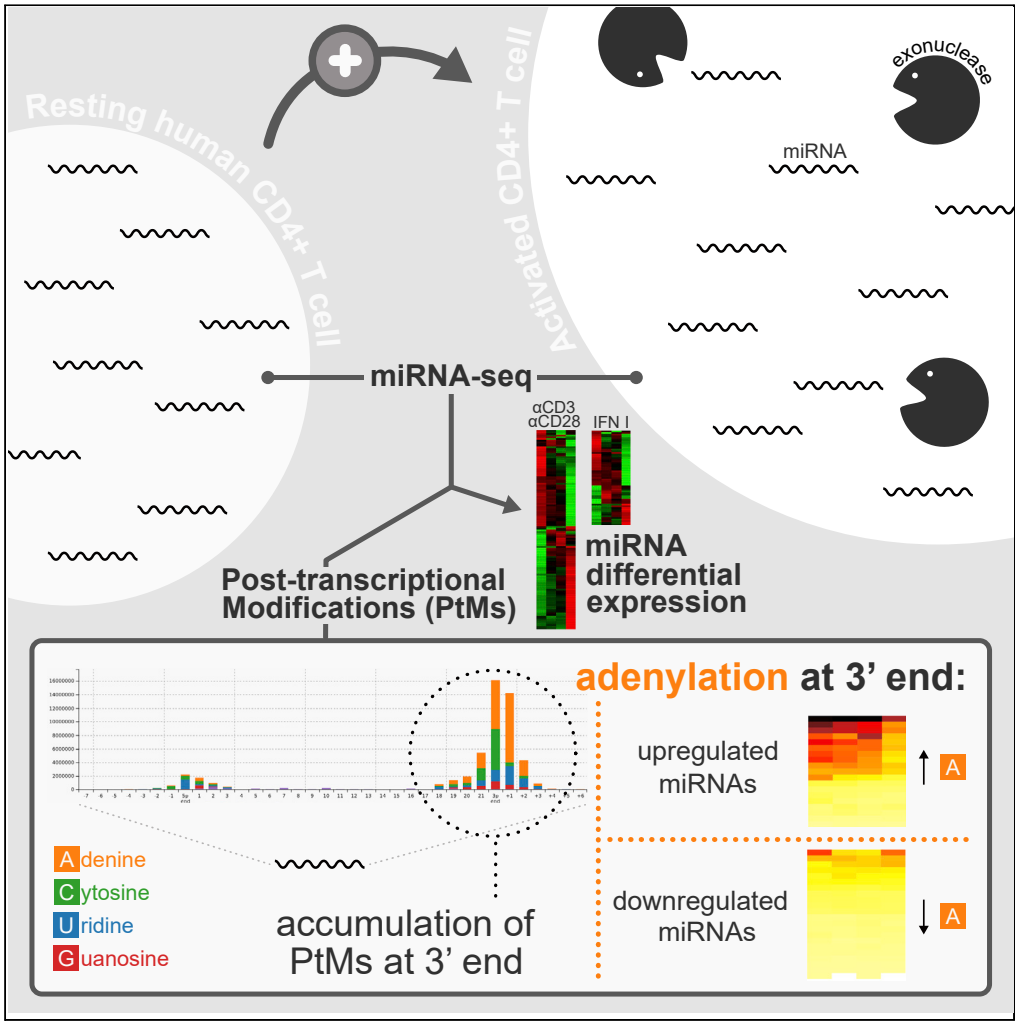

Ana Rodríguez-Galán, Sara G. Dosil, Manuel José Gómez, Irene Fernández-Delgado, Lola Fernández-Messina, Fátima Sánchez-Cabo, Francisco Sánchez-Madrid

fsmadrid@salud.madrid.org

Highlights

TCR and IFN I activation lead to miRNA differential expression in human CD4 T cells.

Upregulated miRNAs count with a stronger 3′ adenylation compared to those downregulated.

Cytosylation is a significant post-transcriptional modification in human T cells.

T cell activation triggers the expression of RNA degrading enzymes.

Rodríguez-Galán et al., iScience 24, 102530 June 25, 2021
https://doi.org/10.1016/j.isci.2021.102530

iScience

CellPress
OPEN ACCESS

Article

MiRNA post-transcriptional modification dynamics in T cell activation

Ana Rodríguez-Galán,[1,2] Sara G. Dosil,[1,2] Manuel José Gómez,[2] Irene Fernández-Delgado,[1,2] Lola Fernández-Messina,[1,2,3] Fátima Sánchez-Cabo,[2] and Francisco Sánchez-Madrid[1,2,3,4,*]

SUMMARY

T cell activation leads to extensive changes in the miRNA repertoire. Although overall miRNA expression decreases within a few hours of T cell activation, some individual miRNAs are specifically upregulated. Using next-generation sequencing, we assessed miRNA expression and post-transcriptional modification kinetics in human primary CD4+ T cells upon T cell receptor (TCR) or type I interferon stimulation. This analysis identified differential expression of multiple miRNAs not previously linked to T cell activation. Remarkably, upregulated miRNAs showed a higher frequency of 3′ adenylation. TCR stimulation was followed by increased expression of RNA modifying enzymes and the RNA degrading enzymes Dis3L2 and Eri1. In the midst of this adverse environment, 3′ adenylation may serve a protective function that could be exploited to improve miRNA stability for T cell-targeted therapy.

INTRODUCTION

MiRNAs are key modulators that fine-tune immune responses (Gracias and Katsikis, 2011; Lindsay, 2008; Mehta and Baltimore, 2016; Podshivalova and Salomon, 2013). During T cell activation, miRNA profile undergoes extensive changes, with a global downregulation of total miRNA levels occurring as early as 4 hr after activation (Bronevetsky et al., 2013). Beyond the overall picture of general reduction, some individual miRNAs stand out for their specific up- or downregulation, as shown by arrays, RT-qPCR and Northern Blot (Bronevetsky et al., 2013; Grigoryev et al., 2011; Gutiérrez-Vázquez et al., 2017; Jindra et al., 2010; Sousa et al., 2017; Teteloshvili et al., 2015; Wu et al., 2007). These studies, which evaluate mouse samples from 18 hr to 7 d and human samples from 2 to 7 d after activation, have been gathered together in a recent review (Rodríguez-Galán et al., 2018).

Little is known regarding the mechanisms that underlie these changes in the T cell miRNA landscape. Previous research from our laboratory pointed to 3′ uridine addition as a potential mechanism guiding miRNA turnover during T cell activation (Gutiérrez-Vázquez et al., 2017). Uridylation is a relatively common post-transcriptional miRNA modification. Next-generation sequencing (NGS) has identified not only nucleotide additions to the expected genomic miRNA sequences but also trimmings and substitutions (Ebhardt et al., 2009; Lee et al., 2010). Post-transcriptional modifications (PtMs) generate multiple variants of the same miRNA (isomiRs) that differ in their 5′, 3′ or internal modifications. PtMs modulate biogenesis, stability, and function (Gebert and MacRae, 2019; Neilsen et al., 2012; de Sousa et al., 2019). Several mechanisms elicit PtMs on the canonical miRNA sequence including: alternative processing by Drosha or Dicer, RNA editing and non-template nucleotide addition.

During miRNA biogenesis, Drosha cleaves the primary-miRNA transcript, generating a hairpin precursor-miRNA which is subsequently processed by Dicer, leading to the generation of a double-stranded miRNA duplex. Drosha and Dicer excisions are slightly flexible, thereby becoming a source of 5′ and 3′ isomiRs (Gu et al., 2012; Kim et al., 2017; Kwon et al., 2019; Starega-Roslan et al., 2011; Wu et al., 2009; Zhou et al., 2012; Zhu et al., 2018).

Other forms of PtMs derive from RNA editing which include conversion of adenosine (A) to inosine (I) by ADARs (adenosine deaminases acting on RNA) (Bazak et al., 2014; Nishikura, 2016; Tan et al., 2017; Yang et al., 2006); or deamination of cytidine (C) to uridine (U) by APOBECs (apolipoprotein B mRNA editing enzyme, catalytic polypeptide-like) (Blanc and Davidson, 2010; Rosenberg et al., 2011). Since I is

[1]Servicio de Inmunología. Hospital Universitario La Princesa, Instituto Investigación Sanitaria Princesa (IIS-IP), Universidad Autónoma de Madrid (UAM), 28006 Madrid, Spain

[2]Vascular Pathophysiology Area. Centro Nacional de Investigaciones Cardiovasculares (CNIC), 28029 Madrid, Spain

[3]CIBER de Enfermedades Cardiovasculares. Instituto de Salud Carlos III, 28029 Madrid, Spain

[4]Lead contact

*Correspondence: fsmadrid@salud.madrid.org

https://doi.org/10.1016/j.isci.2021.102530

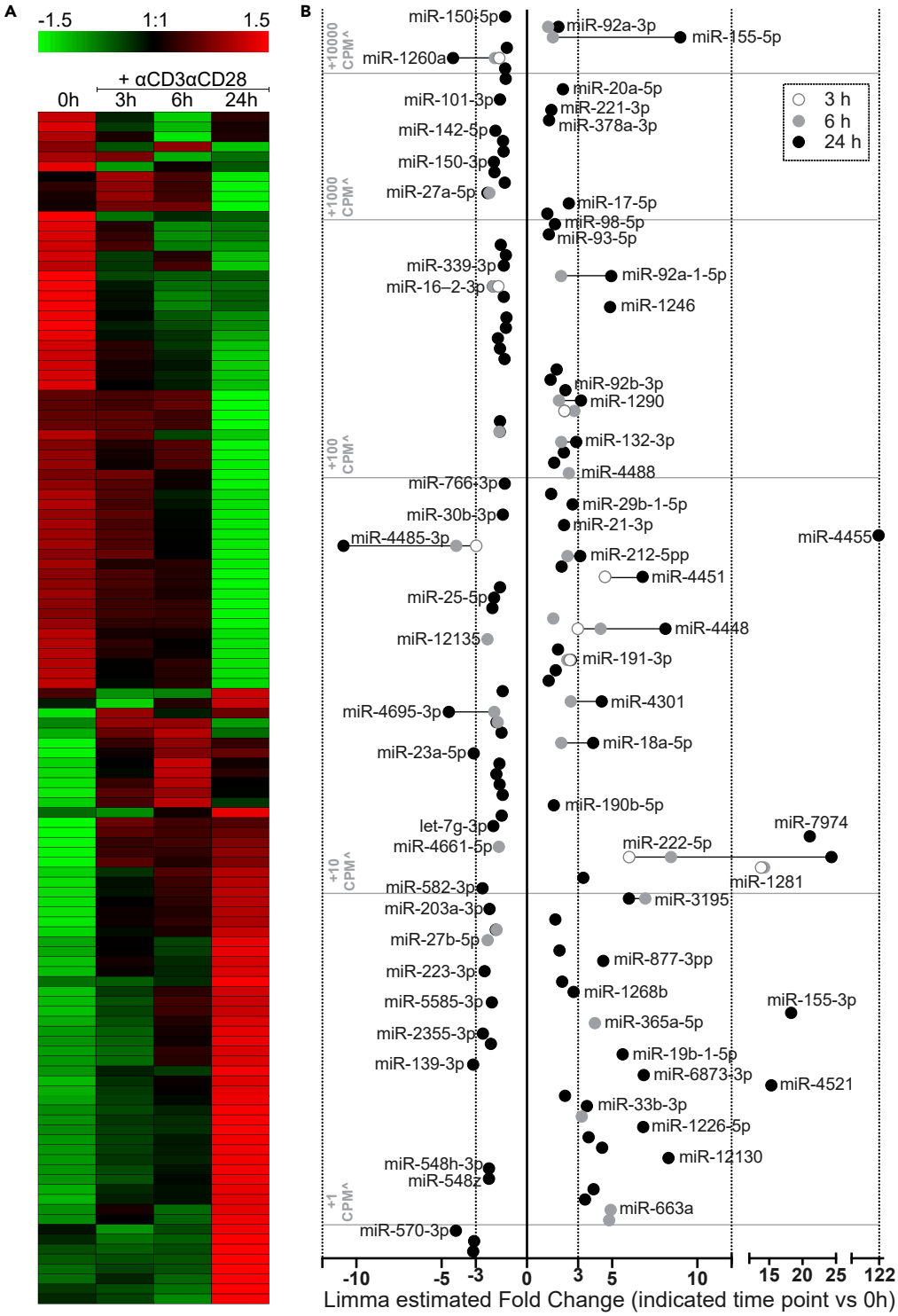

Figure 1. Differential miRNA expression 3h, 6h, and 24h after αCD3αCD28 stimulation of human primary resting CD4+ T cells

(A) The heatmap represents relative expression values for a non-redundant collection of differentially expressed miRNAs (adjusted p value <0.1), detected after stimulation with αCD3αCD28 for 3h, 6h, and 24hr.

Figure 1. *Continued*
(B) Limma estimated Fold Change of differentially expressed miRNAs at 3h, 6h, and 24hr compared to 0h. Representative miRNAs names are included, particularly those with higher fold changes. MiRNAs detected with higher CPM occupy top positions in Y axis (CPM^ = total sum of CPM detected at reference and represented time points; threshold bars indicate values at the bottom of each section). Table S1 contains 1B) raw data.

a guanosine (G) analog, A-to-I editing is equivalent to an A-to-G mutation. For miRNAs, A-to-I editing is well characterized (Li et al., 2018; Wang and Liang, 2018), whereas the physiological relevance of C-to-U modification is currently unknown.

Additional enzymes responsible for miRNA PtMs are terminal nucleotidyl transferases (TENTs). TENTs catalyze non-template additions of nucleotides mainly at the 3′ end (“tailing”) (Warkocki et al., 2018). TENTs are often flexible substrate-wise, but those with a preference toward adding adenosine are known as non-canonical poly(A) polymerases. Other TENTs promote the addition of uridine preferentially namely terminal uridyl transferases (TUTases). Uridylation and adenylation are the most typical 3′ end modifications across animal miRNAs (Burroughs et al., 2010; Chiang et al., 2010; Landgraf et al., 2007; Muller et al., 2014; Wyman et al., 2011). Multiple studies have explored these modifications and their consequences in detail. Conclusions often appear contradictory, likely due to the specific biological context, including different species, cell type or cellular compartment. For instance, GLD-2 (PAPD4/TENT2) 3′ monoadenylation seems to stabilize specific miRNA populations in human fibroblasts (D’Ambrogio et al., 2012) and miR-122 in the liver (Katoh et al., 2009). In mouse early embryos, 3′ mono- and oligoadenylation appears to protect certain miRNAs in a context of large degradation (Yang et al., 2016). However, PAPD5 (TENT4B/GLD4/TUT3) adenylates miR-21-5p on 3′, promoting its degradation by poly(A)-specific ribonucleases (Boele et al., 2014). In human monocytes, knocking down PAPD4 showed no overall effect of 3′ adenylation on miRNA stability, but adenylation instead altered miRNA effectiveness through reduction of their incorporation into the RNA-induced silencing complex (RISC, the complex where miRNAs induce mRNA degradation or inhibit their translation) (Burroughs et al., 2010). Uridylation also promotes diverse outcomes on miRNAs. Pre-let-7 miRNA can be uridylated at its 3′ end by TUT4 (ZCCHC11) or TUT7 (ZCCHC6) (Heo et al., 2009; Thornton et al., 2012). Lin28 (an RNA-binding protein) binds to pre-let-7 and favors oligouridylation (10-20 uridines), which inhibits subsequent Dicer processing and serves as a signal for Dis3L2 miRNA degradation (Chang et al., 2013; Heo et al., 2008, 2009; Thornton et al., 2012; Ustianenko et al., 2013). In the absence of Lin28, pre-let-7 undergoes monouridylation to pursue its maturation process (Heo et al., 2012). Let-7 promotes cell differentiation, and the regulatory mechanism triggered by Lin28 expression maintains pluripotency in stem cells (Büssing et al., 2008; Heo et al., 2009). Non-templated uridine addition also occurs on mature miRNAs, such as miR-26, which has been described to undergo 3′-uridylation by ZCCHC11 (terminal uridylyl transferase 4, TUT4) (Jones et al., 2009). MiR-26a and miR-26b uridylation has been shown to reduce their ability to repress IL-6 (Jones et al., 2009). In addition to Dis3L2, Eri1 is also a 3′ to 5′ exonuclease that exhibits a preference for uridylated RNA substrates (Hoefig et al., 2013).

In order to gain a mechanistic insight in the early changes occurring at the level of miRNA PtMs, we have studied the effect of stimulation of human primary CD4 T cells on miRNAs through NGS.

RESULTS

MiRNA modulation by αCD3αCD28

A total of 120 miRNAs were found to be differentially expressed (adjusted p value < 0.1, 62 upregulated and 58 downregulated) upon stimulation of resting human CD4 T cells with αCD3αCD28 for 3, 6 and 24 hr by NGS analysis [Figures 1A and 1B; Table S1]. Since large changes in total miRNA levels occur very early (Bronevetsky et al., 2013), 3 and 6 hr were chosen as intermediate points for our time course. MiRNAs from 5p and 3p arms were equally identified as differentially expressed with a total of 51% miR-5p and 49% miR-3p (those miRNAs without 5p or 3p included in the nomenclature were classified according to their localization of the mature sequence in miRbase). The most upregulated miRNAs (fold change indicated in brackets) at 24 hr were miR-4455 (122 x), miR-222-5p (24 x), miR-7974 (21 x), miR-155-3p (18 x), and miR-4521 (15 x) [Figure 1B]. Remarkably, miR-1281 showed a 14-fold change upregulation at 3 hr which was maintained at 6 hr but vanished at 24 hr. The most downregulated miRNAs at 24hr were miR-4485-3p (−11 x), miR-4695-3p (-5 x), miR-570-3p (-4 x), and miR-1260a (-4 x). Consistent with previous evidence, we also found downregulation of miR-150-5p, and miR-223-3p; while miR-155-5p, miR-17-5p, and miR-18a-5p

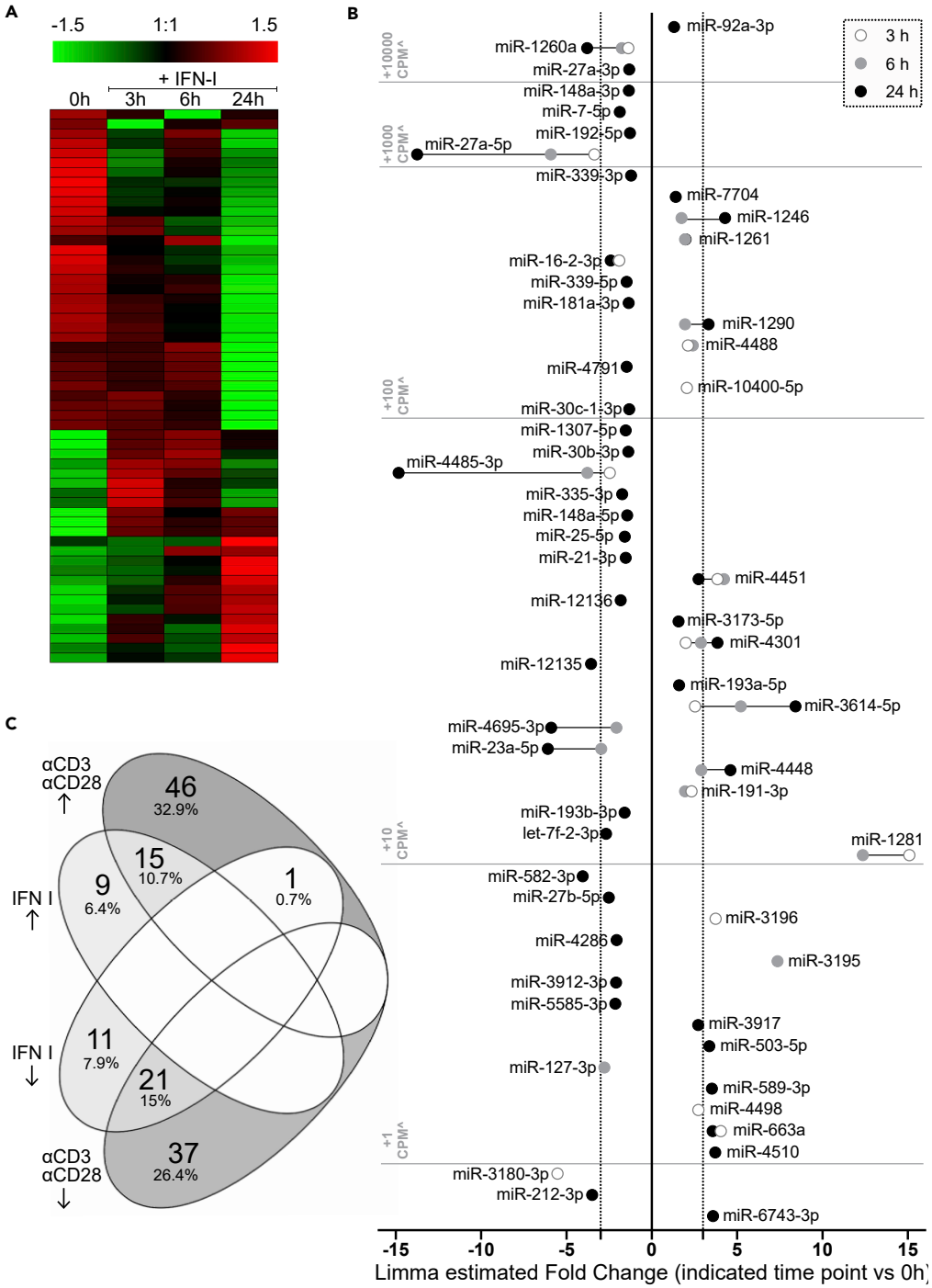

Figure 2. Differential miRNA expression 3h, 6h, and 24h after IFN I stimulation of human primary resting CD4+ T cells

(A) The heatmap represents relative expression values for a non-redundant collection of differentially expressed miRNAs (adjusted p value <0.1), detected after stimulation with IFN I for 3h, 6h, and 24hr.

(B) Limma estimated Fold Change of differentially expressed miRNA at 3h, 6h, and 24hr compared to 0h. MiRNAs detected with higher CPM occupy top positions in Y axis (CPM^ = total sum of CPM detected at reference and represented time points; threshold bars indicate values at the bottom of each section).

(C) Venn diagram with miRNAs differentially up- and downregulated by IFN I and αCD3αCD28. Table S2 contains 2B) raw data.

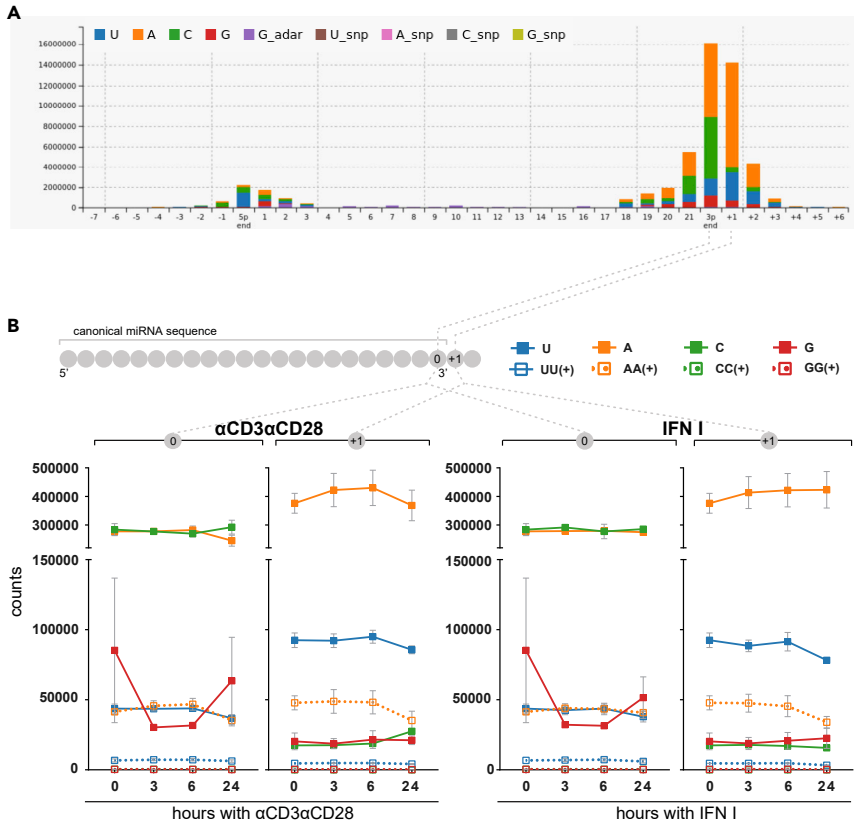

Figure 3. Post-transcriptional miRNA modifications: a global view

(A) Global post-transcriptional modifications (PtMs) profile for all 21 sequenced samples generated by Chimira.

(B) Kinetics of most abundant PtMs (mono-additions: U, A, C, G; and oligo-additions: ≥UU, ≥AA, ≥CC, ≥GG) at positions "3p-end" (0) and "3p-end + 1" (+1), in the population of 626 expressed miRNA species in unstimulated conditions and during activation with αCD3αCD28 (left) or IFN I (right). Mono-additions (solid squares) refer to the specific nucleotide on their own or followed by a different nucleotide, but not followed by the same nucleotide. Oligo-additions (empty squares) include PtMs with two or more equal nucleotides.

were upregulated (Rodríguez-Galán et al., 2018). We confirmed miR-1246 and miR-222-5p upregulation and miR-23a-5p and miR-27a-5p downregulation by qPCR [Figures S1A–S1D]. Ingenuity pathway analysis (IPA) indicated that differentially expressed miRNAs were mainly involved in processes related to cell development, growth, proliferation, and movement [Figure S2A]. Networks of predicted targets for the miRNAs with the highest up- and downregulation show a large overlapping, with 59 genes targeted by at least 2 of the 6 most upregulated miRNAs and 149, targeted by at least 2 of the 6 most downregulated [Figure S3A].

MiRNA modulation by IFN I

In a separate set, resting human CD4+ T cells were stimulated with type I interferon (IFN I). IFN I significantly altered the expression levels of 57 miRNAs (adjusted p value < 0.1): 24 miRNAs were upregulated, and 33 were downregulated [Figures 2A and 2B; Table S2]. Similar to αCD3αCD28 stimulation, 5p and 3p miRNAs were equivalently found as differentially expressed with a total of 49% miR-5p and 51% miR-3p. Compared with the data in Figure 1, we found that 37 miRNAs were common to the IFN I and αCD3αCD28 subsets (15 upregulated and 21 downregulated in both stimulations and 1 miRNA regulated in opposite directions) [Figure 2C]. The most upregulated miRNAs (fold change indicated in brackets) at 24 hr were miR-1281 (15 x, 3h), miR-3195 (7 x, 6h) and miR-3614-5p (8 x, 24hr). The most downregulated miRNAs at 24hr were miR-27a-5p (−14 x) and miR-4485-3p (−15 x) [Figures 2A and 2B]. miR-1246 upregulation and miR-23a-5p and miR-27a-5p downregulation were confirmed by qPCR [Figures S1A–S1D]. IPA revealed that most processes controlled by IFN I-regulated miRNAs were very similar to those observed for cells stimulated

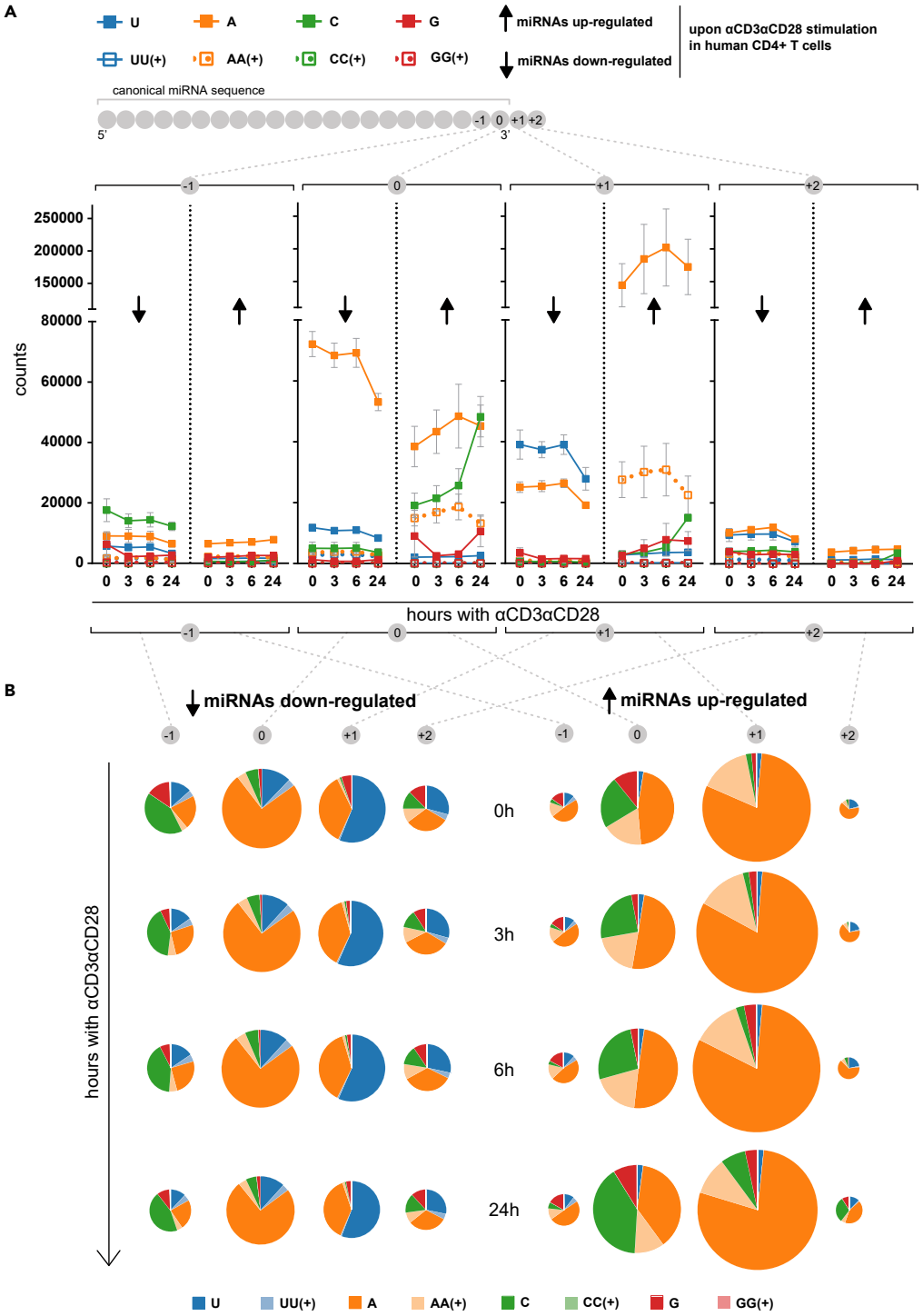

Figure 4. Kinetics of miRNA post-transcriptional modifications for αCD3αCD28 differentially expressed miRNAs

Kinetics of the most abundant PtMs (mono-additions: U, A, C, G; and oligo-additions: ≥UU, ≥AA, ≥CC, ≥GG) at positions "3p-end -1" (−1), "3p-end" (0), "3p-end + 1" (+1), and "3p-end + 2" (+2); for upregulated miRNAs (left) and downregulated miRNAs (right) with an adjusted p value <0.1. Mean and SEM (from three independent experiments) were plotted for each modification counts at specific positions across time points (A) and as pie charts whose area is proportional to the total number of counts for the specific position at indicated time points (B).

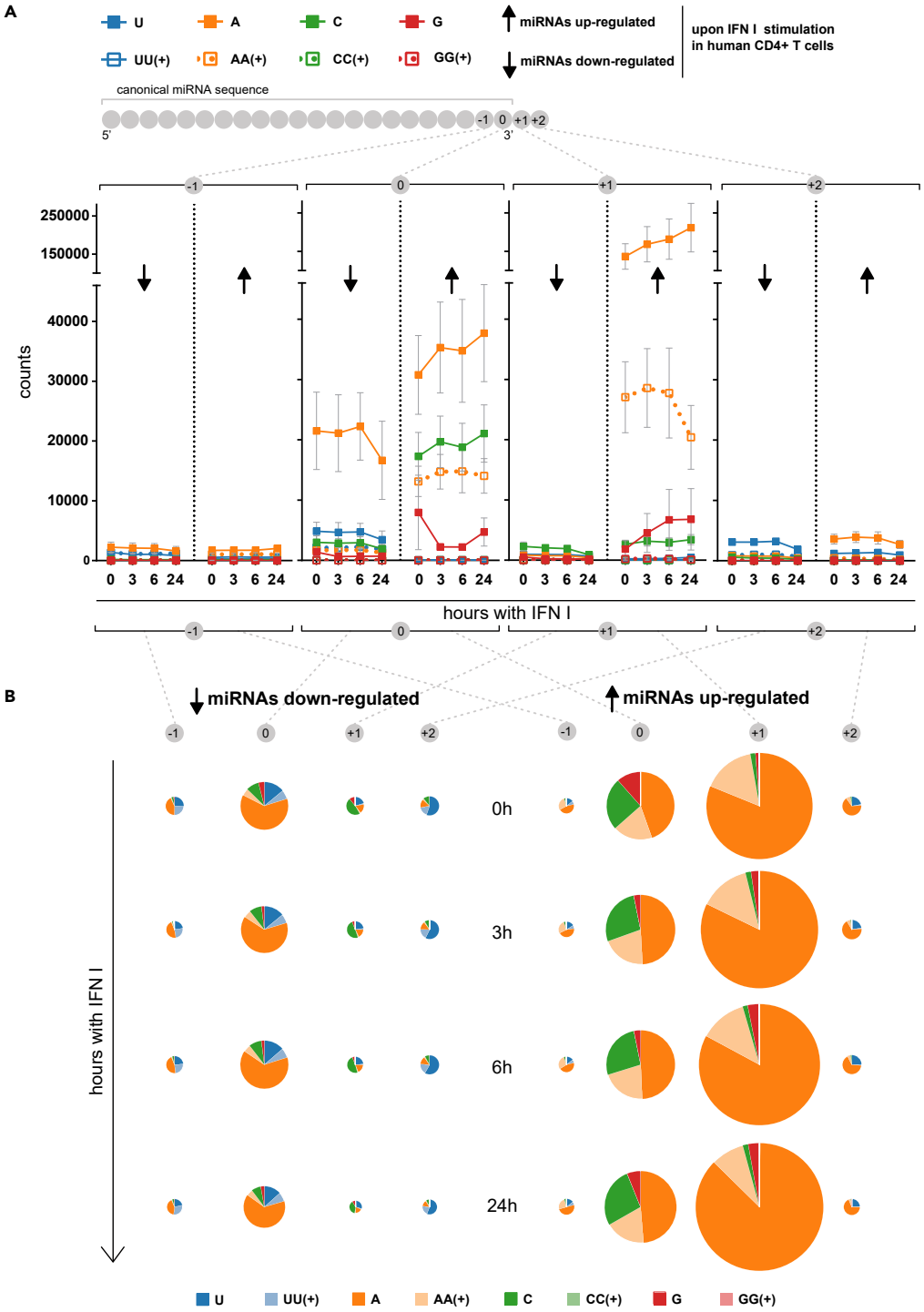

Figure 5. Kinetics of miRNA post-transcriptional modifications for IFN I differentially expressed miRNAs

Kinetics of most abundant PtMs (mono-additions: U, A, C, G; and oligo-additions: ≥UU, ≥AA, ≥CC, ≥GG) at positions "3p-end" (0) and "3p-end + 1" (1) and "3p-end + 2" (2), for upregulated miRNAs (left) and downregulated miRNAs (right) with an adjusted p value <0.1. Mean and SEM (from three independent experiments) were plotted for each modification counts at specific positions across time points (A) and as pie charts whose area is proportional to the total number of counts for the specific position at indicated time points (B).

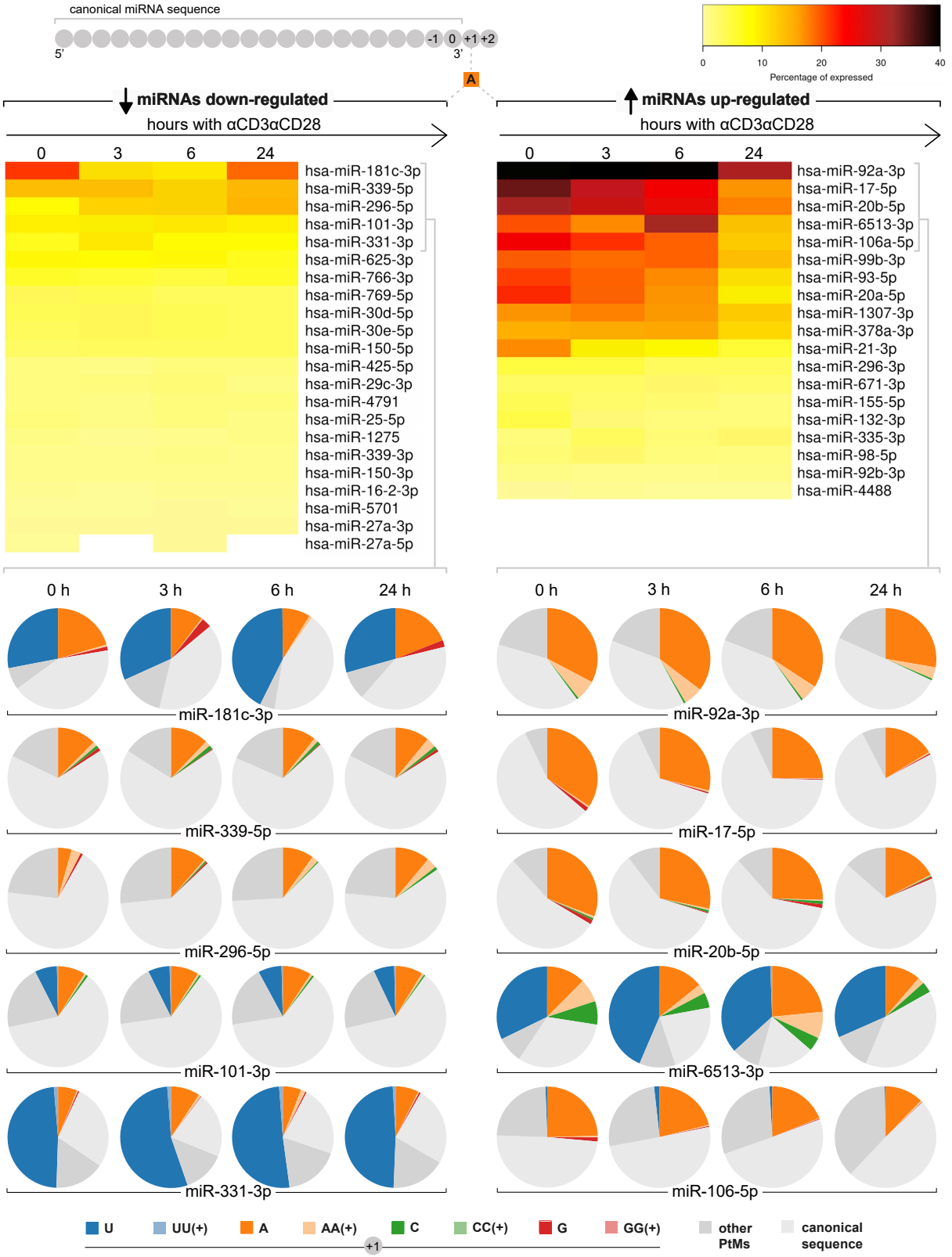
canonical miRNA sequence
5'
-1
0
+1
+2
3'
A
0
10
20
30
40
Percentage of expressed
miRNAs down-regulated
hours with αCD3αCD28
0
3
6
24
hsa-miR-181c-3p
hsa-miR-339-5p
hsa-miR-296-5p
hsa-miR-101-3p
hsa-miR-331-3p
hsa-miR-625-3p
hsa-miR-766-3p
hsa-miR-769-5p
hsa-miR-30d-5p
hsa-miR-30e-5p
hsa-miR-150-5p
hsa-miR-425-5p
hsa-miR-29c-3p
hsa-miR-4791
hsa-miR-25-5p
hsa-miR-1275
hsa-miR-339-3p
hsa-miR-150-3p
hsa-miR-16-2-3p
hsa-miR-5701
hsa-miR-27a-3p
hsa-miR-27a-5p
miRNAs up-regulated
hours with αCD3αCD28
0
3
6
24
hsa-miR-92a-3p
hsa-miR-17-5p
hsa-miR-20b-5p
hsa-miR-6513-3p
hsa-miR-106a-5p
hsa-miR-99b-3p
hsa-miR-93-5p
hsa-miR-20a-5p
hsa-miR-1307-3p
hsa-miR-378a-3p
hsa-miR-21-3p
hsa-miR-296-3p
hsa-miR-671-3p
hsa-miR-155-5p
hsa-miR-132-3p
hsa-miR-335-3p
hsa-miR-98-5p
hsa-miR-92b-3p
hsa-miR-4488
0 h
3 h
6 h
24 h
miR-181c-3p
miR-339-5p
miR-296-5p
miR-101-3p
miR-331-3p
miR-92a-3p
miR-17-5p
miR-20b-5p
miR-6513-3p
miR-106-5p
U
UU(+)
A
AA(+)
C
CC(+)
G
GG(+)
other PtMs
canonical sequence
+1

Figure 6. MiRNAs with significant adenylation at position 1 (αCD3αCD28)

Heatmaps include upregulated (right) and downregulated (left) miRNAs with significant adenylation at position 1, detected in αCD3αCD28 stimulation. Reads with adenine at position 1 are normalized to total reads, in order to visualize the frequency of adenylation for each miRNA. Pie charts are included below for the 5 miRNAs most adenylated within each group. These graphs show in color the percentage of reads with specific modifications at position 1, while reads with modifications at other positions and unmodified reads are depicted in gray.

through αCD3αCD28, mainly: cell development, movement, growth, and proliferation [Figure S2B]. Predicted targets show a more intense network overlapping among the 6 most downregulated miRNAs with 189 targets common to at least 2 miRNAs; while 52 genes would be targeted by at least 2 of the 6 most upregulated [Figure S3B].

Post-transcriptional modifications

A global assessment of PtMs indicated that miRNAs in our samples underwent extensive 3′-end modifications compared to their canonical sequences [Figure 3A]. Unexpectedly, C addition was highly represented in our samples at the most modified position: 0 or "3p end nucleotide". A and C modifications were similarly represented in this position, much more frequently than U and G [Figure 3A]. Modifications at 5′ end and ADAR editing (A to G) were detected on a very limited basis. According to the global profile, positions 0 (3p end) and +1 (3p end +1), were by far the most heavily modified, followed by positions −1 and +2 [Figure 3A]. For this reason, nucleotide modifications at the 3′ end were analyzed in greater detail in an attempt to discover specific sequences that could guide miRNA dynamics in T cells. PtMs patterns found in the 3′ end (positions −4 to 4) were evaluated (data not shown), indicating that the most common modifications across the different samples were: C, A, U, and G mono-additions, and A and U oligo-additions. "AU" was the most frequent multi-nucleotide modification, although sequences combining more than one nucleotide were clearly underrepresented. We also detected UAGU modifications at position −4, as well as AGU and AGUU at −3. We evaluated the presence of U, A, C, G and of UU+, AA+, CC+, GG+ (homopolymers of two or more equal nucleotides) at highly modified 3′-end positions. The results were conjoined for the different stimulation time points [Figure 3B]. Analyzed PtMs remained stable during activation and were clearly associated to a specific 3′ end position [Figure 3B].

To assess whether PtMs could be guiding the differential miRNA expression described in Figures 1 and 2, modifications at positions −1, 0, +1 and +2, were represented considering only data from miRNAs upregulated or downregulated, either upon αCD3αCD28 stimulation [Figures 4A and 4B] or IFN I [Figures 5A and 5B]. Upregulated miRNAs were more extensively modified, with the potential distinctive signature of high levels of A addition at +1 and C addition at 0 [Figures 4A, 4B, 5A, and 5B]. αCD3αCD28 downregulated miRNAs show reduced levels of these specific modifications and a marked presence of U additions, mostly at +1 [Figures 4A and 4B]. Adenine additions at position +1 were much higher in upregulated miRNAs with counts of A mono-additions around 140000-210000, while downregulated miRNAs counts did not go beyond 30,000 in αCD3αCD28 stimulation [Figure 4A] or 2000 in IFN I [Figure 5A]. Additions of two or more adenines were also a specific signature of upregulated miRNAs at 0 and +1 [Figures 4A and 5A].

To gain a better understanding of the most abundant modifications in upregulated miRNAs, we identified the individual miRNAs exhibiting higher adenylation at position 1 and cytosylation at position 0 [Figures 6, 7, S4, and S5]. A higher number of modified miRNAs were found after αCD3αCD28 stimulation [Figures 6 and 7], than in IFN I [Figures S4 and S5]. A group of miRNAs was found to be significantly cytosylated [Figures 7 and S5]. Nevertheless, miR-3195 on its own seems to account for the differential accumulation of cytosylation in upregulated miRNAs. Remarkably, a higher frequency of adenylation was found in upregulated miRNAs [Figures 6 and S4]. MiR-92a-3p, the upregulated miRNA with higher expression both in αCD3αCD28 [Figure 1] and IFN I [Figure 2] stimulations, counts with 31-42% of reads with an adenine at position 1 in all evaluated time points. In αCD3αCD28 stimulation, we have identified a group of upregulated miRNAs which present a higher frequency of adenylation [Figure 6].

Dis3l2, Eri1, TUT4, and TUT7 regulation upon T cell activation

Next, we evaluated the expression kinetics of four proteins related to RNA metabolism: TUT4 and TUT7 (terminal uridylyl transferases), and Dis3L2 and Eri1 time lengths (exonucleases that preferentially degrade uridylated RNA (Chang et al., 2013; Hoefig et al., 2013; Ustianenko et al., 2013)). For these experiments, we stimulated human CD4+ T cells from eight human healthy donors with αCD3αCD28 during various times up to 48 hr. A significant average upregulation was found after activation for all evaluated enzymes [Figures

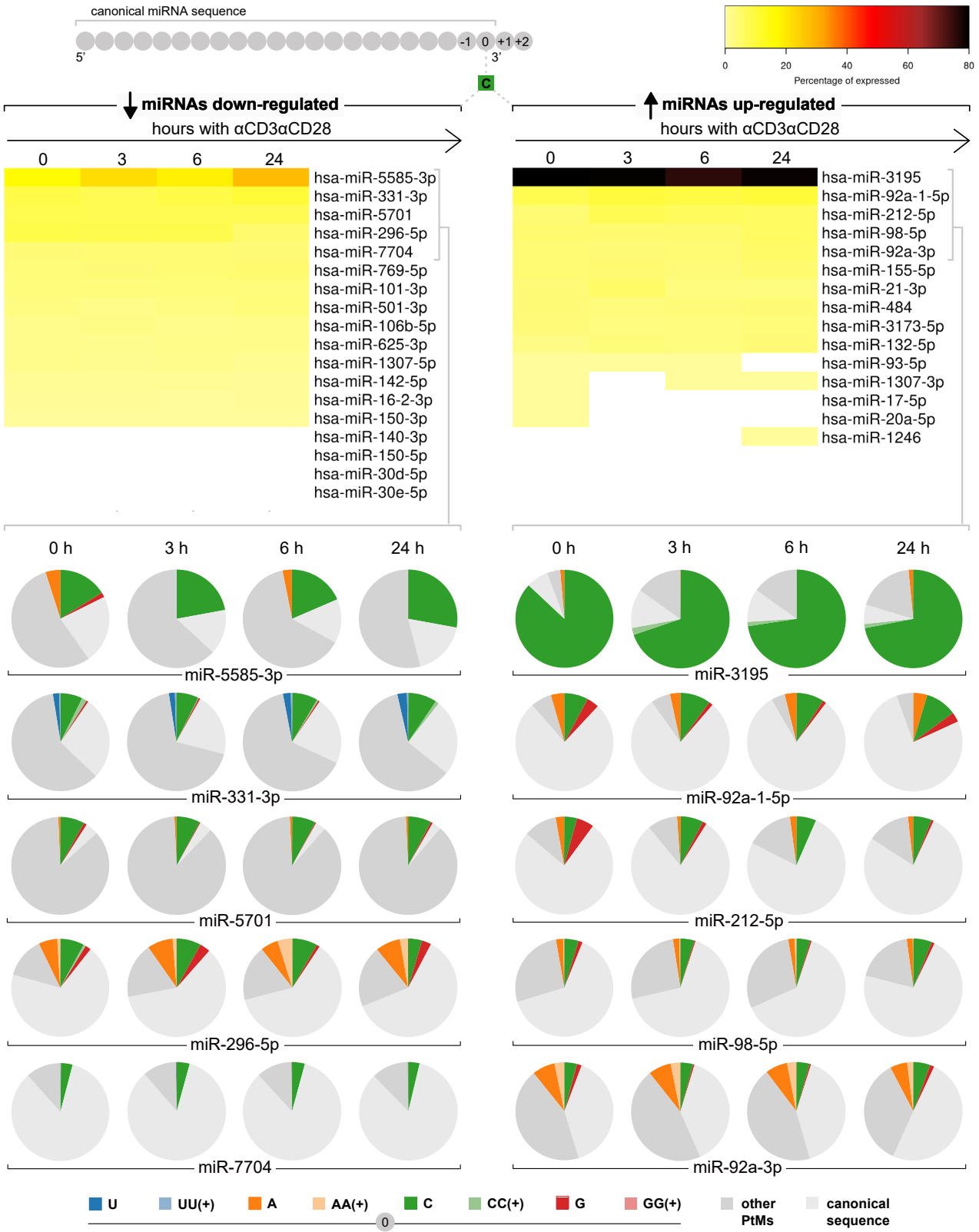
canonical miRNA sequence
5'
-1 0 +1 +2
3'
C
0 20 40 60 80
Percentage of expressed
miRNAs down-regulated
hours with αCD3αCD28
0 3 6 24
hsa-miR-5585-3p
hsa-miR-331-3p
hsa-miR-5701
hsa-miR-296-5p
hsa-miR-7704
hsa-miR-769-5p
hsa-miR-101-3p
hsa-miR-501-3p
hsa-miR-106b-5p
hsa-miR-625-3p
hsa-miR-1307-5p
hsa-miR-142-5p
hsa-miR-16-2-3p
hsa-miR-150-3p
hsa-miR-140-3p
hsa-miR-150-5p
hsa-miR-30d-5p
hsa-miR-30e-5p
miRNAs up-regulated
hours with αCD3αCD28
0 3 6 24
hsa-miR-3195
hsa-miR-92a-1-5p
hsa-miR-212-5p
hsa-miR-98-5p
hsa-miR-92a-3p
hsa-miR-155-5p
hsa-miR-21-3p
hsa-miR-484
hsa-miR-3173-5p
hsa-miR-132-5p
hsa-miR-93-5p
hsa-miR-1307-3p
hsa-miR-17-5p
hsa-miR-20a-5p
hsa-miR-1246
0 h 3 h 6 h 24 h
miR-5585-3p
miR-3195
miR-331-3p
miR-92a-1-5p
miR-5701
miR-212-5p
miR-296-5p
miR-98-5p
miR-7704
miR-92a-3p
U
UU(+)
A
AA(+)
C
CC(+)
G
GG(+)
other PtMs
canonical sequence
0

Figure 7. MiRNAs with significant cytosylation at position 0 (αCD3αCD28)

Heatmaps include upregulated (right) and downregulated (left) miRNAs with significant cytosylation at position 0, detected in αCD3αCD28 stimulation. Reads with cytosine at position 1 are normalized to total reads, in order to visualize the frequency of cytosylation for each miRNA. Pie charts are included below for the 5 miRNAs most adenylated within each group. These graphs show in color the percentage of reads with specific modifications at position 0, while reads with modifications at other positions and unmodified reads are depicted in gray.

8A–8D]. Early upregulation of Eri1 and Dis3L2 could be driving global miRNA downregulation upon T cell activation. The overexpression of TUT4 and TUT7 could be indicating a higher uridylation activity, which could mark miRNA for degradation by Eri1 and Dis3l2.

DISCUSSION

This study aimed to reveal the landscape of PtMs that could control miRNA levels during CD4 T cell activation by antigen T cell receptor and co-receptor (with αCD3αCD28) and by IFN I. We used NGS, since this technique allows the detection of isomiRs variants, offering also for the first time an unbiased exploration of miRNA differential expression at early time points of T cell activation.

Notably, many miRNAs not previously linked with T cell stimulation were significantly down- or upregulated in response to αCD3αCD28. Our repertoire is also consistent with certain miRNAs (e.g. 150-5p, 223-3p, miR-155-5p, miR-17-5p, miR-18a-5p, and miR-4521) previously related with T cell activation in studies performed with arrays, RT-qPCR and Northern Blot (Rodríguez-Galán et al., 2018; Diener et al., 2020), which strengthen our miRNA-seq data. Additionally, we have confirmed our sequencing data through qPCR, including miR-1246 and miR-222-5p ($p = 0.08$) upregulation, and miR-23a-5p and miR-27a-5p downregulation. MiR-1246, miR-23a-5p and miR-27a-5p differential expression was also validated in IFN I stimulation. To our knowledge, no other study has evaluated miRNA changes in human primary T cells stimulated with type I IFN. A recent report reviewed data available on IFN I regulated microRNAs, mainly in the liver cell line Huh7 and human glioma (Forster et al., 2015). Of the 36 miRNAs identified, 7 were described in two or more studies, indicating certain overlapping but also a great diversity across cell types regarding their response to IFN I (Forster et al., 2015). In fact, only one of these 36 miRNAs (miR-212) has been found as differentially expressed in our samples. Two prior studies had assessed immune cells: PBMCs and NK cells. MiRNAs involved in the anti-viral response against Hepatitis C virus (miR-1, miR-30, miR-128, miR-196, and miR-296) were induced in peripheral blood mononuclear cells (PBMCs) upon IFN-α treatment (Scagnolari et al., 2010). In human NK Cells, miRNA-30e and miRNA-378 were downregulated by IFN I (Wang et al., 2012). Our study provides a dataset of IFN I regulated miRNAs in human primary CD4 T cells, which comprises 24 miRNAs that are upregulated and 33 that are downregulated. Of the 57 genes modulated by IFN-I, 37 are also regulated by αCD3αCD28 stimulation.

IPA assessment of IFN-I and αCD3αCD28 regulated miRNAs indicates their involvement in cellular development, growth, proliferation and movement. These processes are indeed essential for activated T cells to perform their function, which includes their differentiation to effector and/or memory phenotypes to combat infection short- and long-term, respectively. In this regard, activated T cells undergo intense cellular reprogramming with an increase in mRNA and protein expression. Accordingly, activated T cells would need to control inhibitory safeguards that prevent abnormal activation that could produce autoimmunity. MiRNA regulation may act as a negative regulator of gene expression, which would need to be withdrawn, at least partially. Several studies support this hypothesis. For instance, mRNAs undergo 3′ UTR shortening upon T lymphocyte activation, thereby reducing the pool of potential target sites for miRNA binding (Sandberg et al., 2008). Moreover, T cell activation promotes a rapid global miRNA downregulation and degradation of Argonaute proteins, which are key effectors of the RISC complex (Bronevetsky et al., 2013). We hypothesize that an active mechanism of miRNA degradation underlies the intense miRNA downregulation observed only a few hours after T cell activation. For this reason, we evaluated the expression of Eri1 and Dis3L2. Both exoribonucleases display a clear preference for uridylated RNA substrates (Chang et al., 2013; Hoefig et al., 2013; Ustianenko et al., 2013); also, Eri1-deficient NK cells and T cells showed increased overall miRNAs levels (Thomas et al., 2012). Here we detected a marked upregulation of both enzymes following T cell activation, pointing toward a context of likely RNA degradation. Enzymes such as, TUT4 and TUT7, which are specifically regulated by αCD3αCD28 stimulation, could be uridylating substrates and labeling them for subsequent degradation by Eri1 or Dis3l2. Interestingly, TUT4 upregulation was not maintained in our samples after 24 hr indicating a potential specific time frame of action for this enzyme.

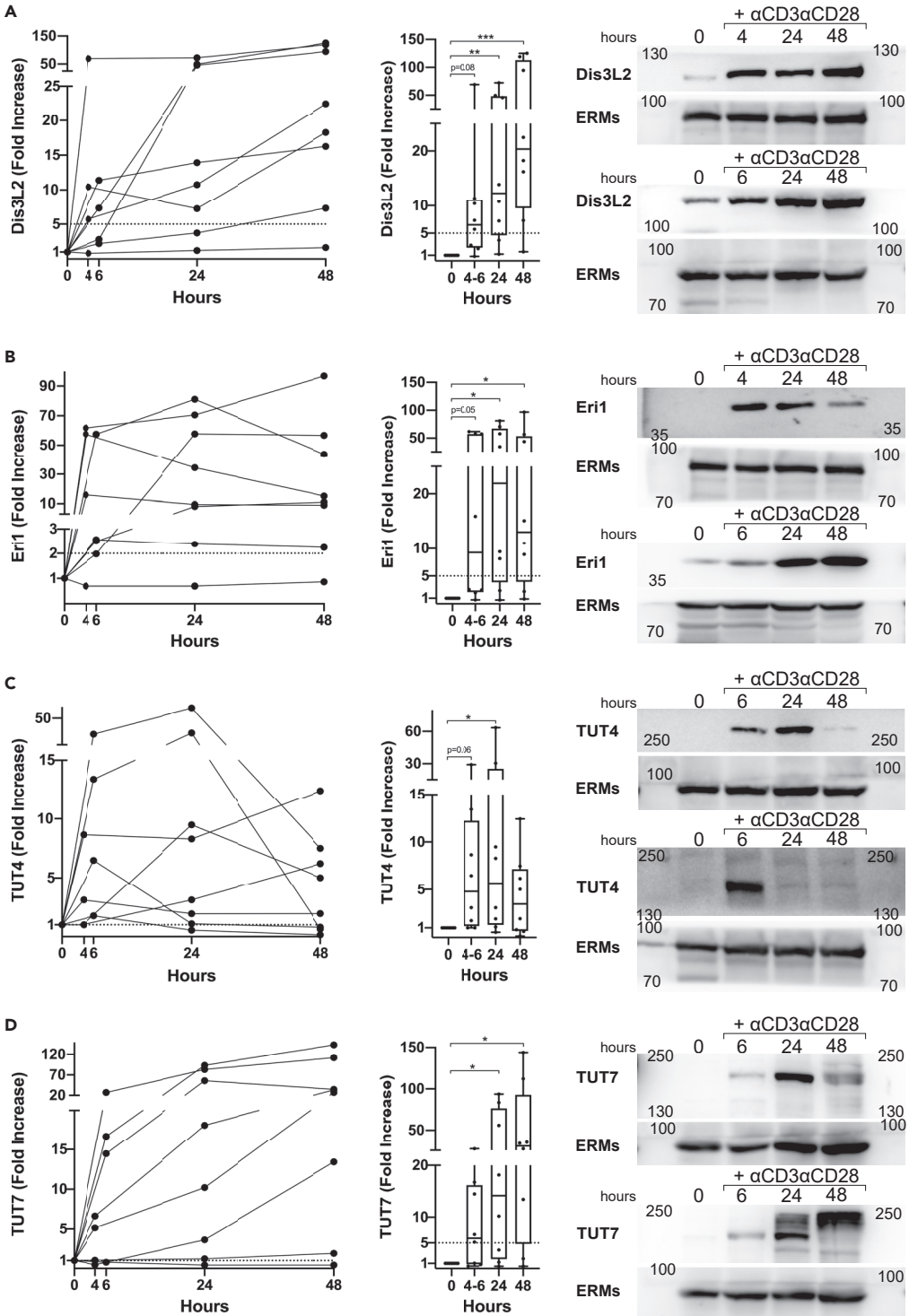

Figure 8. Expression of uridylated RNA degrading enzymes (Dis3L2 and Eri1) and terminal uridyl transferases (TUT4 y TUT7) upon CD4+ T cell activation

Western blot analysis of protein expression in human primary CD4+ T cells from 8 donors stimulated with αCD3αCD28, assessing Dis3L2 (A), Eri1 (B), TUT4 (C) and TUT7 (D). Fold increase compared to non-stimulation was represented for each donor, to observe individual expression evolution upon activation (left panel), and using group median and interquartile range with whiskers ranging from minimum to maximum values (middle panel). Right panels include two examples of different donors for each protein to highlight inter-donor variability in upregulation kinetics. Band intensities were

Figure 8. *Continued*
normalized to ERMs values and relativized to unstimulated conditions. Statistical analysis: Kruskal-Wallis test, Dunn's multiple comparisons test [* p value <0.05, ** p value<0.01, *** p value<0.001; 0.05<p value<0.1: indicated with numbers]. In panel C, TUT4 was separated under two different acrylamide gel concentrations.

Nevertheless, T cells still require certain miRNAs to remain stable even in generally degradative conditions. PtMs could control miRNA stability, promoting degradation but also protecting specific miRNAs. The global PtMs profile of our samples reveals that modification processes were focused on the 3′ end of most miRNAs. A series of upregulated miRNAs, particularly in αCD3αCD28, show a higher degree of adenylation, which could be related with miRNA stability in the context of T cells. Interestingly, the most adenylated miRNA (with up to a 42% of reads adenylated at position 1) is miR-92a-3p which is precisely the upregulated miRNA with higher expression in both studied activation conditions. Other miRNAs highly adenylated such as miR-17-5p, miR-93-5p, miR-20a-5p, and miR-378a-3p are also among those αCD3αCD28-upregulated miRNAs expressed with greater abundance.

While uridylation and adenylation have been the best characterized 3′ end modifications described across animal miRNAs (Burroughs et al., 2010; Chiang et al., 2010; Landgraf et al., 2007; Muller et al., 2014; Wyman et al., 2011), cytosylation was also significantly represented in our samples. Cytosine was specifically found at position 0 (3′ end nucleotide). Although most studies evaluating PtMs have found guanosine and cytosine additions to be barely represented, mono-addition of cytosine was the second most abundant 3′ modification after mono-uridylation, in mouse primordial germ cells and gonadal somatic cells at various embryonic stages (Darnell et al., 2018). The presence of "non-templated cytosylation" has been described in Arabidopsis, which prompted the hypothesis of the existence of a nucleotidyl transferase with a preference for cytosine as substrate (Chou et al., 2015). Cytosine additions could be relevant for miRNA modulation in very specific developmental or differentiation stages.

Consistent with previous studies from our laboratory, which had indicated that uridylation is a miRNA degradation signal in T cells (Gutiérrez-Vázquez et al., 2017), higher levels of U additions were found in αCD3αCD28 downregulated miRNAs. A similar pattern can be observed in IFN I stimulation, although differences are milder, which may be due to a less dynamic miRNA environment; since the number of differentially expressed miRNAs was roughly half of those quantified in cells treated with αCD3αCD28.

In summary, this study offers a data set of differentially regulated miRNAs in early time points of human primary CD4+ T cell activation and the kinetics of their PtMs. Our data also indicate that the RNA degrading enzymes Eri1 and Dis3L2 are upregulated upon activation, which could be part of an active mechanism of miRNA degradation guided by uridylation. Indeed, higher uridylation was found in downregulated miRNAs. Upregulated miRNAs, which manage to multiply their levels in this adverse environment, point toward 3′ adenine addition as a potential protective signal.

Limitations of the study

The present study is technically limited by the lack of solid tools for the study of single miRNA modifications beyond NGS. In addition, our data will need to be further completed with a better understanding of ribonucleases and RNA partners behind the modification landscape observed here. This study will be highly complex due to the numerous potential players and the difficulty to identify proteins with enzymatic activities barely described so far, such as cytosine addition. Therefore, we prefer to make this earlier approach available now to the scientific community, being aware that there is still much to learn on the field.

STAR★METHODS

Detailed methods are provided in the online version of this paper and include the following:

- KEY RESOURCES TABLE
- RESOURCE AVAILABILITY
  - Lead contact
  - Materials availability
  - Data and code availability
- EXPERIMENTAL MODEL AND SUBJECT DETAILS

SUPPLEMENTAL INFORMATION

Supplemental information can be found online at https://doi.org/10.1016/j.isci.2021.102530.

ACKNOWLEDGMENTS

We thank Miguel Vicente-Manzanares and Simon Bartlett for help with English. We also thank the CNIC Genomics and Bioinformatics Units for technical support.

This work was supported by grants SAF2017-82886-R from the Spanish Ministry of Economy and Competitiveness (MINECO), grant S2017/BMD-3671-INFLAMUNE-CM from the Comunidad de Madrid, a grant from the Ramón Areces Foundation "Ciencias de la Vida y la Salud" (XIX Concurso-2018) and a grant from Ayudas Fundación BBVA an Equipos de Investigación Científica (BIOMEDICINA-2018) and ""la Caixa"" Banking Foundation (HR17-00016). BIOIMID (PIE13/041) from Instituto de Salud Carlos III, CIBER Cardiovascular (CB16/11/00272, Fondo de Investigación Sanitaria del Instituto de Salud Carlos III and co-funding by Fondo Europeo de Desarrollo Regional FEDER). The Centro Nacional de Investigaciones Cardiovasculares (CNIC, Spain) is supported by the Ministerio de Economía y Competitividad-Spain and the Pro-CNIC Foundation.

A.R.G., S.G.D., and I.F.D. were supported by the FPU program (Spanish Ministry of Education).

AUTHOR CONTRIBUTIONS

A.R.G. and F.S.M. conceived the study. Experiments were performed by A.R.G., S.G.D., and I.F.D. L.F.M. provided miRNA expertise advice and discussion. M.J.G. and F.S.C. performed the differential expression and PtMs analysis of the miRNA-seq data. A.R.G. analyzed results, made the figures and wrote the manuscript, with input from the rest of authors. F.S.M. supervised and revised all the work.

DECLARATION OF INTERESTS

The authors declare no competing interests.

Received: October 14, 2020
Revised: April 6, 2021
Accepted: May 10, 2021
Published: June 25, 2021

REFERENCES

Bazak, L., Haviv, A., Barak, M., Jacob-Hirsch, J., Deng, P., Zhang, R., Isaacs, F.J., Rechavi, G., Li, J.B., Eisenberg, E., et al. (2014). A-to-I RNA editing occurs at over a hundred million genomic sites, located in a majority of human genes. Genome Res. *24*, 365–376.

Blanc, V., and Davidson, N.O. (2010). APOBEC-1-mediated RNA editing. Wiley Interdiscip. Rev. Syst. Biol. Med. *2*, 594–602.

Boele, J., Persson, H., Shin, J.W., Ishizu, Y., Newie, I.S., Søkilde, R., Hawkins, S.M., Coarfa, C., Ikeda, K., Takayama, K.I., et al. (2014). PAPD5-mediated 3′ adenylation and subsequent degradation of miR-21 is disrupted in proliferative disease. Proc. Natl. Acad. Sci. U S A *111*, 11467–11472.

Bronevetsky, Y., Villarino, A.V., Eisley, C.J., Barbeau, R., Barczak, A.J., Heinz, G.A., Kremmer, E., Heissmeyer, V., McManus, M.T., Erle, D.J., et al. (2013). T cell activation induces proteasomal degradation of Argonaute and rapid remodeling of the microRNA repertoire. J. Exp. Med. *210*, 417–432.

Burroughs, A.M., Ando, Y., de Hoon, M.J.L., Tomaru, Y., Nishibu, T., Ukekawa, R., Funakoshi, T., Kurokawa, T., Suzuki, H., Hayashizaki, Y., et al. (2010). A comprehensive survey of 3′ animal miRNA modification events and a possible role for 3′ adenylation in modulating miRNA targeting effectiveness. Genome Res. *20*, 1398–1410.

Büssing, I., Slack, F.J., and Großhans, H. (2008). let-7 microRNAs in development, stem cells and cancer. Trends Mol. Med. *14*, 400–409.

Chang, H.-M., Triboulet, R., Thornton, J.E., and Gregory, R.I. (2013). A role for the Perlman syndrome exonuclease Dis3l2 in the Lin28-let-7 pathway. Nature *497*, 244–248.

Chiang, H.R., Schoenfeld, L.W., Ruby, J.G., Auyeung, V.C., Spies, N., Baek, D., Johnston, W.K., Russ, C., Luo, S., Babiarz, J.E., et al. (2010). Mammalian microRNAs: experimental evaluation of novel and previously annotated genes. Genes Dev. *24*, 992–1009.

Chou, M.-T., Han, B.W., Hsiao, C.-P., Zamore, P.D., Weng, Z., and Hung, J.-H. (2015). Tailor: a

computational framework for detecting non-templated tailing of small silencing RNAs. Nucleic Acids Res. *43*, 109.

D'Ambrogio, A., Gu, W., Udagawa, T., Mello, C.C., and Richter, J.D. (2012). Specific miRNA stabilization by Gld2-catalyzed monoadenylation. Cell Rep. *2*, 1537–1545.

Darnell, R.B., Ke, S., and Darnell, J.E. (2018). Protein–RNA interactions: structural characteristics and hotspot amino acids. Rna *24*, 1457–1465.

Diener, C., Hart, M., Kehl, T., Rheinheimer, S., Ludwig, N., Krammes, L., Pawusch, S., Lenhof, K., Tänzer, T., Schub, D., et al. (2020). Quantitative and time-resolved miRNA pattern of early human T cell activation. Nucleic Acids Res. *48*, 10164–10183.

Ebhardt, H.A., Tsang, H.H., Dai, D.C., Liu, Y., Bostan, B., and Fahlman, R.P. (2009). Meta-analysis of small RNA-sequencing errors reveals ubiquitous post-transcriptional RNA modifications. Nucleic Acids Res. *37*, 2461–2470.

Fan, Y., and Xia, J. (2018). miRNet—functional analysis and visual exploration of miRNA–target interactions in a network context. In Methods in Molecular Biology (Humana Press Inc.), pp. 215–233.

Forster, S.C., Tate, M.D., and Hertzog, P.J. (2015). MicroRNA as type I interferon-regulated transcripts and modulators of the innate immune response. Front. Immunol. *6*, 1.

Gebert, L.F.R., and MacRae, I.J. (2019). Regulation of microRNA function in animals. Nat. Rev. Mol. Cell Biol. *20*, 21–37.

Gracias, D.T., and Katsikis, P.D. (2011). MicroRNAs: key components of immune regulation. In Advances in Experimental Medicine and Biology (Adv Exp Med Biol), pp. 15–26.

Grigoryev, Y.A., Kurian, S.M., Hart, T., Nakorchevsky, A.A., Chen, C., Campbell, D., Head, S.R., Yates, J.R., and Salomon, D.R. (2011). MicroRNA regulation of molecular networks mapped by global microRNA, mRNA, and protein expression in activated T lymphocytes. J. Immunol. *187*, 2233–2243.

Gu, S., Jin, L., Zhang, Y., Huang, Y., Zhang, F., Valdmanis, P.N., and Kay, M.A. (2012). The loop position of shRNAs and pre-miRNAs is critical for the accuracy of dicer processing in vivo. Cell *151*, 900–911.

Gutiérrez-Vázquez, C., Enright, A.J., Rodríguez-Galán, A., Pérez-García, A., Collier, P., Jones, M.R., Benes, V., Mizgerd, J.P., Mittelbrunn, M., Ramiro, A.R., et al. (2017). 3′ Uridylation controls mature microRNA turnover during CD4 T-cell activation. RNA *23*, 882–891.

Heo, I., Joo, C., Cho, J., Ha, M., Han, J., and Kim, V.N. (2008). Lin28 mediates the terminal uridylation of let-7 precursor MicroRNA. Mol. Cell *32*, 276–284.

Heo, I., Joo, C., Kim, Y.-K., Ha, M., Yoon, M.-J., Cho, J., Yeom, K.-H., Han, J., and Kim, V.N. (2009). TUT4 in concert with Lin28 suppresses microRNA biogenesis through pre-microRNA uridylation. Cell *138*, 696–708.

Heo, I., Ha, M., Lim, J., Yoon, M.J., Park, J.E., Kwon, S.C., Chang, H., and Kim, V.N. (2012). Mono-uridylation of pre-microRNA as a key step in the biogenesis of group II let-7 microRNAs. Cell *151*, 521–532.

Hoefig, K.P., Rath, N., Heinz, G.A., Wolf, C., Dameris, J., Schepers, A., Kremmer, E., Ansel, K.M., and Heissmeyer, V. (2013). Eri1 degrades the stem-loop of oligouridylated histone mRNAs to induce replication-dependent decay. Nat. Struct. Mol. Biol. *20*, 73–81.

Jindra, P.T., Bagley, J., Godwin, J.G., and Iacomini, J. (2010). Costimulation-Dependent expression of MicroRNA-214 increases the ability of T cells to proliferate by targeting Pten. J. Immunol. *185*, 990–997.

Jones, M.R., Quinton, L.J., Blahna, M.T., Neilson, J.R., Fu, S., Ivanov, A.R., Wolf, D.A., and Mizgerd, J.P. (2009). Zcchc11-dependent uridylation of microRNA directs cytokine expression. Nat. Cell Biol. *11*, 1157–1163.

Katoh, T., Sakaguchi, Y., Miyauchi, K., Suzuki, T., Suzuki, T., Kashiwabara, S.I., and Baba, T. (2009). Selective stabilization of mammalian microRNAs by 3′ adenylation mediated by the cytoplasmic poly(A) polymerase GLD-2. Genes Dev. *23*, 433–438.

Kim, B., Jeong, K., and Kim, V.N. (2017). Genome-wide mapping of DROSHA cleavage sites on primary MicroRNAs and noncanonical substrates. Mol. Cell *66*, 258–269.e5.

Kwon, S.C., Baek, S.C., Choi, Y.G., Yang, J., Lee, Y.S., Woo, J.S., and Kim, V.N. (2019). Molecular basis for the single-nucleotide precision of primary microRNA processing. Mol. Cell *73*, 505–518.e5.

Landgraf, P., Rusu, M., Sheridan, R., Sewer, A., Iovino, N., Aravin, A., Pfeffer, S., Rice, A., Kamphorst, A.O., Landthaler, M., et al. (2007). A mammalian microRNA expression atlas based on small RNA library sequencing. Cell *129*, 1401–1414.

Lee, L.W., Zhang, S., Etheridge, A., Ma, L., Martin, D., Galas, D., and Wang, K. (2010). Complexity of the microRNA repertoire revealed by next-generation sequencing. RNA *16*, 2170–2180.

Li, B., and Dewey, C.N. (2011). RSEM: accurate transcript quantification from RNA-Seq data with or without a reference genome. BMC Bioinformatics *12*, 323.

Li, L., Song, Y., Shi, X., Liu, J., Xiong, S., Chen, W., Fu, Q., Huang, Z., Gu, N., and Zhang, R. (2018). The landscape of miRNA editing in animals and its impact on miRNA biogenesis and targeting. Genome Res. *28*, 132–143.

Lindsay, M.A. (2008). microRNAs and the immune response. Trends Immunol. *29*, 343–351.

Martin, M. (2011). Cutadapt removes adapter sequences from high-throughput sequencing reads. EMBnet. J. *17*, 10–12.

Mehta, A., and Baltimore, D. (2016). MicroRNAs as regulatory elements in immune system logic. Nat. Rev. Immunol. *16*, 279–294.

Muller, H., Marzi, M.J., and Nicassio, F. (2014). IsomiRage: from functional classification to differential expression of miRNA isoforms. Front. Bioeng. Biotechnol. *2*, 38.

Neilsen, C.T., Goodall, G.J., and Bracken, C.P. (2012). IsomiRs–the overlooked repertoire in the dynamic microRNAome. Trends Genet. *28*, 544–549.

Nishikura, K. (2016). A-to-I editing of coding and non-coding RNAs by ADARs. Nat. Rev. Mol. Cell Biol. *17*, 83–96.

Podshivalova, K., and Salomon, D.R. (2013). MicroRNA regulation of T-lymphocyte immunity: modulation of molecular networks responsible for T-cell activation, differentiation, and development. Crit. Rev. Immunol. *33*, 435–476.

Ritchie, M.E., Phipson, B., Wu, D., Hu, Y., Law, C.W., Shi, W., and Smyth, G.K. (2015). Limma powers differential expression analyses for RNA-sequencing and microarray studies. Nucleic Acids Res. *43*, e47.

Rodríguez-Galán, A., Fernández-Messina, L., and Sánchez-Madrid, F. (2018). Control of immunoregulatory molecules by miRNAs in T cell activation. Front. Immunol. *9*, 1–10.

Rosenberg, B.R., Hamilton, C.E., Mwangi, M.M., Dewell, S., Papavasiliou, F.N., Struct, N., and Biol, M. (2011). Transcriptome-wide sequencing reveals numerous APOBEC1 mRNA editing targets in transcript 3′ UTRs HHS Public Access Author manuscript. Nat. Struct. Mol. Biol. *18*, 230–236.

Sandberg, R., Neilson, J.R., Sarma, A., Sharp, P.A., and Burge, C.B. (2008). Proliferating cells express mRNAs with shortened 3′ untranslated regions and fewer MicroRNA target sites. Science *320*, 1643–1647.

Scagnolari, C., Zingariello, P., Vecchiet, J., Selvaggi, C., Racciatti, D., Taliani, G., Riva, E., Pizzigallo, E., and Antonelli, G. (2010). Differential expression of interferon-induced microRNAs in patients with chronic hepatitis C virus infection treated with pegylated interferon alpha. Virol. J. *7*, 311.

Sousa, I.G., do Almo, M.M., Simi, K.C.R., Bezerra, M.A.G., Andrade, R.V., Maranhão, A.Q., and Brigido, M.M. (2017). MicroRNA expression profiles in human CD3+T cells following stimulation with anti-human CD3 antibodies. BMC Res. Notes *10*, 124.

de Sousa, M.C., Gjorgjieva, M., Dolicka, D., Sobolewski, C., and Foti, M. (2019). Deciphering miRNAs' action through miRNA editing. Int. J. Mol. Sci. *20*, 6249.

Starega-Roslan, J., Krol, J., Koscianska, E., Kozlowski, P., Szlachcic, W.J., Sobczak, K., and Krzyzosiak, W.J. (2011). Structural basis of microRNA length variety. Nucleic Acids Res. *39*, 257–268.

Sturn, A., Quackenbush, J., and Trajanoski, Z. (2002). Genesis: cluster analysis of microarray data. Bioinformatics *18*, 207–208.

Tan, M.H., Li, Q., Shanmugam, R., Piskol, R., Kohler, J., Young, A.N., Liu, K.I., Zhang, R., Ramaswami, G., Ariyoshi, K., et al. (2017). Dynamic landscape and regulation of RNA editing in mammals. Nature *550*, 249–254.

Teteloshvili, N., Smigielska-Czepiel, K., Kroesen, B.-J., Brouwer, E., Kluiver, J., Boots, A., and van den Berg, A. (2015). T-cell activation induces dynamic changes in miRNA expression patterns in CD4 and CD8 T-cell subsets. MicroRNA *4*, 117–122.

Thomas, M.F., Abdul-Wajid, S., Panduro, M., Babiarz, J.E., Rajaram, M., Woodruff, P., Lanier, L.L., Heissmeyer, V., and Ansel, K.M. (2012). Eri1 regulates microRNA homeostasis and mouse lymphocyte development and antiviral function. Blood *120*, 130–142.

Thornton, J.E., Chang, H.M., Piskounova, E., and Gregory, R.I. (2012). Lin28-mediated control of let-7 microRNA expression by alternative TUTases Zcchc11 (TUT4) and Zcchc6 (TUT7). RNA *18*, 1875–1885.

Ustianenko, D., Hrossova, D., Potesil, D., Chalupnikova, K., Hrazdilova, K., Pachernik, J., Cetkovska, K., Uldrijan, S., Zdrahal, Z., and Vanacova, S. (2013). Mammalian DIS3L2 exoribonuclease targets the uridylated precursors of let-7 miRNAs. RNA *19*, 1632–1638.

Vitsios, D.M., and Enright, A.J. (2015). Chimira: analysis of small RNA sequencing data and microRNA modifications. Bioinformatics *31*, 3365–3367.

Wang, Y., and Liang, H. (2018). When MicroRNAs meet RNA editing in cancer: a nucleotide change can make a difference. BioEssays *40*. https://doi.org/10.1002/bies.201700188.

Wang, P., Gu, Y., Zhang, Q., Han, Y., Hou, J., Lin, L., Wu, C., Bao, Y., Su, X., Jiang, M., et al. (2012). Identification of Resting and Type I IFN-Activated Human NK Cell miRNomes Reveals MicroRNA-378 and MicroRNA-30e as Negative Regulators of NK Cell Cytotoxicity. J. Immunol. *189*, 211–221.

Warkocki, Z., Liudkovska, V., Gewartowska, O., Mroczek, S., and Dziembowski, A. (2018). Terminal nucleotidyl transferases (TENTs) in mammalian RNA metabolism. Philos. Trans. R. Soc. B Biol. Sci. *373*, 20180162.

Wu, H., Neilson, J.R., Kumar, P., Manocha, M., Shankar, P., Sharp, P.A., and Manjunath, N. (2007). miRNA profiling of naïve, effector and memory CD8 T cells. PLoS One *2*, e1020.

Wu, H., Ye, C., Ramirez, D., and Manjunath, N. (2009). Alternative processing of primary microRNA transcripts by Drosha generates 5′ end variation of mature microRNA. PLoS One *4*, e7566.

Wyman, S.K., Knouf, E.C., Parkin, R.K., Fritz, B.R., Lin, D.W., Dennis, L.M., Krouse, M.A., Webster, P.J., and Tewari, M. (2011). Post-transcriptional generation of miRNA variants by multiple nucleotidyl transferases contributes to miRNA transcriptome complexity. Genome Res. *21*, 1450–1461.

Yang, Q., Lin, J., Liu, M., Li, R., Tian, B., Zhang, X., Xu, B., Liu, M., Zhang, X., Li, Y., et al. (2016). Highly sensitive sequencing reveals dynamic modifications and activities of small RNAs in mouse oocytes and early embryos. Sci. Adv. *2*, e1501482.

Yang, W., Chendrimada, T.P., Wang, Q., Higuchi, M., Seeburg, P.H., Shiekhattar, R., and Nishikura, K. (2006). Modulation of microRNA processing and expression through RNA editing by ADAR deaminases. Nat. Struct. Mol. Biol. *13*, 13–21.

Zhou, H., Arcila, M.L., Li, Z., Lee, E.J., Henzler, C., Liu, J., Rana, T.M., and Kosik, K.S. (2012). Deep annotation of mouse iso-miR and iso-moR variation. Nucleic Acids Res. *40*, 5864–5875.

Zhu, L., Kandasamy, S.K., and Fukunaga, R. (2018). Dicer partner protein tunes the length of miRNAs using base-mismatch in the pre-miRNA stem. Nucleic Acids Res. *46*, 3726–3741.

STAR★METHODS

KEY RESOURCES TABLE

REAGENT or RESOURCE	SOURCE	IDENTIFIER
Antibodies		
anti-Dis3L2	Nobus biologicals	Cat# NBP1-84740
anti-Eri1/THEX1	Cell Signaling	Cat#4049
anti-TUT4/ZCCHC11	Pro Sci incorporated	Cat#46-610
anti-TUT7/ZCCHC6	Proteintech	Cat#25196-1-AP
anti-ezrin/radixin/moesin (ERMs) (90/3)	provided by Heinz Furthmayr, Stanford University, CA	N/A
goat anti-rabbit	ThermoFisher Scientific	Cat#31460
rabbit anti-goat	ThermoFisher Scientific	Cat#31402
Biological samples		
Buffy coats	Centro de Transfusión (Comunidad de Madrid, Spain)	N/A
Chemicals, peptides, and recombinant proteins		
Biocoll Separating Solution	Biochrom	Cat# L6115
ImmunoCult™ Human CD3/CD28 T Cell Activator	STEMCELL Technologies	Cat#10971
Human IFN Alpha Hybrid (Universal Type I IFN)	PBL ASSAY SCIENCE	Cat#11200-1
QIAzol Lysis Reagent	Qiagen	Cat#, 79306
Critical commercial assays		
Human Resting CD4+ T cell Isolation Kit	STEMCELL Technologies	Cat#17962
EasySep Human CD4+ T Cell Isolation Kit	STEMCELL Technologies	Cat#17952
miRNeasy Mini Kit	Qiagen	Cat#217004
NEBNext Multiplex SmallRNA Library Prep Set for Illumina	New England Biolabs	Cat#E7580L
miRCURY LNA RT Kit	Qiagen	Cat#339340
miRCURY LNA SYBER Green PCR Kit	Qiagen	Cat#339347
miRCURY LNA miRNA PCR Assay(hsa-miR-1246, hsa-miR-222-5p, hsa-miR-23a-5p, hsa-miR-27a-5p, SNORD44(hsa) and SNORD48(hsa))	Qiagen	Cat#339306
Deposited data		
Raw and processed data	This paper	GEO: GSE156287
Alignments IFN I	This paper	https://genome.ucsc.edu/s/mjgommo/CD4T_IFN_I
Alignments aCD3aCD28	This paper	https://genome.ucsc.edu/s/mjgommo/CD4T_aCD3aCD28
In-house script (CHIMProcessor.R)	This paper	https://github.com/mjgommo/CD4T_miRNA_MOD
Software and algorithms		
FastQC	Babraham Bioinformatics	http://www.bioinformatics.babraham.ac.uk/projects/fastqc/
Cutadapt	Martin (2011)	http://code.google.com/p/cutadapt/
RSEM	Li and Dewey (2011)	http://deweylab.biostat.wisc.edu/rsem
Bioconductor package Limma	Ritchie et al. (2015)	https://bioconductor.org/packages/release/bioc/html/limma.html
Genesis	Sturn et al. (2002)	http://genome.tugraz.at
Chimira	Vitsios and Enright (2015)	http://wwwdev.ebi.ac.uk/enright-dev/chimira/

(*Continued on next page*)

Continued

REAGENT or RESOURCE	SOURCE	IDENTIFIER
Ingenuity Pathway Analysis	Qiagen	Content version: 49932394
MiRNet	Fan and Xia (2018)	www.mirnet.ca
Biogazelle	QbasePlus	https://www.qbaseplus.com
Image Studio Lite	LI-COR Biosciences	https://www.licor.com/bio/image-studio-lite/download

RESOURCE AVAILABILITY

Lead contact

Further information and requests for resources and reagents should be directed to and will be fulfilled by the Lead Contact, Francisco Sánchez-Madrid (fsmadrid@salud.madrid.org).

Materials availability

This study did not generate new unique reagents.

Data and code availability

GEO submission. All raw and processed sequencing data generated in this study have been submitted to the NCBI Gene Expression Omnibus (GEO; https://www.ncbi.nlm.nih.gov/geo/) under accession number GSE156287.

UCSC genome browser sessions. Alignments are accessible at the following UCSC Genome Browser session:

* https://genome.ucsc.edu/s/mjgommo/CD4T_IFN_I
* https://genome.ucsc.edu/s/mjgommo/CD4T_aCD3aCD28

Each session has been configured to allow the visualization of 13 custom tracks, which consist in:

- miRBase_mature track: representing the coordinates of all mature miRNAs described in miRBase, release 22.
-12 BAM alignment tracks, corresponding to three replicate samples for the control condition (0h) and each of the time points (3h, 6h, 24h) for IFN I or αCD3αCD28 treatment.

MiRNA detection and quantification have been performed in this study by aligning NGS processed reads against a transcriptomic reference consisting in all mature miRNA sequences described in miRBAse, release 22, for Homo sapiens. To produce genomic alignments that were fully congruent with those generated for quantification, BAM alignments displayed in the UCSC tracks have been generated with RSEM using a genomic reference constructed with the mature miRNA coordinates described in miRBase, release 22, exclusively. For this reason, coverage is expected only at the intervals corresponding to regions that code for mature miRNAs. MIMAT IDs are used to identify such intervals because they are guaranteed to be unique (locus specific). Visualization of the tracks may require reloading the page, because of timeout issues.

In-house scripts. Chimira results describing miRNA modifications consist in a separate table for each sample. A specialized, in-house R script (CHIMProcessor.R) was developed to process the collection of output files, as well as several other auxiliary files, in order to normalize modification frequencies by library size, merge frequency information from replicate samples, filter data using various parameters and generate combined tables and preliminary plots. The script is available from GitHub, at:

* https://github.com/mjgommo/CD4T_miRNA_MOD

EXPERIMENTAL MODEL AND SUBJECT DETAILS

Human primary cells used in this study were isolated from healthy donor buffy coats. Donor age and sex were not disclosed by the medical center providing the samples.

These studies were performed according to the principles of the Declaration of Helsinki and approved by the local Ethics Committee for Basic Research at the Hospital La Princesa (Madrid), informed consent was obtained from all human volunteers.

Cells were cultured at 37°C in RPMI 1640 (Gibco), supplemented with 10% fetal bovine serum (Sigma), 20mM Hepes (Hyclone), 0.3mg/mL L-glutamine (Hyclone), 100 U/mL penicillin (Gibco) and 100 µg/mL streptomycin (Gibco).

METHOD DETAILS

Human primary CD4 T cell culture

Human peripheral blood mononuclear cells (PBMCs) were isolated from buffy coats, obtained from healthy donors, by separation on Biocoll Separating Solution (Biochrom, L6115) according to standard procedures. Non-adherent cells were separated from PBMCs after a 30 min adherence step at 37°C. $CD4^+$ T cells were purified from non-adherent cells using Human Resting CD4+ T cell Isolation Kit (STEMCELL Technologies, 17962). A specific reagent to isolate resting T cells was selected to avoid the presence of pre-activated CD4+ T cells in sequencing samples. In experiments performed to evaluate protein expression, CD4+ T cells were isolated with EasySep Human CD4+ T Cell Isolation Kit (STEMCELL Technologies, 17952).

For T cell stimulation, we treated CD4+ T cells with either αCD3αCD28 (ImmunoCult™ Human CD3/CD28 T Cell Activator; STEMCELL Technologies, 10971) or IFN I (1:1000, Human IFN Alpha Hybrid (Universal Type I IFN); PBL ASSAY SCIENCE, 11200-1).

RNA isolation, library preparation and NGS

Three independent experiments, with resting CD4+ T cells isolated from different healthy donors were performed. Samples were collected at 0h and after αCD3αCD28 or IFN I stimulation during 3h, 6h and 24h. The 21 samples were lysed in QIAzol Lysis Reagent (Qiagen, 79306) and RNA was extracted using the miRNeasy Mini Kit (Qiagen, 217004). In order to reduce phenol-based reagent contaminations, purified RNA samples were precipitated using sodium acetate (3M, 0.1x sample volume) and ethanol (100%,3x sample volume). RNA integrity was evaluated using an Agilent 2100 Bioanalyzer (Eukaryote Total RNA Nano assay).

A total of 200 ng of total RNA were used to generate barcoded miRNA-seq libraries using the NEBNext Multiplex SmallRNA Library Prep Set for Illumina (New England Biolabs). Briefly, 3′ and 5′ SR adapters were first ligated to the RNA sample. Next, reverse transcription followed by PCR amplification was used to enrich cDNA fragments with adapters at both ends. The quantity and quality of the miRNA libraries were determined using the Agilent 2100 Bioanalyzer High Sensitivity DNA chip.

Libraries were sequenced on a HiSeq2500 (Illumina) to generate 60 bases single reads. FastQ files for each sample were obtained using bcltofastQ 2.20 Software software (Illumina). NGS experiments were performed in the Genomics Unit of the CNIC.

miRNA-seq data analysis

Sequencing reads were pre-processed by means of a pipeline that used FastQC (http://www.bioinformatics.babraham.ac.uk/projects/fastqc/) to assess read quality; and Cutadapt (Martin, 2011) to trim sequencing reads, eliminating Illumina adapter remains, and to discard those that were shorter than 15 nt or longer than 35 nt after trimming. Around 80% of the reads from any of the samples were retained. Resulting reads were aligned against a collection of 2657 human, mature miRNA sequences extracted from miRBase (release 22), to obtain expression estimates with RSEM (Li and Dewey, 2011). Percentages of reads participating in at least one reported alignment were around 40%. Expected expression counts were then processed with an analysis pipeline that used Bioconductor package Limma (Ritchie et al., 2015) for normalization (using TMM method) and differential expression testing, taking into account that samples had been obtained in three batches, and considering only 626 miRNA species for which expression was at least 1 count per million (CPM) in 3 samples. Changes in gene expression were

considered significant if associated to Benjamini-Hochberg adjusted p-value < 0.1. Clustering of expression profiles and production of heatmaps were performed with Genesis (Sturn et al., 2002). Epi-transcriptomic modifications were detected with Chimira (Vitsios and Enright, 2015), an online tool that, after alignment of miRNA-seq reads against miRBAse records, identifies mismatched positions to classify them and to quantify multiple types of 3'-modifications (uridylation, for example), as well as 5'-modifications and internal modifications or variations. Count tables produced by Chimira were further processed with ad-hoc produced R-scripts to normalize modification counts by library size and to calculate summary statistics across groups of replicate samples. Analyses were restricted to the collection of 626 miRNA species with detectable expression. Upregulated and downregulated miRNA groups were defined considering any significant differential expression including all possible time point comparisons, not only those performed versus 0h.

Two core analysis were performed by Ingenuity Pathway Analysis (Content version: 49932394 (Release Date: 2019-11-14), one with all miRNAs differentially expressed at least at one time point after stimulation with αCD3αCD28 and a second one with the corresponding IFN-I regulated miRNAs. MiRNA-target networks were built with miRNet loading the highest upregulated and downregulated miRNAs for each treatment (Fan and Xia, 2018). Venn diagrams were elaborated with Venny (https://bioinfogp.cnb.csic.es/tools/venny/index.html).

miRNA qPCR

RNA was retrotranscribed using miRCURY LNA RT Kit (Qiagen, 339340) and qPCR was performed using miRCURY LNA SYBER Green PCR Kit (Qiagen, 339347) in AB7900. Primers for hsa-miR-1246, hsa-miR-222-5p, hsa-miR-23a-5p, hsa-miR-27a-5p, SNORD44 (hsa) and SNORD48 (hsa) were obtained from miRCURY LNA miRNA PCR Assay (Qiagen, 339306). Data was analyzed with Biogazelle QbasePlus software. Expression values were normalized to both RNU44 and RNU48.

IMMUNOBLOTTING

Cell extracts were prepared in lysis buffer (50 mM Tris pH 7.5, 150 mM NaCl, 1%NP-40, 5 mM EDTA, 50mM NaF, 5mM DTT) supplemented with a protease inhibitor cocktail (Complete, Roche). Cell lysates were cleared of nuclei by centrifugation (15000 g, 15 min). Proteins were separated on 8-10% SDS-PAGE gels and transferred to a nitrocellulose membrane. Membranes were incubated with primary specific antibodies: anti-Dis3L2 (Nobus biologicals, NBP1-84740), anti-Eri1/THEX1 (Cell Signaling, #4049), anti-TUT4/ZCCHC11 (Pro Sci incorporated, 46-610), anti-TUT7/ZCCHC6 (Proteintech, 25196-1-AP), and anti-ezrin/radixin/moesin (ERMs) (90/3) (provided by Heinz Furthmayr, Stanford University, CA). Primary antibodies were used at 1:2000 dilution and peroxidase-conjugated secondary antibodies (goat anti-rabbit, ThermoFisher Scientific #31460; rabbit anti-goat, ThermoFisher Scientific #31402) at 1:5000. Chemoluminescence was measured with LAS-3000 (Fujifilm). Band intensities were quantified with Image Studio Lite (LI-COR Biosciences), normalized to ERMs values and relativized to unstimulated conditions (when no band was detected at 0 h, background was taken as reference signal).

QUANTIFICATION AND STATISTICAL ANALYSIS

MiRNA differential expression changes in miRNA-seq (n=3 donors) were considered significant when associated with a Benjamini-Hochberg adjusted p-value < 0.1. Kruskal-Wallis test and Dunn's multiple comparisons test were applied using GraphPad Prism to perform statistical analysis on western blot (n=8, 8 donors) and qPCR (n=9, 9 donors) data, representing in figures significance as: * p-value <0.05, ** p-value<0.01, *** p-value<0.001; 0.05<p-value<0.1: indicated with numbers. Ingenuity Pathway Analysis uses Fisher's Exact Test p-value with a threshold value 0.05, as stated in the figure legend.

All graphs (except: heatmaps, Venn diagram, miRNet networks and Chimira global profile) were plotted using GraphPad Prism, therefore, for detailed definitions of measures such as mean, median or SEM, program online guides can be reviewed.

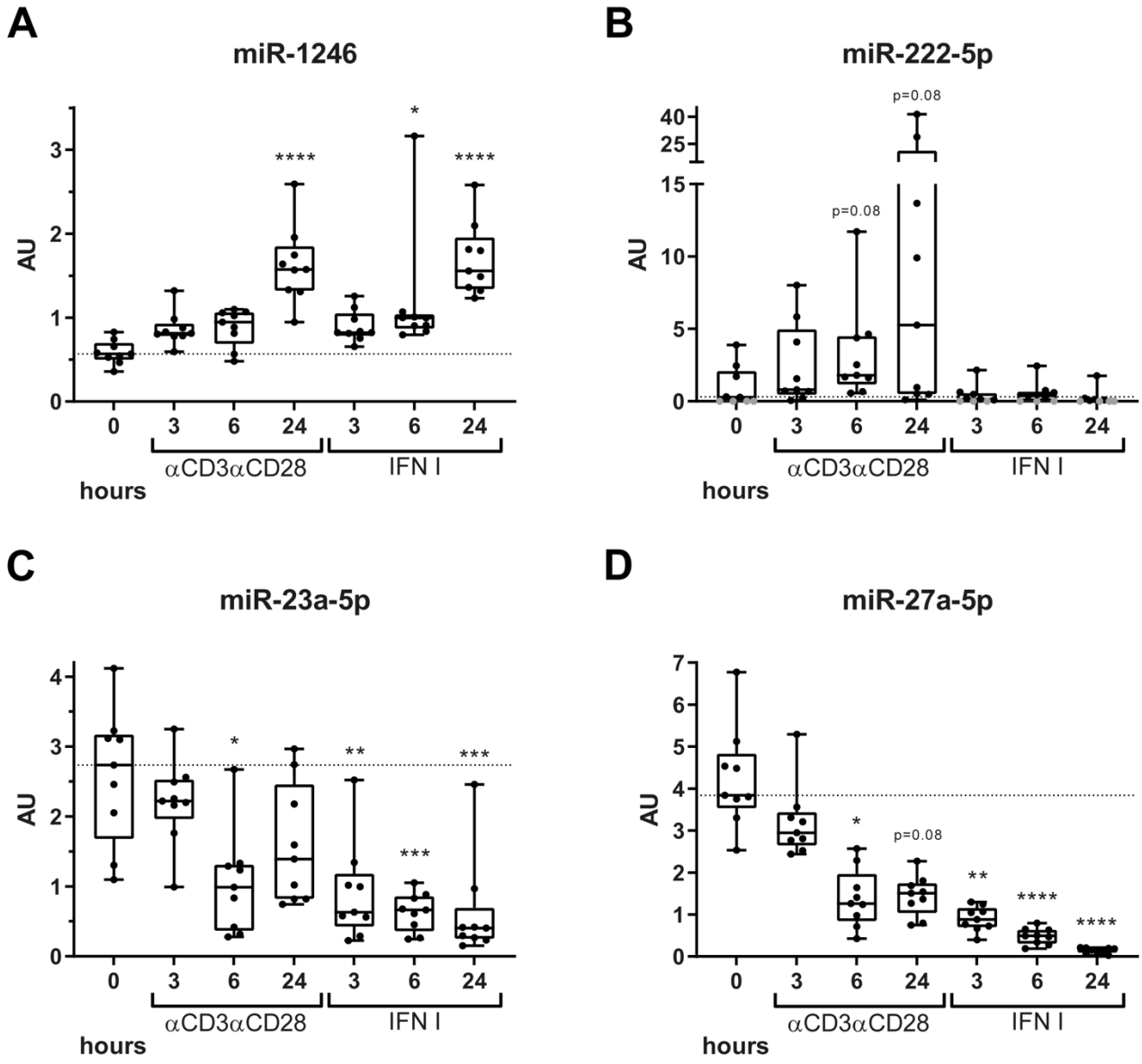

Supplementary Fig.1. qPCR validation of selected miRNAs, related to Figure 1 and Figure 2. qPCR expression values (group median and interquartile range with whiskers ranging from minimum to maximum values) for miR-1246 (A), miR-222-5p(B), miR-23a-5p (C) and miR-27a-5p (D) in CD4+ resting T cells from 9 donors (prior to stimulation and after 3,6 or 24h with αCD3αCD28 or IFN I). Statistical analysis: Kruskal-Wallis test, Dunn's multiple comparisons test [* p-value <0.05, ** p-value<0.01, *** p-value<0.001; 0.05<p-value<0.1: indicated with numbers].

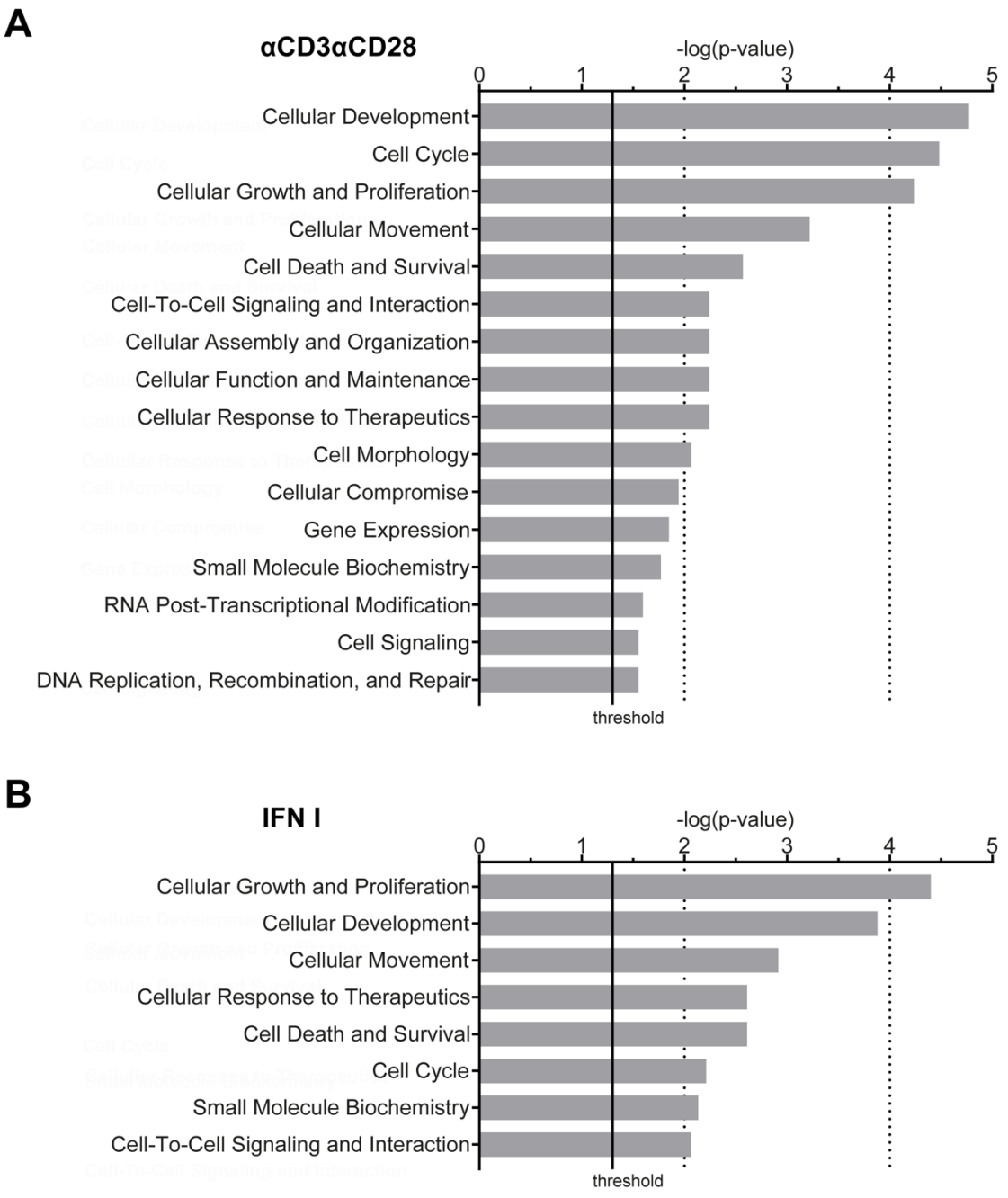

Supplementary Fig.2. Ingenuity Pathway Analysis: molecular and cellular functions, related to Figure 1 and Figure 2.

Core analysis performed with Ingenuity Pathway Analysis on differentially expressed miRNA (adjusted value <0.1) associated to their highest fold change during stimulation. Graphs include molecular and cellular functions found to be significantly represented for αCD3αCD28 miRNAs (A) and IFN I miRNAs (B). Fisher's Exact Test p-value, threshold value 0.05, displaying only entities that have a –log(p-value) greater than 1.3.

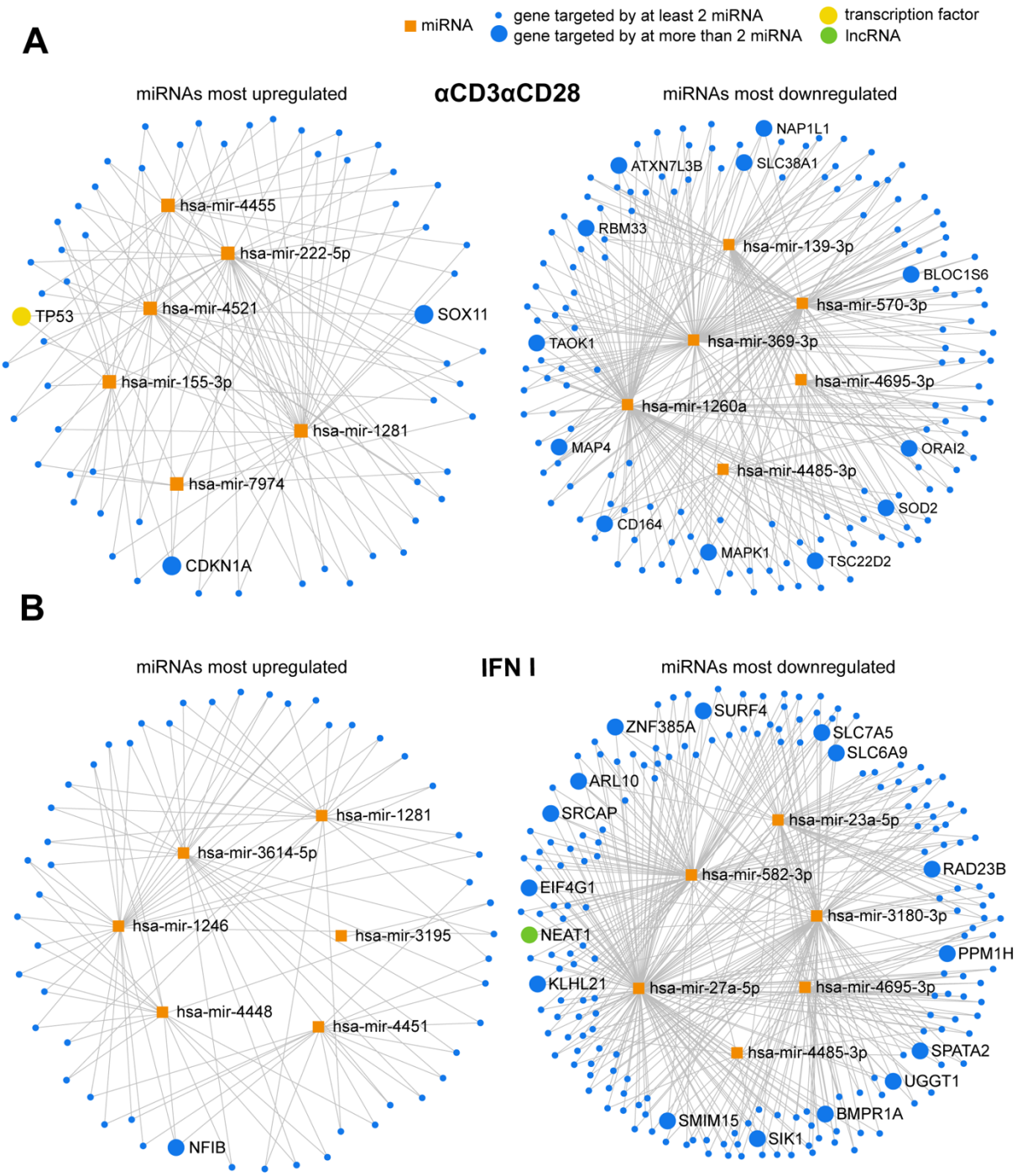

Supplementary Fig. 3. MiRNA predicted targets, related to Figure 1 and Figure 2.
Targets predicted for the 6 miRNAs with highest up (left) and down-regulation (right) in αCD3αCD28 (A) and IFN I (B) sets. Networks include gene targets predicted for at least two of the selected miRNAs. Data were generated using miRNet, applying a degree filter of 1 in all but miRNAs nodes.

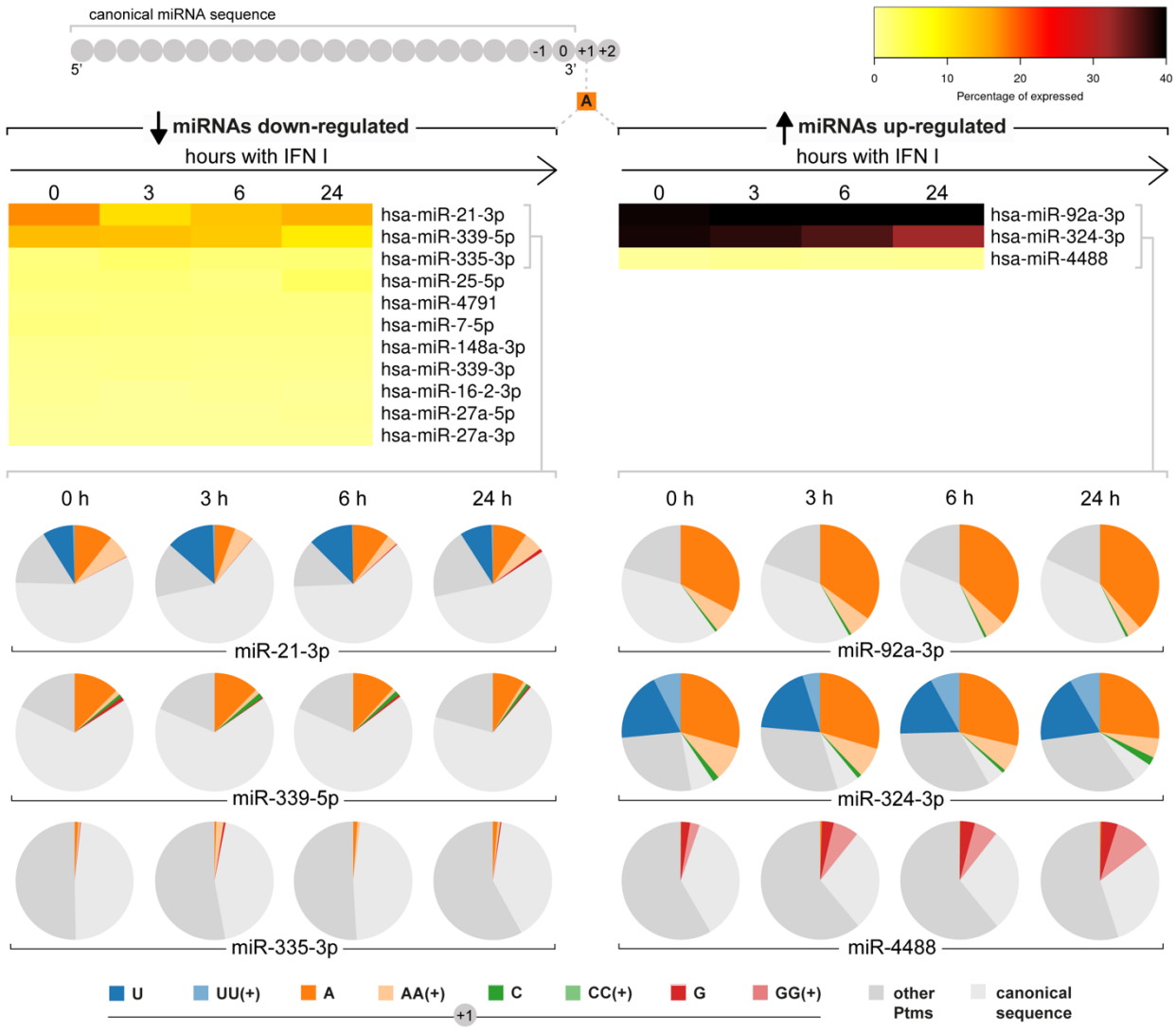

Supplementary Fig.4. MiRNAs with significant adenylation at position 1 (IFN I), related to figure 5.
Heatmaps include upregulated (right) and downregulated (left) miRNAs with significant adenylation at position 1, detected in IFN I stimulation. Reads with adenine at position 1 are normalized to total reads, in order to visualize the frequency of adenylation for each miRNA. Pie charts are included below for the 3 miRNAs most adenylated within each group. These graphs show in colour the percentage of reads with specific modifications at position 1, while reads with modifications at other positions and unmodified reads are depicted in gray.

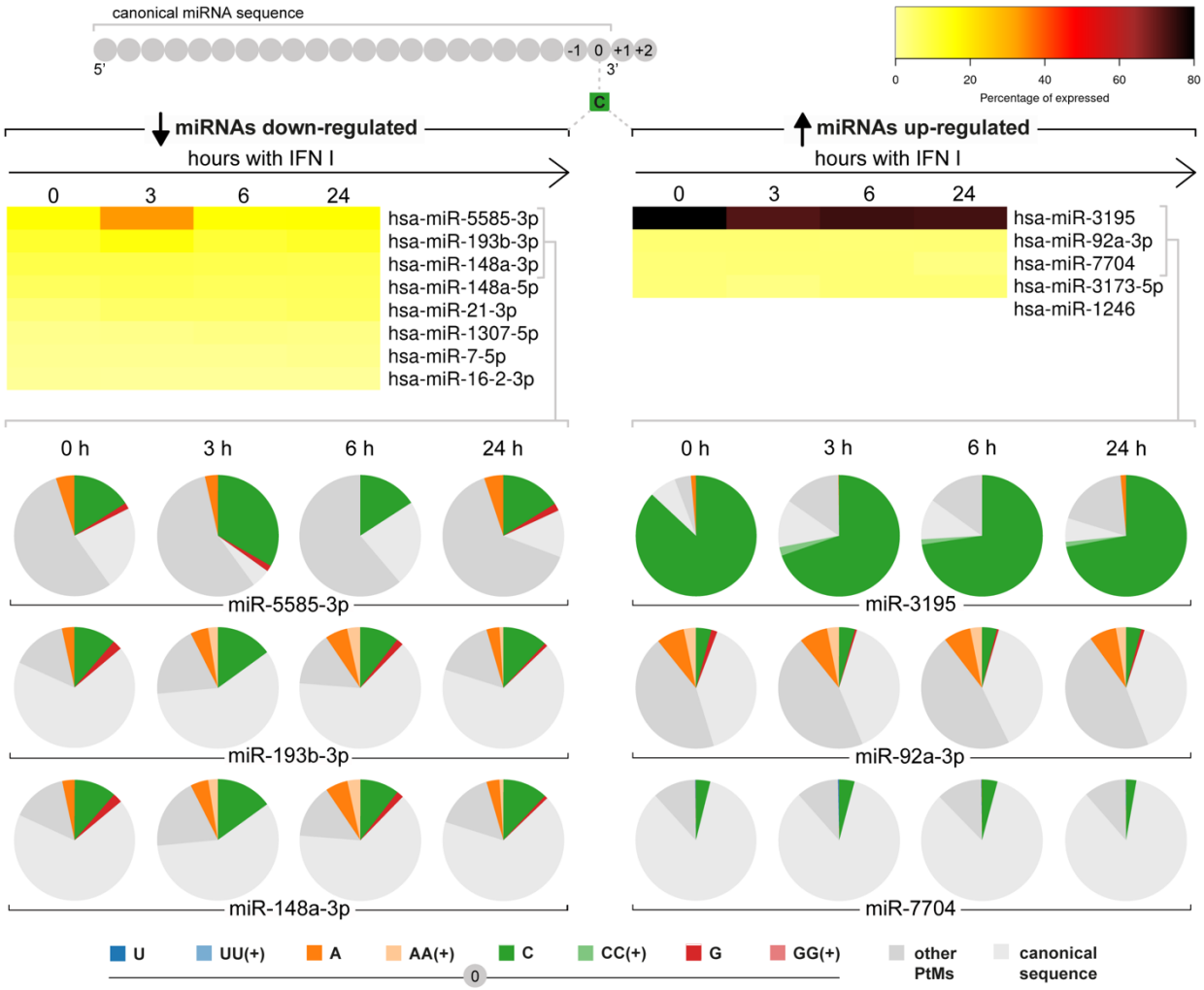

Supplementary Fig.5. MiRNAs with significant cytosylation at position 0 (IFN I), related to figure 5.

Heatmaps include upregulated (right) and downregulated (left) miRNAs with significant cytosylation at position 0, detected in IFN I stimulation. Reads with cytosine at position 1 are normalized to total reads, in order to visualize the frequency of cytosylation for each miRNA. Pie charts are included below for the 3 miRNAs most adenylated within each group. These graphs show in colour the percentage of reads with specific modifications at position 0, while reads with modifications at other positions and unmodified reads are depicted in gray.

UAM
UNIVERSIDAD AUTONOMA
DE MADRID